Nuclear Science
NEA/NSC/WPEC/DOC(2013)445
December 2013
www.oecd-nea.org

Methods and Issues for the Combined Use of Integral Experiments and Covariance Data

OECD
BETTER POLICIES FOR BETTER LIVES

NEA
NUCLEAR ENERGY AGENCY

Nuclear Science
NEA/WPEC-33

NEA/NSC/WPEC/DOC(2013)445

Methods and Issues for the Combined Use of Integral Experiments and Covariance Data

A report by the Working Party
on International Nuclear Data Evaluation Co-operation
of the NEA Nuclear Science Committee

Co-ordinators

M. Salvatores
CEA, Cadarache, France
Idaho National Laboratory
United States

G. Palmiotti
Idaho National Laboratory
United States

Monitor

R.D. McKnight
Argonne National Laboratory
United States

NUCLEAR ENERGY AGENCY

ORGANISATION FOR ECONOMIC CO-OPERATION AND DEVELOPMENT

ORGANISATION FOR ECONOMIC CO-OPERATION AND DEVELOPMENT

The OECD is a unique forum where the governments of 34 democracies work together to address the economic, social and environmental challenges of globalisation. The OECD is also at the forefront of efforts to understand and to help governments respond to new developments and concerns, such as corporate governance, the information economy and the challenges of an ageing population. The Organisation provides a setting where governments can compare policy experiences, seek answers to common problems, identify good practice and work to co-ordinate domestic and international policies.

The OECD member countries are: Australia, Austria, Belgium, Canada, Chile, the Czech Republic, Denmark, Estonia, Finland, France, Germany, Greece, Hungary, Iceland, Ireland, Israel, Italy, Japan, Luxembourg, Mexico, the Netherlands, New Zealand, Norway, Poland, Portugal, the Republic of Korea, the Slovak Republic, Slovenia, Spain, Sweden, Switzerland, Turkey, the United Kingdom and the United States. The European Commission takes part in the work of the OECD. OECD Publishing disseminates widely the results of the Organisation's statistics gathering and research on economic, social and environmental issues, as well as the conventions, guidelines and standards agreed by its members.

NUCLEAR ENERGY AGENCY

The OECD Nuclear Energy Agency (NEA) was established on 1 February 1958. Current NEA membership consists of 31 OECD member countries: Australia, Austria, Belgium, Canada, the Czech Republic, Denmark, Finland, France, Germany, Greece, Hungary, Iceland, Ireland, Italy, Japan, Luxembourg, Mexico, the Netherlands, Norway, Poland, Portugal, the Republic of Korea, the Russian Federation, the Slovak Republic, Slovenia, Spain, Sweden, Switzerland, Turkey, the United Kingdom and the United States. The European Commission also takes part in the work of the Agency.

The mission of the NEA is:

- to assist its member countries in maintaining and further developing, through international co-operation, the scientific, technological and legal bases required for a safe, environmentally friendly and economical use of nuclear energy for peaceful purposes, as well as
- to provide authoritative assessments and to forge common understandings on key issues, as input to government decisions on nuclear energy policy and to broader OECD policy analyses in areas such as energy and sustainable development.

Specific areas of competence of the NEA include the safety and regulation of nuclear activities, radioactive waste management, radiological protection, nuclear science, economic and technical analyses of the nuclear fuel cycle, nuclear law and liability, and public information.

The NEA Data Bank provides nuclear data and computer program services for participating countries. In these and related tasks, the NEA works in close collaboration with the International Atomic Energy Agency in Vienna, with which it has a Co-operation Agreement, as well as with other international organisations in the nuclear field.

Corrigenda to OECD publications may be found online at:

Foreword

The Working Party on International Nuclear Data Evaluation Co-operation (WPEC) has been established under the aegis of the OECD/NEA Nuclear Science Committee (NSC) to promote the exchange of information on nuclear data evaluations, validation and related topics. Its aim is also to provide a framework for co-operative activities between the members of the major nuclear data evaluation projects. This includes the possible exchange of scientists in order to encourage co-operation. Requirements for experimental data resulting from this activity are compiled. The WPEC determines common criteria for evaluated nuclear data files with a view to assessing and improving the quality and completeness of evaluated data.

The parties to the project are: BROND (Russian Federation), ENDF (United States), JENDL (Japan) and JEFF (other NEA Data Bank member countries). Co-operation with evaluation projects of non-NEA countries, specifically the Chinese CENDL project, is organised through the Nuclear Data Section of the International Atomic Energy Agency (IAEA).

The following report has been issued by the WPEC Subgroup 33, whose mission was to review methods and issues of the combined use of integral experiments and covariance data, with the objective of recommending a set of best and consistent practices in order to improve evaluated nuclear data files. In particular, it is shown that the statistical adjustment methodologies used worldwide are well understood and essentially equivalent. The results of the benchmark adjustment exercise indicate common trends for important data, even when they start from different basic nuclear data and different covariance matrices. In this respect, adjustment methodologies can provide a powerful tool to improve nuclear data (and associated uncertainties) if used in an appropriate manner.

The opinions expressed in this report are those of the authors only and do not necessarily represent the position of any member country or international organisation.

Members of Subgroup 33

M. Salvatores
CEA, Nuclear Energy Division, Cadarache, Saint-Paul-lez-Durance, France
Idaho National Laboratory (INL), Idaho Falls, ID, US

G. Palmiotti
Idaho National Laboratory (INL), Idaho Falls, ID, US

G. Aliberti, R. McKnight
Argonne National Laboratory (ANL), Argonne, IL, US

P. Archier, C. De Saint Jean
CEA, Nuclear Energy Division, Cadarache, Saint-Paul-lez-Durance, France

E. Dupont
OECD, Nuclear Energy Agency (NEA), Issy-les-Moulineaux, France

M. Herman
Brookhaven National Laboratory (BNL), Upton, NY, US

M. Ishikawa, K. Sugino
Japan Atomic Energy Agency (JAEA), Tokai-mura, Ibaraki, Japan

T. Ivanova, E. Ivanov
Institut de Radioprotection et de Sureté Nucléaire (IRSN), Fontenay-aux-Roses, France

S.-J. Kim
Korea Atomic Energy Research Institute (KAERI), Daejeon, South Korea

I. Kodeli, A. Trkov
Jozef Stefan Institute (JSI), Ljubljana, Slovenia

G. Manturov
Institute of Physics and Power Engineering (IPPE), Obninsk, Russia

S. Pelloni
Paul Scherrer Institut (PSI), Villigen, Switzerland

C. Perfetti, B.T. Rearden
Oak Ridge National Laboratory (ORNL), Oak Ridge, TN, US

A. Plompen
Institute for Reference Materials and Measurements (IRMM), Geel, Belgium

D. Rochman
Nuclear Research and Consultancy Group (NRG), Petten, The Netherlands

W. Wang, H. Wu
China Institute of Atomic Energy (CIAE), China Nuclear Data Center, Beijing, China

W.-S. Yang
Argonne National Laboratory (ANL), Argonne, IL, US
Purdue University, West Lafayette, IN, US

Acknowledgements

Dick McKnight, the monitor and one of the main initiators of this Subgroup, passed away on the 28 August 2013. With deep regret, all the members of the Subgroup want to dedicate the present report to his memory: his contribution has been essential, as in many other nuclear data activities in the frame of the OECD/NEA. During more than three decades, his outstanding knowledge, scientific vision and technical suggestions have played a key role in defining the right issues and the most appropriate approaches to solve them. Dick had extraordinary human qualities and has been a true friend to most of us. We will very much miss him.

Table of contents

List of Figures

List of Tables

1. Introduction, definition of benchmark steps, choice of integral experiments and target systems

1.1 Introduction

The Working Party on International Nuclear Data Evaluation Co-operation (WPEC) of the OECD Nuclear Energy Agency Nuclear Science Committee has established a subgroup (called "Subgroup 33") on "Methods and issues for the combined use of integral experiments and covariance data". In its mandate "it is proposed for this WPEC subgroup to study methods and issues of the combined use of integral experiments and covariance data with the objective of recommending a set of best and consistent practices in order to improve evaluated nuclear data files. Indications should be provided on how to best exploit existing integral experiments, define new ones if needed, provide trends and feedback to nuclear data evaluators and measurers".

In fact, physicists involved in the early design of fast reactors, proposed to utilise integral experiments to improve multi-group cross-sections by using integral experiments. This approach was justified by the limited knowledge at the time of the great number of nuclear data needed in a wide energy range both for design and for experiment analysis. The development of more powerful computers allowed a continuous improvement of the analytical tools, the reduction of approximations in the solution of the Boltzmann equation and in the multi-group generation algorithms. Hence, the remaining source of uncertainty in the assessment of the total neutron balance and of safety and operational parameters should be found in the nuclear cross-sections data. At the same time, a very large number of high accuracy integral experiments were performed in several critical facilities all over the world, providing evidence of potential significant uncertainties if extrapolation to design was attempted. Only very accurate mock-up experiments, if feasible, could possibly overcome that difficulty.

The mock-up approach was mainly used in the US, while more analytical experimental programmes were performed in France, UK, Japan and the Russian Federation (former USSR). While in the mock-up approach one would attempt to apply directly the observed calculation-to-experiment discrepancies to the calculation of the reference design configuration (with an appropriate use of the integral experiment uncertainties and an appropriate evaluation of possible calculation approximation effects differences between experimental and design configurations), the adjustment methodology was applied when a set of appropriately designed experiments was available. Major requirements for the integral experiments were, from one side, to be as "clean" (e.g. well documented and easy to analyse) as possible and, from another side, to provide complementary information on specific nuclear data (e.g. structural material capture, Pu vs. U fission etc.) in specific energy ranges (e.g. tailoring the neutron spectrum or the neutron leakage component of the core etc.). A careful assessment of experiment uncertainties was systematically performed.

The so-called "adjusted data sets" have been used directly in the design of e.g. fast reactors PHENIX and SUPERPHENIX in France. As an example of the performance of adjusted data, the use of the CARNAVAL-IV adjusted library has allowed predicting the critical mass of SUPERPHENIX with accuracy of the order of 300 pcm.

Despite the success, the adjustment process has raised legitimate questions related to both physical meaning of the individual (i.e. by isotope, reaction type and energy range) "adjustments", and possible compensation effects since integral experiments depend on a great number of parameters. Moreover, the first adjustments depended on uncertainty data essentially based on physicist's judgement and not on any formal approach.

It has also been underlined that there is no clear definition of the application domain of the adjusted multi-group. When a new reactor concept is investigated, it is difficult to define what is the mathematical/physical extrapolation method (if any) to be used together with the previously adjusted data library. As the adjustments are performed at the multi-group level, they will also be related to the weighting function used to produce the original multi-group library and no unique procedure can be used to transfer the adjustments from the broad group level (where the adjustments are usually performed) to a fine group level or, even preferred, to the continuous energy level. Similarly, self-shielding effects cannot be provided explicitly.

Finally, the use of the *a posteriori* covariance matrix (both variances and correlations) is not a self-evident exercise and, in fact, in many cases only *a posteriori* variances are used.

1.2 Activities of the Subgroup

The activity of the subgroup has been focused on providing a deeper understanding of nuclear data adjustment methods and of their application. The general understanding of the adjustment methods, their theory and application implies a number of potential difficulties that should be carefully examined in order to agree on the best approach which would allow taking advantage of the potential of the method.

The first step of the subgroup activity has been the compilation of a detailed report with the assessment of the methodologies that the different participants to this subgroup employ for the adjustment of neutron cross-section data using the observed discrepancies between calculated and measured values of integral experiments. To this purpose, a documentation of the used adjustment methodologies has been provided by ANL, CEA, INL, IPPE, JAEA, JSI, NRG, and ORNL. The report also includes the identification of merits and drawbacks of the existing adjustment methodologies, the comparison of the mathematical formulation and specific characteristics, and the criteria used for assessing the different methodologies.

At first, the assessment has been based on formal observations of formulations of the methodologies and answers provided by the participants on detailed definitions of criteria. In order to better understand the performance of these methodologies several organisations (ANL, CEA, INL, IRSN, JAEA, NRG and ORNL) took part in a common benchmark adjustment exercise. PSI also participated in this benchmark exercise by adopting the JAEA approach, which allows studying some specific issues. In particular, it was agreed that the main objective of the benchmark was to test different methods of nuclear data adjustment/assimilation and different sets of covariance data for the purpose of reducing e.g. the design uncertainties of a particular type of sodium-cooled fast reactor. The benchmark makes use of a single, limited set of selected integral experiments. The final results have been tested on a model of the Advanced Burner Reactor (ABR) with plutonium oxide fuel defined at ANL or/and a model of the JAEA Fast Breeder Reactor core.

This report presents detailed results of the subgroup, a more concise description is available in [1].

1.3 The benchmark exercise

To facilitate comparisons, a common 33-group structure has been adopted for the benchmark input/output. Every participant has been responsible for the conversion of its own data into the adopted group structure. The ANGELO code has, in some cases, been used to convert covariance matrices from one group structure to another. In some cases, it has been necessary to smooth them out (e.g. using lethargy width) on the 33-energy group structure.

Table 1: 33-energy group structure (eV)

Group	Upper Energy	Group	Upper Energy	Group	Upper Energy
1	$1.96\ 10^{7}$	12	$6.74\ 10^{4}$	23	$3.04\ 10^{2}$
2	$1.00\ 10^{7}$	13	$4.09\ 10^{4}$	24	$1.49\ 10^{2}$
3	$6.07\ 10^{6}$	14	$2.48\ 10^{4}$	25	$9.17\ 10^{1}$
4	$3.68\ 10^{6}$	15	$1.50\ 10^{4}$	26	$6.79\ 10^{1}$
5	$2.23\ 10^{6}$	16	$9.12\ 10^{3}$	27	$4.02\ 10^{1}$
6	$1.35\ 10^{6}$	17	$5.53\ 10^{3}$	28	$2.26\ 10^{1}$
7	$8.21\ 10^{5}$	18	$3.35\ 10^{3}$	29	$1.37\ 10^{1}$
8	$4.98\ 10^{5}$	19	$2.03\ 10^{3}$	30	$8.32\ 10^{0}$
9	$3.02\ 10^{5}$	20	$1.23\ 10^{3}$	31	$4.00\ 10^{0}$
10	$1.83\ 10^{5}$	21	$7.49\ 10^{2}$	32	$5.40\ 10^{-1}$
11	$1.11\ 10^{5}$	22	$4.54\ 10^{2}$	33	$1.00\ 10^{-1}$

1.3.1 Benchmark exercise

Every participant to the benchmark exercise used the same integral experiment values (E) and uncertainties, but their own calculated value (C), sensitivity coefficients, and adjustment/assimilation method.

The benchmark consists of a three-phase exercise using:

I. Own initial cross-sections, own nuclear data covariance, w/wo integral experiment correlation.

II. Own initial cross-sections, same nuclear data covariance, w/wo integral experiment correlation.

II-bis. Same initial cross-sections, same nuclear data covariance, w/wo integral experiment correlation.

III. Verification of the impact of the adjustments on a few “Target Systems”.

1.3.2 Benchmark input

In order to limit the calculation effort and to emphasise major trends in a more clear way, the number of isotopes to be adjusted has been limited to 11. In contrast, all major reactions have been considered. Finally, several covariance data sets have been used:

Isotopes

^{10}B for cross-correlation testing;

^{16}O as part of oxide fuel;

^{23}Na as coolant;

^{56}Fe, ^{52}Cr, ^{58}Ni	as major structural materials;
^{235}U	as fuel and for cross correlation testing;
^{238}U	as fuel and for indirect spectra effect (inelastic transfer matrix);
^{239}Pu	as fuel and for cross correlation testing;
^{240}Pu, ^{241}Pu	as fuel and for testing Pu isotopic vector.

Nuclear data

- Elastic scattering infinite-dilution cross-section;
- Total inelastic scattering infinite-dilution cross-section;
- Capture infinite-dilution cross-section (this includes ^{10}B(n,α) reaction);
- Fission infinite-dilution cross-section;
- Average prompt fission neutron multiplicity (Nu-bar);
- Normalised prompt fission neutron spectrum;
- Average cosine of elastically scattered neutrons (Mu-bar);
- Average delayed fission neutron multiplicity (Nu-d), as an optional adjustable parameter (on a voluntary basis). This proposal was driven by consideration on the impact of Nu-d on the integral C/E ratio value and uncertainty for Na void reactivity (measured in dollars). When Nu-d is not adjusted, the participants should have added the corresponding uncertainty to the C/E value of Na void reactivity in order to reduce their statistical weight.

The spectrum of the inelastically scattered neutron has not been part of the benchmark exercise. However, every participant could provide the ^{238}U(n,n') energy transfer matrix used in the exercise.

Nuclear covariance data

Every participant has used its own nuclear covariance data (Phase I, see above). However, in Phase II of the exercise, for comparison purposes and to disentangle effects from different *a priori* cross-sections or covariance data, one common set of covariance data would be used by all the participants, in addition to their own specific sets. The 33-group COMMARA2.0 covariance data, developed at BNL, has been made available for that purpose.

1.4 The selection of the integral experiments

The selection of fast neutron spectrum integral experiments has been based on the availability of well documented specifications and experimental uncertainties and possibly on some indication of uncertainty correlations. The selected experiments cover a wide range of fast neutron energy spectra, and include critical masses, spectral indices and, when available, selected Na-void reactivity coefficients. In the notation used for spectral indices, Fij (or Cij) is the fission (or capture) rate of the isotope 23j of the element 9i (i.e., U, Np, Pu for i=2,3,4, respectively), e.g. F37 is the ^{237}Np fission rate.

Integral experiments

JEZEBEL ^{239}Pu: 1 critical mass, 3 spectral indices: F28/F25, F49/F25, F37/F25;

JEZEBEL ^{240}Pu: 1 critical mass;

FLATTOP-Pu: 1 critical mass, 2 spectral indices: F28/F25, F37/F25;

ZPR6-7 standard configuration: 1 critical mass, 3 spectral indices: F28/F25, F49/F25, C28/F25;

ZPR6-7 high ^{240}Pu content: 1 critical mass;

ZPPR9 1 critical mass, 3 spectral indices: F28/F25, F49/F25, C28/F25;

2 Na void configurations: central void and leakage-dominated configurations;

JOYO 1 critical mass.

Integral data covariance

A specific activity has been devoted to the assessment of integral covariance data (see Chapter 4).

Sensitivity coefficients

Every participant to the benchmark exercise has used its own sensitivity coefficients. An extensive comparison of these coefficients has been performed and is documented in Chapter 2.

1.4.1 Benchmark output

The main benchmark results of the comparison have been:

- adjusted nuclear data;
- final nuclear covariance data;
- initial and final integral C/E's values and associated uncertainties;
- Initial and final results of reactor project calculations including uncertainties.

The initial/final nuclear data and covariance matrices have been tested on the ABR (start-up core, as provided by ANL) configuration and on the JAEA FBR design (Phase III). The specifications of both cores are given in Appendices A and B.

1.5 Corrective factors

The strategy proposed in order to avoid a full reanalysis of all experiments by the participants to the adjustment exercise is to provide corrective factors obtained as a ratio between a very detailed (reference) calculation and a simplified one. Therefore, the participant who does not want to fully reanalyse the experiments using its own cross-sections should obtain its calculated values by carrying out the calculation for the simplified model and then multiplying the results by the corresponding corrective factor.

Hence, the ***C/E*** (**C**alculated/**E**xperimental value) is obtained as:

$$\frac{C}{E} = \frac{C^s * C^f}{E}$$

where E is the experimental value, C^s is the result coming from the simplified model calculation and C^f is the corresponding corrective factor.

The corrective factors have been calculated using ENDF/B-VII data. It has been shown [2] that there is a very weak dependence of the corrective factors from the library used.

Two simplified models are provided: Monte Carlo (continuous energy), and multi-group deterministic. The preferred one is Monte Carlo (with continuous energy files), as this model will avoid any energy collapsing effect on the results.

For the deterministic calculation, one must carefully collapse the cross-sections to the defined 33-group structure and then perform a S_4P_1 calculation.

For the one-dimensional model of the JEZEBEL and FLATTOP experiments no corrective factors are provided for Monte Carlo as the adopted models will generate the reference results. All correction factors have been reported in Appendix C.

For all correction factor calculations, homogeneous compositions were used in fundamental mode flux calculations with critical buckling search in the case of core regions and with out-of-core leakage terms (DB^2) as a source for blankets and other non-fissile regions. The calculation is performed in P1 consistent approximation with a 1968-group energy structure and flux and currents are used to collapse to the 33-energy group level.

2. Sensitivity studies and issues

2.1. Participants and methodologies

2.1.1 Participants

The following institutes, namely JAEA, INL, ANL, CEA and PSI, have provided full sets of unadjusted analytical data in the specified format. Sensitivity coefficients just for the effective multiplication factor k_{eff} have also been generated in a consistent manner by JSI and IRSN.

In addition, on the basis of ENDF/B-VII.0 data, the code APSTRACT ('09) [3], which is basically an in-house version of SUSD3D has been used in conjunction with DANTSYS [4] at KAERI, to generate sensitivity coefficients for *k*.

Based upon SCALE6.1 [5], ORNL has produced for JEZEBEL and FLATTOP, 238-group values by using TSUNAMI-1D discrete ordinates code in conjunction with ENDF/B-VII.0 data. The ORNL sensitivity coefficients were collapsed into the 33-group structure using the TSURFER code [5].

Starting from the so-called Total Monte Carlo approach, NRG has generated sensitivity coefficients for the effective multiplication factor of the seven benchmark systems based upon an innovative stochastic methodology currently under development. The first steps of this approach were to produce thousands of TALYS-based evaluated files using a stochastic sampling of nuclear parameters and benchmark all these files with simulations of integral experiments [6].

CIAE has used an in-house version of the SEN1D code in conjunction with CENDL-3.1 and JENDL-4.0 data, which is currently under development [7], to determine the sensitivity coefficients for *k* of JEZEBEL and FLATTOP.

The ORNL data is not part of this compilation as it cannot easily be compared with the other results, since the specified 33-groups are not a subset of the 238-group structure. Due to their preliminary nature, the KAERI, NRG and CIAE studies were also not included. Nevertheless, some of their key results are used for comparison with an additional solution provided by JSI on the basis of a direct Monte Carlo technique (see Section 2.2.5).

2.1.2 Main methodologies used

(1) For k_{eff}, deterministic values of the sensitivity coefficients have been obtained by Standard Perturbation-Theory (SPT) techniques (see e.g. [8], pages 17 and 31) using transport-theory.

More precisely, the various analyses were carried out on the basis of:

- SAGEP code [9], in conjunction with JENDL-4 data at JAEA;
- ERANOS code [10] in conjunction with ENDF/B-VII.0 data at INL and ANL;
- ERANOS in conjunction with JEFF-3.1.1 and JEFF-3.1 data at CEA and PSI, respectively.

In addition, in conjunction with ENDF/B-VII.0 data, the code SUSD3D [11] was used together with DANTSYS [4] at JSI.

At IRSN, stochastic values of the sensitivity coefficients based on a multi-group approach have been obtained by TSUNAMI-3D which uses an adjoint-based technique and is part of SCALE [12] in conjunction with ENDF/B-VII.0 data. The sensitivity coefficients take into account that a change of a given cross-section may also influence other cross-sections through modifications of their shielding factors. Thus, the TSUNAMI sensitivity coefficients are computed with the total instead of the partial derivatives as:

$$S_{\Sigma^i_{x,g}} = \frac{\frac{dk}{k}}{\frac{d\Sigma^i_{x,g}}{\Sigma^i_{x,g}}} = \frac{\frac{\partial k}{k}}{\frac{\partial\Sigma^i_{x,g}}{\Sigma^i_{x,g}}} + \sum_j \sum_y \sum_h \left(\left(\frac{\frac{\partial k}{k}}{\frac{\partial\Sigma^i_{y,h}}{\Sigma^i_{y,h}}} \right) \left(\frac{\frac{\partial\Sigma^j_{y,h}}{\Sigma^j_{y,h}}}{\frac{\partial\Sigma^i_{x,g}}{\Sigma^i_{x,g}}} \right) \right)$$

In the formula for these "complete" sensitivity coefficients [12], the space variable has been omitted and e.g. $\Sigma^i_{x,g}$ is the cross-section of nuclide *i* for reaction *x* in energy group *g*. The first expression on the right hand side corresponds to the standard definition ("explicit" term), with the additional summations ("implicit" effects) as an indirect term.

(2) For the reaction rates at core centre relative to ^{235}U fission (F25), i.e. F49/F25, F28/F25, F37/F25 and C28/F25, the Generalised Perturbation Theory (GPT) (see e.g. [8], pages 18 and 32) has been consistently used in the deterministic calculations for obtaining their sensitivity coefficients.

(3) The Equivalent Generalised Perturbation Theory (EGPT) in ERANOS terminology (see e.g. [8], pages 28 and 35) has been employed for determining the sensitivity coefficients of the void reactivity effects in ZPPR9 [Na void (Step 3) and Na void (Step 5)].

2.2 Results

The great number of analytical data provided has been scored for any sensitivity coefficient of a given nuclide, reaction and energy group, in terms of (a) its relative difference from the average value among the participants and (b) its relative contribution to the sum over the 33 groups of the coefficients for the same nuclide and reaction, and this in terms of individual absolute values. In order to characterise discrepant data possibly having an impact on the resulting uncertainties, a choice was made according to the result of this score, namely only those sensitivity coefficients exceeding the arbitrary value of 30% for (a), 20% for (b) and with their associated energy profiles having at least one absolute value exceeding 0.001, were considered. The corresponding main findings are summarised below, the sensitivity coefficients of the fission spectrum, delayed data and average cosine of the scattering angle have not been addressed so far due to the scarce availability of analytical data.

2.2.1 Effective multiplication factor

JAEA, INL, ANL, CEA, PSI and JSI have provided deterministic solutions based upon the SPT methodology for the benchmark systems JEZEBEL, (^{239}Pu and ^{240}Pu configurations), FLATTOP (^{239}Pu configuration), ZPR6-7 (standard configuration and high ^{240}Pu content), ZPPR9 and, except JSI, also for JOYO, whereas IRSN has used for all these configurations a stochastic methodology to correspondingly derive "complete" sensitivity coefficients (see Section 2.1.2).

The analytical data are conveniently grouped as follows:

First, the sensitivity coefficients of the actinides referring to the two JEZEBEL bare spheres and to the systems containing sodium i.e. the two ZPR6-7 cores, ZPPR9, and JOYO are considered. The scattering reactions are systematically excluded in this group of analytical data.

Overall consistence is achieved between the participants, as seen in Figure 1. Larger differences in relative terms such as e.g. for ^{239}Pu (n, disappearance) appearing in the case of JEZEBEL (^{239}Pu configuration) are limited to small values of the sensitivity coefficients and are thus unlikely important for the resulting uncertainties.

The sensitivity coefficients, in these cases, are almost independent of the code (deterministic SAGEP, ERANOS and DANTSYS/SUSD3D, stochastic TSUNAMI-3D) and basic nuclear data (JENDL-4, ENDF/B-VII.0 or JEFF-3.1) being used. In particular, as a consequence of the agreement of TSUNAMI-3D with the other codes, it can be concluded that the indirect term should be small, confirming that resonance shielding effects are largely insignificant in these cases.

The second group of analytical data refers to the scattering reactions of the bare spheres and to those sensitivity coefficients of the systems, which contain sodium and which have been so far left out of the first group, namely the sensitivity coefficients for the structural materials, sodium, oxygen, and those for the scattering reactions of the actinides (Figure 2).

Except for the IRSN solution (in magenta), which in several cases differs from the bulk of the other solutions, consistence is also shown. As a consequence, the "implicit" effects of the sensitivity coefficients only considered in the IRSN solution might be larger in these cases. Therefore, despite the fact that these effects characterising the impact of modified resonance shielding on the multi-group cross-sections are normally small in fast reactor applications, they have been specifically studied in greater detail on the basis of the representative sensitivity coefficient of k_{eff} to the elastic scattering cross-section of ^{238}U in the case of ZPR6-7 [standard configuration], (see Figure 2, second picture on the right from the top).

The result of omitting the contribution of the "implicit" effects mainly resulting from ^{23}Na elastic scattering and ^{56}Fe resonances can be deduced from Figure 3, obviously by comparing the black with the red curve obtained at IRSN by means of SCALE6.1/TSUNAMI-3D: The sensitivity coefficient would, in fact, be strongly underestimated for energies around 1 keV. Qualitatively, in the case of an increase in the ^{238}U elastic scattering cross-section, the potential scattering background cross-section for any nuclide other than ^{238}U would also increase, as a consequence, the self-shielding effect for this nuclide would decrease; in the energy region of ^{23}Na and ^{56}Fe resonances, these two elastic cross-sections would, in principle, be less shielded which results in less leakage implying an increased effective multiplication factor, which, in fact, produces a positive "implicit" effect.

PSI has additionally used a direct deterministic methodology taking advantage of the standard JEFF-3.1-based ERANOS library in 33 neutron groups, to determine independently "complete" sensitivity coefficients in the sense of [13]. As shown in Figure 4, there is global agreement with the IRSN data, confirming that "implicit" effects are particularly large around the main sodium elastic scattering resonance.

For completeness, total "complete" sensitivity coefficients, i.e. summed up over the groups, having larger fractions of the "implicit" effects are shown in Figure 5. As expected, these concern elastic scattering only, and when compared to ^{238}U, are all small in magnitude.

Figure 1: Actinides sensitivity profiles of the effective multiplication factor not including scattering reactions for the bare spheres and systems containing sodium

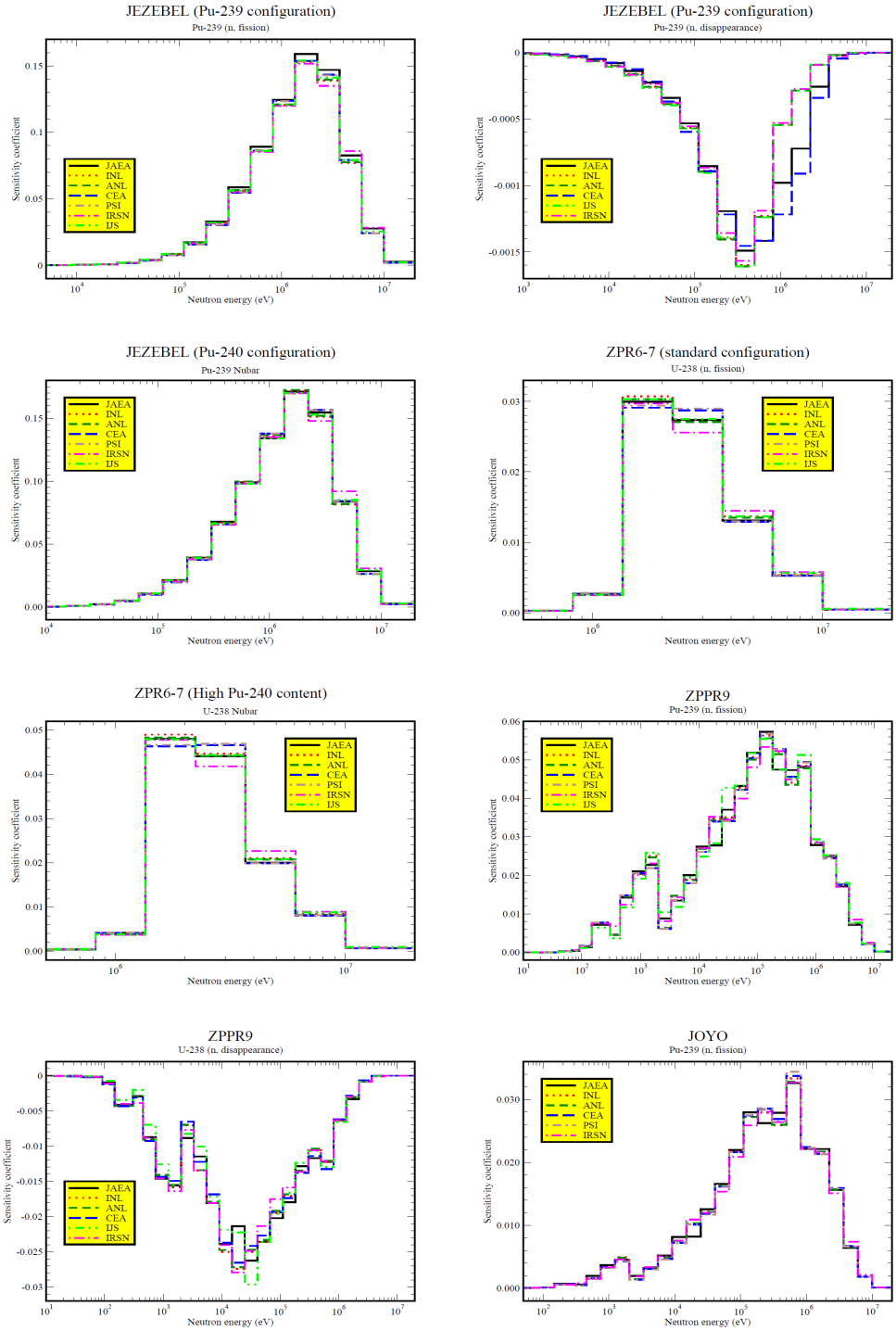

Figure 2: Sensitivity profiles of the effective multiplication factor for structural materials, oxygen, sodium and scattering reactions of actinides

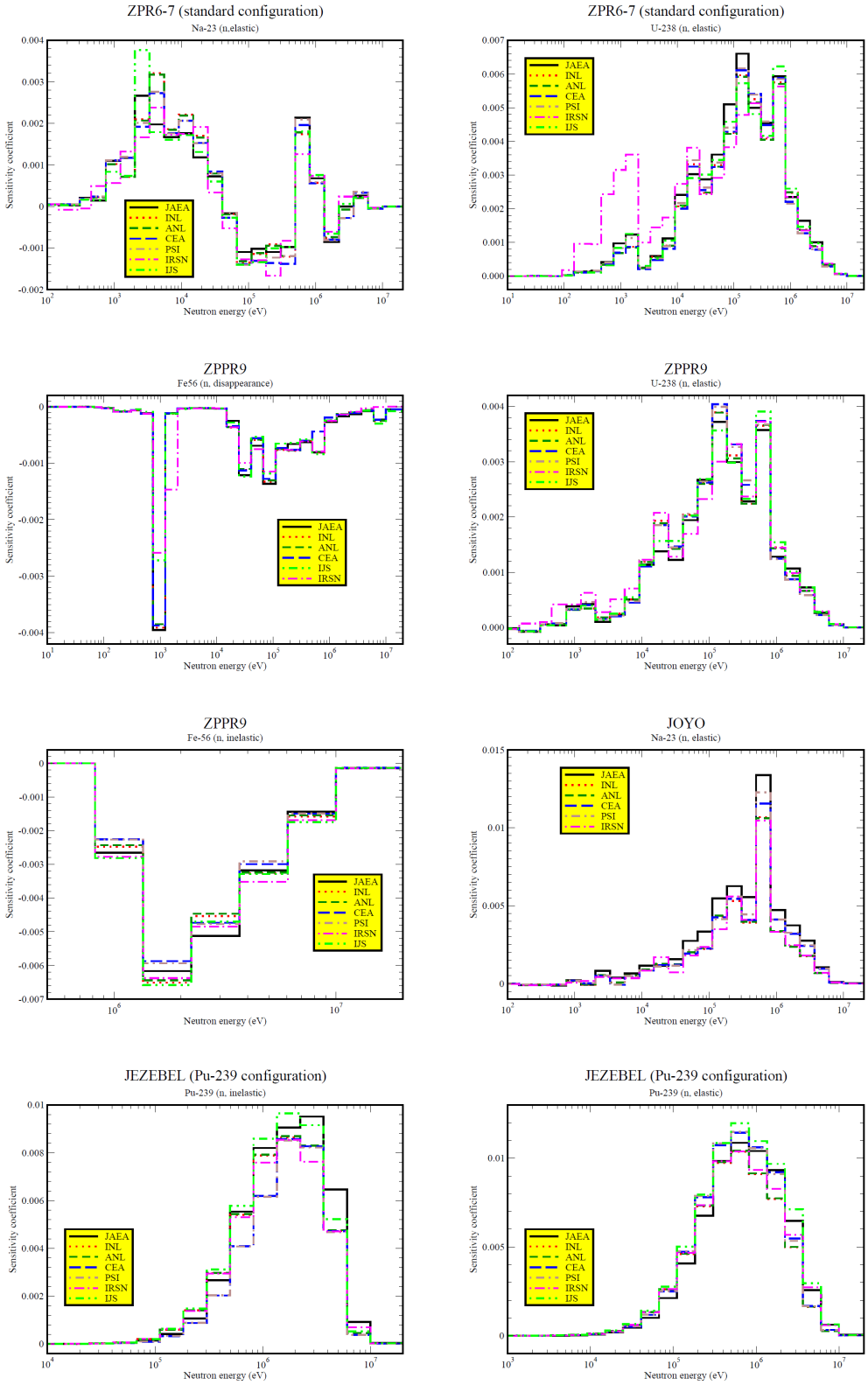

Figure 3: ZPR6-7 (standard configuration): "complete" (red) and "explicit" (black) sensitivity profiles in 238 neutron groups (SCALE structure) for ^{238}U elastic scattering

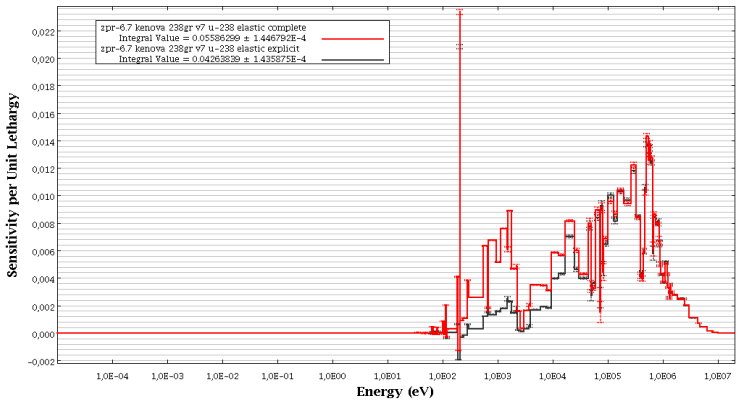

Figure 4: IRSN and PSI solutions

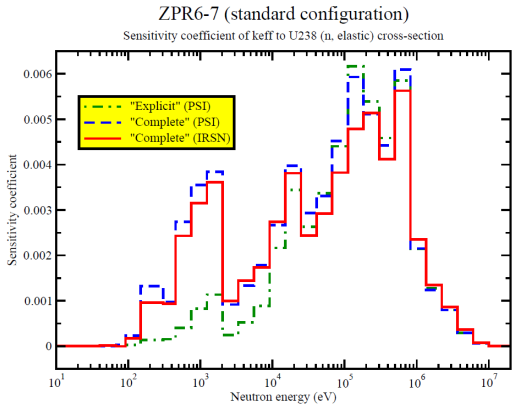

Figure 5: ZPR6-7 (standard configuration): Total sensitivity coefficients with larger fractions of "implicit" effects (IRSN)

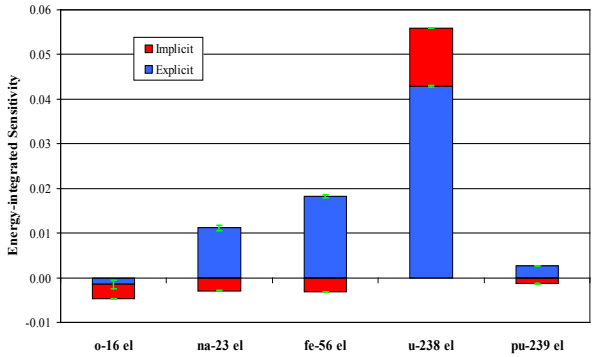

The sensitivity coefficients referring to the FLATTOP core form the third and last group of data. Some of the energy profiles are namely characterised by larger discrepancies, as representatively shown in Figures 6 and 7, respectively for the core and reflector region.

Figure 6: FLATTOP (^{239}Pu configuration): Sensitivity profiles of the effective multiplication factor for Pu isotopes

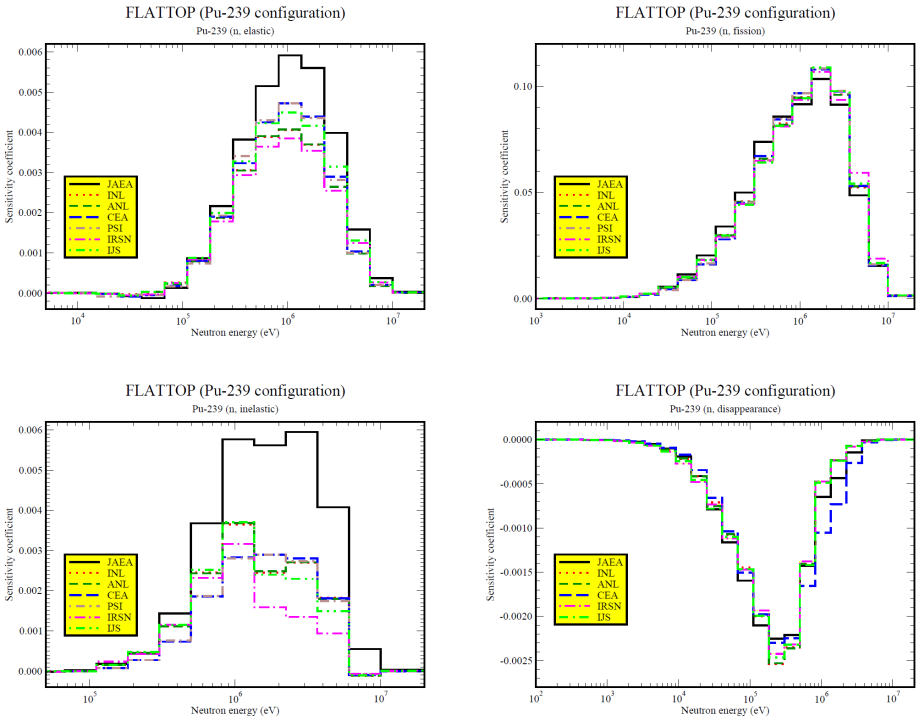

In several cases, the JAEA and IRSN profiles (respectively in black and magenta in these figures) are the two limiting curves.

The ERANOS solutions using the same ENDF/B-VII.0 data (INL and ANL, respectively in red and dark green), as expected, are in good agreement; they also rather agree with the corresponding JSI solution (in light green), and with the corresponding ERANOS solutions based upon JEFF-3 (CEA and PSI), which, in turn, are quite consistent among them (compare the curves in blue with those in brown).

The more significantly deviating JAEA solution could largely be attributed to the use of a 2D (r,z) model with diffusion theory as required in the current version of SAGEP, instead of spherical geometry in conjunction with transport theory used by the other participants. This is causing much larger modelling effect for FLATTOP than for the other systems under investigation (see Appendix D on "In-depth comparison of JAEA and PSI sensitivity coefficients").

Figure 7: FLATTOP (^{239}Pu configuration): Sensitivity profiles of the effective multiplication factor for uranium

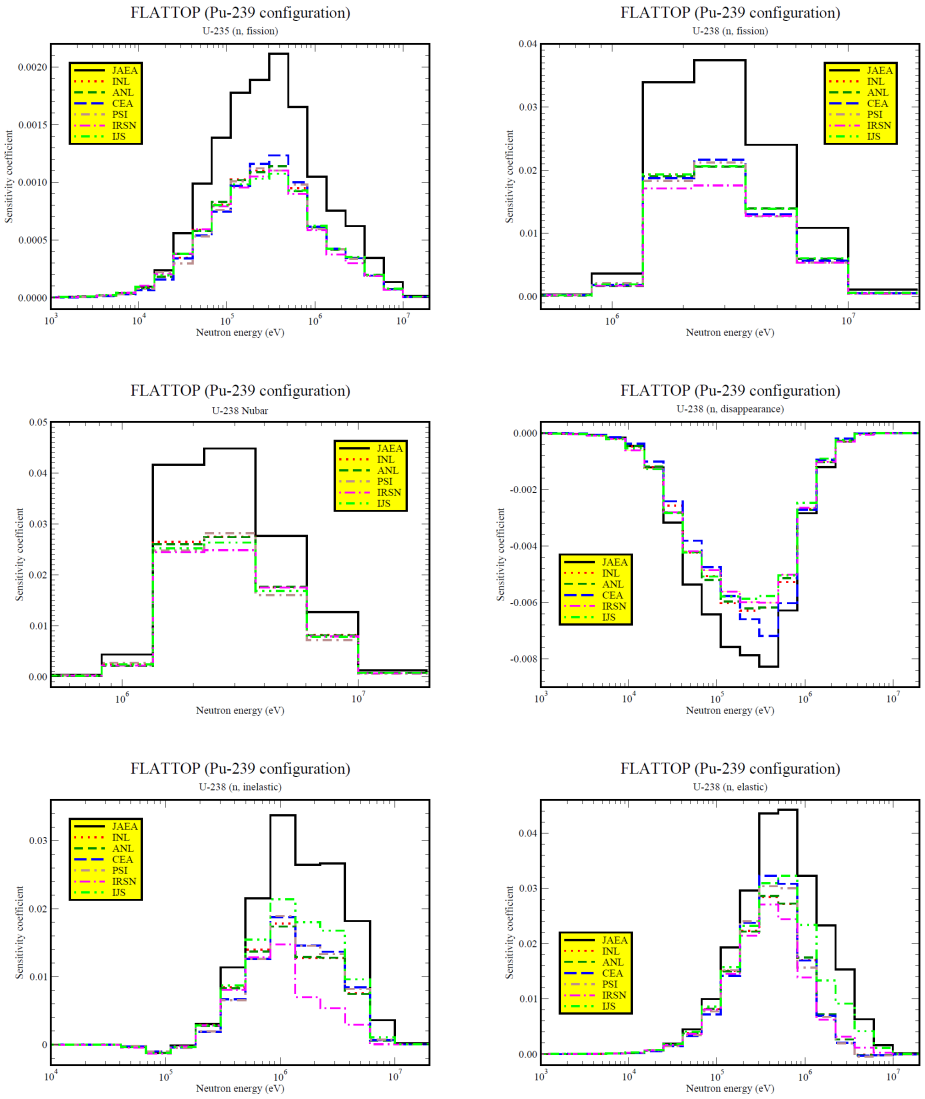

2.2.2 F49/F25

Among the participants (JAEA, INL, ANL, CEA, and PSI) providing deterministic solutions for JEZEBEL, ZPR6-7 (standard configuration) and ZPPR9 based upon the GPT methodology, consistence of the sensitivity coefficients including those for the structural materials, oxygen and sodium in the case of ZPR6-7 and ZPPR9, is shown in Figure 8. Due to the above model difference, the JAEA solution (black curves) might be slightly different from the bulk of the other curves.

Figure 8: Sensitivity profiles of F49/F25

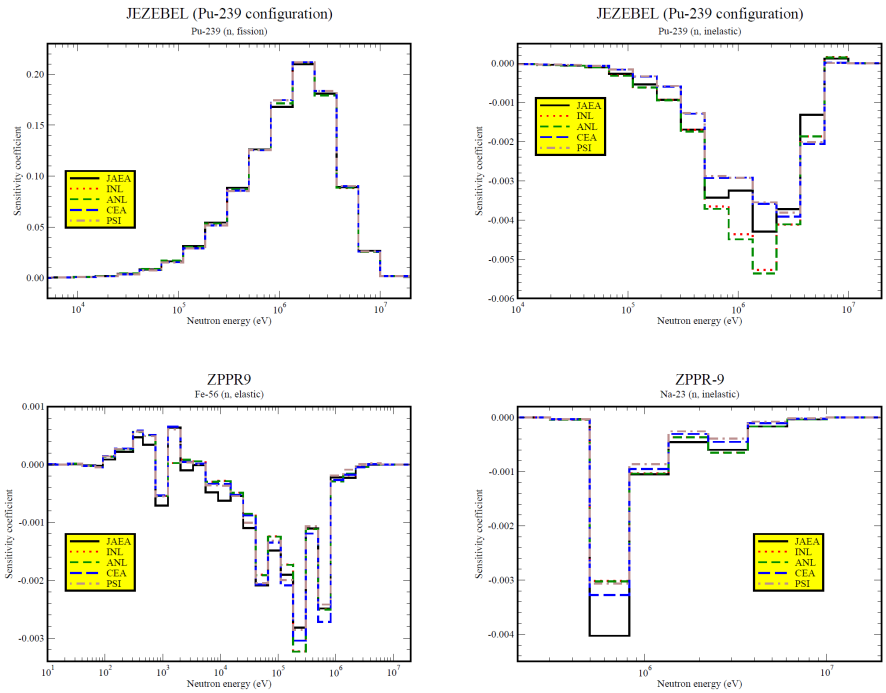

2.2.3 F28/F25, F37/F25 and C28/F25

Similar trends can be observed in relation to F49/F25, i.e. close agreement in most cases, once again with larger deviations of the JAEA solution in the case of FLATTOP (see Figures 9-11).

Figure 9: Sensitivity profiles of F28/F25

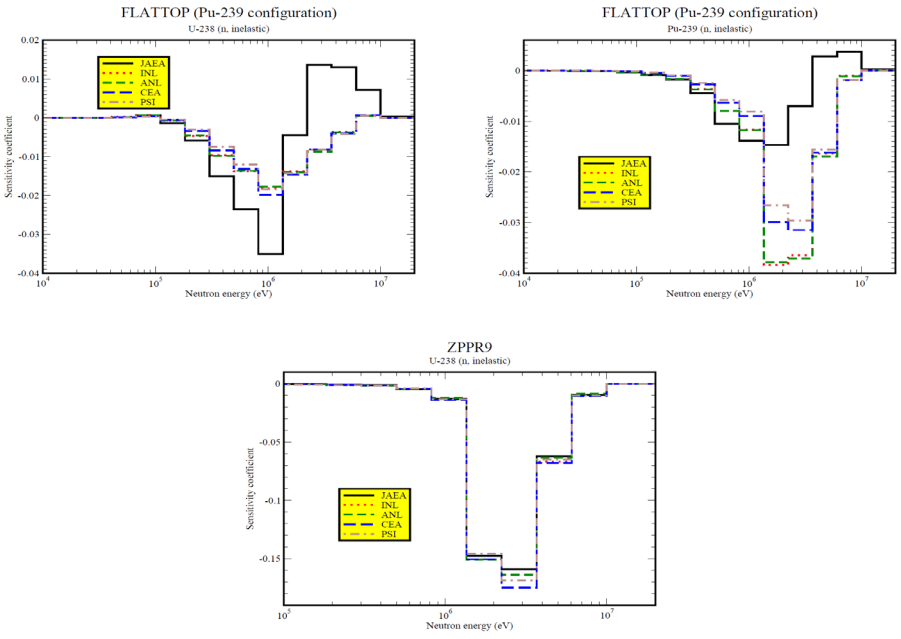

Figure 10: Sensitivity profiles of F37/F25

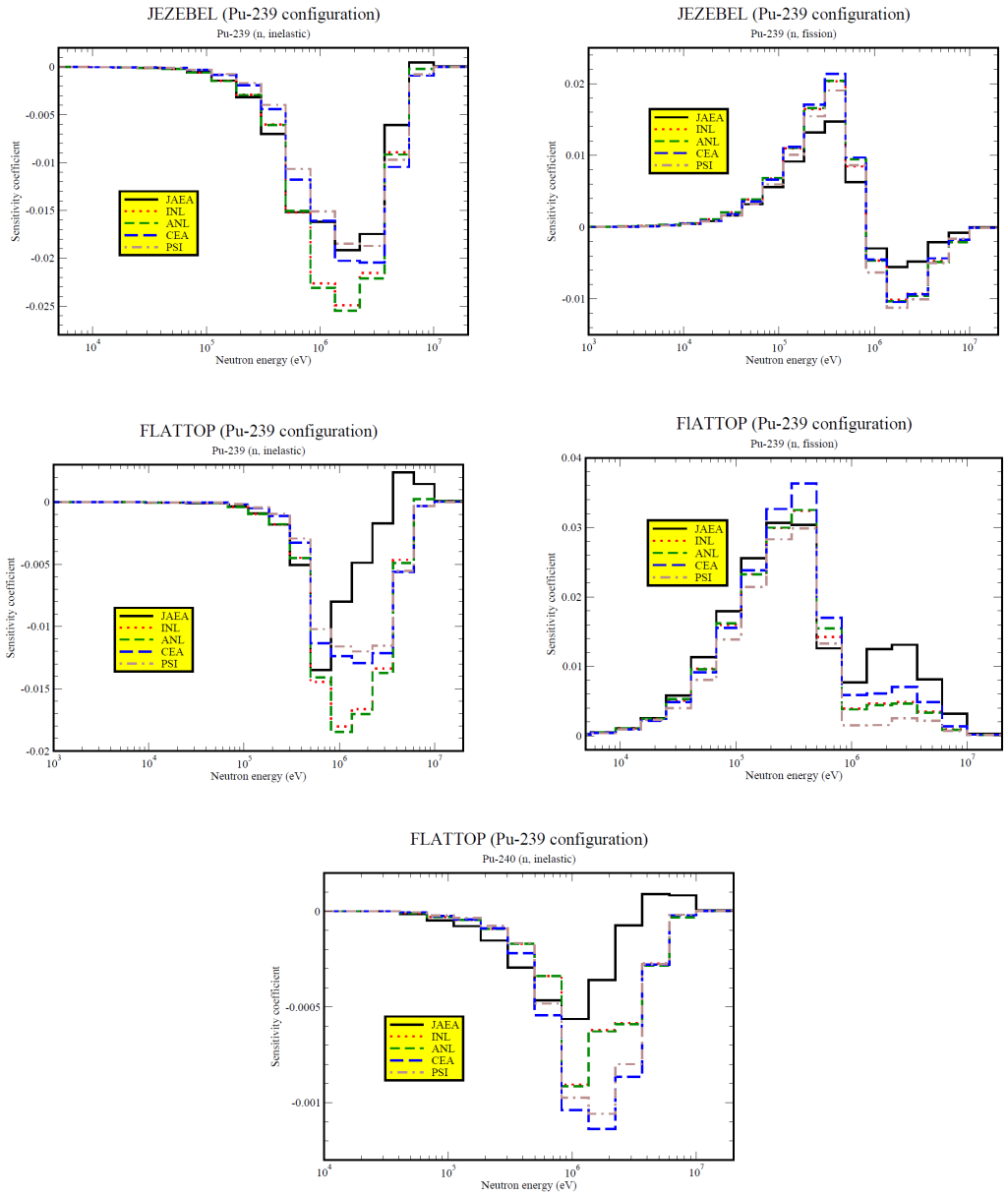

Figure 11: Sensitivity profiles of C28/F25

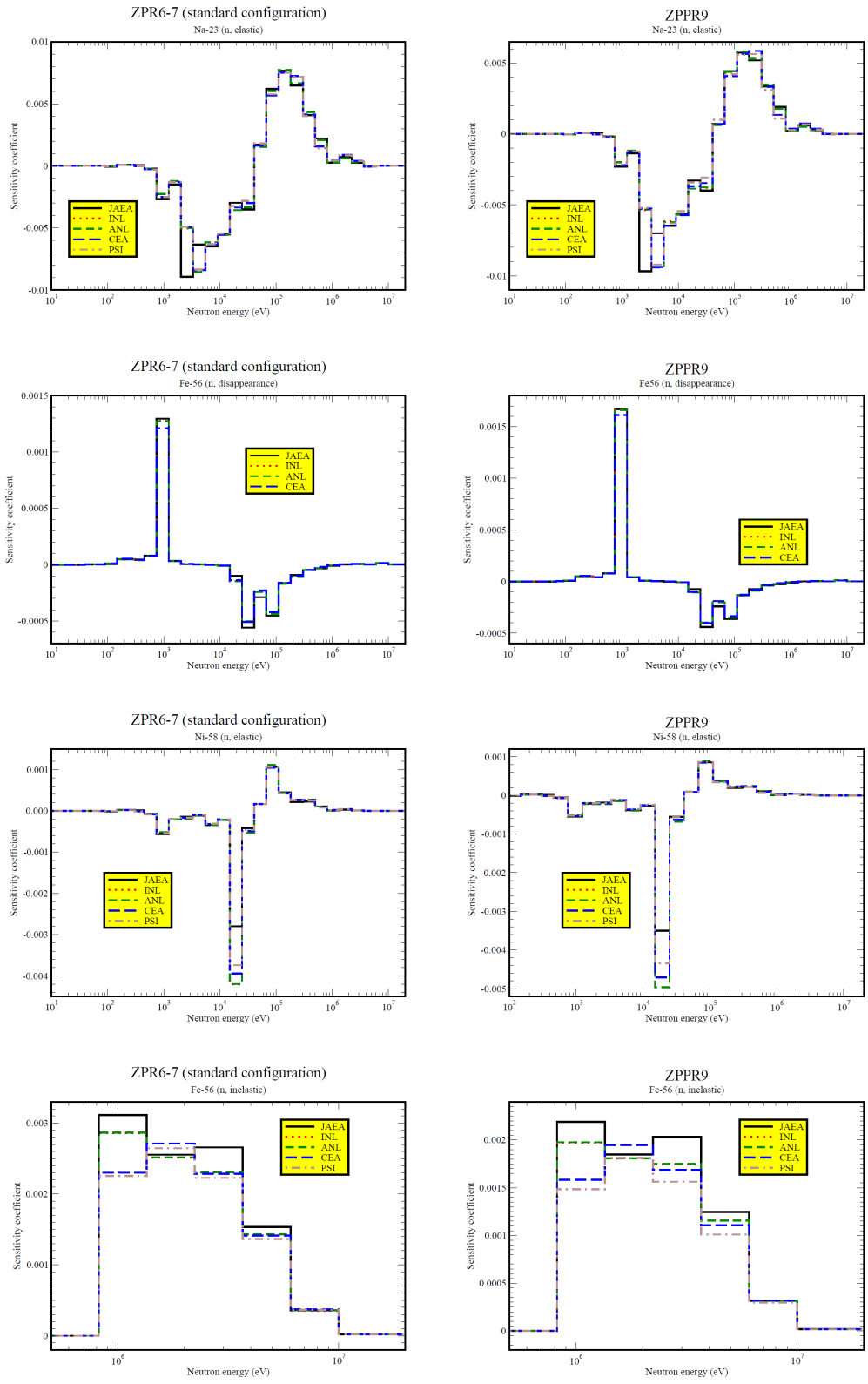

2.2.4 *Na void (Step 3) and Na void (Step 5)*

In general, consistence is shown among the participants (JAEA, INL, ANL, CEA, and PSI) providing for ZPPR9 deterministic solutions based upon the EGPT methodology (see Figure 12).

Figure 12: Sensitivity profiles for the void effect

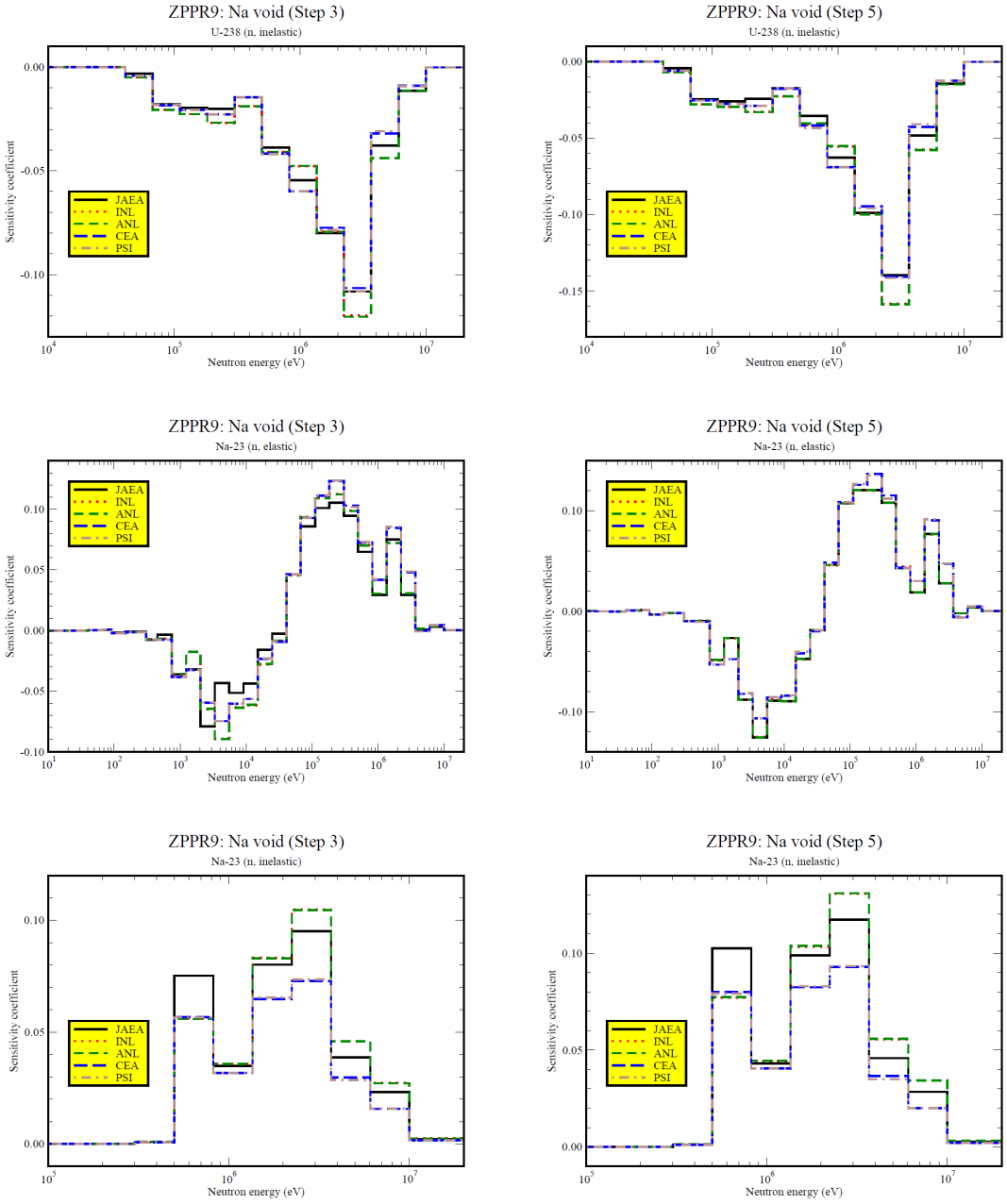

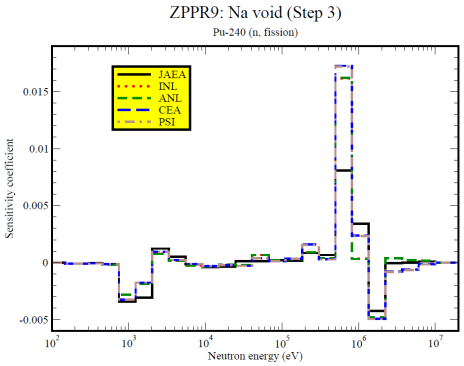
ZPPR9: Na void (Step 3)
Pu-240 (n, fission)
JAEA
INL
ANL
CEA
PSI
Sensitivity coefficient
Neutron energy (eV)

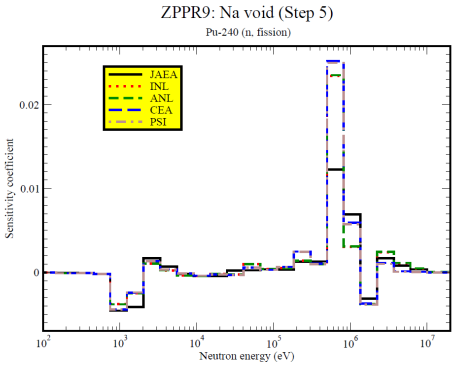
ZPPR9: Na void (Step 5)
Pu-240 (n, fission)
JAEA
INL
ANL
CEA
PSI
Sensitivity coefficient
Neutron energy (eV)

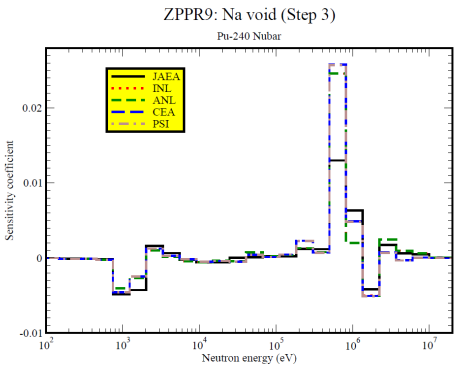
ZPPR9: Na void (Step 3)
Pu-240 Nubar
JAEA
INL
ANL
CEA
PSI
Sensitivity coefficient
Neutron energy (eV)

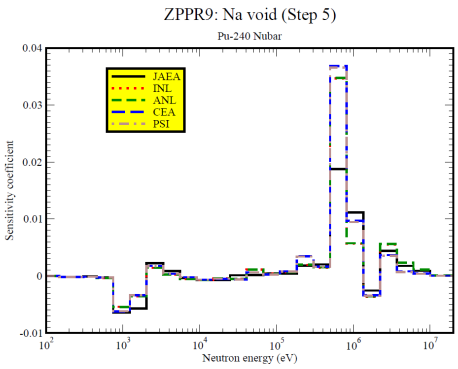
ZPPR9: Na void (Step 5)
Pu-240 Nubar
JAEA
INL
ANL
CEA
PSI
Sensitivity coefficient
Neutron energy (eV)

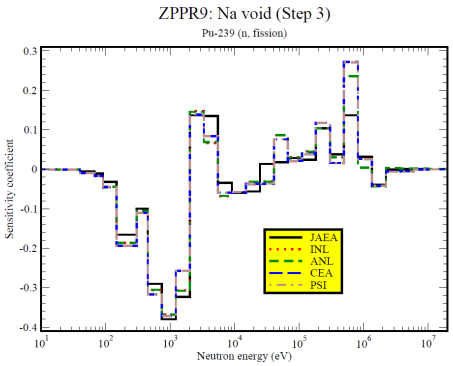
ZPPR9: Na void (Step 3)
Pu-239 (n, fission)
JAEA
INL
ANL
CEA
PSI
Sensitivity coefficient
Neutron energy (eV)

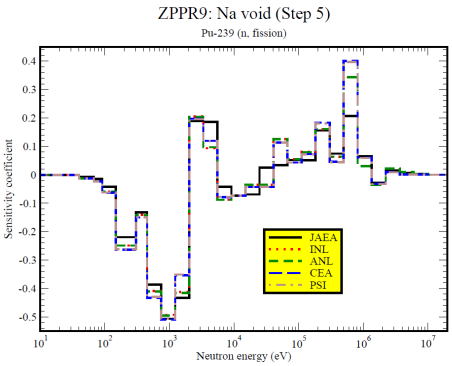
ZPPR9: Na void (Step 5)
Pu-239 (n, fission)
JAEA
INL
ANL
CEA
PSI
Sensitivity coefficient
Neutron energy (eV)

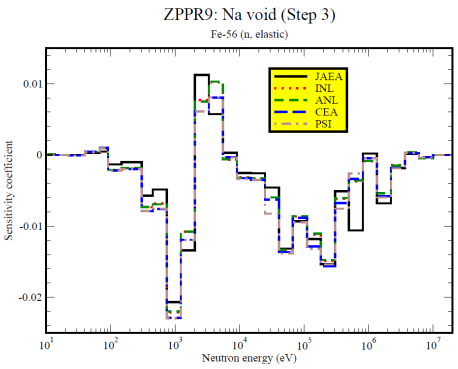
ZPPR9: Na void (Step 3)
Fe-56 (n, elastic)
JAEA
INL
ANL
CEA
PSI
Sensitivity coefficient
Neutron energy (eV)

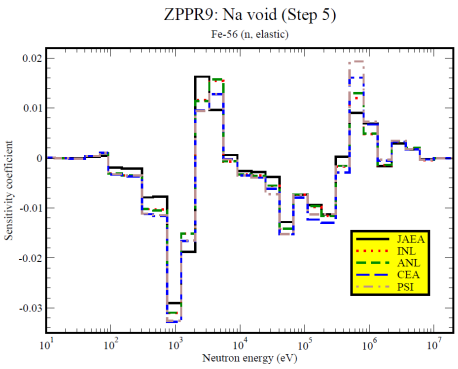
ZPPR9: Na void (Step 5)
Fe-56 (n, elastic)
JAEA
INL
ANL
CEA
PSI
Sensitivity coefficient
Neutron energy (eV)

Some important differences for ^{239}Pu and sodium inelastic scattering having large sensitivity coefficients can be observed. For fission reactions in general, the main discrepancies are observed near 1 MeV, i.e. in group 7 of the 33-group structure, while for sodium inelastic scattering there is e.g. a 30% systematic difference in the fourth group ranging from 2.25 to 3.68 MeV between the ERANOS solutions based on the use of different data.

2.2.5 Additional results

JSI has additionally used a direct stochastic technique in conjunction with dedicated continuous energy ENDF/B-VII.1 libraries [14] to analyse the benchmark system with larger deviations, i.e. FLATTOP (^{239}Pu configuration), see Section 2.2.1.

As a representative example, the sensitivity coefficients of k_{eff} to the ^{238}U elastic scattering cross-section were compared in great detail. Namely, additional JSI deterministic results obtained by a refined P_3 approximation for both the elastic and inelastic scattering cross-sections, SG-33-P3_IJS curve in Figure 13 (a), the aforementioned Monte Carlo-based continuous energy sensitivity coefficient profile determined for a statistical uncertainty of $8{\cdot}10^{-5}$ of the multiplication factor ("FLATTOP-Pu (MC)") and the data taken independently from the International Criticality Safety Benchmark Evaluation Project Handbook (ICSBEP/2), shown in Figure 13 (b), are of particular interest.

As opposed to the previous figures using histogram representations, the Figure 13 curves are eye-guides joining the group average values at the mid-points of the groups for better clarity and distinction between the different cases, and the sensitivity coefficients were divided by the lethargy width, which is 0.5 for most groups.

Figure 13: Sensitivity coefficients of k_{eff} to the ^{238}U elastic scattering cross-section

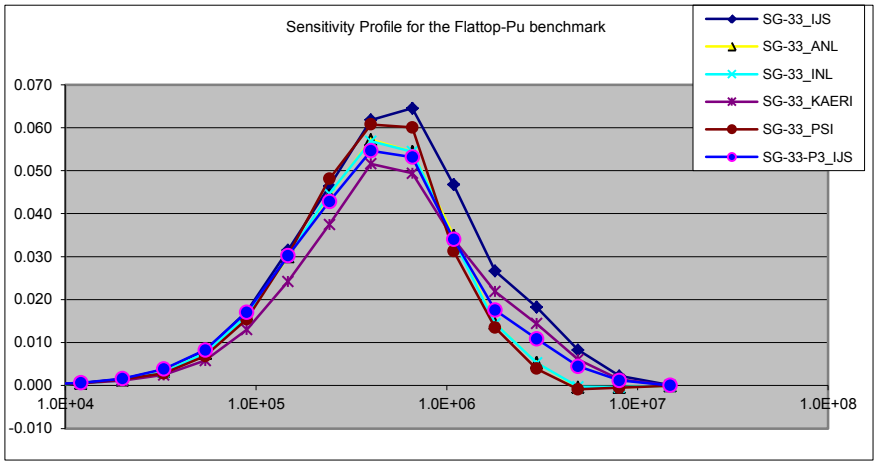

(a)

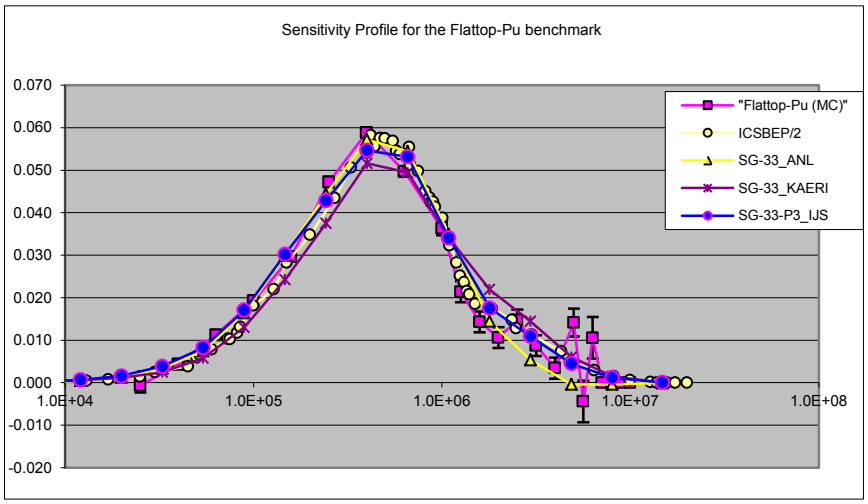

(b)

The main findings are the following:

(a) The reference JSI deterministic values are the largest, especially above 0.3 MeV coinciding with groups 1-8, and peak at a higher energy. Using the P_3 approximation largely removes this difference and leads to agreement for energies up to about 1 MeV with the bulk of the other solutions.

(b) The continuous energy Monte Carlo solution also agrees by bearing in mind that "small" sensitivity coefficients such as for energies below 60 keV and above 5 MeV, are clearly difficult to calculate.

(c) The ORNL values are found to be consistent with ICSBEP/2, which, in turn, appear consistent with the INL and ANL solutions for energies up to about 1.5 MeV, whereas the PSI values are higher near the peak around 0.5 MeV and the KAERI values are systematically lower for energies below 0.6 MeV.

2.3 Conclusions and recommendations

Sensitivity coefficients of the effective multiplication factor have been obtained by JAEA, INL, ANL, CEA, PSI and JSI for the benchmark systems JEZEBEL (^{239}Pu and ^{240}Pu configurations), FLATTOP (^{239}Pu configuration), ZPR6-7 (standard configuration and high ^{240}Pu content), ZPPR9 and, except JSI, for JOYO. Independent deterministic solutions have been provided based upon the standard perturbation theory methodology [8]. In addition, IRSN has used for all these configurations an adjoint-based stochastic methodology to correspondingly derive "complete" sensitivity coefficients (see Section 2.1.2).

Overall consistence of the results has been shown among the participants. The major differences affect FLATTOP, a Pu core surrounded by a U reflector, which is more sensitive to modelling options. The use of "complete" sensitivity coefficients such as in the IRSN study is recommended for analysing the systems which contain sodium, i.e. ZPR6-7, ZPPR9 and JOYO, which are more sensitive to mutual resonance shielding effects (see Section 2.2.1).

Sensitivity coefficients of measured reaction rates at the core centre relative to ^{235}U fission, i.e. F49/F25, F28/F25, F37/F25, and C28/F25 with F49 standing for ^{239}Pu fission, F28 for ^{238}U fission, F37 for ^{237}Np fission and C28 for ^{238}U capture, have been derived by JAEA, INL, ANL, CEA and PSI on the basis of the Generalised Perturbation Theory [8]. In most cases, consistence of the results among the participants has been shown with again larger deviations for FLATTOP (see Sections 2.2.2-2.2.3).

Finally, the Equivalent Generalised Perturbation Theory (EGPT) [8] has been used for determining the sensitivity coefficients of void reactivity effects measured in ZPPR9, i.e. Na void (Step 3) and Na void (Step 5), which show consistence except for more important deviations in the case of ^{239}Pu fission and sodium inelastic scattering (Section 2.2.4, Figure 12).

As a result of this study, it can be concluded that the calculation of sensitivity coefficients is now part of the standard calculation routes in many modern code systems. Moreover, the agreement among results obtained by different methods is remarkable. However, a number of recommendations can be formulated on the basis of the comparisons described above, namely:

- Sensitivity coefficients calculated e.g. for the multiplication factor and reaction rate ratios with different deterministic methods and codes do agree well among them, but one should be careful in specifying definitions and model approximations, such as e.g. the exact detector position and volume in the case of the Generalised Perturbation Theory (GPT) for sensitivity coefficients of reaction rate ratios.
- "Small" sensitivity coefficient values are to be used carefully, since in these cases errors can arise from numerical problems such as those associated to the local convergence of the importance function.
- Resonance shielding effects, which appear insignificant for the present exercise, should be considered with appropriate algorithms.
- Anisotropy of scattering should be accounted for at high energies when calculating sensitivity coefficients to elastic and also inelastic scattering cross-sections.
- EGPT provides a powerful tool to calculate sensitivity coefficients for reactivity effects.
- Adjoint-based and direct Monte Carlo techniques provide an interesting alternative to deterministic methods in particular for complex geometries. However, both methodologies are computationally very intensive. In addition, especially when using the direct method, the calculations should be carried out with a sufficient precision. The sensitivity coefficients are namely computed by means of differences between two independent calculations, and sufficiently large perturbations of the cross-sections must be introduced to obtain statistically significant differences of the results and simultaneously avoid non-linearity.

3. Covariance data for cross-sections: Different sets used and main characteristics

3.1 Introduction

Nuclear data covariances represent one of the important parameters in the cross-section adjustment procedure. Generally, the covariance matrix[1] of a scattered data set, x_i (i=1,…,*n*), with the average value $m_{0i} = \langle x_i \rangle$, is defined as follows [15]:

Variance: $\mu_{ii} = \mathrm{var}(x_i) = \langle (x_i - m_{0i})^2 \rangle \quad for \;\; i = 1, n$

Standard deviation (STD): $\sigma_i = std(x_i) = \sqrt{\mathrm{var}(x_i)}$

Covariance: $\mu_{ij} = \mathrm{cov}(x_i, x_j) = \langle (x_i - m_{0i})(x_j - m_{0j}) \rangle \quad for \;\; i, j = 1, n \;\; with \;\; i \neq j$

Correlation factor (C.F.): $\rho_{ij} = \dfrac{\mu_{ij}}{\sqrt{\mu_{ii}\mu_{jj}}} = \dfrac{\mathrm{cov}(x_i, x_j)}{std(x_i) \times std(x_j)} \qquad where, \; -1 \leq \rho_{ij} \leq 1$

The covariance matrix must be symmetric and positive-definite. In this chapter, first, the current methodologies to evaluate the nuclear data covariances are briefly reviewed. Next, some of the actual covariance data are illustrated. Comparisons are made between JENDL-4.0 (J-4.0 hereafter [16] [17]) and COMMARA-2.0 (C-2.0 hereafter [18]) which is to be used together with the ENDF/B-VII.0 central values [19]. Finally, the effects of different covariance data on the adjusted results are examined and concluded.

3.2 Methodology of covariance evaluation

The covariance data of a library should be evaluated in accordance with the methodology adopted in the library to obtain the central values of the nuclear data. In other words, two covariance data of a cross-section in two libraries could be different even if the central value of the cross-section is accidentally identical, when the evaluation methodologies or the experimental data used differ from each other. Here, typical methodologies to evaluate the covariance data are briefly summarised, according to the recently published covariance data, J-4.0, C-2.0, or ENDF/B-VII.1 [20-22].

1) Generalised Least-Square Method

If plenty of measured data are available to evaluate cross-sections in an energy range, the generalised least-square method with the GMA code (ANL [23]) or the ZOTT code (IAEA [24]) could be used to obtain the best-estimated cross-section values and their covariance data at once. The very critical issue to use the experimental values for the cross-section evaluation is that the systematic and statistical uncertainties[2] of the

[1] Covariance matrix is sometimes called as “variance-covariance matrix”.
[2] The “systematic” and “statistical” means the fully-correlated and uncorrelated, respectively.

measurements must be distinguished and known quantitatively, however, the knowledge of measurement uncertainty would generally be difficult to exactly obtain, according to D.L. Smith [21]. For example, in the evaluation of the JENDL-4.0 covariance for the fission cross-section of the major actinides in the high-energy range, the variances obtained with the simultaneous least-square fitting method using the SOK code (JAEA [25]) were multiplied by a factor of 2 in order to take into account the hidden correlations among measurements [17].

2) Resonance region

To evaluate the covariance of the resolved resonance region for the major actinides such as ^{235}U, ^{238}U, and ^{239}Pu, the results of the full-scale R-matrix solution codes using the SAMMY code [26] are available. The covariance of the resonance parameters is usually too huge to accommodate in a library. Therefore, the resonance parameter uncertainties and correlations are propagated to the cross-section covariance, i.e. File 33 in the ENDF format. As mentioned in the generalised least-square fitting case, the uncertainties of the computed cross-sections from SAMMY were found to be unrealistically underestimated, although the uncertainties of resonance energies and widths seemed realistic. Therefore, in the evaluation of ENDF/B-VII.1 covariance data, systematic uncertainties of background, normalisation, scattering radius and other long-range correlations have been included in the analysis bringing computed cross-section uncertainties to a more plausible level [22]. For the resonance region covariance of minor actinides, the structural isotopes or fission products, more simplified methods such as the kernel approximation (BNL [27]), or the integral method (LANL [28]) are applied, where some *a priori* uncertainty estimations of the resonance parameters such as those by Mughabghab [29] are propagated to the cross-section uncertainty.

3) Kalman-filter method

The basic idea of this method is to optimise the nuclear model parameters by the inclusion of the cross-section measurement information with the Bayesian parameter estimation. In several libraries, the Bayesian code KALMAN (Kyushu University & JAEA [30]) is used with the theoretical nuclear model codes such as GNASH (LANL [31]), EMPIRE (BNL [32]), TALYS (NRG [33]) or CCONE (JAEA [34]). The CONRAD code (CEA [35]) also has the capability to evaluate the cross-section covariance by combining the Bayesian technique with the nuclear theoretical model parameters. The biggest advantage of the KALMAN technique is that even the uncertainty of the cross-section in the energy or reaction for which no experimental data are available can be estimated by extrapolating the obtained uncertainties of nuclear model parameters through the theoretical model. On the other hand, the KALMAN technique has some disadvantages such as the assumption of linearity through the model parameter sensitivities, or the difficulty to take into account the deficiency of the adopted nuclear models themselves [36] [37]. Since the KALMAN method utilises the experimental information, it is also unavoidable to suffer from unrecognised correlation problems.

4) Monte Carlo-based method

Increases in computing power have made it feasible to evaluate nuclear data and their associated covariances using Monte Carlo (MC) methodology (NRG [38] [39]). One of the advantages of the MC-based method is that it does not need the sensitivity of nuclear model parameters, which frees it from the assumption of linearity. However, the MC method requires a fairly large amount of computing time to obtain sufficiently small statistical uncertainties, as well as the need of the prior model parameter uncertainty, shape and correlation for random sampling. These methods face the difficulty to take into account deficiencies in the nuclear reaction models, and the quality and quantity of the cross-section measurements.

3.3 Covariance data used in the SG33 Adjustment Exercise

Table 2 summarises the features of various covariance data treated in the Subgroup 33 exercise. In total, 5 covariance libraries were used.

Table 2: Characteristics of covariance data used in the SG33 Adjustment Exercise

Covariance library	Evaluated isotopes	Covariance data included	Methodology applied to evaluate covariance data	Other features
COMMARA-2.0 (BNL-LANL)	12 light nuclei (coolants and moderators), 78 structural materials and fission products, and 20 actinides.	Reaction cross-sections + nu-bars for 20 actinides +3 PFNS for ^{238}Pu, ^{239}Pu and ^{240}Pu + 2 mu-bars for ^{23}Na and ^{56}Fe.	Generalised Least-Square Method. Resonance R-matrix analysis. Kalman-filter method.	33-energy group structure. To be used together with the ENDF/B-VII.0 central values. Released in October 2010 [18].
JENDL-4.0 (JAEA)	95 nuclides, including ^{10}B, ^{11}B ^{14}N, ^{15}N, ^{16}O, ^{23}Na, ^{48}Ti, ^{52}Cr, ^{53}Cr, ^{55}Mn, ^{56}Fe, ^{59}Co, ^{58}Ni, ^{60}Ni, ^{90}Zr, ^{209}Bi, and all actinides.	Reaction cross-sections + mu-bars for 16 light nuclei and structural materials. Reaction cross-sections. + nu-bars + PFNS+ mu-bars for 79 actinides.	Generalised Least-Square Method. Resonance R-matrix analysis. Kalman-filter method.	ENDF standard format. File 33 is given for resonance energy region. Released in May 2010 [16] [17].
COMAC (CEA) +JENDL/ENDF for some isotopes	24 light and intermediate nuclei, 15 actinides.	Reaction cross-sections+ nu-bars (taken from JENDL-4) +PFNS (taken from JENDL-4).	Generalised Least-Square Method. Resonance R-matrix and Optical Model analysis Marginalisation of systematic experimental uncertainties.	33-energy group structure.
TENDL (NRG)	^{235}U, ^{238}U, ^{239}Pu.	No covariance files but random ENDF files.	Monte Carlo-based method: TMC + selection based on distance minimisation.	Pointwise cross-sections.
SCALE 6.1 (ORNL)	2 isotopes in structural materials and 8 actinides (^{234}U, ^{235}U, ^{238}U, ^{237}Np, ^{239}Pu, ^{240}Pu, ^{241}Pu, ^{242}Pu).	Reaction cross-sections + nu-bars + PFNS.	Generalised Least-Square Method. Delta Chi-Square filter method.	Initially a 44-energy group structure, collapsed to a 33-group structure. Released in June 2011 [40].

3.4 Comparison of JENDL-4.0 and COMMARA-2.0 covariance

Here, the covariance data of J-4.0 and C-2.0 are examined and compared. As for the 11 isotopes treated in the SG33 exercise, that is, ^{10}B, ^{16}O, ^{23}Na, ^{56}Fe, ^{52}Cr, ^{58}Ni, ^{235}U, ^{238}U, ^{239}Pu, ^{240}Pu, and ^{241}Pu, their covariance data are found to be rather similar between the two libraries, probably due to the use of similar evaluation methodology such as the full or simplified R-matrix analysis, the Bayesian estimation connected with some theoretical nuclear model codes, or the simultaneous evaluation for fission data of major actinides, etc. Furthermore, experimental cross-section data from the international library EXFOR [41] are commonly used to fit nuclear reaction model parameters.

However, there are some isotope-reaction-energy regions where the covariance data of the two libraries are notably different. Three examples are shown below:

1) ^{235}U capture data in 3~300 keV energy region

As seen in Figure 14, the standard deviation (STD) of C-2.0 is exactly ±20%, while that of J-4.0 is very small around ±2~4%. Further, the correlations of C-2.0 are almost perfect positive, but those of J-4.0 are partially. The difference of the capture cross-section centre values between ENDF/B-VII.0 and J-4.0 is around -10~+5% in this energy range. From the references [16] [18], C-2.0 applied the Bayesian code KALMAN with the GNASH code for the covariance evaluation, on the other hand, JENDL-4.0 used the generalised least-square code GMA. It seems unlikely that these two methods generate such a large difference, if both methods adopt the same experimental information. It is desirable to investigate the detailed procedures and data used to evaluate the covariance in the fast energy region of ^{235}U capture reaction.

Figure 14: Comparison of JENDL-4.0 and COMMARA-2.0 Covariance: ^{235}U Capture

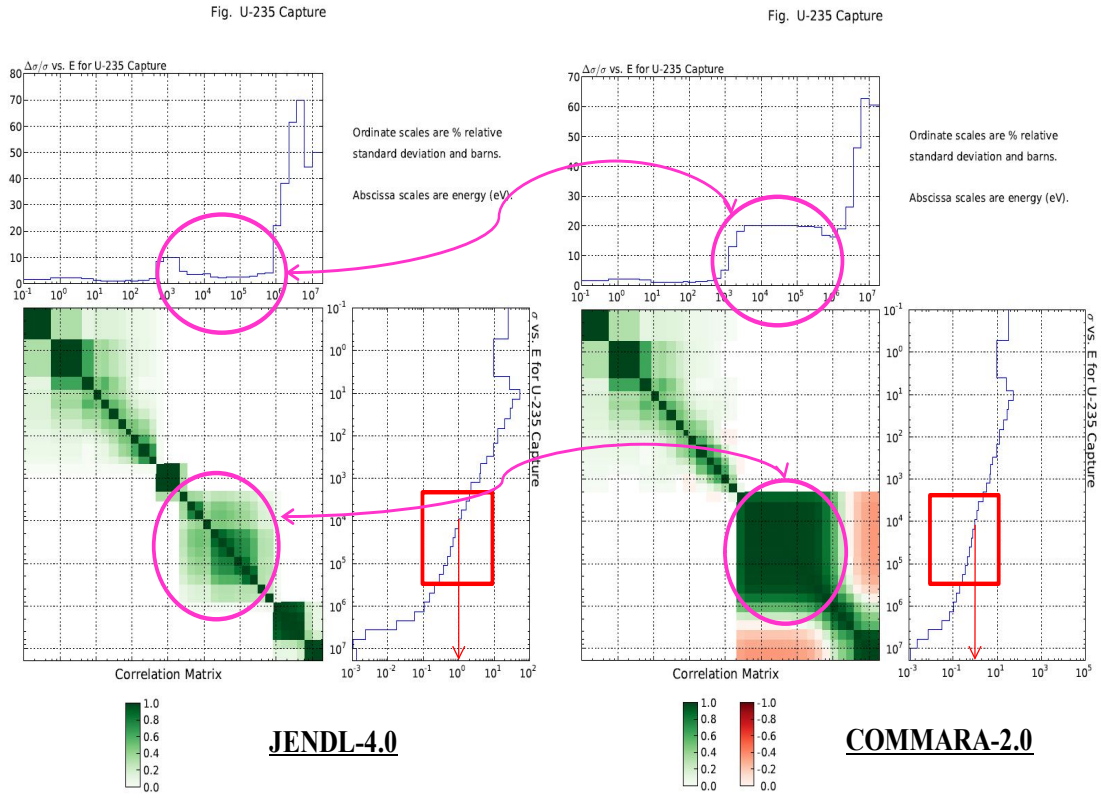

2) ^{23}Na elastic scattering data around 2 keV

In this energy range, there appears a giant resonance peak which significantly affects the sodium-voiding reactivity in sodium-cooled fast reactor cores. As shown in Figure 15, the shape of standard deviation (STD) is extremely different between two libraries, that is, the minimum STD value occurs at the cross-section peak energy in C-2.0, in contrast, the maximum appears there in J-4.0. It can be concluded that the trend of C-2.0 seems more natural, since the larger cross-sections would be more accurate due to the small statistical error in the measurement. The correlations are also quite different. In the C-2.0 covariance, the 2 keV peak has no correlations with other energy[3], while J-4.0 is partially positive everywhere above 100 eV. The covariance of C-2.0 is evaluated by the EMPIRE/KALMAN combination, where the prior resonance model parameter uncertainties are derived from Mughabghab [29], on the other hand, J-4.0 applies the GMA code with some corrections to meet the measured cross-sections with the evaluated ones of J-4.0 which is based on the multi-level Breit-Wigner formula with rather old resonance parameter values recommended by BNL in 1981. The cross-section difference between ENDF/B-VII.0 and J-4.0 is -17~+4% around 2 keV, therefore, the difference of STDs might be reasonable considering the corrections given to J-4.0 covariance.

Figure 15: Comparison of JENDL-4.0 and COMMARA-2.0 Covariance: ^{23}Na Elastic

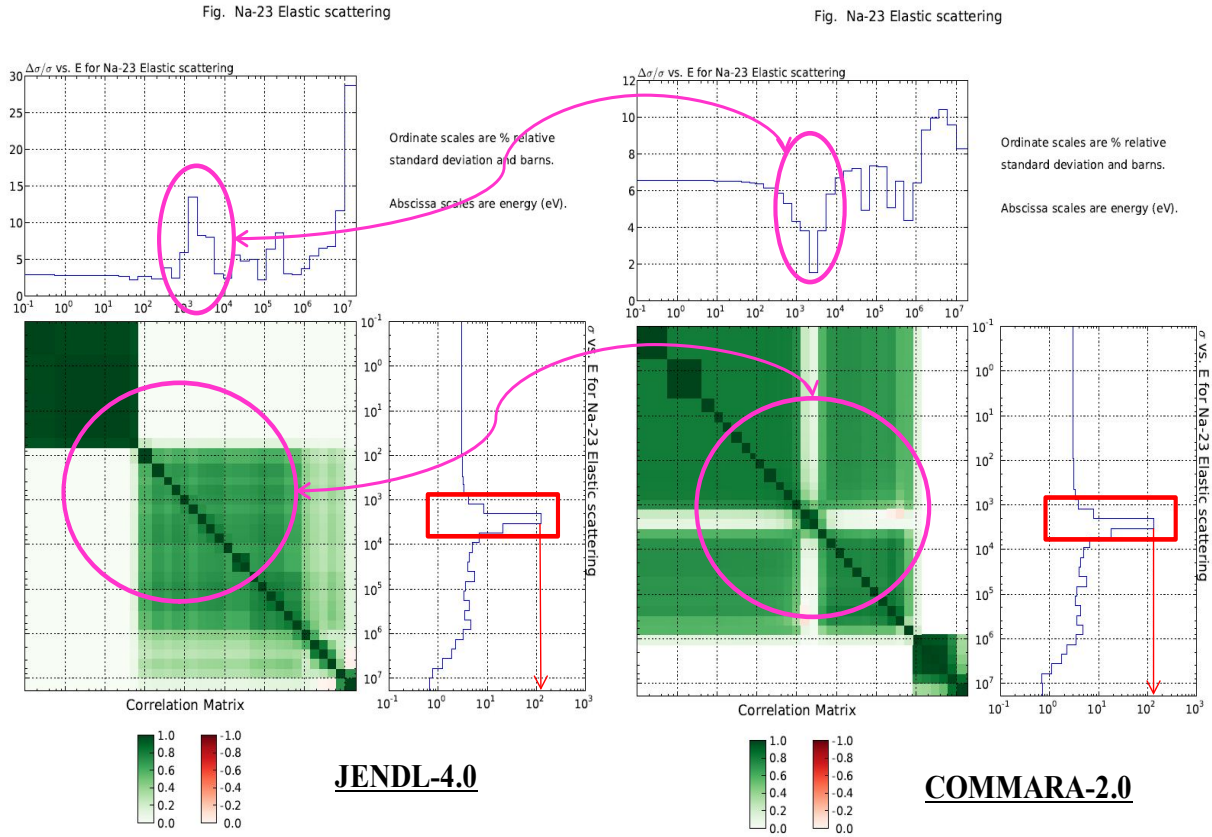

[3] This energy independency of 2 keV peak in the C-2.0 covariance is not well imagined from the general least-square analysis. There might have been some special treatments for the covariance evaluation in this resonance peak.

3) ^{56}Fe elastic scattering data in 0.3~25 keV

The central values of the ^{56}Fe elastic scattering cross-section in the resonance region from 10^{-5} eV through 850 keV are almost identical for ENDF/B-VII.0 and JENDL-4.0, since the resonance parameters adopted in both libraries are based on a common evaluation performed in the 1990s. The covariance data of C-2.0 and J-4.0 were, however, independently evaluated. In the C-2.0 covariance, the resonance region of ^{56}Fe up to 850 keV was evaluated with the kernel approximation and data from Mughabghab [18], on the other hand, the covariance data of J-4.0 were firstly estimated from the experimental data with the GMA code. Then, the estimated variances were modified by considering the difference between the average of the experimental data and that of JENDL-4 [16]. The differences of the STD shapes and the correlations in Figure 16 might stem from these utterly different methodologies of their covariance evaluations, though the energy-averaged STD values seem rather similar with each other, that is, ±5.6% in C-2.0 and ±4.5~11% in J-4.0.

Figure 16: Comparison of JENDL-4.0 and COMMARA-2.0 Covariance: ^{56}Fe Elastic

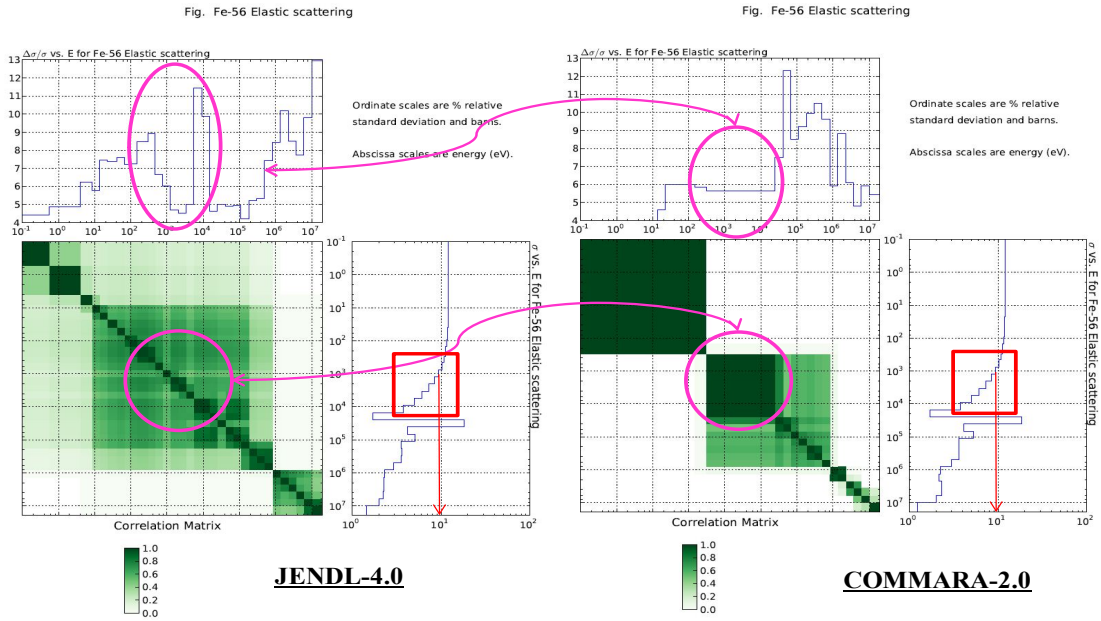

3.5 Concluding remarks

As a result of the study on the covariance data, the followings can be concluded:

In the past decades, huge efforts were made to develop the evaluation methodology of the covariance data all over the world. The latest libraries such as JENDL-4.0, COMMARA-2.0 or ENDF/B-VII.1 provide good covariance data for the users from the viewpoints of both quality and quantity. However, it should also be noted that the covariance data need improving, not only the evaluation methodology but also the quality of the measurement data used, for example, the precise inclusion of complicated correlations.

As a result of the comparison of the actual JENDL-4.0 and COMMARA-2.0 covariance data, reasonable evaluation results as well as questionable results were found. There seems no “golden rule of thumb” to improve the real covariance data. Therefore, the persistent efforts to solve the individual problems would be the only way to reach the success of the covariance fields. The close conversation between the evaluators and the users of nuclear data could be a great help for this long and tough process.

4. Integral experiment covariance data

4.1. Introduction

In the core design of the fast breeder reactors, it is important to improve the prediction accuracy of nuclear characteristics from the perspective of both reducing cost and insuring plant reliability. To utilise the past critical experimental data and power reactor operational experience to the reactor design work, the most powerful method is to adjust a cross-section set based on the Bayesian theory and least-square technique, (see [42]), where all related information including C/E (calculation/experiment) values, experimental and analytical errors, sensitivity coefficients of various experimental cores and parameters, and cross-section covariance, is synthesised with physical consistency. Based on Bayes' theorem, i.e. the conditional probability estimation method, the posterior probability that a cross-section set, $\boldsymbol{T}$, is true, is maximised under the condition that the information of integral experiments, $\boldsymbol{R}$, is obtained as below:

$$J(T) = (T-T_o)^t M^{-1}(T-T_o) + [R_e - R_c(T)]^t [V_e + V_m]^{-1}[R_e - R_c(T)] \quad (4.1)$$

where,

$\boldsymbol{J(T)}$: The error function targeted for the combined set of differential and integral data;

$\boldsymbol{T_o}$: *A prior* cross-section set before adjustment;

$\boldsymbol{M}$: Covariance of the prior cross-section set $\boldsymbol{T_o}$ before adjustment;

$\boldsymbol{V_e}$: Experimental error matrix of an integral experiment set;

$\boldsymbol{V_m}$: Analytical modelling error matrix of the integral experiment set;

$\boldsymbol{R_e}$: Measured values of the integral experiment set;

$\boldsymbol{R_c(T)}$: Analytical values of the integral experiment set obtained with the cross-section set $\boldsymbol{T}$.

To minimise the error function J(T), $dJ(T)/dT = 0$. (4.2)

After analytical derivations, the posterior cross-section set, T', and its covariance, M', after adjustment are obtained as follows:

$$T' = T_o + MG^t[GMG^t + V_e + V_m]^{-1}[R_e - R_c(T_o)] \quad (4.3)$$

$$M' = M - MG^t[GMG^t + V_e + V_m]^{-1}GM \quad (4.4)$$

where,

$\boldsymbol{G}$: Sensitivity coefficients of a cross-section, *t*, to an integral parameter, $\boldsymbol{R}$, that is, $(d\boldsymbol{R}/\boldsymbol{R})/(d\boldsymbol{t}/\boldsymbol{t})$.

As shown in these equations, it is necessary to prepare the error matrices of integral parameters for both the experiments and the analytical modelling, $\boldsymbol{V_e}$ and $\boldsymbol{V_m}$, to perform the cross-section adjustment procedure.

Correlations between two experiments arise if any components of the experimental uncertainty are fully or partially common for those experiments. The importance of accounting for the correlation of experimental uncertainties in the evaluation of calculation uncertainties and in data adjustment methodologies has been demonstrated; (see for example, [43]). A typical procedure for evaluating the integral covariance data is described in [44]. An approach presented by O. Buss *et al.* [45] utilises statistical sampling on uncertain parameters to assess the uncertainty in individual experiments as well as correlations between experiments. Work is underway to implement this stochastic approach in a module called PROTEUS (PaRametric Tool to Engineering Uncertainty analysis in SCALE) [46]. The reader may wish to know that the Expert Group on Uncertainty Analysis for Criticality Safety Assessment (UACSA), established under the guidance of the OECD/NEA Working Party on Nuclear Criticality Safety (WPNCS) to address issues related to sensitivity/uncertainty (S/U) studies for criticality safety calculations, is currently studying the effects of different methodologies to generate integral experiment covariance data.

Section 4.2 now illustrates a reasonable method to quantitatively determine the integral error matrices which include both diagonal terms (standard deviations) and non-diagonal terms (correlation factors). This "Integral covariance estimation method based on the perfect correlation between common error components", or "Error component correlation method" in short, is based closely on the method described in [44]. Section 4.3 provides examples of applying this method to determine the experimental error matrix for the case of sodium void reactivity measurements and the reaction rate ratio measurements in the ZPPR-9 assembly. Section 4.5 develops an evaluation methodology of the analytical modelling error, $\mathbf{V}_m$, which depends on the analytical method adopted to obtain the calculated value of an integral experiment. In the present work developed in SG33, three kinds of analytical methods (continuous-energy Monte Carlo, deterministic, and a combination of Monte Carlo and deterministic methods) are considered.

4.2. Experimental error matrix

Experimental uncertainties of an integral parameter are usually given by the experimenters in the form of components. However, correlations between integral parameters are scarcely found in the experiment reports; therefore, we have to estimate them from the experimental information available. The method adopts the following three steps.

(Stage 1) Classification of Error Components to either Common or Independent

First, all-related components of the experimental errors for "Data A" and "Data B" with quantitative values reported are listed, and each individual component identified either as a "Common error (i.e. the correlation factor is 1.0) between Data A and B", or an "Independent error (i.e. the correlation factor is 0.0)"[4]. If an error component is judged as a mixture of common and independent errors, that is, the correlation factor is not considered as either 1.0 or 0.0, then the error component must be divided into more detailed subcomponents until the error component becomes either a common or independent error. This classification requirement is difficult for the experimenters who evaluate the error components in their report, but today this kind of rigor is essential to retain full value of these experimental quantities. Recent experimental databases like the OECD/NEA ICSBEP and IRPhEP handbooks [47] [48] now include such detailed experimental error evaluation by the continuous efforts of the authors and reviewers.

[4] The words "Common" and "Independent" adopted here are usually referred as "Systematic" and "Statistical", respectively, in many experimental reporting literatures. However, the use of the former labels more clearly expresses the intention of this classification to evaluate their correlation factor for a specific pair of data in a large matrix than the latter labels.

(Stage 2) Summation of Common and Independent Errors

Next, the common and independent errors, respectively, are summed-up statistically to obtain standard deviation, σ_{Total}, the diagonal term of the matrix. The statistical treatment is justified by the assumption that all error components have already been divided until there are no correlations between any error items in the measurement of an integral parameter. The total errors of Data A and B, that is, the diagonal term of error matrix, ***Ve***, are the summation of common and independent errors as below:

Standard deviation of Data A: $$\sigma_{Total,A} = \sqrt{\sigma^2_{Common,A} + \sigma^2_{Independent,A}} \quad (4.5)$$

Standard deviation of Data B: $$\sigma_{Total,B} = \sqrt{\sigma^2_{Common,B} + \sigma^2_{Independent,B}} \quad (4.6)$$

where σ_{Common} : Summing up of all Common error components,

$\sigma_{Independent}$: Summing up of all Independent error components.

(Stage 3) Evaluation of correlation factor

Finally, the correlation factor, non-diagonal term, of Data A and B is derived as the ratio of common errors to the total errors as Equation (4.7). Steps 1 to 3 must be repeated for all matrix elements to generate a full experimental error matrix as the input of adjustment exercise. It should be noted that the correlation factors between several sodium void reactivity measurements would be changed depending on the combination of void steps, even in the same experimental core.

Correlation Factor of Data A and Data B: $$\rho_{A,B} = \frac{\sum_i \sigma_{Common,A,i} \times \sigma_{Common,B,i}}{\sigma_{Total,A} \times \sigma_{Total,B}} \quad (4.7)$$

where, the suffix i represents common error components between Data A and Data B.

4.3. Examples to evaluate experimental error matrix

Typical examples to estimate the experimental error matrix are shown for the sodium void reactivity (SVR) measurement and the reaction rate ratio (RRR) measurement in the ZPPR-9 core.

4.3.1. Sodium void reactivity measurement

Figure 17 summarises the evaluation procedure for the SVR measurement in the ZPPR-9 core. Table 3 shows the measured void step in the ZPPR-9 experiment [49]. Treatment of the error values and their correlation between Step 3 and Step 5 of the SVR measurement in ZPPR-9 is provided as an example. Step 3 is a central void case in the core where neutron non-leakage term is dominant for the reactivity change by sodium voiding, on the other hand, Step 5 is an axially whole-core void case where the non-leakage term of the reactivity is largely cancelled by the leakage term. The net reactivity of both steps is almost the same with the value around +30 cents, though the mass of the removed sodium to simulate sodium voiding is quite different by more than factor 2, that is, 31 kg for Step 3 and 78 kg for Step 5, respectively. The left part of Figure 17 is the result of the experimental error evaluation [49] following the IRPhE evaluation guidance [50], where the error sources are classified into the three categories, (1) measurement technique, (2) geometry, and (3) composition.

(Stage 1) The detailed explanation of the error evaluation for the SVR measurement can be found in "Section 2.4: Evaluation of Reactivity Data" of [49]. First, the quality of the error analysis is assessed and the experimental error components are categorised in order to fulfil the requirement of the necessary error matrix evaluation, that is, the correlation factor of each error component between the two measurements must be 1.0 or 0.0.

Table 3: Results of zone sodium-voiding measurements in ZPPR-9 [51]

Step No.	Total Zone Size Drawers	Zone Depth mm	Total Na Mass[a] kg	Reactivity Change[b] cent		Reactivity Adjustment[c] cent
				Cumulative $\pm\sigma_m$ (σ_t)	Step $\pm\sigma_m$ (σ_t)	
1	9	203.2	2.90	3.03±0.05 (0.10)	3.03±0.05 (0.10)	-0.04
2	37	203.2	11.94	11.56±0.04 (0.19)	8.53±0.06 (0.17)	-1.36
3	97	203.2	31.30	29.39±0.02 (0.36)	17.83±0.04 (0.32)	1.22
4	97	406.4	62.60	37.26±0.01 (0.43)	7.87±0.02 (0.10)	0.84
5	97	508.0	77.88	31.68±0.02 (0.36)	-5.58±0.04 (0.15)	0.13
6	97	685.8	105.11	24.44±0.03 (0.29)	-7.24±0.04 (0.15)	-0.82
Outer core zones						
1	25 (x axis)	203.2	8.07	0.93±0.06 (0.12)		
2	25 (y axis)	203.2	8.07	0.20±0.06 (0.12)		

a: A random uncertainty of 1% is assigned to any mass or mass difference.

b: Counting statistics only are included in σ_m. The value of σ_t includes uncertainties in the reactivity adjustment and a 1.1% uncertainty in the detector calibration.

c: This uncertainty adjustment accounts for differences in experimental conditions between the reference and the particular step. When comparing the reactivity between steps, an uncertainty is assigned based on the magnitude of the adjustment.

Figure 17: Summary of uncertainties in the zone sodium void measurement in ZPPR-9

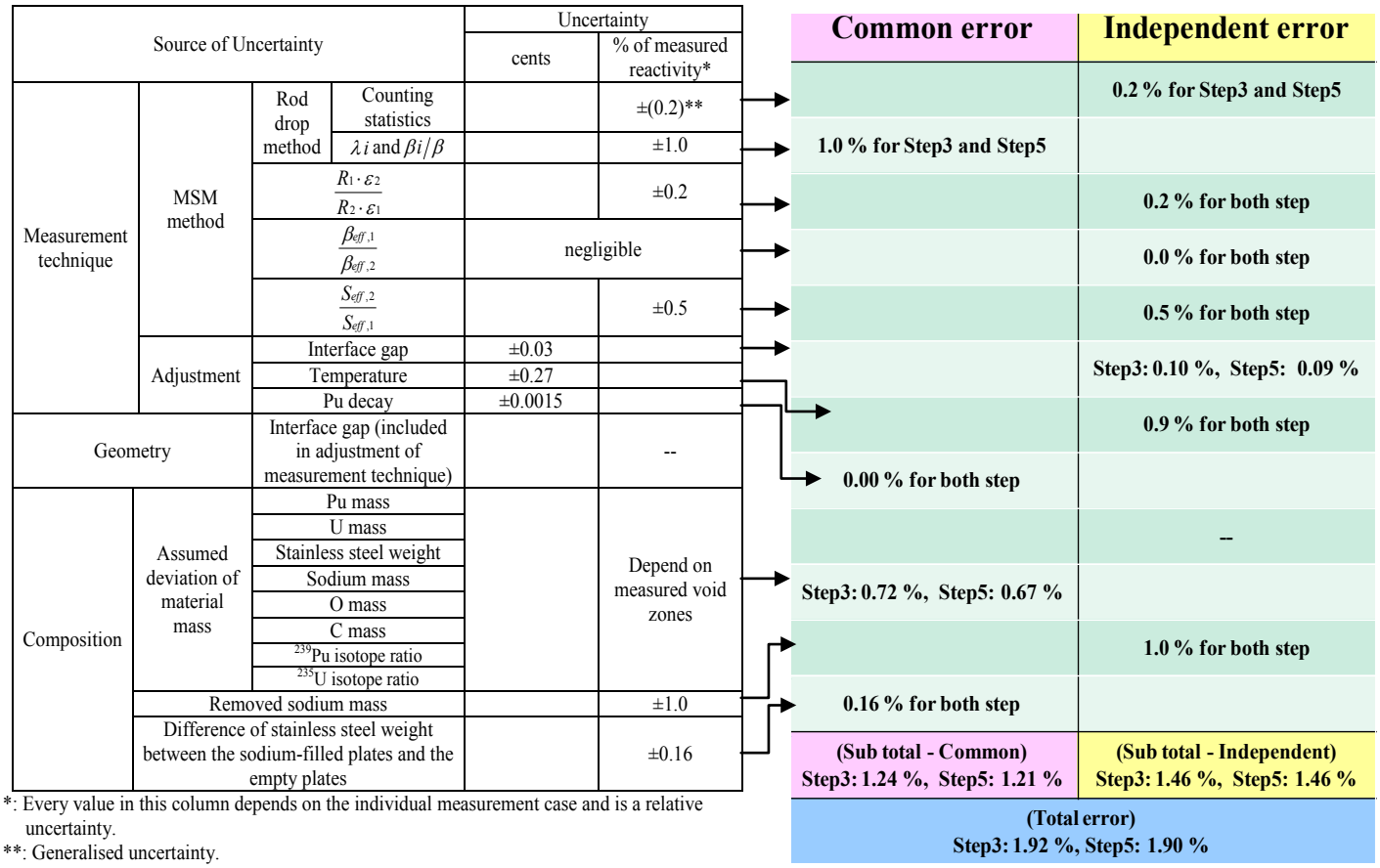

Source of Uncertainty				Uncertainty: cents	Uncertainty: % of measured reactivity*	Common error	Independent error
Measurement technique	MSM method	Rod drop method	Counting statistics		±(0.2)**		0.2 % for Step3 and Step5
			λi and $\beta i/\beta$		±1.0	1.0 % for Step3 and Step5	
		$\frac{R_1 \cdot \varepsilon_2}{R_2 \cdot \varepsilon_1}$			±0.2		0.2 % for both step
		$\frac{\beta_{eff,1}}{\beta_{eff,2}}$		negligible			0.0 % for both step
		$\frac{S_{eff,2}}{S_{eff,1}}$			±0.5		0.5 % for both step
	Adjustment	Interface gap		±0.03			Step3: 0.10 %, Step5: 0.09 %
		Temperature		±0.27			
		Pu decay		±0.0015			0.9 % for both step
Geometry		Interface gap (included in adjustment of measurement technique)			--	0.00 % for both step	
Composition	Assumed deviation of material mass	Pu mass		Depend on measured void zones			--
		U mass				Step3: 0.72 %, Step5: 0.67 %	
		Stainless steel weight					1.0 % for both step
		Sodium mass					
		O mass				0.16 % for both step	
		C mass					
		^{239}Pu isotope ratio					
		^{235}U isotope ratio					
	Removed sodium mass				±1.0		
	Difference of stainless steel weight between the sodium-filled plates and the empty plates				±0.16		
						(Sub total - Common) Step3: 1.24 %, Step5: 1.21 %	(Sub total - Independent) Step3: 1.46 %, Step5: 1.46 %
						(Total error) Step3: 1.92 %, Step5: 1.90 %	

*: Every value in this column depends on the individual measurement case and is a relative uncertainty.
**: Generalised uncertainty.

$$\rho\ (between\ Step3\ \ and\ \ Step5) = \frac{\sum_i \sigma_{Common}(Step3,i) \times \sigma_{Common}(Step5,i)}{\sigma_{Total}(Step3) \times \sigma_{Total}(Step5)} = 0.41$$

The following are brief comments for the important error components in Figure 17 and Table 3. λ_i and β_i/β: To obtain the cent-unit reactivity by solving the inverse kinetics equation from the flux change measured, the family-wise decay constant (λ_i) values of the delayed neutron precursors and the family-wise delayed neutron fraction ratio (β_i/β) were needed as the input data[5]. This error component greatly contributes to the total error with the common characteristics between two measurements, since ANL experimenters used the same λ_i and β_i/β values throughout the measurement.

Temperature adjustment: The correction of temperature difference was needed between two measurements. According to the ANL document, the temperature difference is usually 2 degree-C at maximum, and the uncertainty of the temperature coefficient would be 10%. The resulted error values are quite large with the independent characteristics, since the temperature change between two measurements could be considered as random.

Material mass-induced error: The assumed mass uncertainties were derived from some ANL documents, that is, 0.079% for plutonium, 0.15% for uranium, etc. The mass uncertainties were converted to the reactivity-unit errors using the sensitivity coefficients of each element to each void step, therefore, the error values were slightly changed in Steps 3 and 5. This mass-induced error can be considered as a common component, since the shape of sensitivity coefficients for two measurements are quite similar.

(Stage 2) Summation of the results of the error values for Steps 3 and 5 is shown in Figure 17. The total error for Step 3 is 1.92%, and for Step 5, 1.90%. The contributions of common and independent errors are quite comparable.

(Stage 3) Finally, the correlation factor between Steps 3 and 5 is shown at the bottom of Figure 17. The value is 0.41, which might be physically plausible from the quantitative evaluation of the common and independent error components.

4.3.2. Reaction rate ratio measurement

Figure 18 and Tables 4-7 show the error matrix evaluation process for the RRR measurement in the ZPPR-9 core. Here, the foil activation method for the RRR measurement adopted in the ZPPR facility is provided as an example. Thin metallic activation foils were used to measure reaction rates in ZPPR-9 as illustrated in Figure 18. Uranium and plutonium metal foils were placed between plates in various drawers in the assembly, irradiated and then removed from the drawers. Capture and fission rates in the irradiated foils were determined by counting gamma rays emitted by capture or fission products.

(Stage 1) The error evaluation for the RRR measurement in ZPPR-9 is described in detail in "Section 2.7: Evaluation of Reaction Rate Distributions" [49]. Tables 4-7 show the result of the experimental error evaluation.

Error caused by mapping foil activity measurement: This error component consists of (1) the counting statistics, (2) the positioning of a sample above a gamma-ray counter, (3) the foil mass and (4) the discrete channel boundary in peak integration, whose characteristics are all statistical.

[5] Note this is not concerned with the conversion factor (β_{eff}) of the reactivity from cent-unit to delta k, which is needed to compare the reactivity value of an experiment with that of calculation.

Figure 18: Example of reaction rate ratio measurement in ZPPR9

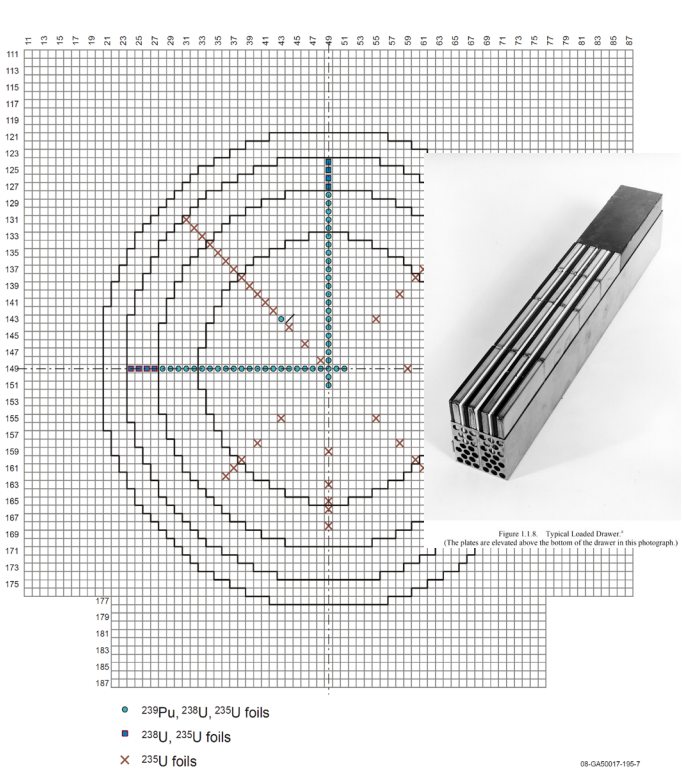

Figure 1.31. Measured Radial Reaction Rate Positions in ZPPR-9.
(Ref. D. N. Olsen, "ZPPR Assembly 9 – Detailed Work Plan No. 3", ZPR-I-306, Argonne National Laboratory (Jun. 1978).)

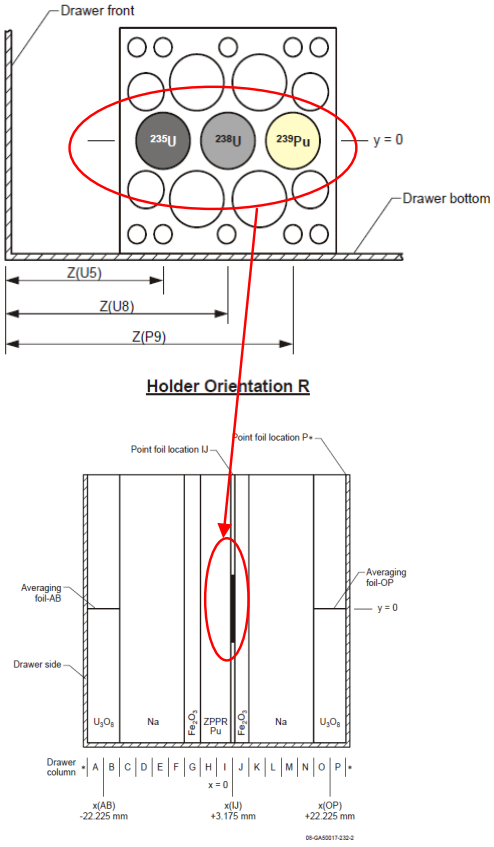

Figure 1.33. Foil Locations in a Drawer (view from front).

Table 4: Uncertainties assigned to the detector calibration

Typical uncertainty (% of measured reaction rate)						
Reaction Rate				Reaction Rate Ratio		
^{239}Pu(n, f)	^{235}U(n, f)	^{238}U (n, f)	^{238}U(n, γ)	^{235}U(n, f)/ ^{239}Pu(n, f)	^{238}U (n, f)/ ^{239}Pu(n, f)	^{238}U(n, γ)/ ^{239}Pu(n, f)
1.5	1.3	1.9	1.0	1.0	1.8	1.2

Table 5: Combined uncertainties of mapping foil data

	Typical uncertainty (% of measured reaction rate)							
	^{239}Pu fission		^{235}U fission		^{238}U fission		^{238}U capture	
	Core	Radial blanket	Core	Radial blanket	Core	Radial blanket	Core	Radial blanket
Measurement technique	1.3*		1.1*		1.7*		1.0*	
Geometry	negligible	--	negligible	1.0	negligible	0.1	negligible	0.9
Composition	0.18	---	0.17	0.08	0.22	0.27	0.18	0.06
Total	1.3	1.3	1.1	1.5	1.7	1.7	1.0	1.3

Table 6: Combined uncertainties of reaction rate ratio (in core region)

			Typical uncertainty (% of measured reaction rate ratio)					
			F25/F49		F28/F49		C28/F49	
			F25	F49	F28	F49	C28	F49
Measurement technique	Mapping foil		1.1	1.3	1.7	1.3	1.0	1.3
		Sub-total	1.7		2.1		1.6	
	Detector calibration		1.0*		1.8*		1.2*	
Geometry			negligible		negligible		negligible	
Composition			0.06		0.22		0.05	
Total			2.0		2.8		2.0	

In ZPPR-9, the reaction rates were measured in the same run and at the same foil place. Common errors of two reaction rate ratios (e.g. F49/F25 and C28/F25) come from the error of the common reaction rate (F25), as shown in the following table and equation.

Table 7: Final values for uncertainties and correlations of reaction rate ratio

Reaction Ratio		F28/F25	F49/F25	C28/F25
Total Error		2.7%	2.0%	1.9%
Correlation factor	F28/F25	1.0		
	F49/F25	0.23	1.0	
	C28/F25	0.23	0.32	1.0

$$\rho\ (between\ F49/F25\ \ and\ \ C28/F25) \approx \frac{1.1\% \times 1.1\%}{\sigma_{Total}(F49/F25) \times \sigma_{Total}(C28/F25)} = 0.32$$

Error caused by detector calibration: The absolute calibration of each reaction is necessary to measure the RRR value, which was made by gamma-ray counting of ^{239}Pu, ^{235}U and ^{238}U foils and deposits in back-to-back fission chambers. Note that the error induced by the detector calibration has the systematic characteristics to determine the absolute value of a kind of RRR, such as by averaging the F49/F25 values in the whole core, however, it has a statistical characteristic when the correlation between two kinds of RRRs, such as between F49/F25 and C28/F25, is considered.

Composition-induced error: Since the error caused by the foil composition is included in the mapping foil error, the composition row in Table 5 is related to the chemical analysis error of the core fuel and other core materials, and possesses the common characteristics between two RRRs. The composition error to the reactivity was converted with the sensitivity coefficients like the SVR case, but the magnitude was found to be negligible, compared with other common error mentioned below.

(Stage 2) In the ZPPR experiment, the activation foils of ^{239}Pu, ^{235}U and ^{238}U were irradiated in the same run, and at the same foil folders in a drawer. This means that the common error of two RRRs such as F49/F25 and C28/F25 must include the contribution from the common denominator, F25 in this case. The results of the error values for F49/F25 and C28/F25 are shown in Table 7. The total error for F49/F25 is 2.0%, and for C28/F25, is 1.9%.

(Stage 3) The correlation factors between F49/F25 and C28/F25 become 0.32 as shown in the last row of Table 7.

4.4. Full experimental error matrix in SG33 Exercise

Applying the above-mentioned methodology, the full covariance matrix for the 20 experiments treated in the SG33 exercise is summarised in Figure 19. Additional comments are given below:

(1) The correlation factors of the RRRs in JEZEBEL-^{239}Pu, FLATTOP and ZPR6-7 are borrowed from those of ZPPR-9, since the denominator of the RRRs, F25, is common in these experiments, and there is scarce information for the former three experiments to evaluate the common and independent components of the RRRs. The F37/F25 ratio is assumed to possess similar characteristics with F28/F25 which has threshold characteristics against neutron energy.

(2) From the fuel composition tables of [49] and [52], the plutonium fuel plates used in ZPR6-7, ZPR6-7 ^{240}Pu and ZPPR-9 experiments were found as identical ones. This means at least that the criticality of these three cores must be correlated through the composition errors. In Figure 19, the evaluated correlation factors with the sensitivity coefficients of core compositions are added[6]. The correlations among other parameters of these three cores are neglected here, since the effects of common core material to other parameters are usually small compared with that to the criticality.

4.5. Analytical modelling error matrix

The evaluation methodology of the analytical modelling error, $\mathbf{V}_m$, depends on the analytical method adopted to obtain the calculation value of an integral experiment. Here, we consider three kinds of analytical methods: (1) continuous-energy Monte Carlo method based on the as-built experimental geometry and compositions (MC method, hereafter), (2) deterministic analytical method based on the combination of the standard calculation and the corrections by the most-detailed analytical models (deterministic method), and (3) combination of the deterministic analytical calculation based on the simplified geometry and the correction by the Monte Carlo calculation with as-built geometry (combined method).

[6] The common errors induced by composition errors are only considered here, since there is no information on other common error components among these.

Figure 19: Experimental error matrix V_e applied in SG33 Exercise

No.	Core		1	2	3	4	5	6	7	8	9	10	11	12	13	14	15	16	17	18	19	20
1	Jezebel - Pu239	keff	0.2																			
2		F28/F25	0	1.1																		
3		F49/F25	0	0.23	0.9																	
4		F37/F25	0	0.23	0.32	1.4																
5	Jezebel - Pu240	keff	0	0	0	0	0.2															
6	Flattop	keff	0	0	0	0	0	0.3														
7		F28/F25	0	0	0	0	0	0	1.1													
8		F37/F25	0	0	0	0	0	0	0.23	1.4												
9	ZPR6-7	keff	0	0	0	0	0	0	0	0	0.23											
10		F28/F25	0	0	0	0	0	0	0	0	0	3.0										
11		F49/F25	0	0	0	0	0	0	0	0	0	0.23	2.1									
12		C28/F25	0	0	0	0	0	0	0	0	0	0.23	0.32	2.4								
13	ZPR6-7 Pu240	keff	0	0	0	0	0	0	0	0	0.13	0	0	0	0.22							
14	ZPPR-9	keff	0	0	0	0	0	0	0	0	0.31	0	0	0	0.30	0.117						
15		F28/F25	0	0	0	0	0	0	0	0	0	0	0	0	0	0	2.7					
16		F49/F25	0	0	0	0	0	0	0	0	0	0	0	0	0	0	0.23	2.0				
17		C28/F25	0	0	0	0	0	0	0	0	0	0	0	0	0	0	0.23	0.32	1.9			
18		Central Na void	0	0	0	0	0	0	0	0	0	0	0	0	0	0	0	0	0	1.9		
19		Large Na void	0	0	0	0	0	0	0	0	0	0	0	0	0	0	0	0	0	0.41	1.9	
20	Joyo	keff	0	0	0	0	0	0	0	0	0	0	0	0	0	0	0	0	0	0	0	0.18

* Diagonal term: Error value (1 sigma, %)
** Non-diagonal term : Correlation factor (between -1 and +1)

4.5.1. *MC Method*

The standard deviation (diagonal term) of the analytical modelling error should be supplied from the statistical error value evaluated by the adopted MC code. However, there is one caution to adopt the statistical error evaluated by the MC code. According to [53] and [54], the existing MC codes cannot depend on the effect of correlation among the fission source over successive MC cycles to evaluate the statistical error. This ignorance will result in the underestimation bias of the real statistical error, by the range of the factor 1.4 to 3.1 [53] depending on the target calculation systems, or by 69% for a small-size reactor core and by 80% for a medium-size one [54]. Here, it is recommended to multiply the statistical error evaluated with a MC code by a factor of 2, in order to prepare the analytical modelling error as the input data of the cross-section adjustment.

The correlation factors of the analytical modelling error with the MC method are basically 0.0 from the random nature of the Monte Carlo methodology. This would be also valid even for the correlation between two reaction rates at the same position in a core, since the detailed energy structure of two cross-sections are not identical, therefore, the energy-integrated reaction rate would be independent from each other. Only one exception is the correlation between two reaction rate ratios (RRRs) which have the same denominator such as F49/F25 and C28/F25. If the calculation results of two RRRs are obtained by one MC code run, these RRRs have the correlation of +0.5 if the statistical errors of each RRR are the same. Figure 20 shows an example of the analytical modelling error matrix $\mathbf{V}_m$ applied in SG33 Exercise, where all calculations are based on the MC method.

4.5.2. *Deterministic method*

There is no established methodology to evaluate the analytical modelling error matrix for the deterministic analysis yet. Here a possible estimation method is submitted, which is based on a kind of "sensitivity consideration" to the detailed degree of a physical modelling. The basic assumption is that the error value of analytical modelling would be large, if the analytical result significantly changes when the degree of physical modelling is replaced from simple one to detailed, such as from the diffusion theory to the transport theory. In other words, the error would be large if the sensitivity to the analytical modelling is large. Figure 21 summarises the actual procedure to estimate the analytical modelling error matrix.

(1) First, the correction items of an integral parameter, the criticality for two experimental cores, ZPPR-9 [49] and JOYO Mk-I [55] in Figure 21, are listed up with their calculated values. The explanation of each correction is found in Section 4 of [56].

(2) For each correction item, a certain percent[7] of the "smaller" correction value is assumed as the common error between two cores. The concept of this treatment for the transport-theory correction is illustrated in Figure 22. The physical mechanism of transport correction comes from the approximated treatment of neutron-flux gradient, which is common between ZPPR-9 and JOYO.

Figure 20: Example of the analytical modelling error matrix V_m applied in SG33 Exercise

(All calculations are based on continuous-energy Monte Carlo method.)

No.	Core		1	2	3	4	5	6	7	8	9	10	11	12	13	14	15	16	17	18	19	20
1	Jezebel - Pu239	keff	0.03																			
2		F28/F25	0	0.9																		
3		F49/F25	0	0.5	0.8																	
4		F37/F25	0	0.5	0.5	0.8																
5	Jezebel - Pu240	keff	0	0	0	0	0.03															
6	Flattop	keff	0	0	0	0	0	0.03														
7		F28/F25	0	0	0	0	0	0	0.8													
8		F37/F25	0	0	0	0	0	0	0.5	0.7												
9	ZPR6-7	keff	0	0	0	0	0	0	0	0	0.03											
10		F28/F25	0	0	0	0	0	0	0	0	0	2.2										
11		F49/F25	0	0	0	0	0	0	0	0	0	0.5	1.4									
12		C28/F25	0	0	0	0	0	0	0	0	0	0.5	0.5	1.2								
13	ZPR6-7 Pu240	keff	0	0	0	0	0	0	0	0	0	0	0	0	0.03							
14	ZPPR-9	keff	0	0	0	0	0	0	0	0	0	0	0	0	0	0.02						
15		F28/F25	0	0	0	0	0	0	0	0	0	0	0	0	0	0	2.1					
16		F49/F25	0	0	0	0	0	0	0	0	0	0	0	0	0	0	0.5	1.2				
17		C28/F25	0	0	0	0	0	0	0	0	0	0	0	0	0	0	0.5	0.5	1.4			
18		Central Na void	0	0	0	0	0	0	0	0	0	0	0	0	0	0	0	0	0	5.3		
19		Large Na void	0	0	0	0	0	0	0	0	0	0	0	0	0	0	0	0	0	0	5.0	
20	Joyo	keff	0	0	0	0	0	0	0	0	0	0	0	0	0	0	0	0	0	0	0	0.03

* Diagonal term: Error value (1 sigma, %)
** Non-diagonal term : Correlation factor (between -1 and +1)

[7] The "a certain percent" means that value of the analytical modelling error is assumed to be proportional to the value of correction by the detailed models.

Figure 21: Example of the weak correlation case of the analytical modelling error

Experiment / Analytical Item		Keff of ZPPR-9 (: A) Value (Ref.2)	Common Error	Independent Error	Keff of JOYO Mk-I (: B) Value (Ref.5)	Common	Independent Error
keff by basic method		0.99372	*multiplied by 0.3*		0.98060		
Correction by detailed model (unit: pcm)	Transport theory	+248	±74	0	+1760	±74	±523
	Mesh-size effect	-93	±28	0	-210	±28	±56
	Ultra-fine energy effect	+103	0	±31	-50	0	±15
	Multi-drawer effect	+47	0	±14	0	0	0
	Cell-asymmetry effect	-52	0	±16	0	0	0
Total		0.99625	±79	±37	0.99560	±79	±526
			±88 pcm			±532 pcm	

assumed as common

assumed as independent

$$\rho\ (between\ ZPPR-9\ and\ JOYO) = \frac{\sum_i \sigma_{Common}(ZPPR-9)\times\sigma_{Common}(JOYO)}{\sigma_{Total}(ZPPR-9)\times\sigma_{Total}(JOYO)} = 0.14$$

Figure 22: Illustration of the common-error concept in the analytical modelling error estimation

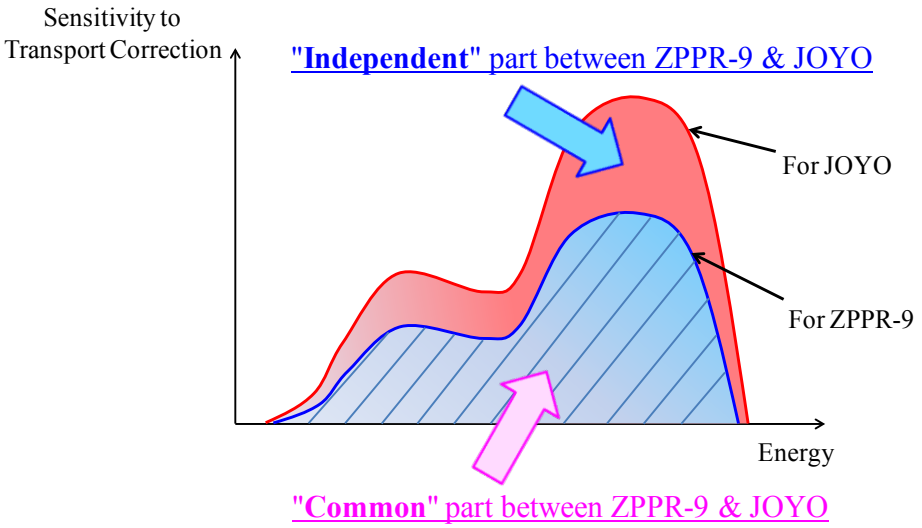

However, the sensitivity of the transport effect to JOYO is larger than that to ZPPR-9, since JOYO is a smaller core with steep flux gradient. We assume here that the overlapped part of the transport correction would be common between these two cores, and the un-overlapped part might be an independent characteristic of JOYO only. If the signs of the correction values for the two cores are opposite, which is the case of the ultra-fine energy effect in Figure 21, this correction item would be judged as independent because the physical mechanism must be different from each other.

(3) The percentage value of the correction should be estimated by other engineering judgments, and a value of 30% is suggested from the past adjustment experiences where the chi-square balancing was investigated among the set of the C/E-1 values, the integral experimental errors, the cross-section covariances and the analytical modelling errors.

(4) The following procedures are similar with those of the experimental error matrix evaluation. The total error values of two cores are calculated by summing up both the common errors and the independent errors as in Equations (4.5) and (4.6). The correlation factor is evaluated by the ratio of the common errors to the total errors as in Equation (4.7).

Figure 21 shows the example of k_{eff} correlations between a large core, ZPPR-9, and a small core, JOYO. The correlation between them is expected to be quite weak, and the estimated result was 0.14. On the other hand, Figure 23 is an example of the strong correlation case. The integral data evaluated are the criticality of ZPPR-10A, a 600MWe-class FBR core, and that of ZPPR-10C, a 800MWe-class FBR core [57]. The drawer structures and arrangements of both cores are almost identical except a small difference of core sizes, therefore, the correlation between them is expected to be strong, and the estimated factor was 0.82. These results would coincide with our physical intuition.

Figure 23: Example of the strong correlation case of the analytical modelling error

Experiment / Analytical Item		Keff of ZPPR-10A (: A) (600 MWe-class FBR)			Keff of ZPPR-10C (: B) (800 MWe-class FBR)		
		Value (Ref.6)	Common Error	Independent Error	Value (Ref.7)	Common	Independent Error
keff by basic method		0.9913			0.9916	*multiplied by 0.3*	
Correction by detailed model (unit: pcm)	Transport theory	+530	±129	±93	+430	±129	0
	Mesh-size effect	-130	±33	±21	-110	±33	0
	Ultra-fine energy effect	+150	±42	±16	+140	±42	0
	Multi-drawer effect	+40	±12	0	+40	±12	0
	Cell-asymmetry effect	-60	±15	±10	-50	±15	0
Total		0.9966	±141	±97	0.9961	±141	0
			±171 pcm			±141 pcm	

assumed as common

$$\rho\ (between\ ZPPR-10A\ and\ ZPPR-10C) = \frac{\sum_i \sigma_{Common}(ZPPR-10A) \times \sigma_{Common}(ZPPR-10C)}{\sigma_{Total}(ZPPR-10A) \times \sigma_{Total}(ZPPR-10C)} = 0.82$$

4.5.3. *Combined method*

The MC method could be generally regarded as the most desirable analysis tool to obtain the best-estimated calculation values and their error values for the complicated as-built geometry. However, the current computer power is still not enough to calculate small reactivity changes or local reaction rates by the MC method with realistic computing time. Further, the input data of the MC method tends to be huge if the core compositions are very complicated, such as the burn-up conditions of a power reactor. On the other hand, the deterministic method has the advantage that the computing time is relatively short, and it is rather practical to treat such complicated compositions, although the complicated as-built geometry is difficult to directly simulate by the deterministic method. To make use of the merits of both methods, there is a possibility to combine the MC method with the deterministic method to obtain the best-estimated calculation values. The idea is to make the calculation result of the deterministic method equivalent to that of the MC method by the correction. The final values of the combined method, $R_{Combined}$ (best-estimated), would be expressed as follows:

$$\begin{aligned} R_{Combined}\text{ (best-estimated)} = {} & \mathbf{R}_{Det}\text{ (simplified geometry, as-built composition)} + \\ & \mathbf{R}_{MC}\text{ (as-built geometry, simplified composition)} - \\ & \mathbf{R}_{Det}\text{ (simplified geometry, simplified composition)} \end{aligned} \qquad (4.8)$$

where:

$\mathbf{R}_{Det}$: calculated value by the deterministic method and

$\mathbf{R}_{MC}$: calculated value by the MC method.

In this case, the standard deviation of the combined method could be considered as the same of the MC method, under the condition that the correction values, the second term of the right hand in Equation (4.8), are obtained through well-organised simulation models from the analytical modelling error viewpoint, in other words, if the analytical errors caused by two calculations with the deterministic method are cancelled in Equation (4.8). The correlation factors of the combined method would be also the same with those of the MC method, under such conditions.

4.6. Concluding remarks

In order to make the cross-section adjustment, the preparation of the integral experimental and analytical modelling errors is inevitable with the form of matrix, that is, the combination of standard deviations and correlation factors. A methodology and a procedure to evaluate/estimate both matrices have been proposed herein, and in the hope that these will be used in the actual adjustment exercise and improved to more sophisticated methods in the future.

5. Comparison of integral experiment initial C/E's, uncertainties, and target system uncertainties

5.1 Introduction

In this chapter we will examine the results provided by the benchmark participants regarding the initial C/E's, uncertainties associated to the integral experimental analysis (both experimental and calculation), as well as those related to nuclear data, and target system uncertainties (nuclear data related).

The integral experimental analysis results have been provided by the following organisations:

- ANL: ENDF/B-VII.0 cross-sections, MCNP5 for experiment analysis, and ERANOS system and COMMARA 2.0 covariance data for uncertainty analysis;
- CEA: JEFF3.1.1 cross-sections, ERANOS/PARIS (in conjunction with corrective factors) for experimental analysis, and ERANOS/PARIS and COMAC covariance data for uncertainty analysis;
- INL: ENDF/B-VII.0 cross-sections, MCNP5 for experiment analysis, and SANDRA code and COMMARA 2.0 covariance data for uncertainty analysis;
- IRSN: ENDF/B-VII.0 cross-sections, SCALE-6 for experiment analysis, and BERING code and COMMARA 2.0 covariance data for uncertainty analysis (only k_{eff} quantities provided);
- JAEA: JENDL-4 cross-sections, MVP for experimental analysis, and SAGEP code and JENDL-4 covariance data for uncertainty analysis;
- JSI: ENDF/B-VII.0 cross-sections, DANTSYS for experiment analysis, and SUSD3D system and COMMARA 2.0 covariance data for uncertainty analysis (only k_{eff} quantities were provided with the exclusion of JOYO MK-I). P_1 and S_4 with the built-in Gaussian quadrature constants were used in DANTSYS transport calculations;
- KAERI: ENDF/B-VII.0 cross-sections, DANTSYS for experiment analysis, DANTSYS/SUSD3D system and COMMARA 2.0 covariance data for uncertainty analysis (only k_{eff} quantities provided for uncertainty evaluation);
- ORNL: ENDF/B-VII.0 cross-sections, TSUNAMI-1D for experiment analysis, and TSURFER code and ORNL covariance data for uncertainty analysis (only 1D results analysed);
- PSI: JEFF3.1 cross-sections, ERANOS (in conjunction with corrective factors) for experimental analysis, and ERANOS and COMMARA 2.0 covariance data for uncertainty analysis.

In the following sections, the analysis of the participants' results is provided.

5.2 C/E's

Table 8 compares the (E-C)/C results provided by the participants expressed in %. For all k_{eff} values, with the exception of KAERI, the discrepancies between experimental and calculation results lie in a quite narrow range of ~250 pcm. This indicates that the current cross-section libraries are in very good agreement for the set of experiments selected for the exercise that are often used for the validation of these cross-section data sets.

However, one must not forget that k_{eff} is an integral quantity and therefore the agreement can be the result of cancellation of errors. One exception is F28/F25 of ZPR6-7.

The spectral indice discrepancies are contained in a more widespread range of 4%. There is still some disagreement between CEA and PSI results, both of which used the JEFF3.1 cross-section set. This could be due to differences during the cell calculations with the ECCO code. It should be noted that the general tendency for all cross-section sets is to underestimate the fission spectral indices results.

Finally, for sodium void results the discrepancy spread is within a ~6% range. It should be noted that both ENDF/B-VII.0 and JEFF3.1 cross-section sets have different signs between the spectral component experiment (Step 3) and the leakage component one (Step 5), while JENDL-4 overestimates the results in both cases.

5.3 Experimental and calculation uncertainties on C/E's

Table 9 shows the (quadratic) combination of experimental and calculation uncertainties on the C/E's provided by the participants. As indicated in the exercise, all the participants have adopted the same experimental uncertainties provided in the original documentation of the experiment benchmark models; therefore, the observed differences have to be attributed to the diverse assumptions the participants have taken on their calculation values. However, the following organisations have chosen not to apply any calculation uncertainties: CEA, JSI, and KAERI. IRSN has applied a constant 0.1% calculation uncertainty to seven k_{eff}, the only quantities they have considered for the exercise.

In general, the uncertainties are relatively low and quite consistent among the different participants. There are a few exceptions. For the sodium void reactivities, the participants that have adopted the Monte Carlo (instead of deterministic) codes have quite high uncertainties (~7%). This is due to the intrinsic (statistical) difficulty that stochastic methods encounter when confronted with small reactivity variations. It has to be kept in mind that for a reliable adjustment, it is necessary for both experimental and calculation uncertainties to stay as low as possible.

Low experimental uncertainties provide good quality results, thus giving credibility to the adjustment process. Low calculation uncertainties prevent the adjustment from compensating for shortcomings present in the calculation route. In other words, if the calculation uncertainties are high, there is a danger that the changes in the cross-sections coming from the adjustment are not physical, but the result of an artificial compensation. However, the integral data which have large calculation uncertainty do not have impact on the adjusted results, since the weight of the data become small and give fewer effects to the cross-section changes. There is a risk of underestimating the calculation uncertainty because, in such cases, the cross-sections are un-physically changed to force the adjusted C/E values to be 1.0.

Table 8: (E-C/C) results provided by the participants expressed in %

CORE	Quantity	ANL	CEA	INL	IRSN	JAEA	JSI	KAERI	ORNL	PSI
JEZEBEL239	k_{eff}	0.014	0.187	0.014	0.051	0.130	-0.091	-0.296	-0.001	0.059
JEZEBEL239	F28/F25	2.351	0.026	2.354	-	3.242	-	1.630	2.232	1.791
JEZEBEL239	F49/F25	2.534	1.412	2.533	-	1.667	-	2.019	2.570	1.539
JEZEBEL239	F37/F25	1.319	1.526	1.317	-	2.103	-	2.680	1.244	-0.013
JEZEBEL240	k_{eff}	0.019	-0.255	0.019	0.051	0.160	-0.235	-0.267	-0.079	-0.373
FLATTOP-PU	k_{eff}	-0.100	0.020	-0.097	-0.112	0.140	-0.953*	-0.944	-0.255	0.071
FLATTOP-PU	F28/F25	1.811	1.034	1.812	-	2.323	-	1.278	3.030	1.386
FLATTOP-PU	F37/F25	0.446	1.535	0.442	-	0.756	-	1.469	0.989	-0.697
ZPR6-7	k_{eff}	-0.040	-0.270	-0.043	-0.216	-0.527	-0.188	-0.091	-	-0.144
ZPR6-7	F28/F25	-0.446	4.207	-0.448	-	-3.251	-	1.183	-	-0.441
ZPR6-7	F49/F25	3.761	3.752	3.756	-	2.145	-	-1.320	-	4.244
ZPR6-7	C28/F25	-0.973	-0.445	-0.970	-	-1.643	-	-2.387	-	-0.467
ZPR6-7 240	k_{eff}	0.060	-0.221	0.063	-0.099	-0.329	-0.171	-0.003	-	-0.091
ZPPR-9	k_{eff}	0.080	0.005	0.078	-0.133	-0.210	-0.160	-0.133	-	0.004
ZPPR-9	F28/F25	2.985	3.664	2.987	-	1.750	-	0.948	-	4.104
ZPPR-9	F49/F25	1.956	2.417	1.958	-	0.080	-	1.131	-	2.480
ZPPR-9	C28/F25	-0.918	-0.334	-0.921	-	-1.845	-	-2.586	-	-0.372
ZPPR-9	Na Void Step 3	-1.887	-3.401	-1.884	-	-6.385	-	-4.585	-	-2.804
ZPPR-9	Na Void Step 5	2.752	3.126	2.754	-	-4.970	-	-6.978	-	2.759
JOYO MK-I	k_{eff}	0.249	0.083	0.255	0.219	0.180	-	-0.504	-	0.056

*Results very sensitive to S_NP_N order (S_6P_1:-0.81, S_8P_1:-0.48, $S_{12}P_1$:-0.24, $S_{16}P_1$:-0.15, $S_{48}P_3$:-0.17).

Table 9: Combination of experimental and calculation uncertainties on the C/E's (%)

CORE	Quantity	ANL	CEA	INL	IRSN	JAEA	JSI	KAERI	ORNL	PSI
JEZEBEL239	k_{eff}	0.201	0.200	0.201	0.224	0.202	0.200	0.200	0.200	0.224
JEZEBEL239	F28/F25	1.421	1.100	1.421	–	1.447	-	1.100	1.100	1.487
JEZEBEL239	F49/F25	0.949	1.400	0.949	–	1.172	-	0.900	0.900	1.345
JEZEBEL239	F37/F25	1.432	0.900	1.432	–	1.612	-	1.400	1.400	1.720
JEZEBEL240	k_{eff}	0.201	0.200	0.201	0.224	0.202	0.200	0.200	0.200	0.224
FLATTOP-PU	k_{eff}	0.303	0.300	0.302	0.316	0.302	0.300	0.300	0.300	0.316
FLATTOP-PU	F28/F25	1.860	1.100	1.860	–	1.384	-	1.100	1.100	1.487
FLATTOP-PU	F37/F25	1.432	1.402	1.432	–	1.561	-	1.400	1.400	1.720
ZPR6-7	k_{eff}	0.230	0.230	0.230	0.251	0.231	0.230	0.230	-	0.250
ZPR6-7	F28/F25	3.499	2.100	3.499	–	3.744	-	3.000	-	3.162
ZPR6-7	F49/F25	2.524	3.000	2.524	–	2.541	-	2.100	-	2.326
ZPR6-7	C28/F25	2.683	2.400	2.683	–	2.692	-	2.400	-	2.600
ZPR6-7 240	k_{eff}	0.221	0.220	0.221	0.242	0.222	0.220	0.220	-	0.241
ZPPR-9	k_{eff}	0.120	0.117	0.117	0.154	0.119	0.117	0.117	-	0.153
ZPPR-9	F28/F25	2.915	2.700	2.915	–	3.414	-	2.700	-	2.879
ZPPR-9	F49/F25	2.119	2.000	2.119	–	2.338	-	2.000	-	2.236
ZPPR-9	C28/F25	1.992	1.900	1.992	–	2.354	-	1.900	-	2.147
ZPPR-9	Na Void Step 3	7.737	1.900	7.737	–	5.593	-	1.900	-	4.225
ZPPR-9	Na Void Step 5	7.543	1.900	7.543	–	5.311	-	1.900	-	4.133
JOYO MK-I	k_{eff}	0.181	0.180	0.181	0.206	0.182	-	0.180	-	0.206

5.4 Nuclear data uncertainties

Table 10 illustrates the nuclear data uncertainties evaluated by the participants on the experimental quantities considered for the adjustment exercise. ORNL used ENDF/B-VII.0 covariance information that was collapsed to fit the 33-group format of the exercise. Six organisations (ANL, INL, IRSN, JSI, KAERI, and PSI) have used the same covariance data matrix, COMMARA 2.0. As one would expect that there is a good agreement among the results of these organisations with the exception of KAERI. The problem is likely related to the sensitivity coefficients (see related discussion in the chapter devoted to this subject).

In general, JENDL-4 showed consistently lower uncertainties values than COMMARA 2.0. Exceptions are the spectral indices of fission ^{239}Pu and ^{238}U capture, indicating that for these two reactions JENDL-4 carries larger variances than COMMARA 2.0. Uncertainties calculated by CEA using the COMAC covariance matrix are higher than corresponding results using COMMARA 2.0. The only exception is for ^{237}Np fission spectral indices. Quite remarkably, the k_{eff} uncertainty values span a range from ~1500 to ~2000 pcm. Relatively high values (up to more than 10%) are associated to the ^{238}U fission spectral indices.

Finally, concerning the uncertainties attached to the sodium reactivity coefficients, there is a fairly good agreement among all the participants. ZPPR9 Step 3 results lie in the range between 6 and 7%, and Step 5 results between 7 and 10%.

5.5 Uncertainty consistency for adjustment

In this section, we examine the consistency of the combined experimental, calculation, and nuclear data uncertainties with the observed discrepancies between experimental and calculation results. In order to establish this consistency let us define the adjustment margin ***AM***:

$$\boldsymbol{AM} = \boldsymbol{U^{ND}} + \boldsymbol{U^{\frac{C}{E}}} - \left|\frac{\boldsymbol{E}-\boldsymbol{C}}{\boldsymbol{C}}\right| \tag{5.1}$$

Where $\boldsymbol{U^{ND}}$ is the uncertainty associated to nuclear data, $\boldsymbol{U^{C/E}}$ is the quadratic combination of the experimental and calculation uncertainty, $\boldsymbol{E}$ is the experimental result and $\boldsymbol{C}$ the calculation one. The ***AM*** quantity indicates if the adjustment has sufficient margin to accommodate the **C/E** discrepancy. Of course, the **C/E** discrepancy has to take into account its associated uncertainty. If the ***AM*** values are negative, this implies that there is not enough uncertainty for the adjustment in the one sigma range. This will be reflected, afterwards, in the χ^2 values. One could interpret the appearance of negative values as a signal of some inconsistency in the covariance matrix (usually due to too low uncertainties associated to specific cross-sections). The ***AM*** quantity is relatively similar to the χ_i quantity used by JAEA (Equation (8) of Appendix A5 of [58]). The χ_i is used with a three-sigma-range criterion for deciding the elimination of an experiment from the adjustment. Table 11 reports the ***AM*** values for the different solutions provided by the participants.

Table 10: Uncertainties due to nuclear data (%)

CORE	Quantity	ANL	CEA	INL	IRSN	JAEA	JSI	KAERI	ORNL	PSI
JEZEBEL239	k_{eff}	0.640	2.072	0.636	0.611	0.693	0.658	0.117	1.186	0.511
JEZEBEL239	F28/F25	3.720	7.342	3.696	-	3.198	-	-	3.311	2.426
JEZEBEL239	F49/F25	0.830	2.811	0.823	-	0.625	-	-	0.809	0.719
JEZEBEL239	F37/F25	2.390	1.483	2.354	-	1.505	-	-	7.204	1.604
JEZEBEL240	k_{eff}	0.660	1.763	0.656	0.540	0.649	0.634	0.123	0.982	0.579
FLATTOP-PU	k_{eff}	0.760	1.913	0.764	0.519	1.257	0.719	0.123	1.128	0.829
FLATTOP-PU	F28/F25	3.120	7.885	3.093	-	2.936	-	-	2.616	1.948
FLATTOP-PU	F37/F25	2.050	1.585	2.034	-	1.444	-	-	7.076	1.421
ZPR6-7	k_{eff}	0.970	1.586	0.968	0.972	0.816	0.943	0.313	-	0.972
ZPR6-7	F28/F25	6.400	9.959	6.395	-	4.819	-	-	-	6.400
ZPR6-7	F49/F25	0.840	2.378	0.836	-	1.147	-	-	-	0.833
ZPR6-7	C28/F25	1.510	3.916	1.512	-	2.004	-	-	-	1.493
ZPR6-7 240	k_{eff}	0.970	1.559	0.971	0.970	0.812	0.948	0.311	-	0.973
ZPPR-9	k_{eff}	1.180	1.666	1.191	1.202	0.902	1.183	0.384	-	1.203
ZPPR-9	F28/F25	7.850	10.688	7.896	-	5.277	-	-	-	7.742
ZPPR-9	F49/F25	0.870	2.387	0.870	-	1.152	-	-	-	0.846
ZPPR-9	C28/F25	1.550	3.894	1.545	-	2.030	-	-	-	1.521
ZPPR-9	Na Void Step 3	7.670	6.493	7.563	-	5.950	-	-	-	7.228
ZPPR-9	Na Void Step 5	9.920	8.543	9.679	-	7.311	-	-	-	9.157
JOYO MK-I	k_{eff}	0.890	1.416	0.863	0.867	0.583	-	0.348	-	0.878

Table 11: Adjustment margin values *AM* expressed in %

CORE	Quantity	ANL	CEA	INL	IRSN	JAEA	JSI	KAERI	ORNL	PSI
JEZEBEL239	k_{eff}	0.827	2.085	0.823	0.784	0.764	0.767	0.021	1.385	0.676
JEZEBEL239	F28/F25	2.790	8.417	2.763	-	1.404	-	-	2.179	2.122
JEZEBEL239	F49/F25	-0.755	2.799	-0.761	-	0.129	-	-	-0.861	0.525
JEZEBEL239	F37/F25	2.503	0.857	2.469	-	1.014	-	-	7.360	3.311
JEZEBEL240	k_{eff}	0.842	1.708	0.838	0.726	0.691	0.598	0.056	1.103	0.430
FLATTOP-PU	k_{eff}	0.963	2.193	0.969	0.723	1.418	0.602	-0.521	1.173	1.075
FLATTOP-PU	F28/F25	3.169	7.950	3.141	-	1.997	-	-	0.686	2.048
FLATTOP-PU	F37/F25	3.036	1.452	3.024	-	2.249	-	-	7.487	2.444
ZPR6-7	k_{eff}	1.160	1.545	1.155	1.008	0.520	0.985	0.453	-	1.079
ZPR6-7	F28/F25	9.453	7.852	9.446	-	5.312	-	-	-	9.121
ZPR6-7	F49/F25	-0.397	1.626	-0.396	-	1.543	-	-	-	-1.085
ZPR6-7	C28/F25	3.220	5.871	3.225	-	3.053	-	-	-	3.626
ZPR6-7 240	k_{eff}	1.131	1.559	1.129	1.116	0.705	0.997	0.528	-	1.123
ZPPR-9	k_{eff}	1.220	1.778	1.230	1.224	0.811	0.957	0.368	-	1.352
ZPPR-9	F28/F25	7.780	9.724	7.825	-	6.941	-	-	-	6.516
ZPPR-9	F49/F25	1.033	1.970	1.031	-	3.410	-	-	-	0.602
ZPPR-9	C28/F25	2.625	5.460	2.616	-	2.539	-	-	-	3.296
ZPPR-9	Na Void Step 3	13.520	4.995	13.416	-	5.158	-	-	-	8.649
ZPPR-9	Na Void Step 5	14.711	7.317	14.468	-	7.653	-	-	-	10.531
JOYO MK-I	k_{eff}	0.822	1.513	0.789	0.854	0.585	-	0.024	-	1.029

There are only seven (highlighted in blue) negative values. The KAERI FLATTOP k_{eff} would be challenging to adjust in view of the associated quite large negative ***AM*** (-521 pcm). This is the result of different contributions: a quite unusually large initial C/E discrepancy (almost 1000 pcm), no calculation uncertainty provided, and, finally, the sensitivity coefficient problem previously mentioned. PSI has a relative high negative ***AM*** for the ^{239}Pu fission spectral index in ZPR-6-7, *a priori* indicating some difficulty in adjusting this integral parameter.

The ANL and INL four negative values are relative to the ^{239}Pu fission spectral indices and are likely due to the low uncertainty associated by COMMARA 2.0 to ^{239}Pu fission. The only negative value for CEA is associated to the fairly low uncertainty on ^{237}Np fission for COMAC previously observed in Section 5.4. For all these five negative ***AM*** values one should expect, after adjustment, a difficulty for the ***C/E*** to reach the unity value even including the new evaluated associated uncertainty in the one-sigma-range. This is indeed the case if one inspects such quantities after adjustment (see related chapter). The impact on χ^2 is not expected to be large for two reasons. First, the negative ***AM*** values are relatively low (<1% for spectral indices), and then, because the χ^2 is normalised to (divided by) the number of experiments (degrees of freedom). Having only one or two small inconsistencies will not appear in an adjustment with 20 experiments.

Equation (5.1) reveals that a not negligible role is played by the $\boldsymbol{U^{C/E}}$ term. As indicated in Section 5.3, the desirable situation is to have this quantity as low as possible in order to provide a reliable adjustment. Let us define the experiment merit ***EM,*** where in Equation (5.1) we suppress the term $\boldsymbol{U^{ND}}$. In this investigation positive values are targeted. Positive ***EM*** will indicate that the experiment does not provide enough useful information (i.e. has not enough merit to be included in the adjustment) because there is too much uncertainty associated to the observed ***C/E***. In practice, these experiments could be excluded from the adjustment because they are not valuable either for poor experimental quality or/and because the employed calculation analysis carries too much uncertainty, or kept in order to provide a constraint that should not be changed by the adjustment.

In all fairness, in terms of usefulness of an experiment, correlations in the experimental uncertainties should be established and one should examine also the case where only the experimental uncertainty is considered. In fact, the calculation uncertainty component depends on circumstances independent from the experiment. Besides, another criterion for retaining or discarding an experiment would be to examine their correlation through the cross product of sensitivities weighted with the covariance matrix (the so-called representativity factor). If the correlation factor is very close to 1, one of the two experiments should be discarded as it provides redundant information (unless the configurations are not experimentally correlated), and kept only for *a posteriori* verification with the new adjusted cross-sections and covariance matrix data.

On the other hand, because ***EM*** values neglect the uncertainty coming from the nuclear data $\boldsymbol{U^{ND}}$, this could, in some circumstances, lead to misleading conclusions about the usefulness of an experiment. In particular, let us consider the case where there is a very good agreement between calculation and experimental results so that the ***E-C/C*** is almost zero, and, therefore, ***EM*** is positive. If the initial nuclear data uncertainties are greater than the $\boldsymbol{U^{C/E}}$, still the resulting *a posteriori* uncertainty will be reduced, after adjustment, for the experiment under consideration. Therefore, one has to be very careful in drawing conclusions, and, undoubtedly, this subject of experimental selection deserves further investigations.

EM values corresponding to the benchmark solutions provided by participants are shown in Table 12. This table provides the following conclusions regrouped by type of integral parameters:

- Critical Masses – For organisations using ENDF/B-VII.0 cross-sections only the JOYO experiment provides a useful contribution to the adjustment. This can be readily seen examining the column of IRSN that has considered only critical masses due the good performance of ENDF/B-VII.0 for Pu-fuelled fast cores, while the significant amount of ^{235}U in JOYO requires an adjustment (in particular for the capture, as will be explained in Chapter 7). In contrast, organisations using JEFF3.1 (CEA, and PSI) and JENDL-4 (JAEA) perform well for JOYO. CEA will take advantage of adjustment associated to the discrepancies in k_{eff} of JEZEBEL ^{240}Pu (and not so much with ^{239}Pu), ZPR6-7 but not for the harder cores (FLATTOP). The exact opposite is true for JAEA (good agreement for harder cores, adjustment needed for softer cores). It is not clear why for PSI, that uses JEFF3.1, the Pu-fuelled cores do not need any adjustment.
- Spectral Indices – ^{238}U capture spectral indices have positive ***EM*** values for everybody (with exception of KAERI), and, therefore, it seems not to provide any contribution to the adjustment except as a constraint. For the fission spectral indices the situation is more complex. ^{238}U fission spectral indices require adjustments in harder cores practically for all participants, while JEFF3.1 needs it also for softer cores. ^{239}Pu fission indices need adjustment in all cores. One exception is JAEA, which has positive ***EM*** values for the ZPR6-7 and ZPPR-9 cores, indicating that the adjustment needed for the Pu-fuelled softer cores k_{eff} does not concern the ^{239}Pu fission but rather some other reactions (or isotope). For ^{237}Np fission spectral indices the situation is mixed. These spectral indices are not important for the adjustment of ENDF/B-VII.0 users, while action is needed for CEA on both JEZEBEL and FLATTOP, and JAEA (but only for JEZEBEL). The fact that PSI has positive ***EM*** values for these indices indicates that the institute is probably using a version of JEFF3.1 with different ^{237}Np cross-sections with respect to CEA.
- Sodium Void Reactivity Coefficients – ENDF/B-VII.0 does not benefit from these experiments, the main reason being the high uncertainties associated to the ***C/E's***. JAEA will use the information from the experiment dominated by the central component, while CEA will also benefit from that dominated by the leakage component. There is no agreement on the ***EM*** values of CEA and PSI. This time, the indication is that they are probably using different ^{23}Na cross-sections.

Table 12: Experiment merit values *EM* expressed in %

CORE	Quantity	ANL	CEA	INL	IRSN	JAEA	JSI	KAERI	ORNL	PSI
JEZEBEL239	k_{eff}	0.187	0.013	0.187	0.173	0.072	0.109	-0.096	0.199	0.165
JEZEBEL239	F28/F25	-0.930	1.074	-0.933	-	-1.795	-	-0.530	-1.132	-0.305
JEZEBEL239	F49/F25	-1.585	-0.012	-1.584	-	-0.496	-	-1.119	-1.670	-0.193
JEZEBEL239	F37/F25	0.113	-0.626	0.115	-	-0.491	-	-1.280	0.156	1.707
JEZEBEL240	k_{eff}	0.182	-0.055	0.182	0.186	0.042	-0.035	-0.067	0.121	-0.149
FLATTOP-PU	k_{eff}	0.203	0.280	0.205	0.204	0.162	0.188	-0.644	0.045	0.245
FLATTOP-PU	F28/F25	0.049	0.066	0.048	-	-0.939	-	-0.178	-1.930	0.100
FLATTOP-PU	F37/F25	0.986	-0.133	0.990	-	0.805	-	-0.069	0.411	1.023
ZPR6-7	k_{eff}	0.190	-0.040	0.187	0.035	-0.296	0.042	0.139	-	0.106
ZPR6-7	F28/F25	3.053	-2.107	3.051	-	0.493	-	1.817	-	2.721
ZPR6-7	F49/F25	-1.237	-0.752	-1.232	-	0.396	-	0.780	-	-1.918
ZPR6-7	C28/F25	1.710	1.955	1.713	-	1.050	-	0.013	-	2.133
ZPR6-7 240	k_{eff}	0.161	-0.001	0.158	0.143	-0.107	0.049	0.217	-	0.150
ZPPR-9	k_{eff}	0.040	0.112	0.039	0.021	-0.091	-0.226	-0.016	-	0.149
ZPPR-9	F28/F25	-0.070	-0.964	-0.071	-	1.664	-	1.752	-	-1.225
ZPPR-9	F49/F25	0.163	-0.417	0.161	-	2.257	-	0.869	-	-0.244
ZPPR-9	C28/F25	1.075	1.566	1.071	-	0.509	-	-0.686	-	1.775
ZPPR-9	Na Void Step 3	5.850	-1.501	5.853	-	-0.792	-	-2.685	-	1.421
ZPPR-9	Na Void Step 5	4.791	-1.226	4.789	-	0.341	-	-5.078	-	1.374
JOYO MK-I	k_{eff}	-0.068	0.097	-0.074	-0.013	0.002	-	-0.324	-	0.150

In contrast to ***EM***, let us define the theoretical adjustment margin ***TAM*** where in Equation (5.1) we suppress the $\boldsymbol{U^{C/E}}$ term. This corresponds to the ideal situation where we have perfect measured experiment and perfect calculation tools with no error or uncertainty associated. Even though this is a more academic exercise, the negative ***TAM*** values can provide stronger recommendations for the quality of the covariance data. Again negative ***TAM*** will point out the inability of the covariance data to accommodate the adjustment, where now all the discrepancies have to be attributed to shortcomings in the nuclear data. Table 13 shows the ***TAM*** values for the solutions provided by the participants. As expected, there are more negative ***TAM*** values than ***AM*** ones. If one excludes the columns of KAERI and ORNL (very low or zero $\boldsymbol{U^{ND}}$ values for the reasons previously indicated), it is quite striking that the rows for the ^{239}Pu fission spectral indices have practically all negative ***TAM*** values. This stresses out that all cross-section files have overly optimistic uncertainties for ^{239}Pu fission cross-sections.

Another good reason for examining the ***TAM*** values is the following: if the method uncertainty is very large, the ***AM*** and χ_i, quoted above, would suggest that an experiment is still useful for the adjustment, despite the fact that the use of better methods (e.g. with fewer approximations) would make clear that the specific experiment is not useful. In other words, why should one compensate weaknesses of the calculation methods with cross-section modifications? This compensation effect was an early criticism to any statistical adjustment method.

One should bear in mind that the method uncertainty reduction is a necessary condition in order to provide unambiguous indications on the integral experiment selection. This is also consistent with the fact that in most cases what we call "method uncertainty" is, in fact, more a systematic uncertainty or even a bias, with rather limited "statistical" meaning. This is especially true when deterministic methods are used in the experiment analysis. When stochastic methods are used the uncertainty is more statistical in nature, provided that the Monte Carlo code employed in the analysis has no errors or computational approximation (e. g. treatment of unresolved resonances in early versions of MCNP4).

5.6 Target system uncertainties

In this section, we will examine the uncertainty analysis on target systems, as defined in Chapter 1, using the unadjusted covariance matrix data. Five organisations have provided solutions. In what follows the details associated with these solutions are provided:

- ANL: Covariance matrix COMMARA 2.0. Uncertainties with breakdown by isotope and reaction provided for k_{eff} only of the four target systems: ABR oxide, JAEA FBR, ABR metal, and ABR oxide with recycled compositions;
- CEA: Covariance matrix COMAC. Uncertainties with breakdown by isotope and reaction provided for k_{eff} only of the four target systems;
- INL: Covariance matrix COMMARA 2.0. Uncertainties with breakdown by isotope and reaction provided for k_{eff} and sodium void of the four target systems;
- JAEA: Covariance matrix JENDL-4. Uncertainties, with no breakdown, provided for k_{eff} only of the three target systems: ABR oxide, JAEA FBR, and ABR metal;
- PSI: Covariance matrix COMMARA 2.0. Uncertainties with breakdown by isotope and reaction provided for k_{eff} of the four target systems and for the sodium void of the FBR on the basis of finite difference, discrete ordinates P_1S_4 calculations in (r,z) geometry with JEFF-3.1 data. Neither fission spectrum uncertainties nor fission product data are considered.

Table 14 reports the total uncertainties provided by the four organisations by reactor and integral quantities.

ANL and INL have very comparable results because they use practically the same data and tools. The only existing difference is that ANL has included also the mu-bar effect. The general behaviour is that the lower values are attached to the JENDL-4 calculations, while the highest ones are relative to COMAC. ANL and CEA have not introduced minor actinides (e. g. ^{244}Cm and ^{245}Cm) in their analysis for the ABR oxide core with recycling. In fact, the aim of considering this system in the exercise was to show that, after adjustment, the minor actinides would provide a bigger contribution to total uncertainty because they were not adjusted.

JAEA has not provided a breakdown by reaction and isotope, and, therefore, a more detailed analysis cannot be carried out. However, we can make some more detailed comparisons between the COMMARA 2.0 (we use ANL results and PSI ones) and COMAC (CEA results) uncertainty evaluation. In Tables 15-17, the breakdown (in terms of reactions) comparison for the ABR oxide, JAEA FBR, and ABR metal k_{eff} cases is provided for selected isotopes with the largest contributions to total uncertainties.

In all three cases the trends are very similar. For COMAC the largest contribution by far, comes from ^{239}Pu fission (more than 5 times the corresponding uncertainty in COMMARA), whereas the COMMARA uncertainty is dominated by the ^{238}U inelastic. While the total uncertainty in ^{238}U is comparable, in COMAC the capture and fission are significantly larger, with the opposite happening for the inelastic term. Other notable trends are: larger ν and χ contribution for ^{239}Pu in COMAC, larger ^{240}Pu capture and χ, ^{56}Fe elastic and inelastic, and ^{16}O capture (n,α) in COMMARA. COMAC shows a not negligible ^{241}Pu χ contribution for the JAEA FBR case that is not present in COMMARA.

The PSI and ANL independent calculations are similar except for the basic cross-sections. This is reflected in similar uncertainties except for ^{56}Fe.

Table 13: Theoretical adjustment margin values *TAM* expressed in %

CORE	Quantity	ANL	CEA	INL	IRSN	JAEA	JSI	KAERI	ORNL	PSI
JEZEBEL239	k_{eff}	0.626	1.885	0.622	0.560	0.562	0.567	-0.179	1.185	0.453
JEZEBEL239	F28/F25	1.369	7.317	1.342	-	-0.043	-	-	1.079	0.635
JEZEBEL239	F49/F25	-1.704	1.399	-1.710	-	-1.042	-	-	-1.761	-0.820
JEZEBEL239	F37/F25	1.071	-0.043	1.037	-	-0.599	-	-	5.960	1.591
JEZEBEL240	k_{eff}	0.641	1.508	0.637	0.502	0.489	0.398	-0.144	0.903	0.207
FLATTOP-PU	k_{eff}	0.660	1.893	0.667	0.407	1.116	0.462	-0.821	0.873	0.759
FLATTOP-PU	F28/F25	1.309	6.850	1.281	-	0.613	-	-	-0.414	0.562
FLATTOP-PU	F37/F25	1.604	0.050	1.592	-	0.688	-	-	6.087	0.724
ZPR6-7	k_{eff}	0.930	1.315	0.925	0.757	0.289	0.755	0.223	-	0.828
ZPR6-7	F28/F25	5.954	5.752	5.947	-	1.568	-	-	-	5.958
ZPR6-7	F49/F25	-2.921	-1.374	-2.920	-	-0.998	-	-	-	-3.411
ZPR6-7	C28/F25	0.537	3.471	0.542	-	0.361	-	-	-	1.026
ZPR6-7 240	k_{eff}	0.910	1.339	0.908	0.871	0.483	0.777	0.308	-	0.882
ZPPR-9	k_{eff}	1.100	1.661	1.113	1.069	0.692	0.840	0.251	-	1.198
ZPPR-9	F28/F25	4.865	7.024	4.909	-	3.526	-	-	-	3.637
ZPPR-9	F49/F25	-1.086	-0.030	-1.088	-	1.072	-	-	-	-1.634
ZPPR-9	C28/F25	0.632	3.560	0.624	-	0.185	-	-	-	1.149
ZPPR-9	Na Void Step 3	5.783	3.095	5.679	-	-0.434	-	-	-	4.424
ZPPR-9	Na Void Step 5	7.168	5.417	6.925	-	2.341	-	-	-	6.398
JOYO MK-I	k_{eff}	0.641	1.333	0.608	0.648	0.402	-	-0.156	-	0.823

Table 14: Uncertainties of target systems (pcm for k_{eff}, % for Na void)

Reactor	Parameter	ANL	CEA	INL	JAEA	PSI
ABR Oxide	k_{eff}	882	1554	830	778	939
	Na void	-	-	8.7	-	-
JAEA FBR	k_{eff}	1018	1311	1015	804	1114
	Na void	-	-	10.6	-	5.3
ABR Metal	k_{eff}	1008	1744	969	810	1069
	Na void	-	-	7.7	-	-
ABR Oxide Recycled	k_{eff}	1016	1245	1042	-	1136
	Na void	-	-	7.6	-	-

Table 15: ABR oxide k_{eff} uncertainty breakdown by reaction and isotope (pcm)

Isotope	Covariance	σ^{capt}	σ^{fiss}	σ^{elas}	σ^{inelas}	υ	χ	Total
^{238}U	COMMARA (ANL)	294	32	116	577	119	-	669
	COMMARA (PSI)	285	33	116	642	125	-	724
	COMAC	561	259	-36	311	-	-	690
^{239}Pu	COMMARA (ANL)	326	235	33	79	75	174	453
	COMMARA (PSI)	324	244	31	65	77	-	419
	COMAC	271	1306	11	21	142	310	1377
^{240}Pu	COMMARA (ANL)	64	47	5	17	87	25	125
	COMMARA (PSI)	61	53	6	19	93		124
	COMAC	34	23	5	17	30	41	68
^{16}O	COMMARA (ANL)	107	-	38	2	-	-	113
	COMMARA (PSI)	153	-	47	2	-	-	160
	COMAC	27	-	30	1	-	-	40
^{56}Fe	COMMARA (ANL)	50	-	167	155	-	-	286*
	COMMARA (PSI)	166	-	274	155	-	-	356
	COMAC	154	-	71	64	-	-	181
^{23}Na	COMMARA (ANL)	2	-	19	78	-	-	111*
	COMMARA (PSI)	2	-	21	77	-	-	80
	COMAC	13	-	12	39	-	-	42
^{52}Cr	COMMARA (ANL)	20	-	44	19	-	-	53
	COMMARA (PSI)	22	-	51	17	-	-	58
	COMAC	8	-	29	17	-	-	35

* The quadratic sum includes contributions coming from the mu-bar uncertainty.

Table 16: JAEA FBR k_{eff} uncertainty breakdown by reaction and isotope (pcm)

Isotope	Covariance	σ^{capt}	σ^{fiss}	σ^{elas}	σ^{inelas}	υ	χ	Total
^{238}U	COMMARA (ANL)	319	36	169	784	138	-	875
	COMMARA (PSI)	327	38	176	882	147	-	969
	COMAC	596	324	-74	414	-	-	790
^{239}Pu	COMMARA (ANL)	244	176	23	71	56	148	348
	COMMARA (PSI)	252	186	22	59	59	-	326
	COMAC	195	953	6	19	104	242	1008
^{240}Pu	COMMARA (ANL)	132	105	12	45	192	63	267
	COMMARA (PSI)	131	118	13	51	207	-	277
	COMAC	74	49	11	45	65	98	154
^{241}Pu	COMMARA (ANL)	101	81	1	22	38	-	136
	COMMARA (PSI)	130	87	2	6	41	-	161
	COMAC	120	79	1	6	37	121	191
^{16}O	COMMARA (ANL)	126	-	54	3	-	-	137
	COMMARA (PSI)	185	-	65	3	-	-	196
	COMAC	32	-	35	2	-	-	47
^{56}Fe	COMMARA (ANL)	88	-	44	105	-	-	144*
	COMMARA (PSI)	86	-	50	105	-	-	145
	COMAC	85	-	21	43	-	-	97
^{23}Na	COMMARA (ANL)	2	-	22	83	-	-	103*
	COMMARA (PSI)	2	-	30	81	-	-	86
	COMAC	11	-	20	38	-	-	44

* The quadratic sum includes contributions coming from the mu-bar uncertainty.

Table 17: ABR metal k_{eff} uncertainty breakdown by reaction and isotope (pcm)

Isotope	Covariance	σ^{capt}	σ^{fiss}	σ^{elas}	σ^{inelas}	υ	χ	Total
^{238}U	COMMARA (ANL)	221	41	183	759	150	-	826
	COMMARA (PSI)	212	41	177	814	151		874
	COMAC	684	268	-120	376	-	-	812
^{239}Pu	COMMARA (ANL)	238	250	43	78	77	201	421
	COMMARA (PSI)	238	255	39	79	78	-	368
	COMAC	195	1474	17	23	143	330	1530
^{240}Pu	COMMARA (ANL)	32	39	5	5	13	21	88
	COMMARA (PSI)	30	43	5	15	72	-	90
	COMAC	22	16	5	12	29	35	55
^{56}Fe	COMMARA (ANL)	152	-	253	167	-	-	348*
	COMMARA (PSI)	150	-	410	158	-	-	464
	COMAC	122	-	118	60	-	-	180
^{23}Na	COMMARA (ANL)	2	-	24	73	-	-	144*
	COMMARA (PSI)	2	-	42	74	-	-	86
	COMAC	11	-	17	37	-	-	42
^{52}Cr	COMMARA (ANL)	20	-	79	19	-	-	84
	COMMARA (PSI)	21	-	85	16	-	-	89
	COMAC	6	-	53	16	-	-	55

* The quadratic sum includes contributions coming from the mu-bar uncertainty.

6. Adjustment procedures

This chapter summarises the nuclear data adjustment methodologies used by the participants to the benchmark exercise and the main conclusions of the assessment of these methodologies performed by the members of Subgroup 33. A "teaching example" of the adjustment method is provided in Appendix E. More detailed information on the adjustment methodologies used by ANL, CEA, INL, IPPE, JAEA, JSI, NRG and ORNL is available in [58]. PSI has adopted the JAEA adjustment methodology and the documentation on the methodology used by IRSN is available in Appendix F.

6.1 General description

Let $\vec{E} = \overrightarrow{E_i}$ ($i = 1 \ldots N_E$) denote some experimental integral variables, and let $\vec{\sigma} = \overrightarrow{\sigma_i}$ ($i = 1 \ldots N_\sigma$) denote the multi-group parameters defining the model used to simulate these integral experiments, and $\vec{C}(\sigma)$ the associated calculated values to be compared with $\vec{E}$. Let $\vec{\sigma}_m$ and M_σ define the *a priori* expectation and covariance matrix of the multi-group parameters, and M_E define the experimental covariance matrix, including analytical modelling covariance information, when appropriate. The evaluation of posterior expectation and covariances is done by finding the minimum of the following cost function (a generalised least-square):

$$\chi^2_{GLS} = (\vec{\sigma} - \vec{\sigma}_m)^t M_\sigma^{-1} (\vec{\sigma} - \vec{\sigma}_m) + \left(\vec{E} - \vec{C}(\sigma)\right)^t M_E^{-1} \left(\vec{E} - \vec{C}(\sigma)\right).$$

Information related to integral simulations is included in the $\vec{C}$ values as well as in their derivatives with respect to the multi-group parameters. Using a first order approximation, one can write:

$$\vec{C}(\sigma) = \vec{C}(\sigma_m) + S \cdot (\vec{\sigma} - \vec{\sigma}_m).$$

S is a matrix ($N_E \times N_\sigma$) of calculated derivatives supposed to be constant (when the cross-sections slightly change). Most of the time, S is referred to relative sensitivity coefficients:

$$S_{ij} = \frac{\delta C_i / C_i}{\delta \sigma_j / \sigma_j}.$$

From a mathematical point of view, the method is quite general and has been extensively used for many kinds of inverse problems. In the field of reactor physics, this approach has been already applied to validate and/or further improve the nuclear data used in the simulation of thermal and fast reactors.

6.2. Assessment of participants' methods

The methodology adopted by each participant to adjust the differential nuclear data using the information from integral experiments was reported and compared in Table 18 [58].

Table 18: Comparison of adjustment methodology by participants [57]

Organization	Theory	Basic equation	Reference
ANL (USA)	Generalized least-square method	$\delta = C_p S^T (SC_p S^T + C_E)^{-1} E$ $C_p' = C_p - C_p S^T (SC_p S^T + C_E)^{-1} SC_p$	Poenitz, "GMADJ", 1980
CEA (France)	Bayes' theorem method	$\vec{\sigma} - \vec{\sigma}_m = M_\sigma \cdot S^T (M_E + S \cdot M_\sigma \cdot S^T)^{-1} \cdot (\vec{E} - \vec{C}(\sigma_m))$ $M_{\sigma'} = M_\sigma - M_\sigma \cdot S^T (M_E + S \cdot M_\sigma \cdot S^T)^{-1} \cdot S \cdot M_\sigma$	Gandini, Symposium,Tokyo, 1973
INL (USA)	Lagrange multiplier's method	$\tilde{y} - y = -(I - B_y A^T G^{-1} A)v$ $B_{\tilde{y}} = (I - B_y A^T G^{-1} A) B_y (I - B_y A^T G^{-1} A)^T$	Gandini, "AMARA", 1973
IPPE (Russia)	Maximum likelihood method	$C' - C = WH^T (V + HWH^T)^{-1} (I - I_p)$ $W' = W - WH^T (V + HWH^T)^{-1} HW$	Manturov, "INDECS", 1984
JAEA (Japan)	Baysian parameter-estimation method	$T' = T_0 + MG^t \left[GMG^t + V_e + V_m\right]^{-1} \left[R_e - R_c(T_0)\right]$ $M' = M - MG^t \left[GMG^t + V_e + V_m\right]^{-1} GM$	Dragt, NSE 62, 1977
JSI (Slovenia)	Partitioned least-square method	ZOTT-99 code	Muir, NSE 101, 1989
NRG (Netherlands)	Total Monte Carlo method	TALYS, NJOY and MCNP codes	Koning, Annals N.E. 35, 2008
ORNL (USA)	Generalized linear least-square method	$\Delta\alpha = -\left[C_{\alpha\alpha} S_k^T \left(S_k C_{\alpha\alpha} S_k^T + F_{m/k} C_{mm} F_{m/k}\right)^{-1}\right] \vec{d}$ $C_{\alpha'\alpha'} = C_{\alpha\alpha} - \left[C_{\alpha\alpha} S_k^T \left(S_k C_{\alpha\alpha} S_k^T + F_{m/k} C_{mm} F_{m/k}\right)^{-1} S_k C_{\alpha\alpha}\right]$	Broadhead, NSE 146, 2004

The following observations can be made:

- Eight organisations (ANL, CEA, INL, IPPE, JAEA, JSI, IRSN and PSI) apply equivalent equations for the adjustment, though the names of the theory differ.
- ORNL uses similar equations as the above organisations. However, a correction factor ($F_{m/k}$) is applied to the covariance matrix of integral experiments to account for the E/C discrepancy.
- The NRG approach is completely different. It is based on the Total Monte Carlo method to produce thousands of TALYS-based evaluated files using MC sampling of nuclear parameters. The so-called Petten method solves the inverse problem of nuclear data adjustment by selecting the optimal combination of random files that best reproduce all integral experiments.

Criteria for assessing the different methodologies have been defined and agreed upon among participants. These criteria (in the form of questions) have been submitted to the participants and the responses are provided in [58].

We briefly summarise here the main characteristics that emerge from the answers of the participants.

What is the rank of the matrix (or matrices) to be inverted?

All methodologies end up inverting a matrix that has the rank of the integral experiments used in the adjustment. This, of course, minimises the number of operations as the number of cross-sections to be adjusted is larger than the number of integral experiments used.

Does the adjustment procedure use an iterative method?

Only JSI uses an iterative Gauss-Newton method for explicit treatment of non-linear effects.

Is there any computational limitation (number of variables, experiments, etc.)?

No limitations from the computer power are imposed, except those dictated by the coding of the programme, e.g. JSI has a limitation of 3 600 integral experiments.

What is a typical running time for a defined number of variables/experiments?

Today, computing time is no longer an issue and has become quite negligible. For a reasonable number of variables only a few seconds are needed.

Are all cross-sections taken into account?

Participants consider all cross-sections, except INL that limits the number of adjusted parameters using criteria based on the product of sensitivity coefficients and nuclear data covariances.

Are all reactions taken into account (e.g. fission prompt and delayed neutron spectra/data)?

Generally, all participants are able to treat all reactions if specified by the user and if associated sensitivity coefficients and covariances are provided.

Can self-shielding effects be explicitly treated?

JAEA, ORNL and IRSN can explicitly treat the self-shielding. CEA can do so only for nuclear parameter adjustment, not for multi-group. ANL, INL and IPPE can treat the self-shielding factors as separate variables in the adjustment. JSI cannot treat it.

Can high-order effects be taken into account?

Most participants can treat higher-order effects only through an iterative, mostly manual, application of the adjustment procedure. This is due to the inherent linear characteristic of the sensitivity coefficients. Only JSI can directly treat non-linear effects through the Gauss-Newton method.

Can method uncertainties/bias be accounted for?

Only JAEA treats this directly through explicit inclusion of the calculation uncertainty in the adjustment methodology. Other participants include it in the C/E uncertainty.

How are inelastic matrices and secondary energy distributions treated?

In most cases, the total inelastic cross-section is adjusted. Secondary energy distribution is adjusted depending on the capability of calculating associated sensitivity coefficients with stochastic codes and on the capability of evaluating associated covariance matrices.

Is a consistency test present?

All participants use a χ^2 test to check the consistency of nuclear data and integral information. In the JSI code, there is an option to alter the diagonal element of the input covariance matrix to assign lower weight to inconsistent experiments.

Are cross-correlations among nuclear data and integral experiments taken into account?

Yes, for all participants when related data are provided.

Are correlations among nuclear data and experiments taken into account?

Only INL can treat this correlation, but these are not common data.

Is a new covariance data set produced?

All participants produce a new covariance data set after adjustment.

Is the solution unique (local minima)?

All participants that use non-iterative methods in the adjustment produce a unique solution, which should correspond to the minimum. When applying a non-linear technique JSI can produce local minima.

7. Adjustment analysis

7.1 Introduction

The comparison of the adjustment exercises and to draw a conclusion can be very difficult due to the great number of results given by several laboratories.

Thus, we will focus on several methods of presenting and analysing the results on cross-sections:

- analyse adjustment results only within an adjustment made by each participant to ensure that the adjustment shows coherent trends with respect to uncertainties;
- compare results where everything is different: Phase I;
- compare results having fixed one or several parts of the adjustment: that may be the covariances (Phase II) or covariances and initial nuclear data library (Phase II-bis);
- add or remove from the adjustment a few elements (such as spectrum), keep/do not keep some experiments, experimental correlations or not for one chosen adjustment activity (i.e. CEA here);
- present analysis related to change on initial C/E values to infer the influence of initial starting points in order to complement what was initiated in this sub-group.

To treat Gigabytes of results on covariances, ad-hoc plots will also be presented to synthesise the number of results.

To analyse the effect of each experiment and some influent nuclear data, the concept of Cook's distance (commonly used in regression analysis) is proposed.

In addition, in this analysis only laboratories having done the whole adjustment exercise will be discussed: ANL/INL, JAEA, CEA and PSI. A few additional points may be added when considered as exemplary compared with other laboratories results. Furthermore, as INL and ANL have the same results (having the same inputs), conclusions given for each of them will stand for both. The detailed benchmark results are available on the NEA website as Appendix G.

7.2 General analysis

7.2.1 C/E's impacts and final results

First, general considerations will be reviewed with respect to C/E's before and after adjustment on benchmarks and their related uncertainties.

The deviations from unity of C/E's are, in fact, due to the following key points:

- Correction factors C/C' are not sufficient: C values display discrepancies far from the "true" (in terms of validation to Monte-Carlo) reference calculation (example of quadrature choices for PSI calculation are in this sense important);
- C values reflect the direct impact of the nuclear data individually or the indirect impact of the whole library (especially for k_{eff}).

In principle, if C/C' values are properly calculated and with no residual biases, one should expect that several different nuclear data libraries should converge to the same nuclear data sets, within the limits of the nuclear data uncertainties.

For teams not doing the whole exercise (i.e. having their own reference calculation) the fact that correction factors were estimated with MCNP and ENDF nuclear data library might be important. The latter might present a problem as other libraries may give different reference C/E values (MCNP+JENDL for example). It was shown [2] by comparing two data sets of the same nuclear data library (ENDF/B-VI and ENDF/B-VII), that this problem had low influence. Nevertheless, it needs to be pointed out that:

- Some corrective factors may not be sufficient for having the proper C/E's: if the deterministic modelling is far from what is proposed by INL (ERANOS+S_4P_1), an additional extra correction factor may be required.
- Even so, in some cases the nuclear data library may have an impact on correction factors.

ANL/INL

Figure 24 shows initial and final C/E-1 with respect to initial/final calculated uncertainties for ANL/INL results.

Figure 24: ANL/INL C/E comparison before and after adjustment

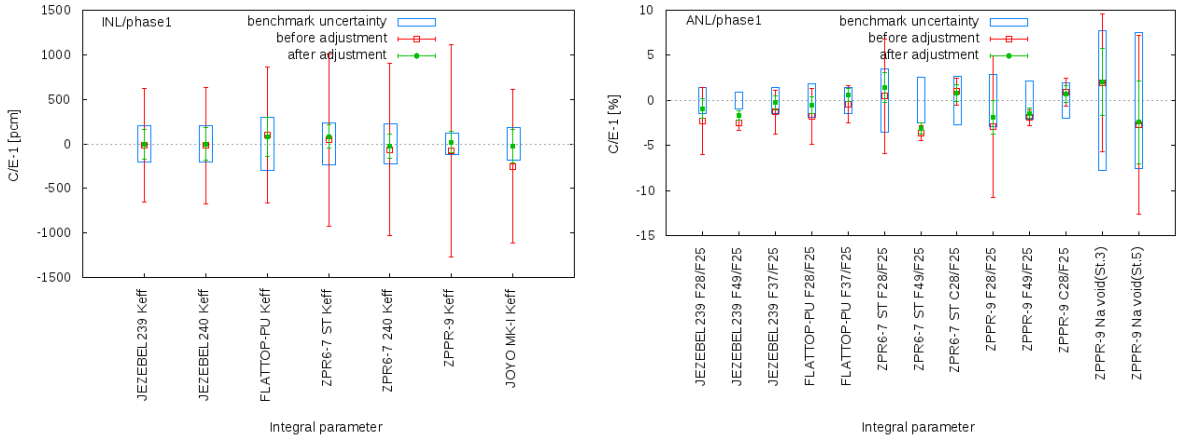

JAEA

Figure 25 shows initial and final C/E-1 with respect to initial/final calculated uncertainties for JAEA results.

Figure 25: JAEA C/E comparison before and after adjustment

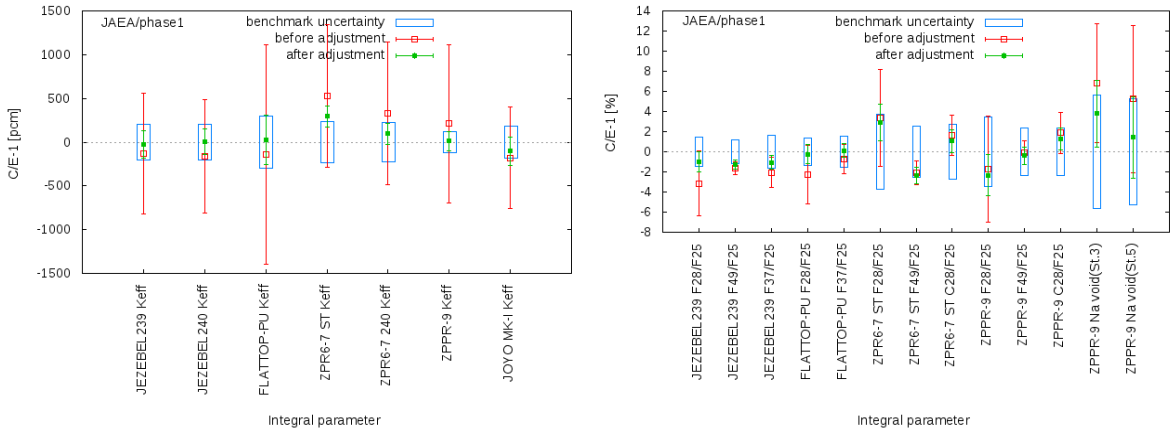

CEA

Figure 26 shows initial and final C/E-1 with respect to initial/final calculated uncertainties for JAEA results.

Figure 26: CEA C/E comparison before and after adjustment

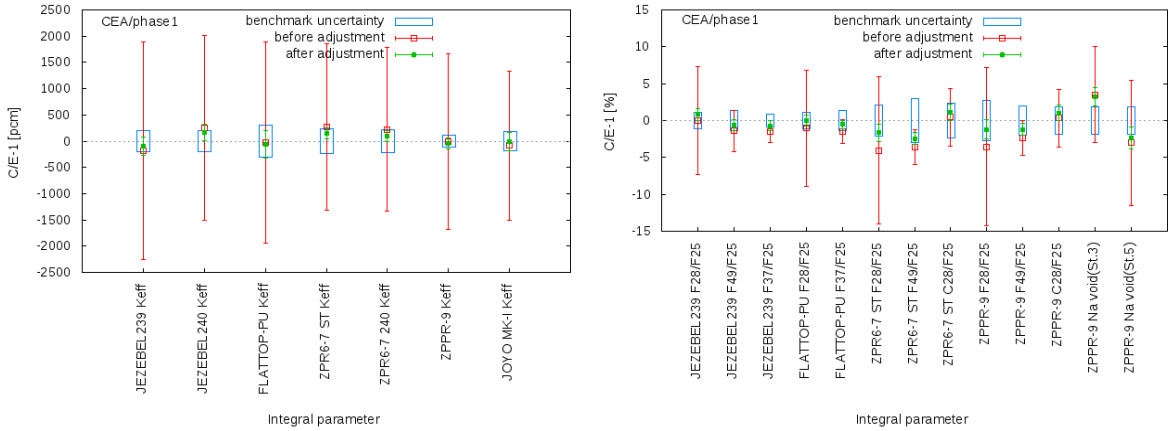

PSI

Figure 27 shows initial and final C/E-1 with respect to initial/final calculated uncertainties for PSI results.

Figure 27: PSI C/E comparison before and after adjustment

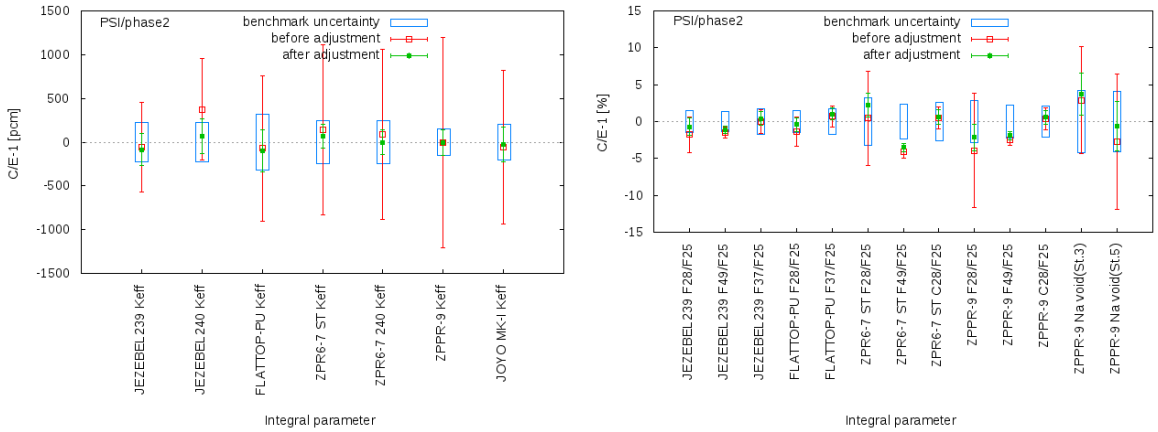

Comparisons

As Figures 24, 25, 26, and 27 show, each adjustment exercise of Phase I gives consistent results:

- All integral experiments information is assimilated by the adjustment exercise: no outlier remains (except the ZPPR9-Na void cases for CEA, but still within 1σ uncertainty);
- *A posteriori* uncertainties are coherent with experimental given uncertainties →no overt uncertainty reduction appears;
- ANL/INL, JAEA, CEA and PSI come to an end with similar *a posteriori* uncertainties.

In addition, we can see that ANL/INL/PSI initial C/E's were rather close to unity: the final results do not show big changes after adjustments. In contrast, for JAEA and CEA, the general overall C/E's after adjustment are far better. Furthermore, JAEA and CEA initial C/E shows more or less the same initial discrepancies (signs of C/E-1 equal) but not always with the same magnitude. These C/E's different initial values between ANL/INL and JAEA/CEA reveal some hints of what happened in detail on cross-sections adjustment trends.

Finally, Phase II and Phase II-bis do not exhibit additional behaviours. Nevertheless, this absence of effect in final C/E's is quite important to notice. Figure 28 shows the JAEA results in terms of C/E's by using INL *a priori* covariances (Phase II).

Figure 28: JAEA Phase I and Phase II integral calculations

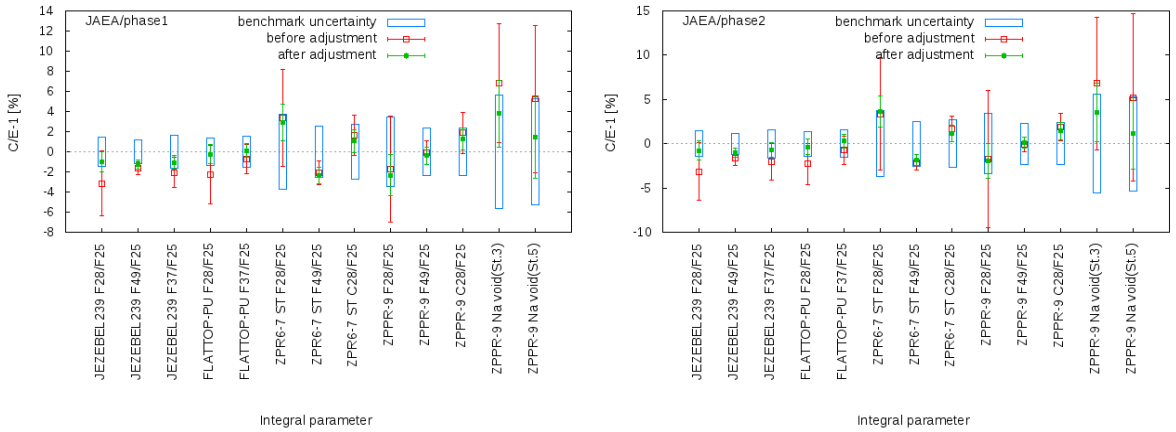

The last figure shows that the initial *a priori* for covariance does not seem to influence the final C/E values or their uncertainties. The latest point is due to the form of generalised least-square equations.

Let us remind the form of the equation for *a posteriori* covariances:

$$M_\sigma' = M_\sigma - M_\sigma \cdot S^T \left(M_E + S \cdot M_\sigma \cdot S^T\right)^{-1} \cdot S \cdot M_\sigma \qquad (7.1)$$

If $S \cdot M_\sigma \cdot S^T >> M_E \ (or\ M_E + M_M)$, then the posterior uncertainties on experiments due to the new cross-section data, $S \cdot M_\sigma^{'} \cdot S^T$, are almost equal to $M_E \ (or\ M_E + M_M)$.

M_E stands for integral experiments covariances and M_M for analytical modelling errors.

In the next chapters, the influence of *a priori* covariance on trends will be presented.

7.2.2 Analysis of each adjustment

In this section, the analysis grid will be devoted to examining each adjustment work. We will thus focus on the "physical solution" given by each laboratory on cross-sections and analyse:

- variation/trends within initial and final uncertainty;
- posteriori covariances;
  - New correlations?
  - Unphysical correlations?

In most results for Phase I, no incoherent trends are found when compared to initial uncertainties. Figure 29 presents this major effect through some illustrative examples.

Figure 29: Several examples of trend compared with a priori and *a posteriori* uncertainties

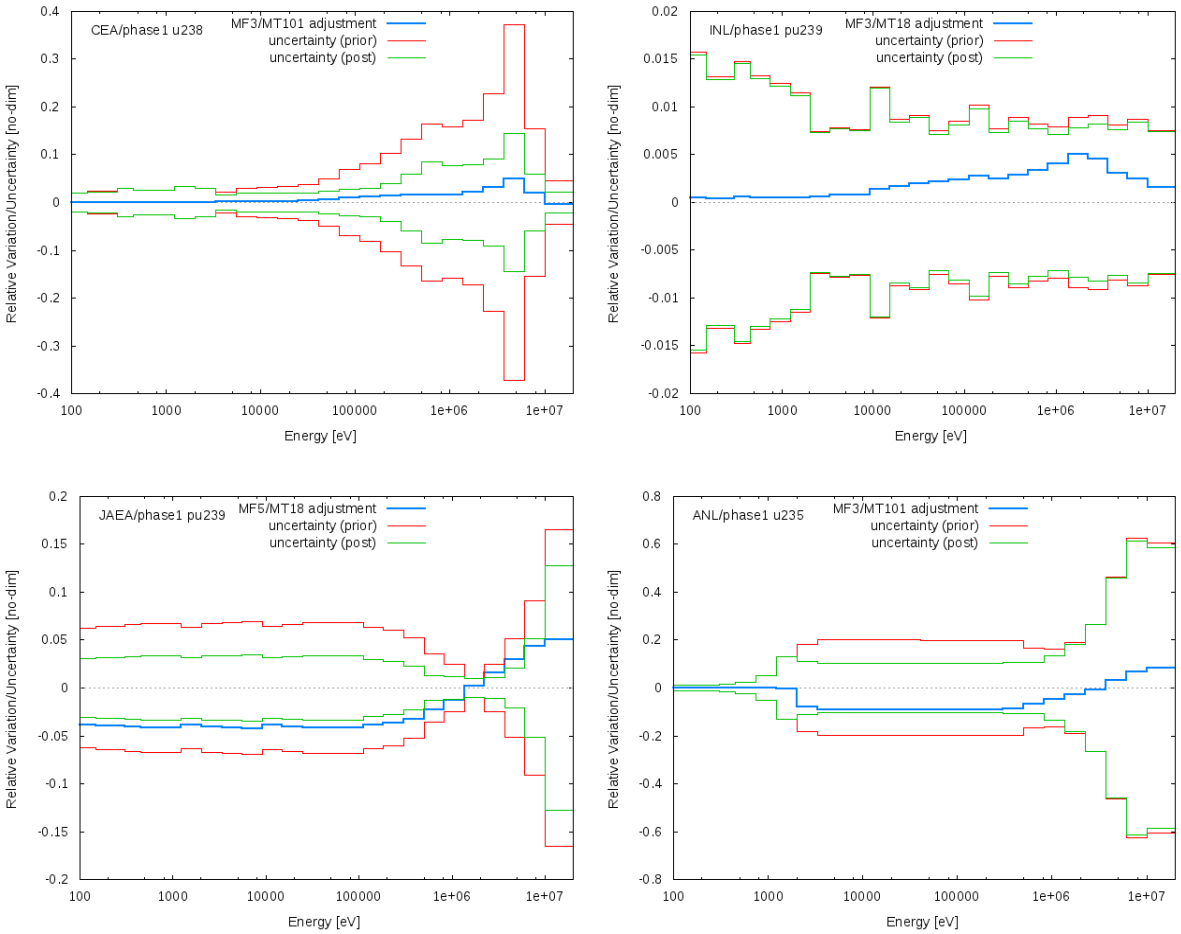

One additional remarkable point is that variances are not so much reduced between prior and posterior cross-section uncertainties (except for CEA, where initial uncertainties for some isotopes may be found pessimistic and some minor cross-sections). This means that the final overall uncertainty reductions on benchmarks calculation or concept calculation are mainly due to correlations created by the adjustment. Later, we need to examine these correlations (see next paragraph on correlations).

One additional comment on general results is the fact, that it seems like only a few (~5) initial isotopes exert an influence on the adjustment procedure. ^{58}Ni, ^{52}Cr, ^{10}B, ^{241}Pu do not seem to be interesting as vectors of data assimilation/adjustment. (See, for instance, Figure 30 for examples of trends found for ^{58}Ni elastic cross-sections).

This figure suggests that the trends found by all adjustments are really negligible, even if the initial cross-section data can be different (see comparison of JAEA and INL for example).

Figure 30: ^{58}Ni trends on elastic cross-section and comparison with INL for JAEA

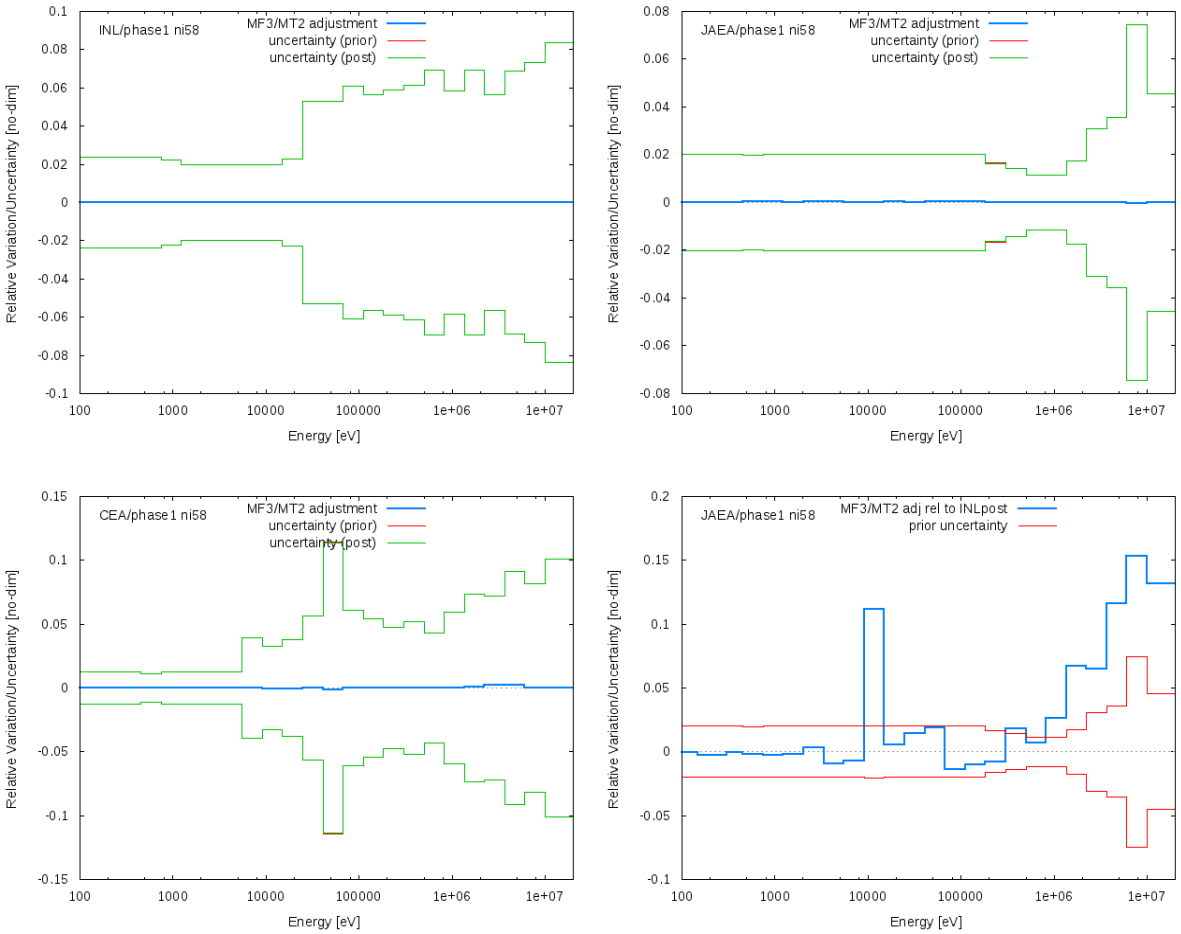

7.2.3 General Correlations: Prior/Posterior

CEA

The effects of changing initial cross-section covariances on *a posteriori* matrices were compared. Same C/E, same sensitivity sets and same experimental covariances are thus considered here.

Adjustment analysis results with COMAC-V0 (with Chi)

Figure 31: Full nuclear data prior correlation matrix with COMAC-V0

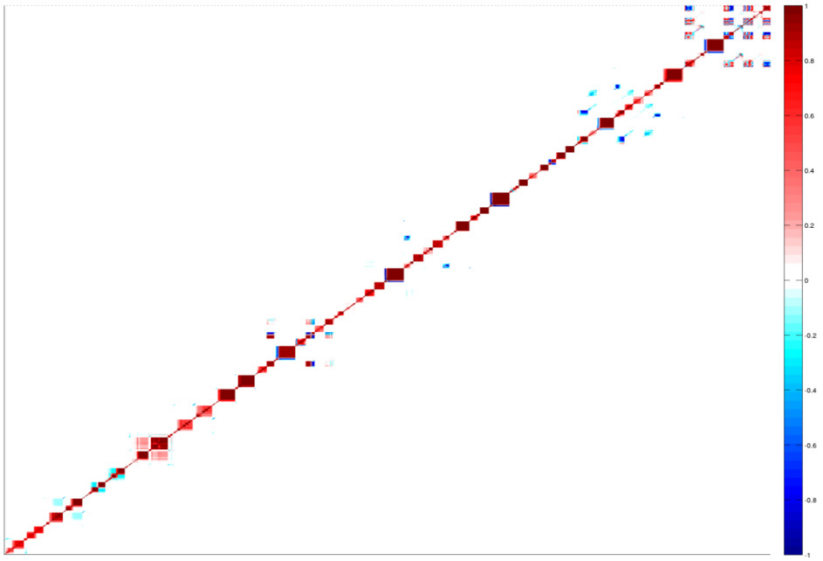

Figure 32: Full nuclear data posterior correlation matrix with COMAC-V0

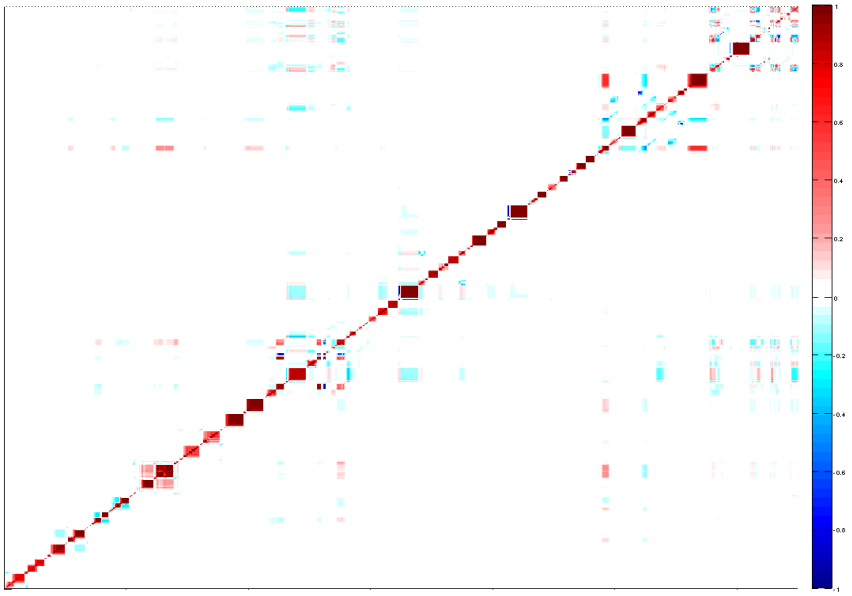

Changes on correlations appear for:

- Structural materials (^{23}Na, ^{56}Fe): correlations, mostly positive, are created with ^{239}Pu and uranium isotopes with scattering reactions (elastic, inelastic). No notable changes were found for correlations between cross-sections of ^{56}Fe. Small anti-correlations are created between elastic and inelastic of ^{23}Na (see Figure 33).
- ^{239}Pu: anti-correlations between Chi and Chi of other fissile isotopes (^{240}Pu, ^{235}U, ^{238}U). Also, quite strong anti-correlations were found (~0.4) between Chi and Nu of ^{239}Pu. New correlations can be observed between capture and fission of ^{239}Pu in the resolved resonance range (Figure 34).

- ^{240}Pu: correlations between reactions of ^{240}Pu;
- ^{235}U: strong correlations were found between capture and Nu in the high energy domain, as shown in Figure 35, which explains the fact that both large trends and no uncertainty reduction were obtained on ^{235}U capture. Some anti-correlations were found between capture and Chi, and also between elastic and Nu. The strong prior anti-correlations between capture and elastic in the high energy domain are quite diluted for the *a posteriori* correlations. Small correlations were found with ^{238}U.
- ^{238}U: the strong correlations and anti-correlations are softer (1 → 0.4, -1 → -0.4) after the adjustment, i.e. capture-capture, capture-inelastic and elastic-inelastic cross-correlations in the high energy range in Figure 36.

In this adjustment exercise no spurious covariances are created with non-sensitive parameters such as ^{10}B, ^{58}Ni, ^{52}Cr, ^{241}Pu.

Figure 33: ^{23}Na prior and posterior correlation matrices with COMAC-V0

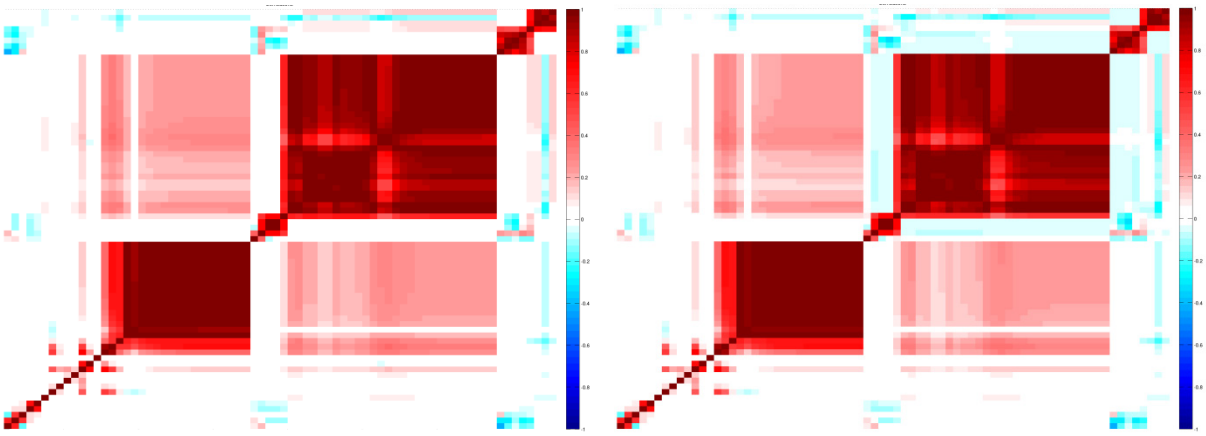

Figure 34: ^{239}Pu prior and posterior correlation matrices with COMAC-V0

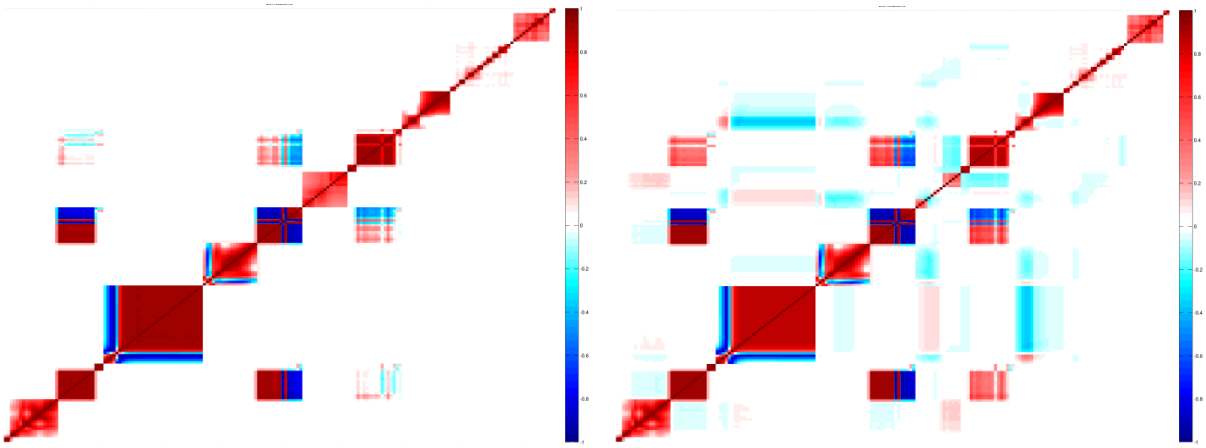

Figure 35: ^{235}U prior and posterior correlation matrices with COMAC-V0

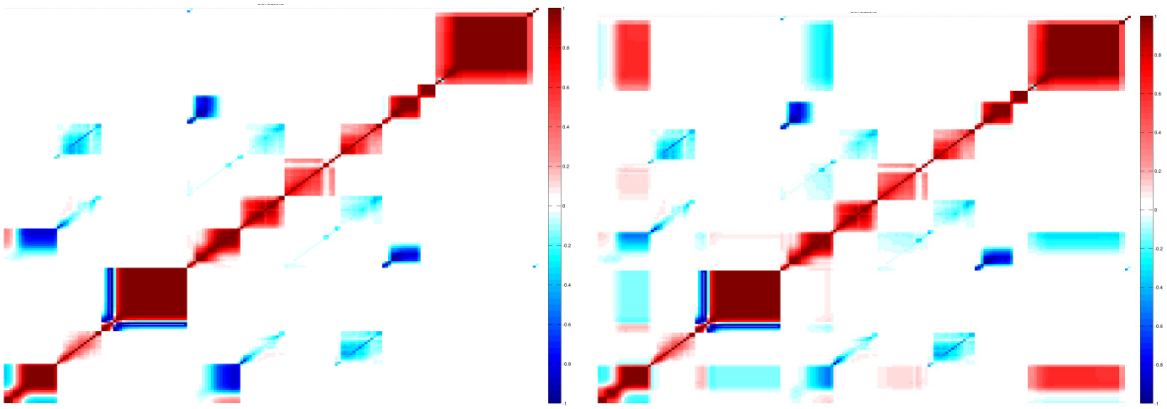

Figure 36: ^{238}U prior and posterior correlation matrices with COMAC-V0

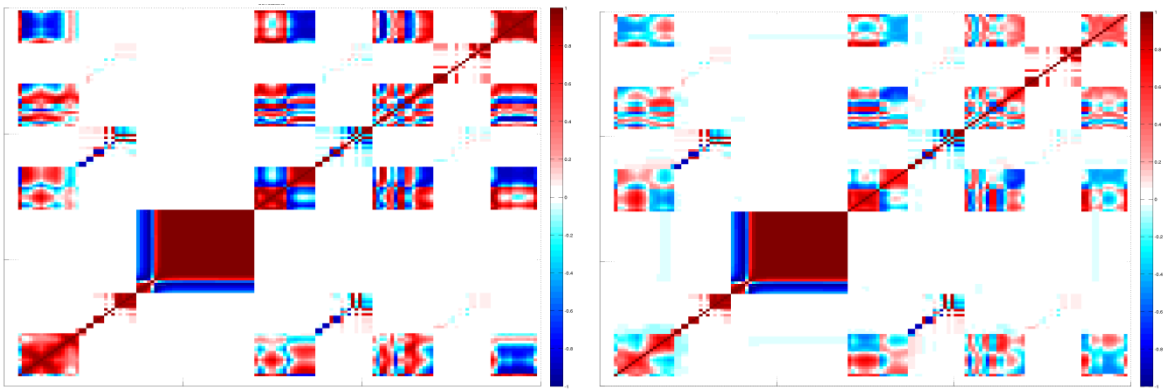

Adjustment analysis results with COMMARA:

Figure 37: Full nuclear data prior correlation matrix with COMMARA

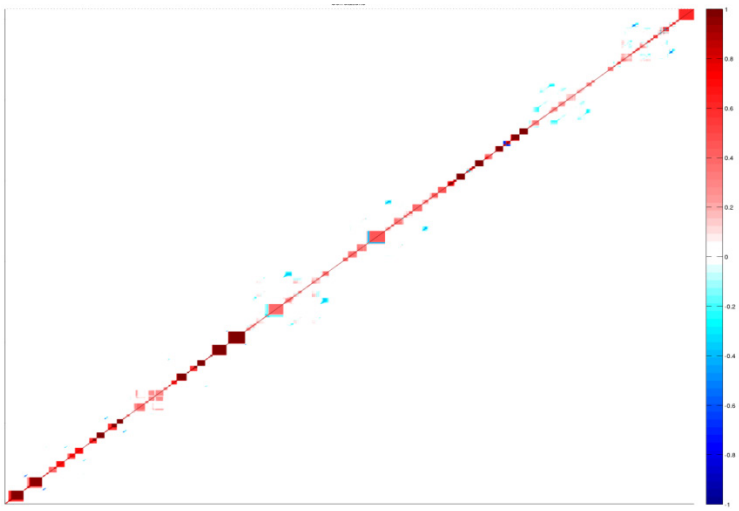

Figure 38: Full nuclear data posterior correlation matrix with COMMARA

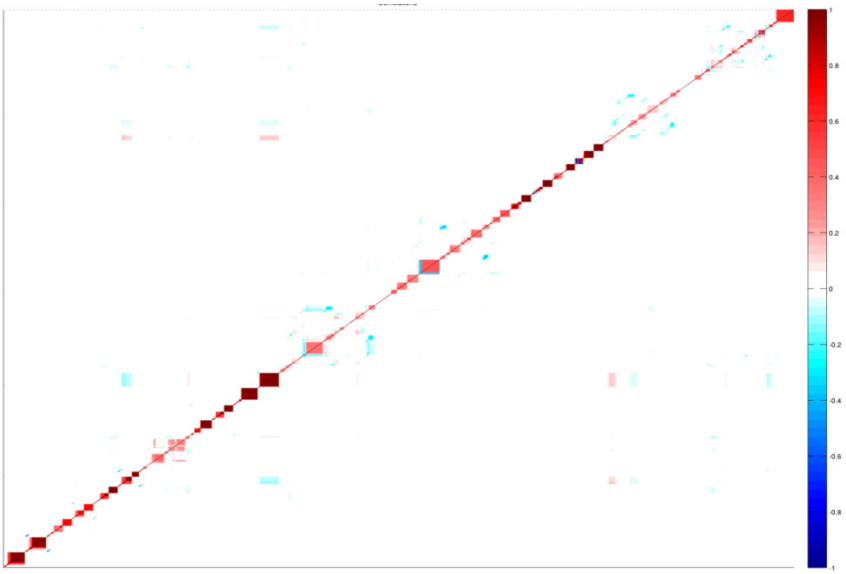

Very small changes can be observed between the prior and posterior covariance matrices. Some small positive and negative correlations appear between the spectra of fissile isotopes (Figure 38).

Effect of experimental correlations on posterior correlation matrix (Ve matrix from JAEA):

Figure 39: Full nuclear data posterior correlation matrix with COMAC-VO and experimental correlation matrix Ve

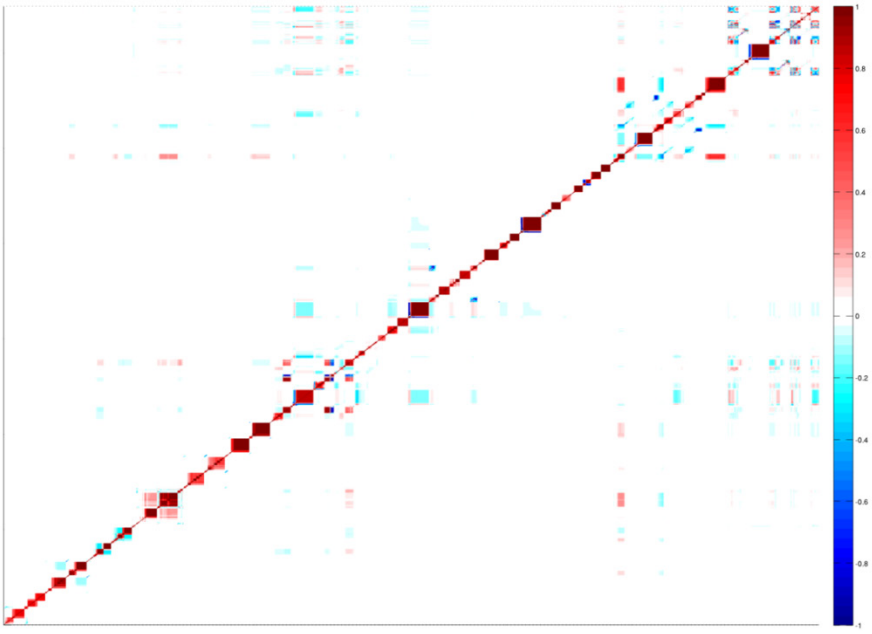

Comparison of Figures 31 and 38 shows no visual differences. The Ve matrix is quite sparse and contains rather small correlation (<0.3), which can explain the very few effects in this adjustment.

Effect of correlations (prior/posterior) on Target System uncertainties (Phase III)

In this exercise, where only COMAC-V0 covariance matrices were used, the importance of correlations before and after adjustment on target system uncertainties (only k_{eff}) is evaluated. The following uncertainty propagation calculations are presented:

- Case 1: full prior/posterior covariance matrix;
- Case 2: remove, from previous case, correlations between different isotopes (such as no correlation between $^{235}U/^{238}U$);
- Case 3: remove, from previous case, correlations on reactions for each isotope (such as inelastic/elastic for ^{238}U);
- Case 4: keep only variances.

ABR Oxide	**Prior covariances**	**Posterior covariances**
Case 1	1550 pcm	170 pcm
Case 2	1550 pcm	510 pcm
Case 3	1720 pcm	680 pcm
Case 4	1200 pcm	820 pcm
JAEA FBR	**Prior covariances**	**Posterior covariances**
Case 1	1310 pcm	220 pcm
Case 2	1310 pcm	490 pcm
Case 3	1560 pcm	610 pcm
Case 4	1170 pcm	900 pcm
ABR Metal	**Prior covariances**	**Posterior covariances**
Case 1	1740 pcm	250 pcm
Case 2	1740 pcm	560 pcm
Case 3	2020 pcm	730 pcm
Case 4	1290 pcm	850 pcm
ABR Oxide Recycled	**Prior covariances**	**Posterior covariances**
Case 1	1250 pcm	260 pcm
Case 2	1250 pcm	490 pcm
Case 3	1400 pcm	590 pcm
Case 4	1080 pcm	820 pcm

For all target systems[8], the uncertainty using prior and posterior covariance matrices converged when correlations are deleted. It is visible that:

- correlations between isotopes are important (after adjustment), and take part in the uncertainty reduction: a factor 2-3 appears on target system uncertainties;

[8] For ABR Oxide Recycled case, no minor actinide uncertainties are taken into account.

- correlations between reactions for each isotope and the correlation between energy groups for each reaction are significant;
- for prior covariances, consideration of cross-correlations (between reactions and energy groups) tends to give an overall uncertainty of the same order of magnitude (Case 4 → Case 1), except for ABR Metal core. However, the effect of the energy group is related to an increase in the uncertainty (Case 4 → Case 3) and the effect of constraint on the reaction tends to lower this uncertainty (Case 3 → Case 2 = Case 1).
- In contrast, for posterior covariances, consideration of correlations always produces a reduction Case 4 → Case 3 → Case 2 → Case 1.

JAEA

Figures 40 and 41 show prior and posterior correlation matrices for the JAEA exercise (JENDL4 for nuclear data and covariances). Changes using all JAEA between prior/posterior correlations are similar to the work of CEA with the COMAC set. However, mostly new correlations are negative (mix of positive/negative in COMAC).

Figure 40: Full nuclear data prior correlation matrix with JENDL4

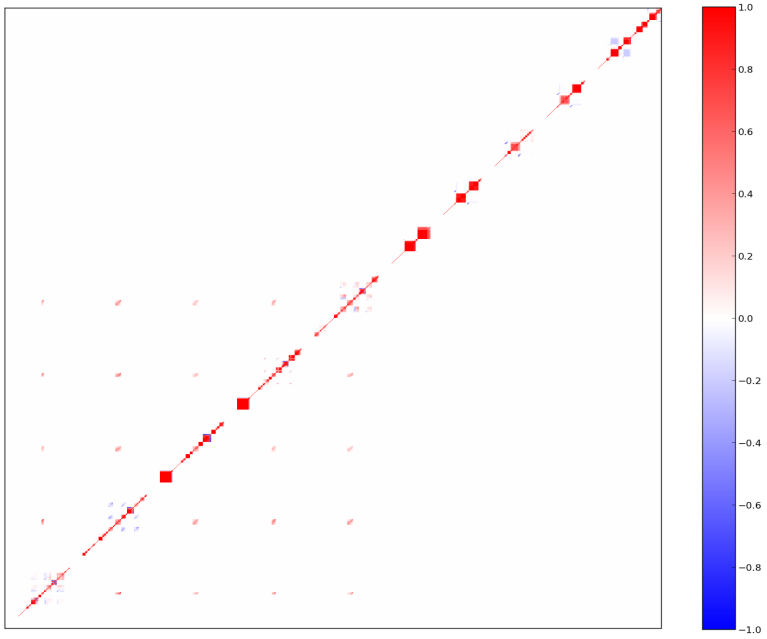

Figure 41: Full nuclear data posterior correlation matrix with JENDL4

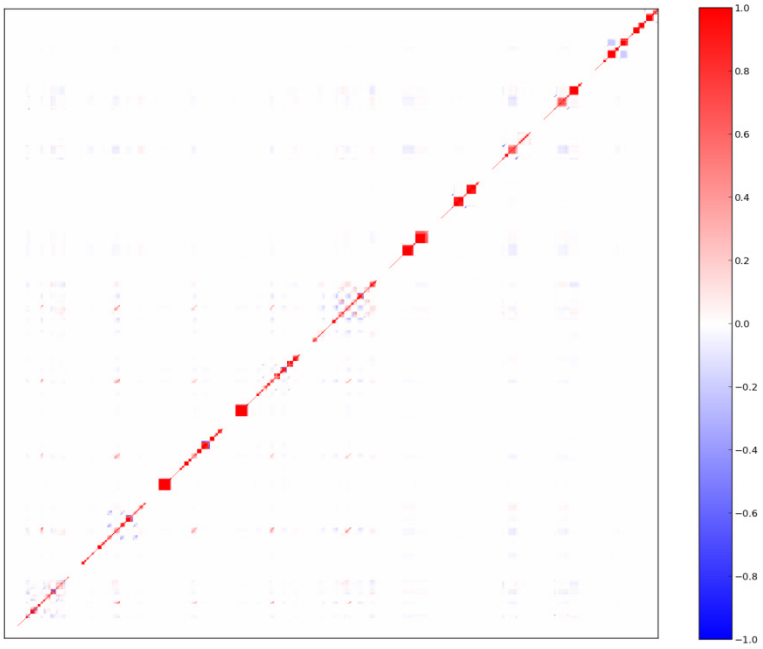

7.3 Comparison of adjustments exercises for Phase I, II

Our aim here is to find physical issues from the comparison of laboratory exercises. The analyses will focus on a limited set of isotopes: ^{238}U, ^{239}Pu, ^{235}U, ^{23}Na, ^{56}Fe.

The data compared will be:

- Final cross-sections →convergence of final cross-sections?
- *A posteriori* Covariances INL/CEA/JAEA
  - New correlations of the same type?
  - variance magnitudes;
  - unphysical correlations;
  - Noticeable differences between Phases I and II results?
- Effect of *a priori* covariances CEA/INL/JENDL
  - on cross-sections;
  - on trends;
  - on *a posteriori* covariances;
- Effect of libraries.

7.3.1 ^{238}U

As shown in Figure 42, JAEA trends on (n,n') cross-sections show a need for slightly increasing this cross-section. In contrast, ANL/INL do not show this trend, and CEA and PSI even propose a slight reduction.

Figure 42: ^{238}U trends on inelastic cross-section and comparison with INL for JAEA and CEA

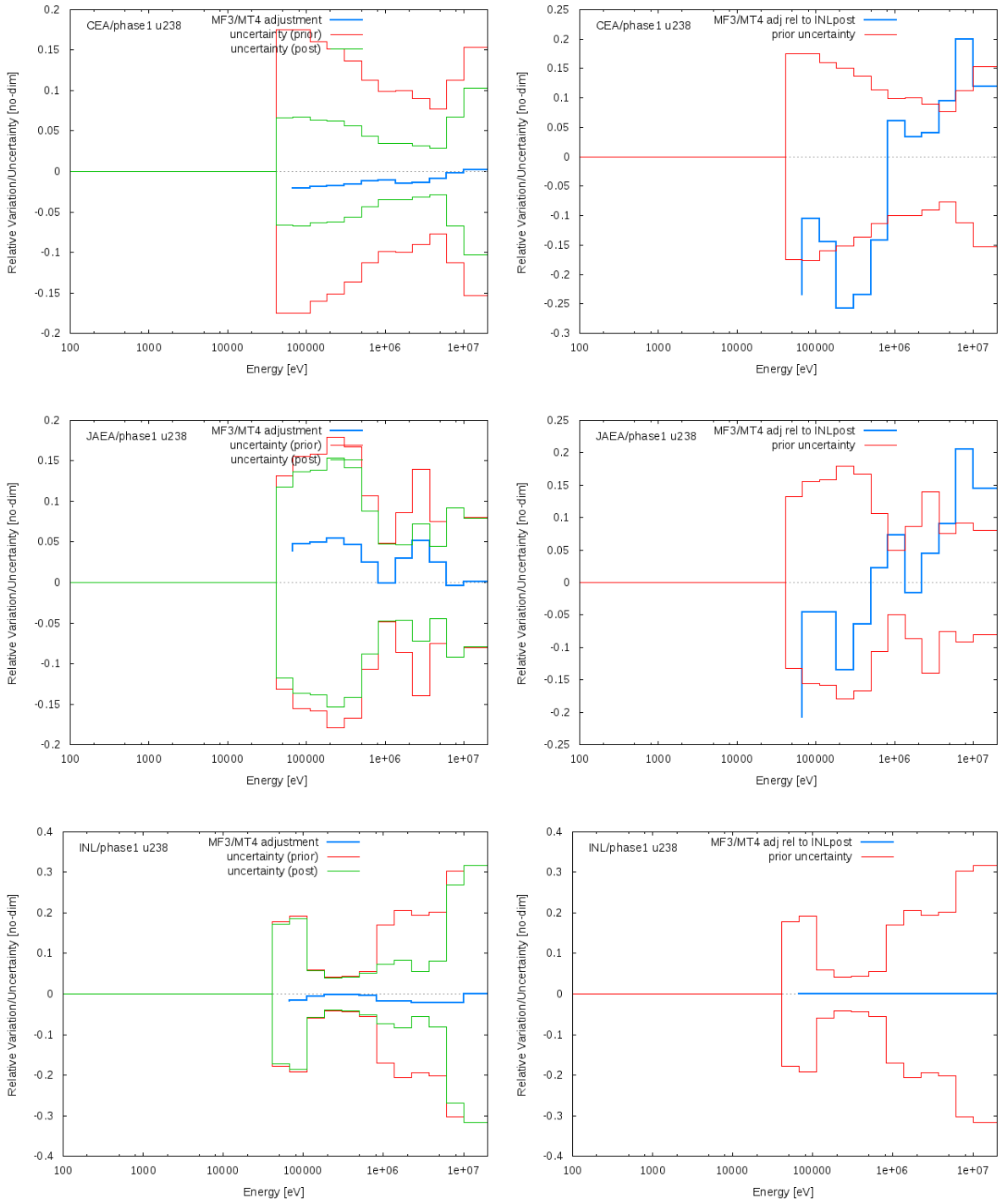

Another puzzling effect is related to uncertainty reduction which is important for CEA, limited and similar for INL/ANL and PSI, and negligible for JAEA. This is due to the covariance proposed by CEA, which shows important correlations on inelastic cross-sections and other reactions which make the adjustment reduce the uncertainty in the whole energy range. The uncertainty values for the inelastic cross-sections in the three files are rather different in magnitude and energy trend. E.g. in the range of 1-20 MeV, the COMMARA 2.0 uncertainties are 2-3 times higher than in the JENDL 4.0 (and in the CEA) covariance dataset. Below ~1 MeV that trend is reversed between the two files.

The above data suggest a drastic impact of *a priori* covariance choices on trends.

The ^{238}U inelastic cross-section adjustments of the present benchmark are rather small and often much smaller than the uncertainties, and the *a posteriori* cross-sections are only marginally more consistent that the *a priori* values. In fact, CEA and INL/ANL emphasise the need for a reduced decrease in this reaction.

For CEA, there is an adjustment of the fission cross-section of ^{238}U (a slight decrease of ~1% in the energy range ~400 keV-1 MeV), while the INL and PSI adjustments show a slight decrease of nu-bar. CEA variance is too pessimistic and the INL/CEA difference is outside the scope of INL/CEA relative difference.

Figure 43: ^{238}U trends on fission cross-section and comparison with INL for CEA

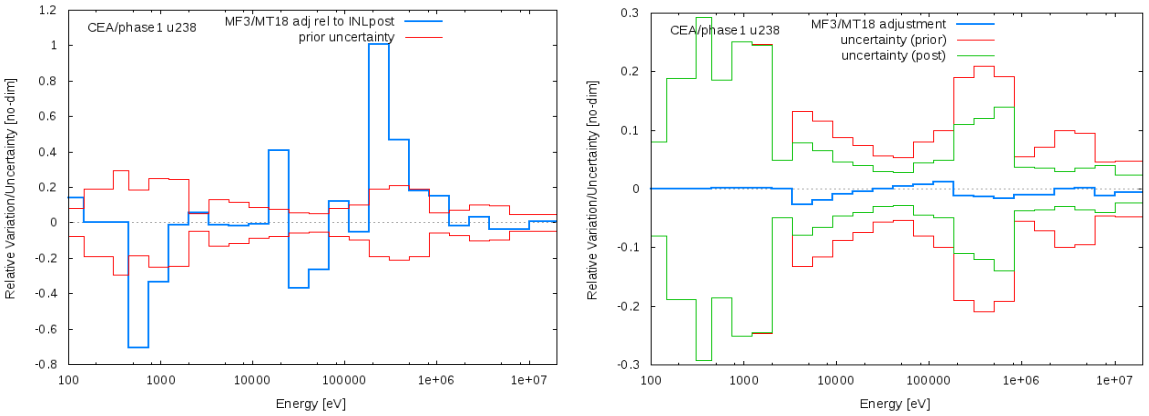

Phase II results show that in the case of CEA/ANL/JAEA, considering COMMARA *a priori* covariances with merely impossible fission cross-section adjustment will not display the same trends as Phase I. NRG proposes a drastic change in ^{238}U elastic cross-section. This may be due to the discrepant initial data as compared to other libraries (see Figure 44).

Figure 44: ^{238}U trends on elastic cross-section for NRG

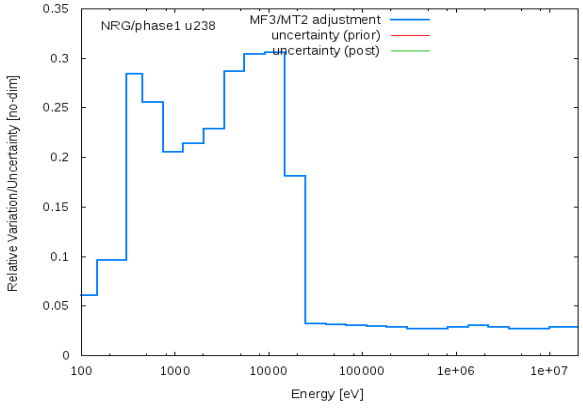

7.3.2 ^{239}Pu

A first investigation of the adjustment results (Phase I) for some selected data as obtained by JAEA, INL (very close to ANL), CEA and PSI is given below:

^{239}Pu capture (Figure 45)

In the energy range ~3 keV-~500 keV, the uncertainties in the three covariance data sets (JAEA: J 4.0, CEA, COMMARA2.0) are rather similar and the uncertainty is in the range ~6-9% to 7-12%. As for the adjustments, they consistently indicate an increase in the capture cross-section by ~1-2% up to a maximum of ~10%

In the range ~5-50 keV, the suggested increase of the capture cross-sections in the three files are such that even the adjusted data look very consistent and still close to each other, like before adjustment.

For this isotope and this reaction, a clear trend seems to emerge.

The same relative difference exists between CEA/JAEA/NRG and INL/ANL/PSI nuclear data, as a result, we can observe the same trends on capture around +3-5% increase in keV-MeV. But, it should be noted that the uncertainty is not affected in this case. No reduction is found after adjustments.

Figure 45: ^{239}Pu trends on capture cross-section ANL/INL, JAEA, CEA and NRG

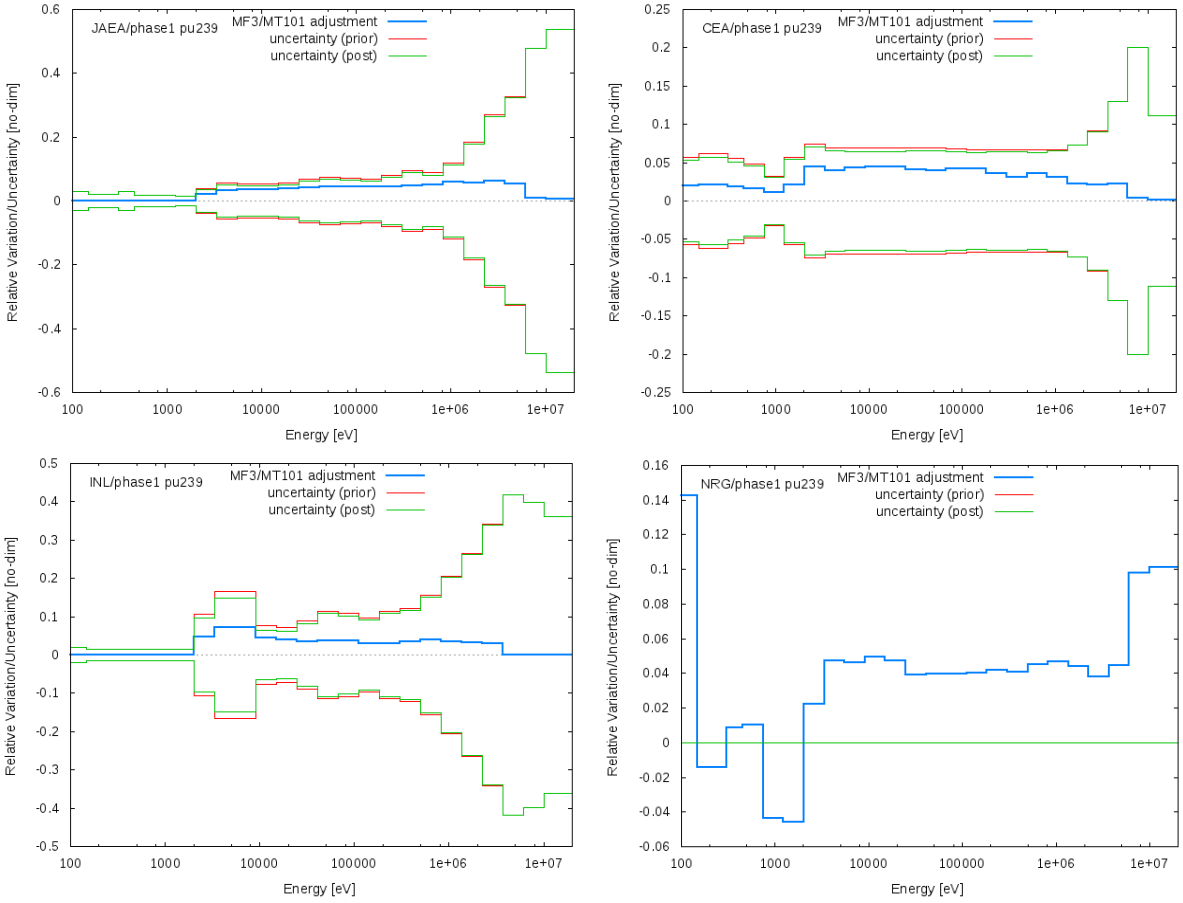

^{239}Pu inelastic and prompt fission neutron spectrum (Figure 46)

^{239}Pu inelastic is an important parameter (i.e. large sensitivities) when ^{239}Pu is a major component of the core (e.g. JEZEBEL and FLATTOP), in particular for k_{eff} and F28/F25.

In general, a decrease in the inelastic is suggested for each file. This trend allows getting a better agreement on e.g. F28/F25, which is underestimated for both JEZEBEL and FLATTOP by all groups, since negative sensitivity coefficients for the F28/F25 parameter to variations of the ^{239}Pu inelastic are calculated as expected (even if not in perfect agreement) by all groups .

However, the changes in the inelastic cross-section are the highest for INL and the lowest for CEA. As regards PSI using the JEFF-3.1 library, a decrease of up to 10% occurs for energies larger than 1 MeV, which is counterbalanced by an increase in the inelastic scattering cross-section of up to 10% around 100 keV for lower energies. PSI did not adjust the fission spectrum yet, which may explain this particular behaviour.

Even if after adjustment a rather better agreement is found among the three data sets, a good understanding of the trends is obtained only if the ^{239}Pu inelastic cross-section adjustments are considered together with the prompt fission neutron spectrum adjustments. In fact, only JAEA and CEA results show significant adjustments for that parameter while INL and ANL show very small adjustments. The lower adjustment (decrease) of the inelastic in the JAEA and CEA results is partly compensated for by the decrease in the energy fission spectrum below ~3.5 MeV suggested both in the JAEA and in the CEA results. When a smaller decrease in the inelastic cross-section is suggested, this is associated to a higher reduction of the prompt fission neutron (see CEA with respect to JAEA adjustments of the two parameters). In fact, a lower inelastic cross-section at high energies allows fewer neutrons below e.g. 1-2 MeV and the same effect is produced by a lower amount of prompt fission neutrons in that energy range. In other words, since both adjustments of the JAEA and CEA results (i.e. decrease in inelastic and harder fission spectrum) consistently harden the neutron spectrum and help e.g. to improve the C/E of F28/F25 in FLATTOP and JEZEBEL, in the INL adjustment a larger inelastic decrease is needed since a lower inelastic decrease (JAEA and CEA) is "compensated" for by the fission spectrum hardening. In summary, the net result is better C/E (i.e. close to 1) values for e.g. the FLATTOP and JEZEBEL F28/F25 (and F37/F25) with the four adjustments (JAEA, CEA, INL and PSI, which, however, does not need to improve F37/F25, see Figure 27).

Finally, the suggested change of the prompt neutron fission spectrum both in the JAEA and in the CEA cases, is very consistent.

The Phase II results from CEA/JAEA show the same trends equivalent to Phase I.

Figure 46: ^{239}Pu trends on inelastic cross-section

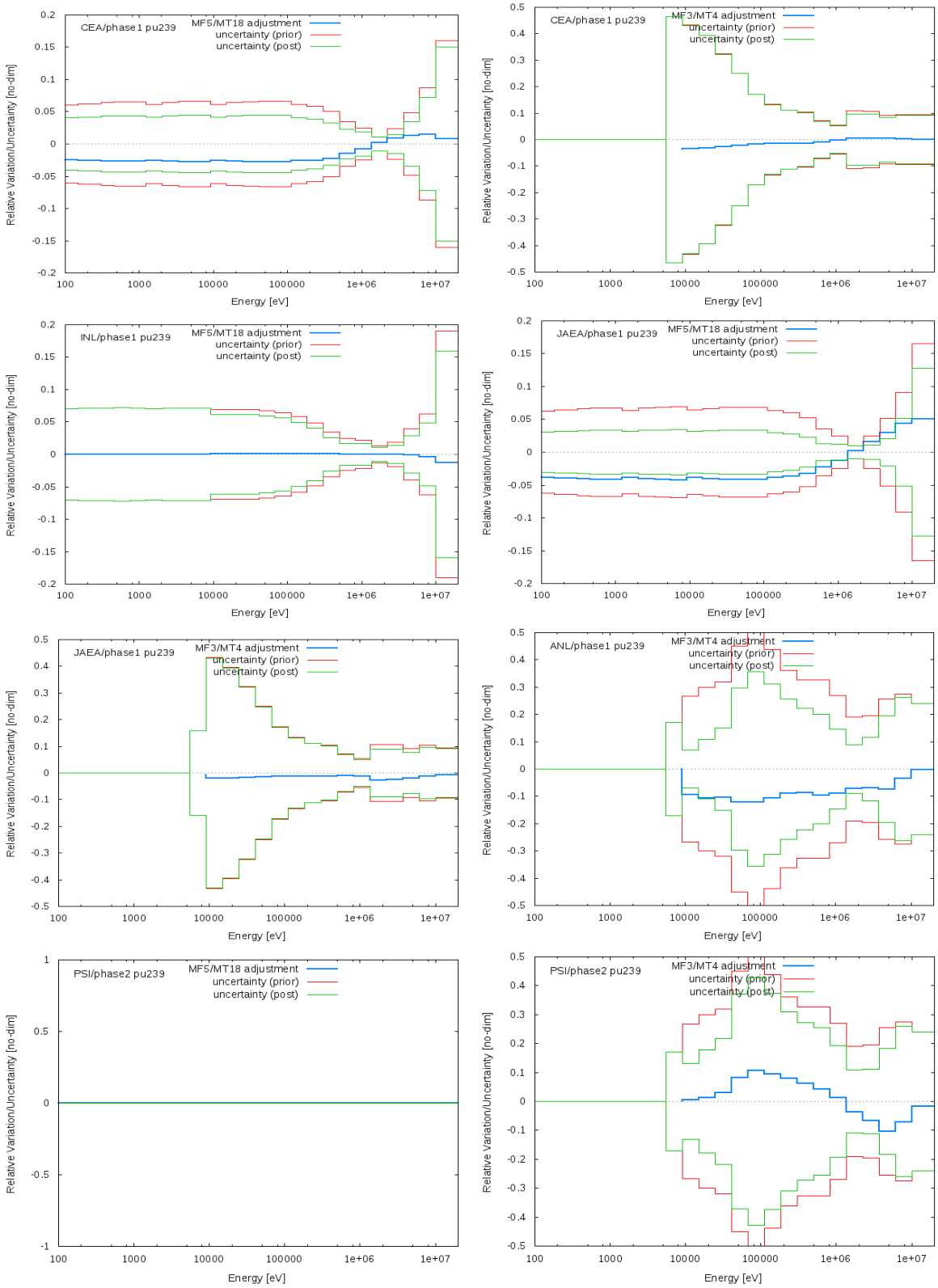

7.3.3 ^{235}U

^{235}U capture

The uncertainty values on this parameter are significantly different among the different covariance data files. As a result, as shown in Figure 47, the end result is a common trend for this cross-section but with different magnitude among the participants. The larger uncertainties in COMMARA 2.0 (and in CEA covariance data) allow a significant decrease in the cross-section, essentially to improve the k_{eff} under prediction of INL. In the CEA and PSI cases, the overall ^{235}U capture decrease is smaller (of maximum 7% for PSI, not shown), since the discrepancy on the k_{eff} is rather small and in the CEA case, it is of opposite sign. Finally, the JAEA adjustment is a decrease of the capture cross-section only at very high energies where the JENDL 4.0 uncertainties are higher. Elsewhere, the low uncertainty data in JENDL 4.0 do not allow any significant decrease in the ^{235}U capture data.

It is to be noted that most teams underline the necessity of decreasing the ^{235}U capture cross-section in the unresolved resonance range. An equivalent conclusion was given by the WPEC Subgroup 29 in 2011.

Figure 47: ^{235}U trends on capture cross-section

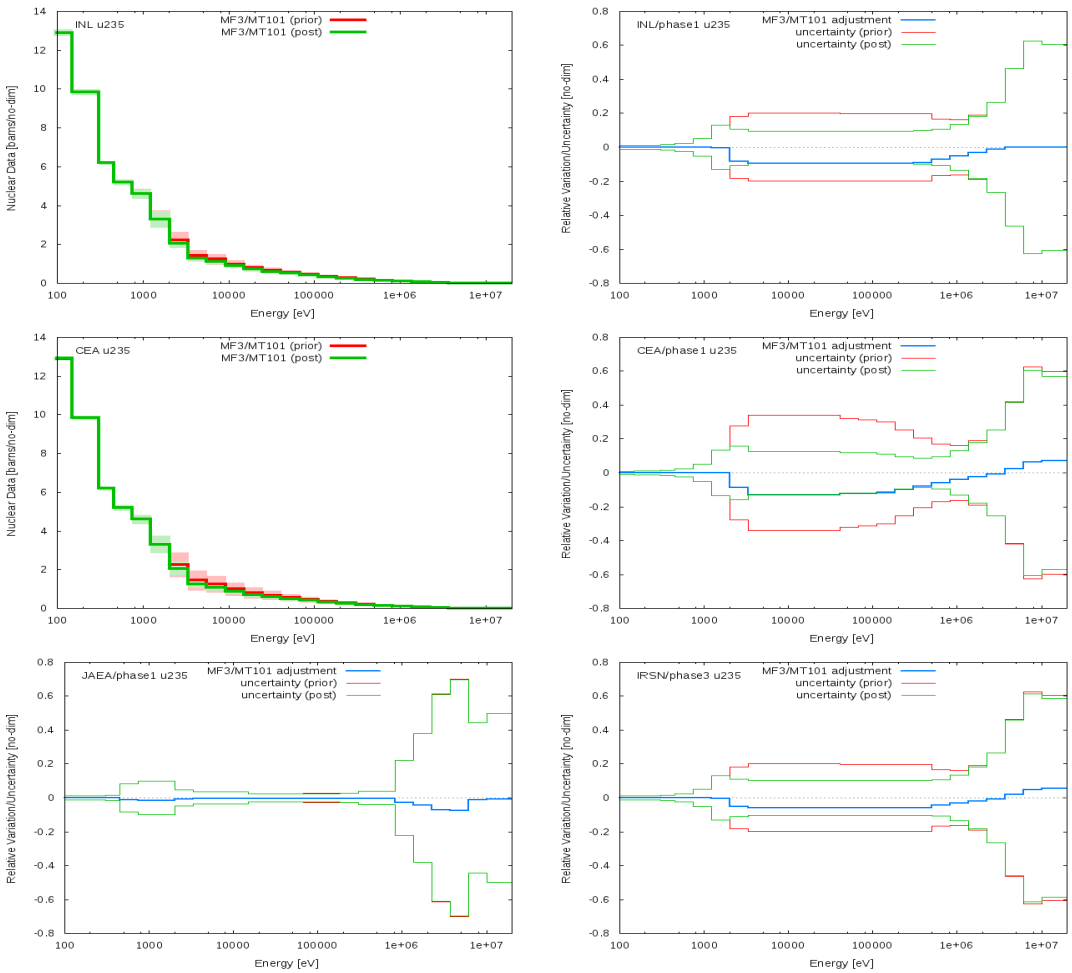

7.3.4 Other data

For other data, e.g. ^{23}Na inelastic and elastic, ^{56}Fe inelastic cross-sections, the adjustments are rather small and it is rather difficult to extract clear common trends.

7.4 Relative effects of input data: Covariances, C/E's, experiments

7.4.1 Effect of Different Covariance Data on Adjustment: JAEA

In principle, the central cross-section values and the corresponding covariance data of a library must be consistent. However, here we intentionally replace the covariance data used in the adjustment procedure, though we use the same values of other adjustment parameters, especially the C/E's values which completely depend on the central cross-sections, to depict the pure effects of the different covariance data to the adjusted results.

Three adjustment cases are surveyed as follows:

Case J (Phase I): This is the reference adjustment case. Cross-sections and covariance data are both based on the JENDL-4.0 library J-4.0 [16] [17].

Case B0: The covariance data in Case J are replaced with those of COMMARA-2.0 C-2.0, [18], with the exception that the missing covariance data in C-2.0 below are substituted with those of J-4.0.

- Mu-bar of ^{235}U, ^{238}U, ^{239}Pu, ^{240}Pu, ^{241}Pu, ^{10}B, ^{16}O, ^{52}Cr, ^{58}Ni;[9]
- Nu-d of ^{235}U, ^{238}U, ^{239}Pu, ^{240}Pu, ^{241}Pu.[10]

The other adjustment parameters are identical with Case J.

Case B2 (Phase II): The covariance data are only adopted from C-2.0. No J-4.0 covariance data are supplemented. The other adjustment parameters are identical with Case J.

To investigate the effect of different covariance data, we focus on the results of the criticality and the sodium void reactivity below.

Criticality (k_{eff})

Figure 48 compares the k_{eff} C/E changes of the three cases by adjustment. It is found that the adjusted C/E values of the three cases are almost identical for k_{eff} of small through large cores. In detail, however, there are some differences between Case J and Case B0/B2 for the k_{eff} of the JOYO Mk-I core, which contains the ^{235}U fuel as well as plutonium, while the other cores do not include ^{235}U in fuel. The use of C-2.0 shows better improvement of JOYO C/E values than J-4.0.

The nuclide- and reaction-wise contributions for the C/E changes of JOYO k_{eff} in the three cases are shown in Figure 49. As can be seen, the contribution of ^{235}U capture cross-section is significantly different by 400 pcm between the J-4.0 and C-2.0 covariance data. Further, those of ^{23}Na and ^{56}Fe elastic scattering are even opposite in sign.

[9] mu-bar covariance data of Na-23, Fe-56 are adopted from C-2.0.
[10] There are no nu-d covariance data in C-2.0.

Figure 48: Change of C/E values by adjustment: Criticality (k_{eff})

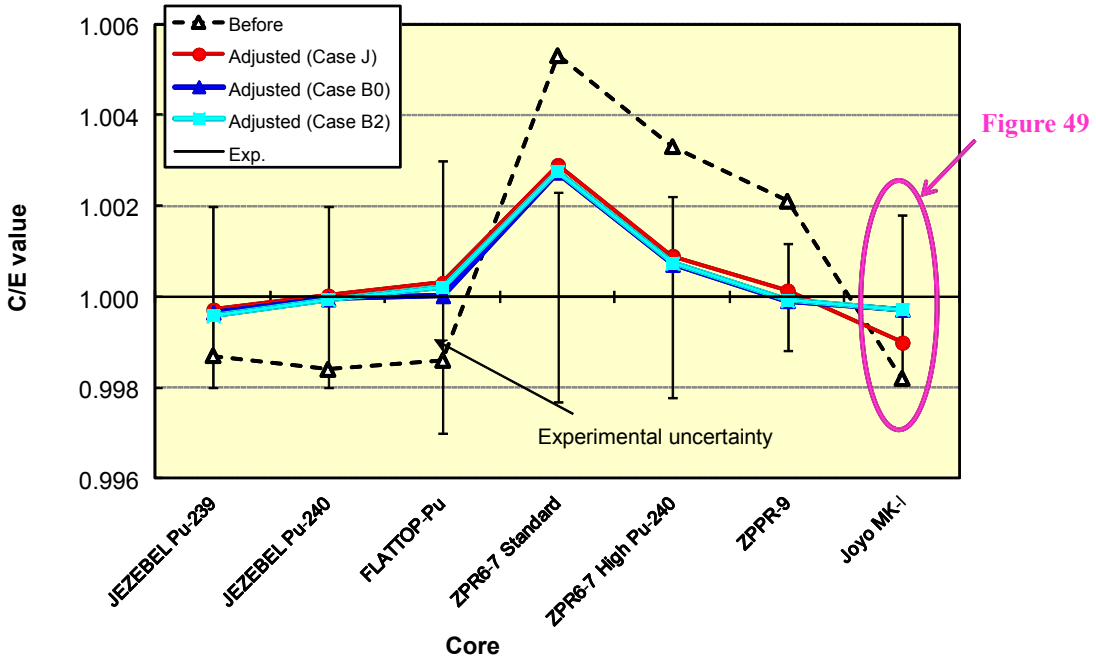

Figure 49: Contribution to C/E changes by adjustment: k_{eff} of JOYO Mk-I

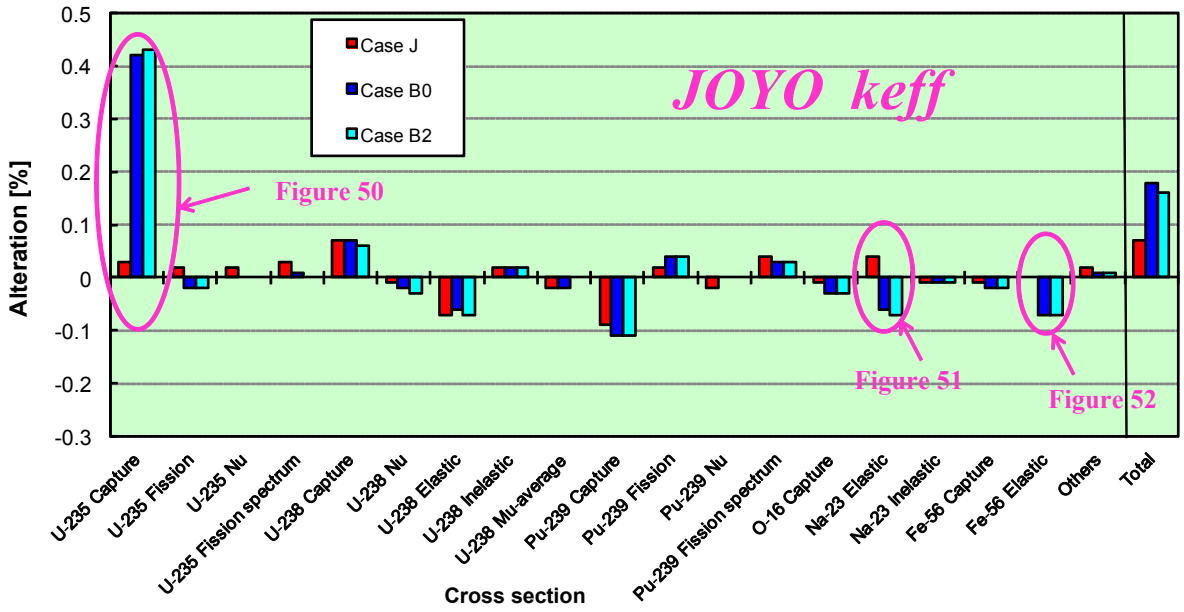

The reasons for these contribution differences could be inferred from Figures 50-52. As for ^{235}U capture, the difference of STDs between C-2.0 and J-4.0 significantly affected the changing rate of the cross-section. The small STD of J-4.0 must constrain the alteration of the cross-section by the adjustment. The large STD of C-2.0 allows high changing rates of the ^{235}U capture cross-sections to improve the C/E value of JOYO k_{eff} by the adjustment[11]. The decrease of ^{23}Na elastic cross-section in C-2.0 would result in the increase of the neutron leakage from the JOYO core, i.e. the negative reactivity. In contrast, the increase in J-4.0 would be the positive reactivity. The effect of ^{56}Fe elastic contribution to JOYO k_{eff} could be explained by the same mechanism, where the changing rate of C-2.0 is constant in energy due to the strong positive correlations, as shown in Figure 52.

Figure 50: Change of cross-sections by adjustment: ^{235}U, Capture

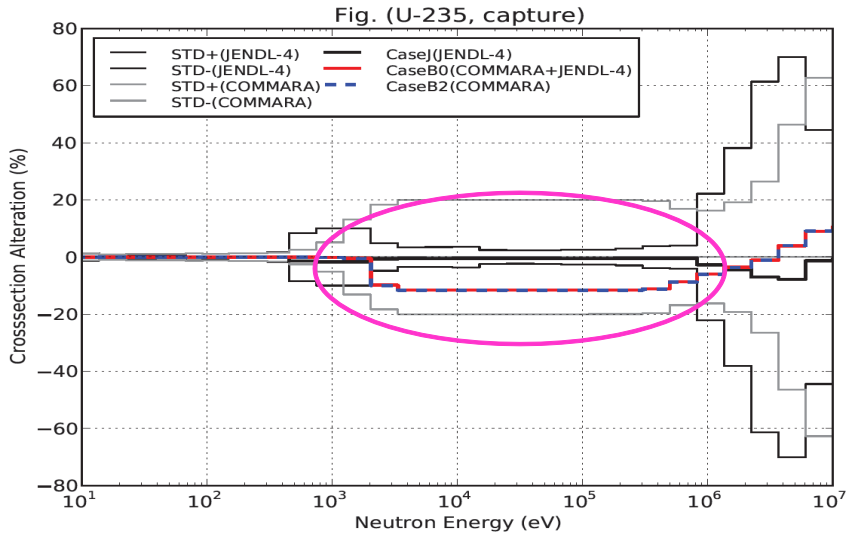

Figure 51: Change of cross-sections by adjustment: ^{23}Na, elastic scattering

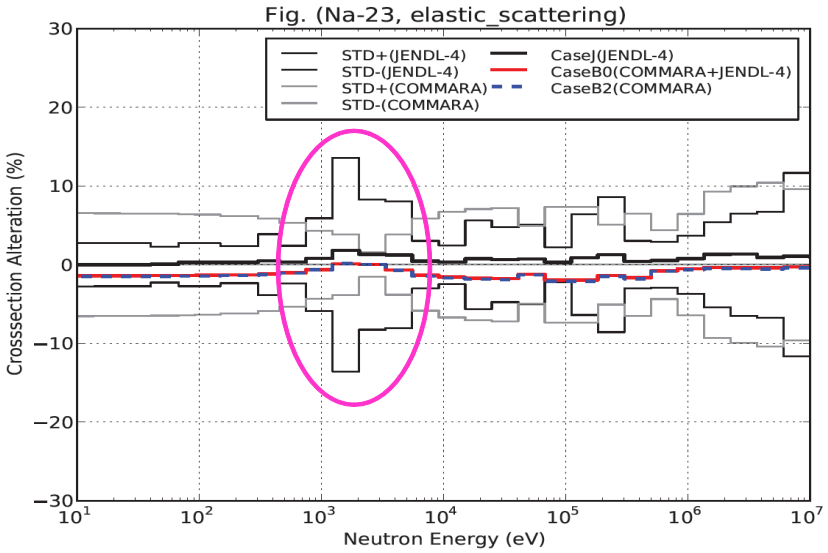

[11] The change of C-2.0 might be consistent with the conclusion of WPEC/SG29, that is, the possibility of the ^{235}U capture overestimation in the ENDF/B-VII.0 library.

Figure 52: Change of cross-sections by adjustment: ^{56}Fe, elastic scattering

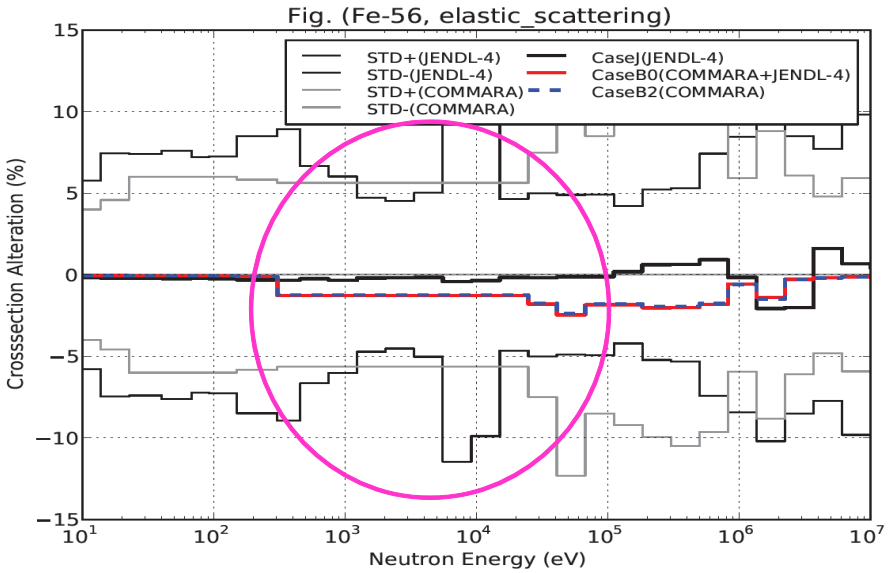

Sodium void reactivity

Figure 53 shows the adjusted C/E values of the sodium void reactivity in ZPPR-9. All three cases improve the C/E values by 4-6%. In detail, the C/E values of Case B0 seem somewhat better than those of Case B2, the major difference of which is whether to adjust the delayed neutron data (Nu-d) or not. As seen in Figure 54, Nu-d of ^{238}U and ^{239}Pu certainly contribute to improving the reactivity C/E values, though the amount is rather small compared with those of other cross-sections such as ^{238}U inelastic, capture or ^{23}Na inelastic cross-sections. Table 19 summarises the uncertainties of Nu-d and the changing rates by the adjustment for the three cases.

Table 19: Change of delayed neutron data (Nu-d) by adjustment

Fission isotope	Standard deviation (%)	Change by adjustment		
		Case J	Case B0	Case B2
U-235	2.7 %	+0.00 %	+0.00 %	-
U-238	3.4 %	-0.49 %	-0.37 %	-
Pu-239	4.4 %	-0.41 %	-0.30 %	-
Pu-240	4.9 %	+0.00 %	+0.00 %	-
Pu-241	5.0 %	+0.00 %	+0.00 %	-

When the reactivity parameters are included in the adjustment, Nu-d might be included in the adjusted data, since it has a certain amount of the sensitivity and uncertainty[12].

Figure 53: Change of C/E values by adjustment: Sodium void reactivity of ZPPR-9

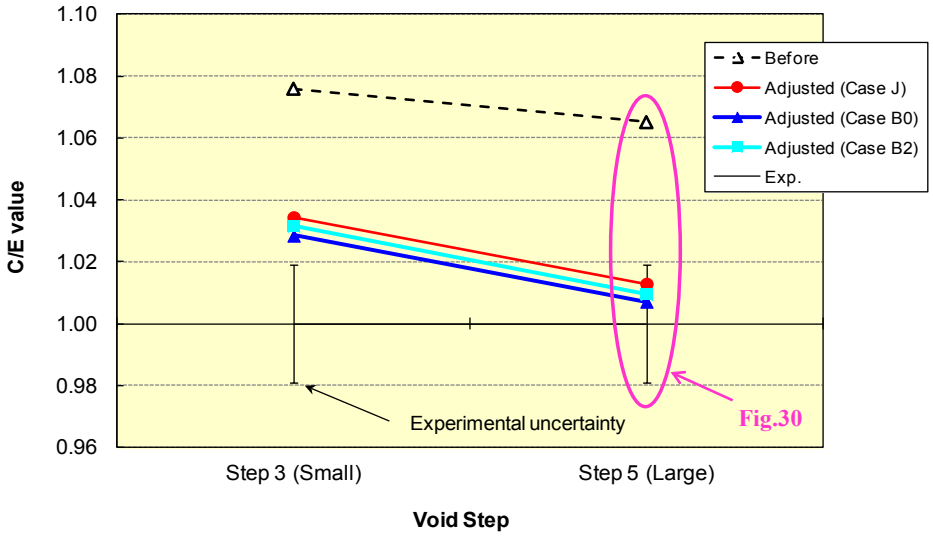

Figure 54: Contribution to C/E changes by adjustment: Sodium void reactivity of ZPPR-9 (Step5)

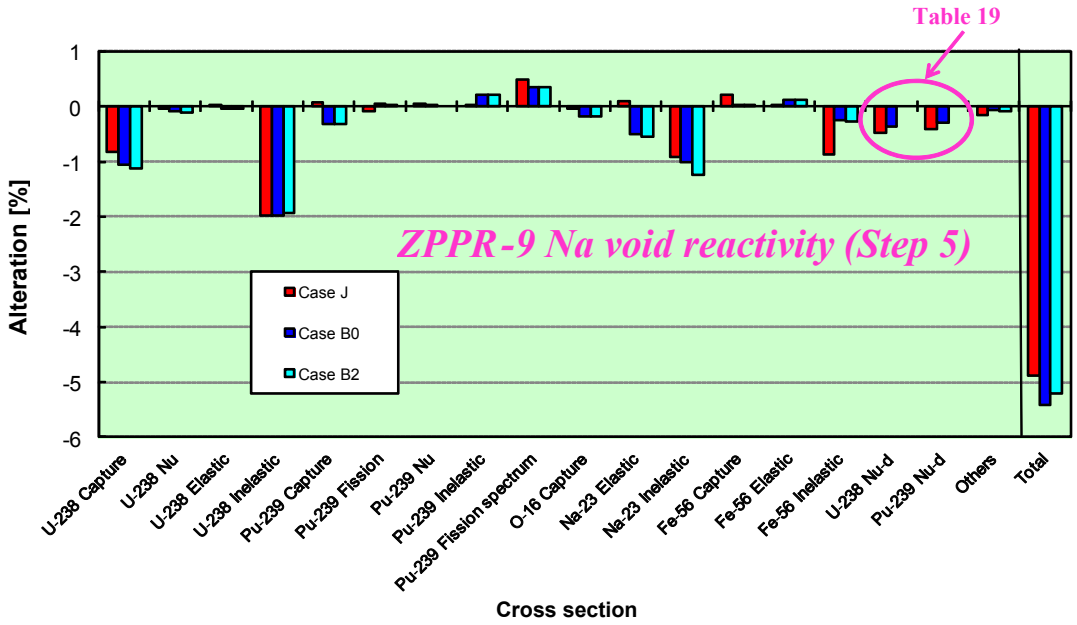

[12] If we treat other reactivity data such as the control rod worth of ZPPR in the adjustment, the contribution would be quite important, since it was largely overestimated by both JENDL and ENDF in general.

7.4.2 Effect of initial C/E's

C/E change exercise

CEA made two different calculations based on different C/E values:

Table 20: C/E's values of integral parameters obtained with reference and simplified calculations

Core	Quantity	CEA Reference calculation	CEA Simplified calculation
JEZEBEL239	k_{eff}	0.187	0.312
JEZEBEL239	F28/F25	0.026	2.181
JEZEBEL239	F49/F25	1.526	2.626
JEZEBEL239	F37/F25	1.412	1.751
JEZEBEL240	k_{eff}	-0.256	-0.066
FLATTOP-PU	k_{eff}	0.020	0.676
FLATTOP-PU	F28/F25	1.034	3.209
FLATTOP-PU	F37/F25	1.535	3.032
ZPR6-7	k_{eff}	-0.270	-0.207
ZPR6-7	F28/F25	3.752	4.080
ZPR6-7	F49/F25	4.207	4.971
ZPR6-7	C28/F25	-0.445	-1.085
ZPR6-7 240	k_{eff}	-0.220	-0.164
ZPPR-9	k_{eff}	0.005	-0.103
ZPPR-9	F28/F25	3.664	9.662
ZPPR-9	F49/F25	2.417	3.355
ZPPR-9	C28/F25	-0.334	-0.809
ZPPR-9	Na void Step 3	-3.401	-2.468
ZPPR-9	Na void Step 5	3.126	4.200
JOYO MK-I	k_{eff}	0.083	-0.172

With a simplified calculation route the adjustment procedure produces a slight increase in inelastic. With a better C/E, a decrease is preferable, as shown in Figure 55.

Figure 55: ^{238}U trends on inelastic cross-section: with reference and simplified C/E's calculation

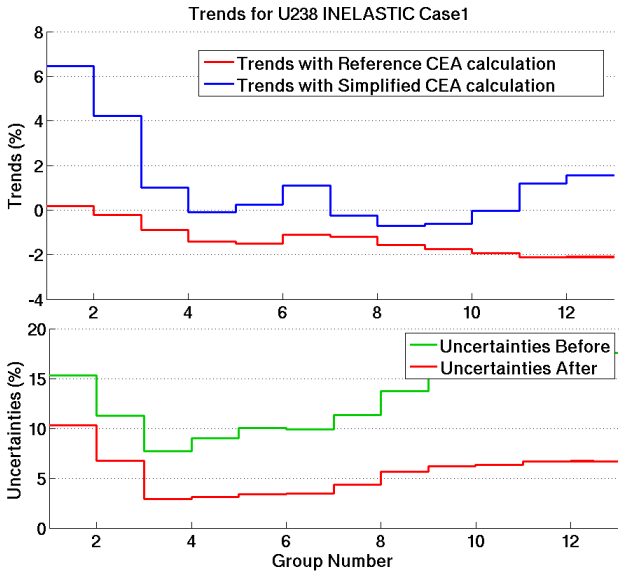

Correction factors and the calculation scheme used to properly calculate initial C/E are thus key to performing adjustment on multi-group cross-section.

The high sensitivity of trends with respect to C/E's shows that reference calculations always need to be performed, if possible, with Monte-Carlo, to avoid misleading trends. In addition, as a consequence of the form of the *a posteriori* cross-section covariance equation (see Equation (7.1)), trends and initial C/E's have no influence on the final covariances. The only important point for *a posteriori* covariances is the competition between the *a priori* covariance matrix and the initial experimental matrix.

7.4.3 How to measure the influence of experiments or parameters?

Definition of Cook's distance

In statistics, Cook's distance is used to estimate the influence of experimental data points when performing least-squares analysis. These data points could be a given observation (here an integral experiment) or a given parameter (for example Chi or inelastic cross-section, etc.).

Data points with large residuals (outliers) and/or high uncertainties may distort accuracy and conclusion of the adjustment. Points with a large Cook's distance are to be assessed.

If the adjustment is done by discarding a chosen integral data point, I, the results (adjusted cross-sections) are noted: $\{\sigma_p^I\}$. The original adjustment is noted $\{\sigma_p\}$. Cook's distance is calculated using the following formula:

$$D_I = (\sigma_p^I - \sigma_p)^T (M_\sigma{}')^{-1} (\sigma_p^I - \sigma_p)$$

Low values of D, show negligible impact on the remote data point. High values of D indicate a very influential experiment. This last point may be due to very low experimental uncertainties and a very important influence on final multi-group cross-sections.

Calculation of Cook's distance

The calculation of Cook's distance is carried out using COMAC-V0 covariances. The results (blue bars) are shown in Figure 56. The influence of each experiment is detailed by type:

- K_{eff}:
  - JOYO is by far the most important experiment in the adjustment for two reasons: all isotopes have an impact on the reactivity of the core (^{235}U + ^{239}Pu fuel) and the experimental uncertainty is rather small (180 pcm). If we change this specific uncertainty manually, from 180 pcm to 500 pcm, we obtain the red bars in Figure 56, where the weight of JOYO is reduced by almost a factor of 10.
  - JEZEBEL ^{240}Pu and ^{239}Pu are the second and third experiments with the most leverage mostly because of the low experimental uncertainty.
  - FLATTOP is 4 times less important than JEZEBEL ^{239}Pu because of its large experimental uncertainty (300 pcm instead of 200 pcm).
  - ZPPR-9 has the same influence as JEZEBEL ^{239}Pu, due to its very small experimental uncertainty (118 pcm).
  - ZPPR-6-7 and ZPPR-6-7 ^{240}Pu have a negligible impact, in comparison with ZPPR-9, mostly due to their experimental uncertainties (~230 pcm).
- Sodium void reactivity experiments seem to be important (the same order of magnitude with JEZEBEL 240 and JOYO). Structural materials such as ^{23}Na and ^{56}Fe are more sensitive to this kind of experiment than in the multiplication factor, which can explain the weight of sodium void in the adjustment. Also, the experimental uncertainties for ZPPR-9 Step 3 and Step 5 are quite low.
- Reaction rate ratio experiments have a very limited impact in the adjustment because the sensitivities are mostly focused on only two reactions in the whole set of cross-section parameters.

Figure 56: Cook's distance on experiments, using full experimental set (blue bars) and when experimental uncertainty of JOYO goes from 180pcm to 500pcm (red bars)

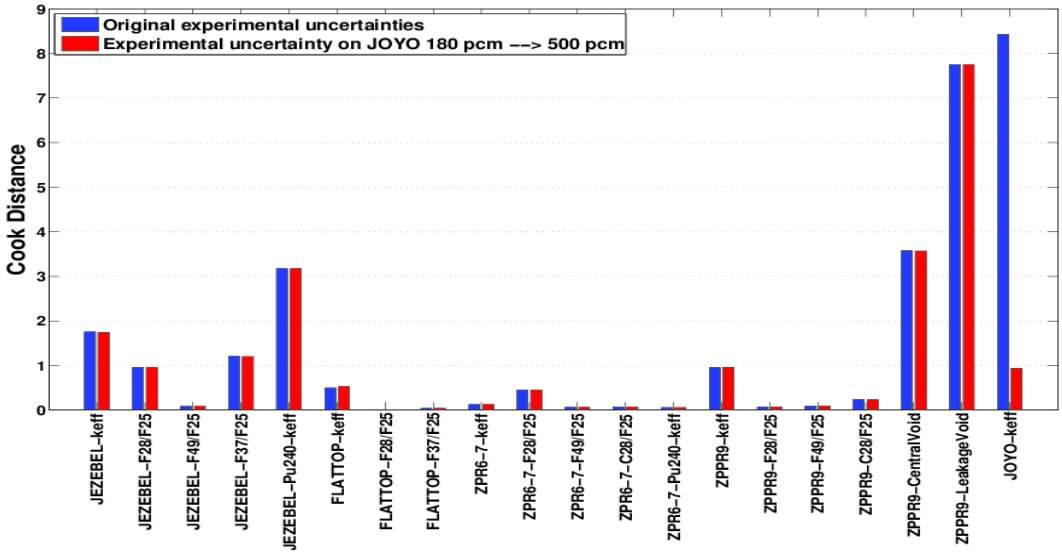

7.5 Conclusions

In summary, this first analysis indicates that:

- Adjustment should include all significant parameters in order to provide a meaningful indication (see the case of inelastic and Chi of ^{239}Pu), and a wide range of integral experiments with different sensitivity profiles.
- Very different covariance data give rise to different adjustments (the cases of ^{238}U inelastic and ^{235}U capture). This point reinforces the need to produce very reliable covariance data and to understand the impact of very small variance data and of correlations (in energy, among reactions, etc.).
- Initial C/E's drive the path to adjustment in some cases (see the example of CEA ^{238}U inelastic trends depending on C/E values).
- Experimental uncertainties have to be correctly quantified, because they drive the weight in the adjustment process (see Cook's distance). In other words, a misestimated experimental uncertainty can lead to biased trends on cross-sections and over-estimation of the uncertainty reduction.
- Final calculated uncertainties on benchmarks do not seem to depend on chosen *a priori* cross-section covariance: uncertainty reduction through an integral experiment is driven by integral experiment uncertainties.
- *a posteriori* cross-section covariances are only driven by the competition between the *a priori* covariance matrix and the initial experimental matrix with a deterministic adjustment procedure.

8. Stress tests and their impact

8.1 Objective

In the SG33 study, the cross-section adjustment exercise treats typical 20 benchmarks of the fast reactor experiments as the reference case. As seen in the previous chapters, the adjusted results of the reference case are quite satisfactory from both points of view of the integral and differential data. The objective of this chapter is to study the impact on the adjusted results when an integral experiment with different nature from the standard 20 data is added to the reference case, which is called as the "Stress test" here. Further, we will add other peculiar integral data with very inadequate C/E (calculation/experiment) values to the reference case to examine what would occur in the adjusted results.

8.2 Survey cases

Three adjustment cases are assessed as follows:

- Case J4: This is the reference adjustment case with the standard 20 integral data. Cross-sections and covariance data[13] are based on the JENDL-4.0 library [16] [17].
- "Stress test": One integral experiment, criticality (k_{eff}, hereafter) of the ZPR-9/34 core [59], is added to the reference Case J4. The unique characteristics of the ZPR-9/34 core are:
  - core region consists of 93% enriched-uranium and iron;
  - height and diameter of the core are 1.8 m and 1.2 m, respectively,
  - core region is surrounded by stainless steel reflector.
- Case B: Four extra integral data are added to Case J4.
  - k_{eff} of the ZPR-9/34 core, which is added in the "Stress test";
  - k_{eff} of the ZPR-3/53 core [60], the core region of which consists of plutonium, ^{238}U and carbon, and is surrounded by ^{238}U blanket;
  - k_{eff} of ZPR-3/54 core [61], the core of which is almost identical with that of ZPR-3/53, but is surrounded by iron reflector;
  - k_{eff} of the ZPR-6/10 core [62], the core of which consists of plutonium, carbon and stainless steel, and is surrounded by stainless steel reflector.

The experimental and analytical information of all 24 integral data treated in this chapter is summarised in Table 21. Numbers 1 through 20 are the data applied in the reference Case J4. Number 21 is the ZPR-9/34 core data added to Case J4 as the "Stress test". It should be emphasised that the k_{eff} value of ZPR-9/34 is overestimated by +1,420 pcm, on the other hand, k_{eff} values of six cores treated in Case J4, numbers 1, 5, 6, 9, 13 and 20, are within only ±530 pcm. The concern of the "Stress test" is whether the adjustment operation could

[13] Carbon which only appears in Case B is the exception. Since JENDL-4.0 does not contain the covariance of carbon, that of COMMARA-2.0 [18] based on ENDF/B-VII is used here.

manage this inadequate C/E value of ZPR-9/34 without harmful influence on other integral data and/or cross-sections. Further, numbers 21 through 24 are the data added to Case J4 as the extreme Case B, where the k_{eff} value of ZPR-6/10 is overestimated by +3,380 pcm. In this sense, the ratio of the C/E-1 value to the one-sigma total uncertainty, that is, the square root for the variance summation of the experimental uncertainty, the analytical modelling uncertainty and the cross-section-induced uncertainty, is more than 3.5, as shown in the right-most column of Table 24. This means that the probability to realise this inadequate C/E value is less than 0.02% (=1-0.9998) assuming the normal distribution of the related uncertainty components. It should be noted that some problems or mistakes might have occurred in the experimental procedure of the ZPR-6/10 core, in the analytical modelling, and/or in the evaluation of cross-section covariance.

As for Table 21, the experimental k_{eff} values and uncertainties[14] from cores number 21 to 24 are based on the ICSBEP handbook [59-62]. The analytical k_{eff} values of the four cores are calculated by a continuous-energy Monte Carlo code with two-dimensional homogenised (r,z) benchmark models, and applied with the corrective factors between the simplified (r,z) model and the as-built three-dimensional heterogeneous model which are provided in the handbook. The analytical modelling uncertainties are based on the uncertainty estimation associated with the "Monte Carlo transformation of model" correction factors to convert the simplified (r,z) model values to the as-built model which is also provided in the handbook. The Monte Carlo statistical uncertainties[15] of the simplified (r,z) model calculation are also added to the analytical modelling uncertainties, though they are negligible compared with the model transformation uncertainties.

Table 21: Integral data for adjustment to be applied in Case J4, "Stress test" and Case B

Case J4) Reference adjustment based on JENDL-4.0 (20 integral data) (+Stress test +Case B)

Case B (extreme case) " Stress test " Case J4 (reference case)

No.	Core	Parameter	Parameter value		C/E value	Relative uncertainty (%)		
			Experiment	Calculation		Experiment	Analytical modeling	*Sum*
1	JEZEBEL-Pu239	keff	1.0000	0.9987	0.9987	0.20	0.03	*0.202*
2		F28/F25	0.2133	0.2066	0.9686	1.1	0.94	*1.447*
3		F49/F25	1.461	1.437	0.9836	0.9	0.75	*1.172*
4		F37/F25	0.9835	0.9632	0.9794	1.4	0.80	*1.612*
5	JEZEBEL-Pu240	keff	1.0000	0.9984	0.9984	0.20	0.03	*0.202*
6	FLATTOP-Pu	keff	1.0000	0.9986	0.9986	0.30	0.03	*0.302*
7		F28/F25	0.1799	0.1758	0.9773	1.1	0.84	*1.384*
8		F37/F25	0.8561	0.8497	0.9925	1.4	0.69	*1.561*
9	ZPR-6/7	keff	1.0005	1.0058	1.0053	0.23	0.03	*0.231*
10		F28/F25	0.02230	0.02305	1.0336	3.0	2.24	*3.74*
11		F49/F25	0.9435	0.9237	0.9790	2.1	1.43	*2.54*
12		C28/F25	0.1323	0.1345	1.0167	2.4	1.22	*2.69*
13	ZPR-6/7 High-Pu240	keff	1.0008	1.0041	1.0033	0.22	0.03	*0.222*
14	ZPPR-9	keff	1.0008	1.0030	1.0021	0.12	0.02	*0.119*
15		F28/F25	0.02070	0.02034	0.9828	2.7	2.09	*3.41*
16		F49/F25	0.9225	0.9217	0.9992	2.0	1.21	*2.34*
17		C28/F25	0.1296	0.1320	1.0188	1.9	1.39	*2.35*
18		Central Na void*	29.39	31.39	1.0682	1.9	5.26	*5.59*
19		Large Na void*	31.68	33.34	1.0523	1.9	4.96	*5.31*
20	JOYO Mk-I	keff	1.0011	0.9992	0.9982	0.18	0.03	*0.182*
21	ZPR-9/34	keff	1.0004	1.0145	1.0142	0.11	0.24	*0.263*
22	ZPR-3/53	keff	1.0017	1.0101	1.0084	0.09	0.21	*0.230*
23	ZPR-3/54	keff	0.9981	1.0119	1.0139	0.17	0.21	*0.272*
24	ZPR-6/10	keff	1.0016	1.0355	1.0338	0.13	0.22	*0.256*

*Cent unit (beta value of ZPPR-9 by JENDL-4.0 = 0.003594)

[14] The experimental uncertainties among the additional ZPR cores might be correlated with other cores through the fuel composition uncertainties and/or experimental technique uncertainties, but it is assumed here that they are independent of each other, since there is no information on such correlations in the ICSBEP handbook.

[15] The uncertainty of the Monte Carlo (MC) calculation is set as twice of the statistical uncertainty value evaluated by the MC code here, taking into account the effect of correlation among the fission sources over successive MC cycles.

8.3 Adjustment results

8.3.1 *Change of all C/E values*

The C/E value changes for all integral data in Case J4, "Stress test" and Case B are summarised in Figure 57 and Table 22 through 24. It appears that both "Stress test" and Case B do not seem to have critical impact on the standard 20 integral data of Case J4. In detail, the C/E values of two ^{238}U capture/^{235}U fission ratios (C28/F25) data are changed by -2% in Case B, but these are still within the summation of the experimental and analytical modelling uncertainties, as shown in the right-most column of Table 21. The reason of these C28/F25 alterations will be explained later.

Figure 57: Change of C/E values by adjustment (all integral data)

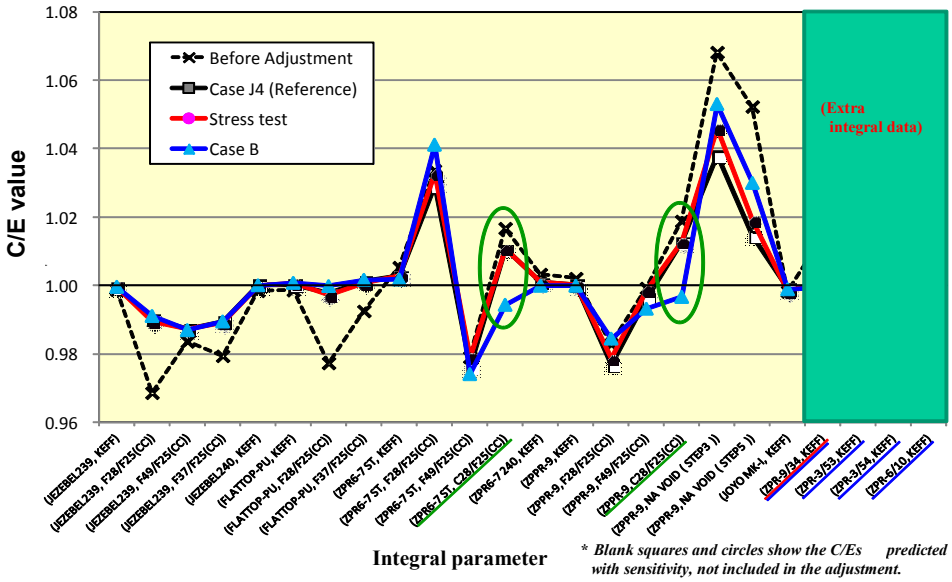

Table 22: Results of adjustment (Case J4: Standard 20 data)

Result of Case J4: Reference adjustment based on JENDL-4.0 (20 integral data)

No.	Core	Parameter	C/E value		Relative uncertainty (%)		Nuclear-data-induced uncertainty (%)		Ratio of C/E-1 to prior total uncertainty*
			Before	After	Experiment (Ve)	Analytical modeling	Before (GMG)	After (GMG)	
1	JEZEBEL-Pu239	keff	0.9987	0.9997	0.20	0.03	0.69	0.15	0.18
2		F28/F25	0.969	0.990	1.1	0.94	3.20	1.02	0.89
3		F49/F25	0.984	0.987	0.9	0.75	0.63	0.47	1.23
4		F37/F25	0.979	0.989	1.4	0.80	1.50	0.67	0.93
5	JEZEBEL-Pu240	keff	0.9984	1.0001	0.20	0.03	0.65	0.14	0.24
6	FLATTOP-Pu	keff	0.9986	1.0002	0.30	0.03	1.26	0.28	0.11
7		F28/F25	0.977	0.998	1.1	0.84	2.94	0.97	0.70
8		F37/F25	0.993	1.001	1.4	0.69	1.44	0.72	0.35
9	ZPR-6/7	keff	1.0053	1.0029	0.23	0.03	0.82	0.12	0.62
10		F28/F25	1.034	1.029	3.0	2.24	4.82	1.85	0.55
11		F49/F25	0.979	0.976	2.1	1.43	1.15	0.83	0.75
12		C28/F25	1.017	1.011	2.4	1.22	2.00	1.12	0.50
13	ZPR-6/7 High-Pu240	keff	1.0033	1.0010	0.22	0.03	0.81	0.12	0.39
14	ZPPR-9	keff	1.0021	1.0001	0.117	0.02	0.90	0.11	0.23
15		F28/F25	0.983	0.977	2.7	2.09	5.28	2.02	0.27
16		F49/F25	0.999	0.996	2.0	1.21	1.15	0.83	0.03
17		C28/F25	1.019	1.013	1.9	1.39	2.03	1.12	0.60
18		Central Na void*	1.068	1.038	1.9	5.26	5.95	3.32	0.84
19		Large Na void*	1.052	1.014	1.9	4.96	7.31	4.04	0.58
20	JOYO Mk-I	keff	0.9982	0.9990	0.18	0.03	0.58	0.16	0.29
Chi-square/Freedom = 0.53									

* = (C/E-1)/[(GMG+Ve+Vm)**0.5]

Table 23: Results of adjustment ("Stress test": 21 data)

Result of "Stress test": Addition of keff of ZPR-9/34 to Case J4

No.	Core	Parameter	C/E value		Relative uncertainty (%)		Nuclea-data-induced uncertainty (%)		Ratio of C/E-1 to prior total-uncertainty*
			Before	After	Experiment (Ve)	Analytical modeling	Before (GMG)	After (GM'G)	
1	JEZEBEL-Pu239	keff	0.9987	0.9997	0.20	0.03	0.69	0.15	0.18
2		F28/F25	0.969	0.989	1.1	0.94	3.20	1.02	0.89
3		F49/F25	0.984	0.987	0.9	0.75	0.63	0.47	1.23
4		F37/F25	0.979	0.989	1.4	0.80	1.50	0.67	0.93
5	JEZEBEL-Pu240	keff	0.9984	1.0000	0.20	0.03	0.65	0.14	0.24
6	FLATTOP-Pu	keff	0.9986	1.0007	0.30	0.03	1.26	0.28	0.11
7		F28/F25	0.977	0.997	1.1	0.84	2.94	0.97	0.70
8		F37/F25	0.993	1.001	1.4	0.69	1.44	0.72	0.35
9	ZPR-6/7	keff	1.0053	1.0028	0.23	0.03	0.82	0.12	0.62
10		F28/F25	1.034	1.033	3.0	2.24	4.82	1.84	0.55
11		F49/F25	0.979	0.979	2.1	1.43	1.15	0.81	0.75
12		C28/F25	1.017	1.011	2.4	1.22	2.00	1.12	0.50
13	ZPR-6/7 High-Pu240	keff	1.0033	1.0009	0.22	0.03	0.81	0.12	0.39
14	ZPPR-9	keff	1.0021	1.0002	0.117	0.02	0.90	0.11	0.23
15		F28/F25	0.983	0.979	2.7	2.09	5.28	2.01	0.27
16		F49/F25	0.999	0.999	2.0	1.21	1.15	0.82	0.03
17		C28/F25	1.019	1.013	1.9	1.39	2.03	1.12	0.60
18		Central Na void*	1.068	1.046	1.9	5.26	5.95	3.29	0.84
19		Large Na void*	1.052	1.019	1.9	4.96	7.31	4.03	0.58
20	JOYO Mk-I	keff	0.9982	0.9984	0.18	0.03	0.58	0.16	0.29
21	ZPR-9/34	keff	1.0142	1.0012	0.11	0.24	1.15	0.25	1.21
Chi-square/Freedom = 0.63									

* = (C/E-1)/[(GMG+Ve+Vm)**0.5]

Table 24: Results of adjustment (Case B: 24 data)

Result of Case B: Addition of keff of ZPR-9/34 and other 3 cores to Case J4

No.	Core	Parameter	C/E value		Relative uncertainty (%)		Nuclea-data-induced uncertainty (%)		Ratio of C/E-1 to prior total-uncertainty*
			Before	After	Experiment (Ve)	Analytical modeling	Before (GMG)	After (GM'G)	
1	JEZEBEL-Pu239	keff	0.9987	0.9996	0.20	0.03	0.69	0.15	0.18
2		F28/F25	0.969	0.991	1.1	0.94	3.20	1.01	0.89
3		F49/F25	0.984	0.987	0.9	0.75	0.63	0.47	1.23
4		F37/F25	0.979	0.989	1.4	0.80	1.50	0.67	0.93
5	JEZEBEL-Pu240	keff	0.9984	1.0000	0.20	0.03	0.65	0.14	0.24
6	FLATTOP-Pu	keff	0.9986	1.0007	0.30	0.03	1.26	0.28	0.11
7		F28/F25	0.977	1.000	1.1	0.84	2.94	0.97	0.70
8		F37/F25	0.993	1.002	1.4	0.69	1.44	0.72	0.35
9	ZPR-6/7	keff	1.0053	1.0017	0.23	0.03	0.82	0.11	0.62
10		F28/F25	1.034	1.041	3.0	2.24	4.82	1.79	0.55
11		F49/F25	0.979	0.974	2.1	1.43	1.15	0.79	0.75
12		C28/F25	1.017	0.994	2.4	1.22	2.00	1.02	0.50
13	ZPR-6/7 High-Pu240	keff	1.0033	0.9999	0.22	0.03	0.81	0.11	0.39
14	ZPPR-9	keff	1.0021	0.9999	0.117	0.02	0.90	0.11	0.23
15		F28/F25	0.983	0.984	2.7	2.09	5.28	1.98	0.27
16		F49/F25	0.999	0.993	2.0	1.21	1.15	0.79	0.03
17		C28/F25	1.019	0.997	1.9	1.39	2.03	1.02	0.60
18		Central Na void*	1.068	1.053	1.9	5.26	5.95	3.27	0.84
19		Large Na void*	1.052	1.030	1.9	4.96	7.31	4.01	0.58
20	JOYO Mk-I	keff	0.9982	0.9988	0.18	0.03	0.58	0.16	0.29
21	ZPR-9/34	keff	1.0142	0.9993	0.11	0.24	1.15	0.25	1.21
22	ZPR-3/53	keff	1.0084	1.0006	0.09	0.21	0.62	0.16	1.28
23	ZPR-3/54	keff	1.0139	0.9980	0.17	0.21	0.83	0.22	1.59
24	ZPR-6/10	keff	1.0338	1.0044	0.13	0.22	0.93	0.21	3.52
Chi-square/Freedom = 1.11									

* = (C/E-1)/[(GMG+Ve+Vm)**0.5]

8.3.2 Change of k_{eff} C/E values

The C/E values of k_{eff} data are further discussed in Figure 58, where the blank squares and circles mean the posterior C/E values which are not included in the adjustment operation itself, but predicted with sensitivity coefficients. If we study carefully the adjusted results, the following facts can be found:

1) Case J4: Even applying the cross-sections adjusted by the reference Case J4, there are no improvements at all to predict the extra four data, numbers 21 through 24. This means that the adjusted results of the integral data and cross-sections are expected to be quite different between Case J4 and the other two cases.

2) "Stress test": The adjusted results seem as good as in Case J4. Even the C/E value of the extra ZPR-9/34 k_{eff}, which is newly added to the adjustment, changes to almost 1.00. The other three extra data, number 22 through 24, which are not included in the "Stress test", are also partly improved if the cross-sections adjusted by the "Stress test" are applied. This means that the extra three data possess somewhat similar sensitivity coefficients with those of ZPR-9/34.

3) Case B: The adjusted results seem good. Even the doubtful k_{eff} of ZPR-6/10 seems to be successfully adjusted.

Figure 58: Change of C/E values by adjustment (Only k_{eff} data)

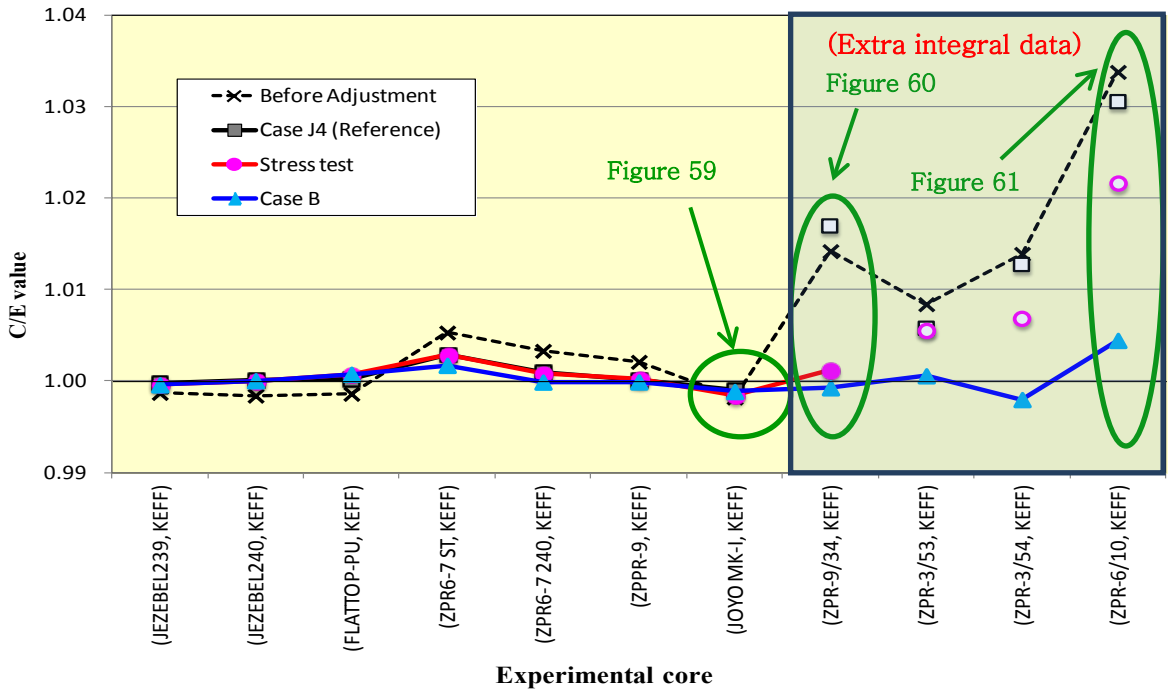

8.3.3 Component of contribution to k_{eff} changes

It is necessary to confirm that the adjustment has no impact on not only the integral data, but on the differential cross-sections. Here, we check the nuclide- and reaction-wise contributions to the total k_{eff} alterations by the adjustment by comparing the three survey cases.

Figure 59 shows the breakdown of the contributions for the k_{eff} alterations of the JOYO Mk-I core, which is included in the three cases. The total k_{eff} alterations are rather similar among the three cases, but the components of the cross-section contributions are found to be significantly different from each other. In the "Stress test", ^{56}Fe contributes largely compared with that of Case J4, the reason of which would be caused by the stainless steel reflector effect of the extra ZPR-9/34 core. In the extreme Case B, it should be emphasised that some major cross-sections such as ^{238}U and ^{239}Pu capture, contribute extremely, but cancelled with each other because of the opposite directions of the reactivity. It should be confirmed whether these large cross-section changes are reasonable from the nuclear data viewpoint or not.

The components of the k_{eff} alteration in the ZPR-9/34 core are compared for the three cases[16] in Figure 60. In the "Stress test", it is found that the large improvement of the C/E value, -1,300 pcm, is attained by the cross-section changes of ^{56}Fe capture and elastic scattering reactions, which are considered to result in the negative reactivity of the absorption effect by the iron in the core region, and the neutron leakage enhancement by the stainless steel reflector. These trends of the ^{56}Fe cross-section alterations are exaggerated in the extreme Case B, but the ^{235}U cross-sections are also changed here to keep the adjusted C/E value around 1.0. Again, it is needed to investigate this reasonability from the nuclear data viewpoint.

The contributions of cross-sections to the ZPR-6/10 k_{eff} alterations are summarised in Figure 61. Note that the ZPR-6/10 k_{eff} is only included in the Case B adjustment, therefore, those of the other two cases show the prediction values with sensitivity. In the reference Case J4, there are small contributions of cross-section changes to the ZPR-6/10 k_{eff}. In the "Stress test", the predicted k_{eff} change is -1,200 pcm totally, which is close to that of the ZPR-9/34 core, because of the similar sensitivity coefficients of ^{56}Fe between ZPR-6/10 and ZPR-9/34. In the extreme Case B, the alteration of the ZPR-6/10 k_{eff} reaches -2,940 pcm to make the adjusted C/E value very close to 1.0. This large k_{eff} alteration is caused not only by the contributions of ^{56}Fe but by those of ^{239}Pu capture reaction. When needed, this negative reactivity by this ^{239}Pu alteration is cancelled by other isotopes, for example, ^{238}U in the JOYO Mk-I core as already seen.

Figure 59: Contribution to C/E changes by adjustment: JOYO Mk-I, k_{eff}

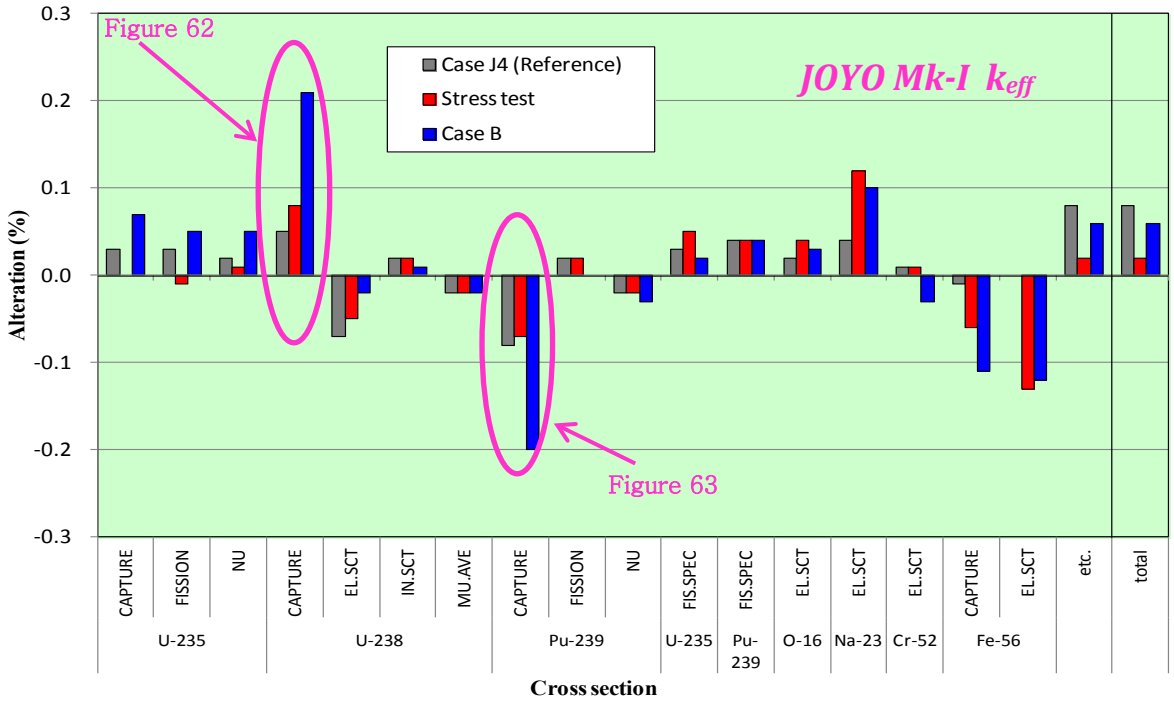

[16] In the reference Case J4, ZPR-9/34 is not included in the adjustment. The components with blank elements in the figure mean the predicted alterations of k_{eff} obtained by the sensitivity coefficients and the cross-section changes of Case J4.

Figure 60: Contribution to C/E changes by adjustment: ZPR-9/34, k_{eff}

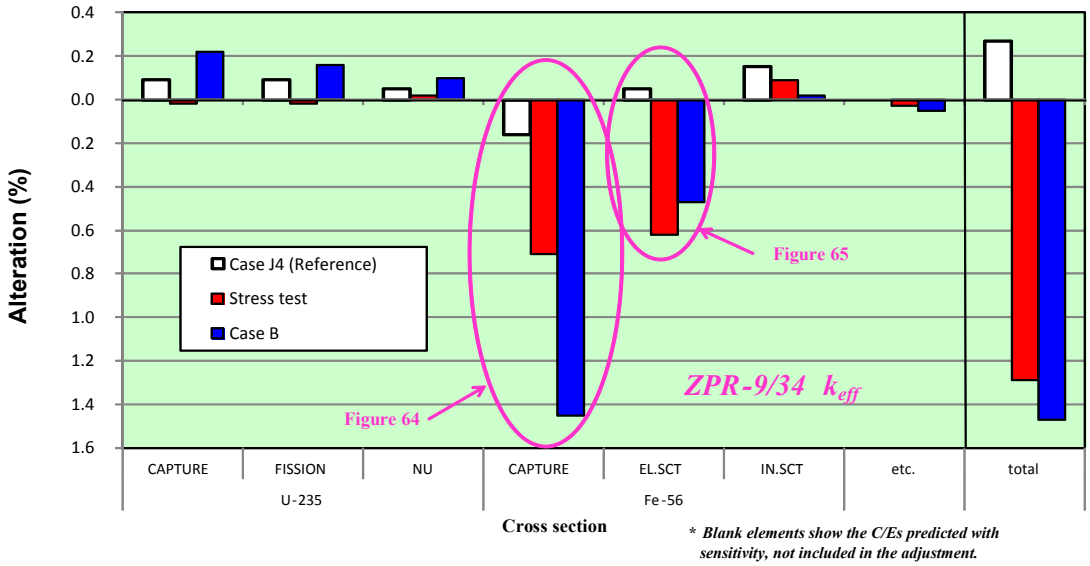

Figure 61: Contribution to C/E changes by adjustment: ZPR-6/10, k_{eff}

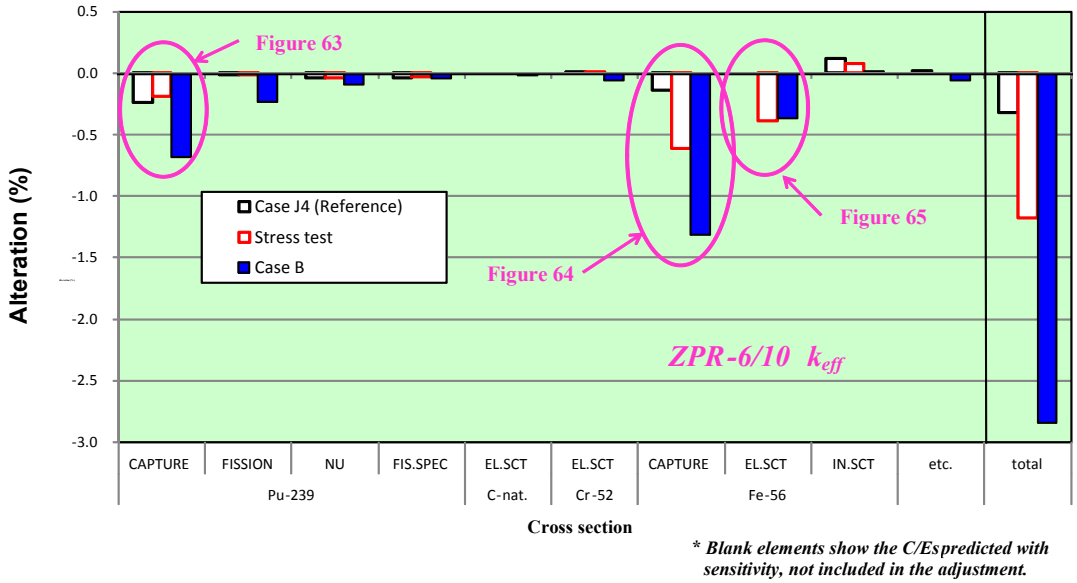

8.3.4 *Cross-section alteration by adjustment*

For the three survey cases, it is investigated here whether the cross-section alteration by the adjustment is physically reasonable from the nuclear data viewpoint or not.

Figure 62 shows the cross-section alterations of the ^{238}U capture reaction with neutron energy. For the reference Case J4 and the "Stress test", there is little movement of ^{238}U capture, but in the extreme Case B, it is decreased by -2~-3% in the important energy region, a few through 100 keV, in order to cancel the negative reactivity due to the ^{239}Pu capture changes in JOYO Mk-I and other cores such as ZPR-6/7 or ZPPR-9. This affects the

C/E values of C28/F25 as seen in Figure 57, but the degrees of the C/E value alterations are within the experimental and analytical modelling uncertainties as already mentioned.

The alterations of the ^{239}Pu capture cross-sections by the adjustment are depicted in Figure 63. In Case J4 and the "Stress test", the change is approximately +3~5%, which is within one standard deviation (STD) value of the JENDL-4.0 covariance, that is, ±6~9% in the dominant energy region. However, in the extreme Case B, ^{239}Pu capture is significantly increased by +9~13%, to adjust the k_{eff} of ZPR-6/10. This cross-section alteration of ^{239}Pu capture reaction could be considered quite improbable from the statistical viewpoint, since it largely exceeds the STD value.

More drastic cross-section alteration appears for the ^{56}Fe capture reaction in Figure 64. In the reference Case J4, there are small changes of the cross-sections. However, quite large cross-section alterations occur in the "Stress test". The degree is +11% below 100 keV, which is very close to the STD value, ±10%. The changes of this magnitude might be close to the limitation of allowance from the viewpoint of the nuclear data evaluation. In the extreme Case B, the cross-section alterations exceed +24%, more than twice of the STD value, which is definitely unacceptable.

Figure 65 illustrates the changes of the ^{56}Fe elastic scattering cross-sections. In the Case J4, there are small alterations. On the other hand, in the "Stress test" and the Case B, the ^{56}Fe elastic cross-sections are decreased to adjust k_{eff} values of the stainless steel or iron reflector cores, ZPR-9/34, -3/54 and -6/10. These cross-section changes are quite large, but still within the STD values, which may be acceptable from the nuclear data viewpoint.

It is also necessary to examine the adjusted results of the carbon-natural which are newly introduced in Case B adjustment, since its elastic scattering cross-sections have very large sensitivity to the k_{eff} values of the ZPR-3/53, -3/54 and -6/10 cores. Figure 66 shows that the carbon elastic cross-sections are not altered by the adjustment at all, the reason for which would be the very small STD values of the COMMARA-2.0 covariance adopted here.

Figure 62: Change of cross-sections by adjustment: ^{238}U capture

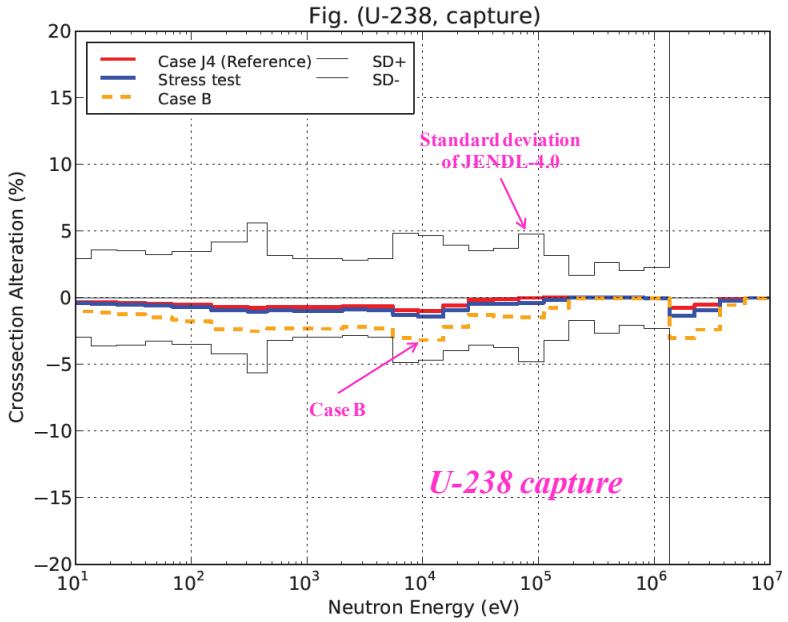

Figure 63: Change of cross-sections by adjustment: ^{239}Pu, capture

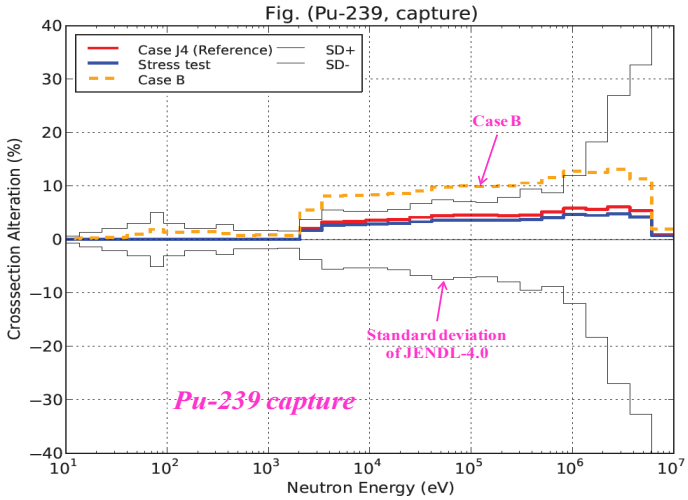

Figure 64: Change of cross-sections by adjustment: ^{56}Fe, capture

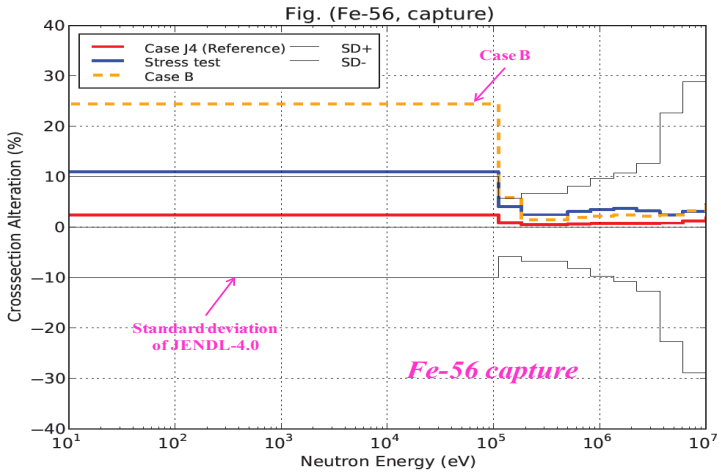

Figure 65: Contribution to C/E changes by adjustment: ^{56}Fe, elastic scattering

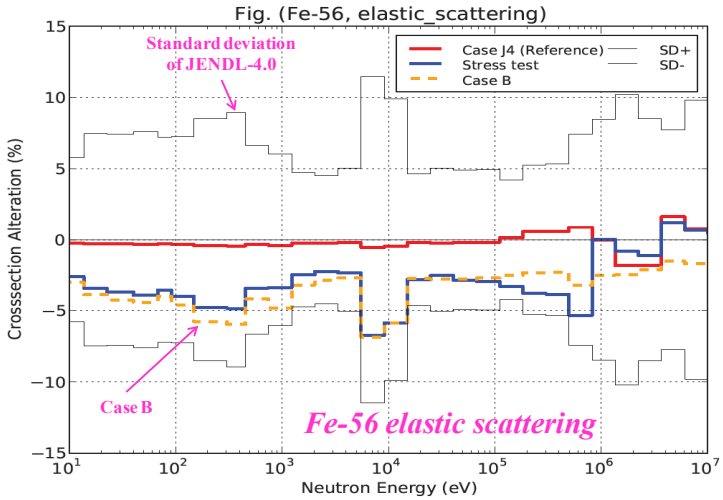

Figure 66: Contribution to C/E changes by adjustment: C-natural, elastic scattering

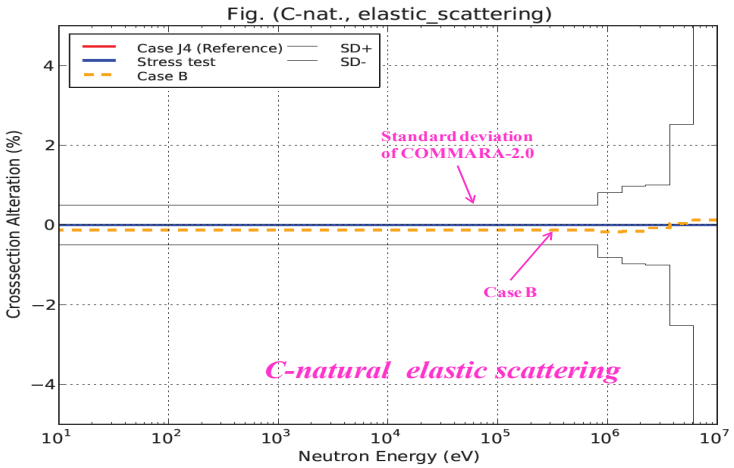

8.4 Effects on target cores

Applying the adjusted cross-section sets of the three cases to the SG33 targets, that is, JAEA-FBR, ABR-Oxide and ABR-Metal cores mentioned in Chapter 1, the influence of the extra integral data is studied. Table 25 compares the k_{eff} changes of the target cores with the adjusted data of Case J4, the "Stress test", and Case B.

As for the k_{eff} value of the JAEA-FBR core, there are no effects regardless of the adjustment cases. On the other hand, for the ABR-Oxide core, the "Stress test" affects the k_{eff} value by -120 pcm, but Case B by -400 pcm, compared with the reference Case J4. Figure 67 clearly reveals the reason, that is, the differences of the k_{eff} changes between the JAEA-FBR and ABR-Oxide cores among adjustment cases are caused by the differences of those sensitivity coefficients to the capture cross-sections of ^{56}Fe and ^{239}Pu.

Table 25: Effects of adjustment on k_{eff} of target cores

Core	Change of keff by adjustment		
	Case J4 (Reference)	Stress test	Case B
JAEA-FBR	-0.18 %Δk	-0.16 %Δk	-0.18 %Δk
ABR-Oxide	-0.25 %Δk	-0.37 %Δk	-0.65 %Δk
ABR-Metal	-0.22 %Δk	-0.40 %Δk	-0.55 %Δk

Figure 67: Contribution to k_{eff} changes of target cores by adjustment

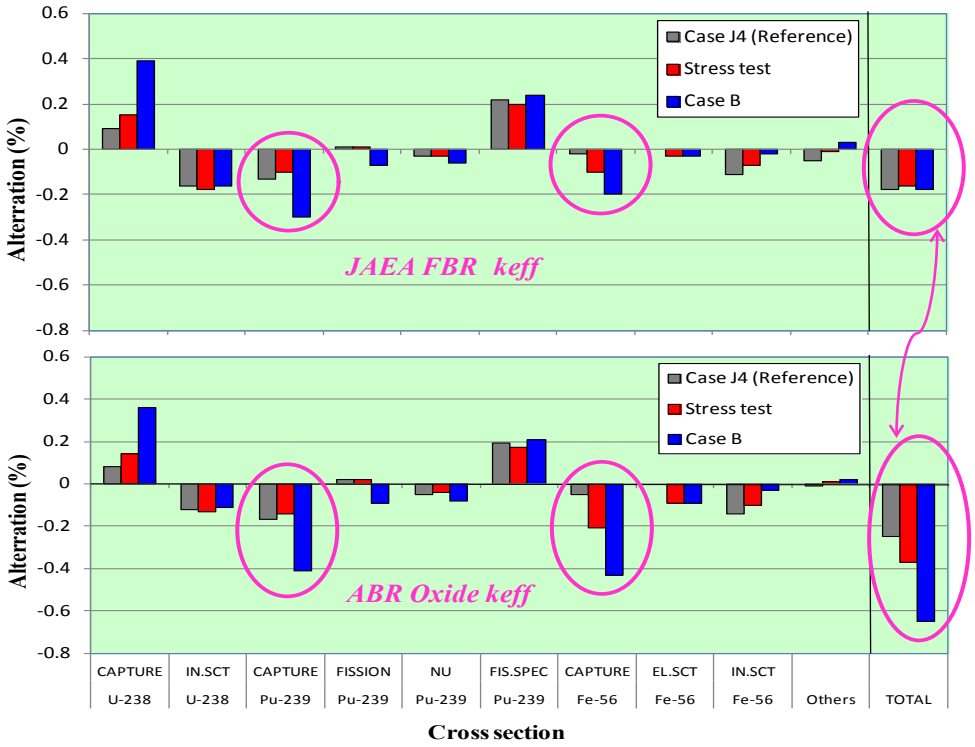

8.5. Concluding remarks

The lessons from the "Stress test" and the extreme Case B are summarised as follows:

- In the "Stress test", the overestimation of k_{eff} for the extra core, ZPR-9/34 (+1,400 pcm) was successfully adjusted without impact on the standard 20 integral data and the nuclear data based on JENDL-4.0. It is judged that the "Stress test" of the SG33 adjustment exercise was passed to demonstrate its robustness.
- In the extreme Case B (maximum: +3,400 pcm), some cross-sections were changed unacceptably exceeding their STD ranges, though the all C/E values seemed to be successfully adjusted immediately.
- It would be required to eliminate some doubtful or abnormal integral data from the adjustment procedure. A proposal of the measure is that the ratio of absolute C/E-1 value to the total uncertainty (= the square root for the variance summation of the cross-section-induced uncertainty, the experimental uncertainty and the analytical modelling uncertainty) must be less than 1.5~2 to adopt the data in the adjustment[17].

[17] To confirm this recommendation, one extra adjustment case was studied, where the doubtful ZPR-9/10 k_{eff} was removed from the Case B data. As for the remaining 23 integral data, the ratios of the C/E-1 values to the total uncertainties are all less than 1.6, as shown in Table 24. The adjusted results of the extra 23 data case were found to be rather similar with those of the "Stress test", which is reasonable from not only the integral but nuclear data viewpoint.

9. Conclusions

The statistical data adjustment methods have been applied successfully in the design of reactors, in particular fast and innovative (e.g. Generation-IV) reactors for four decades. However, only recently these methods have been recognised as powerful tools to be used also for the improvement of nuclear data files within a very wide range of applications. The establishment of science-based covariance data motivated by the need to understand and to quantify uncertainties in reactor design parameters, has been one of the most important developments in order to achieve both goals, i.e. improvements of evaluated data files and reduction of design parameters uncertainties.

However, other important achievements have been necessary to pursue those objectives: improved integral experiment analysis and experimental uncertainty assessments (including correlations), sensitivity methods, critical analysis of the adjustment characteristics, both *a priori* and *a posteriori*.

Subgroup 33 has provided a deeper understanding of nuclear data adjustment methodologies and of their applications. The findings of Subgroup 33 have revealed that the statistical adjustments methodologies in use worldwide for different reactor analysis and design purposes are well understood and they are essentially equivalent.

For some important data, the results of the benchmark adjustments indicate common trends for modification even if they start from different basic nuclear data and different covariance matrices. The results obtained also show a remarkable degree of robustness in the sense that the observed trends can "survive" rather severe "stress tests".

In this respect, these methodologies can provide a powerful tool for nuclear data (and associated uncertainties) improvement if used in an appropriate manner. In fact, it has been indicated that the associated sensitivity analysis requires the careful use of existing methods, and specific recommendations have been made.

Moreover, the choice of specific integral experiments of different types (critical masses but also reaction rates, reactivity coefficients and irradiation experiments) and the significant sensitivity in different neutron energy spectra is of high importance to avoid compensating effects in adjustments.

Finally, it has been emphasised the crucial role of the covariance data used, both those associated with the nuclear data and those associated with the integral experiments. The *a posteriori* correlations are mainly responsible for the uncertainty reduction of the parameters of the reference design systems. Their physical meaning and appropriate utilisation will require further investigation.

The deeper understanding of the methodologies and of their applications implies that the role for cross-section adjustment is more and more perceived as one providing useful feedback to evaluators and differential measurement experimentalists in order to improve the knowledge of neutron cross-sections to be used in a wider range of applications.

This new role for cross-section adjustment requires addressing and solving a new series of issues such as: definition of criteria to assess the reliability and robustness of an adjustment; requisites to assure the quantitative validity of the covariance data; criteria to alert for inconsistencies between differential and integral data; definition of consistent approaches to use both adjusted data and *a posteriori* covariance data to improve

quantitatively nuclear data files; provide methods and define conditions to generalise the results of an adjustment in order to evaluate the "extrapolability" of the results to a different range of applications (e.g. different reactor systems) for which the adjustment was not initially intended; suggest guidelines to enlarge the experimental database in order to avoid as much as possible compensations and to meet needs that were identified by the cross-section adjustment.

Future development should then focus on a research activity to provide criteria and practical approaches for the effective use of the results of sensitivity analyses and cross-section adjustments. As a result, it will be possible to provide feedback to evaluators and differential measurement experimentalists in order to improve the knowledge of neutron cross-sections, uncertainties, and correlations to be used in a wide range of applications.

References

[1] M. Salvatores *et al.* (2014), "Methods and issues for the combined use of integral experiments and covariance data: Results of a NEA international collaborative study", Nucl. Data Sheets, 115.

[2] G. Palmiotti: "Corrective Factors Dependence from Cross-Sections Data Sets"4th Subgroup meeting, NEA, 29-30 November 2010.

[3] S.J. Kim *et al.* (2012), "Results of Nuclear Data S&U Analysis for Benchmark Exercises Using DANTSYS/SUSD3D with COMMARA-2.0", private communication, SG33 group meeting (22-23 May 2012).

[4] R.E. Alcouffe *et al.* (1995), "DANTSYS: A Diffusion Accelerated Neutral Particle Transport Code System", Los Alamos National Laboratory report, LA-12969-M.

[5] ORNL (2009), "SCALE, A modular code system for performing standardized computer analyses for licensing evaluations". Version 6: Report available from the Radiation Safety Information Computational Center at Oak Ridge National Laboratory as CCC-750, ORNL/TM-2005/39.

[6] D. Rochman (2012), "Adjusting ^{235}U, ^{238}U and ^{239}Pu nuclear data with a Monte Carlo technique", private communication, SG33 group meeting (22-23 May, 2012).

[7] H. Wu (2012), "Progress on nuclear data adjustment", private communication, SG33 group meeting (22-23 May, 2012).

[8] J. Tommasi (2007), "ERANOS User's manual- Applications of perturbation theory with finite difference diffusion and S_n transport flux solvers", CEA report, SPRC/LEPh 07-003.

[9] M. Ishikawa (2005), "Recent application of nuclear data to fast reactor core analysis and design in Japan", *International Conference on Nuclear Data for Science and Technology*.

[10] G. Rimpault *et al.* (2002), "The ERANOS data and code system for fast reactor neutronic analyses", Proceedings of the International Conference on the New Frontier of Nuclear Technology: Reactor Physics, Safety and High-Performance Computing (PHYSOR 2002), Seoul, Korea.

[11] I. Kodeli (2001), "Multidimensional Deterministic Nuclear Data Sensitivity and Uncertainty Code System: Method and Application", *Nuclear Science and Engineering*, 138, pp. 45-66.

[12] ORNL (2009), "TSUNAMI-3D Control module for three-dimensional cross-section sensitivity and uncertainty analysis for criticality (SCALE, VOL I, Sect. C9),Technical Report ORNL/TM-2005/39.

[13] M.L. Williams *et al.* (2001), "Eigenvalue sensitivity theory for resonance-shielded cross sections", *Nuclear Science and Engineering*, 138, 177–191.

[14] A. Trkov (2012), "Direct Monte Carlo Calculation of the Sensitivity Coefficients", Private communication.

[15] D.L. Smith (1991),"Probability, Statistics, and Data Uncertainties in Nuclear Science and Technology", An OECD Nuclear Energy Agency Nuclear Data Committee Series, *Nuclear Physics and Nuclear Data in Science and Technology*, Volume 4.

[16] K. Shibata, O. Iwamoto, T. Nakagawa, N. Iwamoto, A. Ichihara, S. Kunieda, S. Chiba, K. Furutaka, N. Otuka, T. Ohsawa, T. Murata, H. Matsunobu, A. Zukeran, S. Kamada, J. Katakura (2011), "JENDL-4.0: A New Library for Nuclear Science and Engineering", *Journal of Nuclear Science and Technology*, Vol.48, No.1, pp.1-30, JENDL-4.0 homepage, http://wwwndc.jaea.go.jp/jendl/j40/j40.html.

[17] O. Iwamoto, T. Nakagawa, S. Chiba (2011), "Covariance Evaluation for Actinide Nuclear Data in JENDL-4.0", *Journal of Korean Physical Society (Proceedings of International Conference on Nuclear Data for Science and Technology*, ND2010), Vol.59, No.2, pp.1224-1229.

[18] M. Herman, P. Obložinský, C.M. Matoon, M. Pigni, S. Hoblit, S.F. Mughabghab, A. Sonzogni, P. Talou, M.B. Chadwick, G.M. Hale, A.C. Kahler, T. Kawano, R.C. Little, P.G. Young (2011),"COMMARA-2.0 Neutron Cross Section Covariance Library", BNL-94830-2011, U.S. Department of Energy.

[19] M.B. Chadwick, P. Oblozinsky, M. Herman, N.M. Greene, R.D. McKnight, D.L. Smith, P.G. Young, R.E. MacFarlane, G.M. Hale, S.C. Frankle, A.C. Kahler, T. Kawano, R.C. Little, D.G. Madland, P. Moller, R.D. Mosteller, P.R. Page, P. Talou, H. Trellue, M.C. White, W.B. Wilson, R. Arcilla, C.L. Dunford, S.F. Mughabghab, B. Pritychenko, D. Rochman, A.A. Sonzogni, C.R. Lubitz, T.H. Trumbull, J.P. Weinman, D.A. Brown, D.E. Cullen, D.P. Heineichs, D.P. McNabb, H. Derrien, M.E. Dunn, N.M. Larson, L.C. Leal, A.D. Carlson, R.C. Block, J.B. Briggs, E.T. Cheng, H.C. Huria, M.L. Zerkle, K.S. Kozier, A. Courcelle, V. Oronyaev, S.C. van der Mark (2006), "ENDF/B-VII.0: Next Generation Evaluated Nuclear Data Library for Nuclear Science and Technology", *Nuclear Data Sheets,* Volume 107, Number 12, pp.2931-3060.

[20] M.B. Chadwick, M. Herman, P. Obložinský, M.E. Dunn, Y. Danon, A.C. Kahler, D.L. Smith, B. Pritychenko, G. Arbanas, R. Arcilla, R. Brewer, D.A. Brown, R. Capote, A.D. Carlson, Y.S. Cho, H. Derrien, K. Guber, G.M. Hale, S. Hoblit, S. Holloway, T.D. Johnson, T. Kawano, B.C. Kiedrowski, H. Kim, S. Kunieda, N.M. Larson, L. Leal, J.P. Lestone, R.C. Little, E.A. McCutchan, R.E. MacFarlane, M. MacInnes, C.M. Mattoon, R.D. McKnight, S.F. Mughabghab, G.P.A. Nobre, G. Palmiotti, A. Palumbo, M.T. Pigni, V.G. Pronyaev, R.O. Sayer, A.A. Sonzogni, N.C. Summers, P. Talou, I.J. Thompson, A. Trkov, R.L. Vogt, S.C. van der Marck, A. Wallner, M.C. White, D. Wiarda, P.G. Young (2011),"ENDF/B-VII.1 Nuclear Data for Nuclear Science and Technology: Cross Sections, Covariances, Fission Product Yields and Decay Data", *Nuclear Data Sheets,* Volume 112, Number 12, pp.2887-2996.

[21] D.L. Smith (2011), "Evaluated Nuclear Data Covariances: The Journey from ENDF/B-VII.0 to ENDF/B-VII.1", Nuclear Data Sheets 112, pp.3037-3053.

[22] M. Herman (2011), "Development of ENDF/B-VII.1 and Its Covariance Component", *Journal of Korean Physical Society (Proceedings of International Conference on Nuclear Data for Science and Technology,* ND2010), Vol.59, No.2, pp.1034-1039.

[23] W.P. Poenitz (1981), "Data Interpretation, Objective Evaluation Procedures and Mathematical Techniques for the Evaluation of Energy-dependent Ratio, Shape and Cross Section Data", *Proceedings of the Conference on Nuclear Data Evaluation Methods and Procedures,* Brookhaven National Laboratory, New York, Sep. 22-25, 1980, BNL-NCS-51363, pp.249-289.

[24] D.W. Muir (1999), "ZOTT99, Data Evaluation Using Partitioned Least-Squares", Code package IAEA1371/01, NEA Computer Program Service.

[25] T. Kawano, H. Matsunobu, T. Murata, A. Zukeran, Y. Nakajima, M. Kawai, O. Iwamoto, K. Shibata, T. Nakagawa, T. Ohsawa, M. Baba, T. Yoshida (2000),"Simultaneous Evaluation of Fission Cross Sections of Uranium and Plutonium Isotopes for JENDL-3.3", *Journal of Nuclear Science and Technology*, Vol.37, No.4, pp.327-334.

[26] N.M. Larson (2008), "Updated Users' Guide for SAMMY: Multilevel R-matrix Fits to Neutron Data using Bayes' Equations", Oak Ridge National Laboratory, ORNL/TM-9179/R8.

[27] P. Obložinský, Y.-S. Cho, C.M. Mattoon, S.F. Mughabghab (2010), "Formalism for neutron cross-section covariances in the resonance region using kernel approximation", Brookhaven National Laboratory, BNL-91287-2010.

[28] R.C. Little, T. Kawano, G.D. Hale, M.T. Pigni, M. Herman, P. Obložinský, M.L. Williams, M.E. Dunn, G. Arbanas, D. Wiarda, R.D. McKnight, J.N. McKamy, J.R. Felty (2008), "Low-fidelity Covariance Project", *Nuclear Data Sheets* 109, pp.2828–2833.

[29] S.F. Mughabghab (2006), "Atlas of Neutron Resonances, Resonance Parameters and Thermal Cross Sections, Z = 1-100, 5th Edition", Elsevier, Amsterdam.

[30] T. Kawano, K. Shibata (1997), "Covariance Evaluation System", Japan Atomic Energy Research Institute, JAERI-Data/Code 97-037.

[31] P.G. Young, M.B. Chadwick, R.E. MacFarlane, P. Talou, T. Kawano, D.G. Madland, W.B. Wilson, C.W. Wilkerson (2007), "Evaluation of Neutron Reactions for ENDF/B-VII: $^{232-241}$U and ^{239}Pu", *Nuclear Data Sheets* 108, pp.2589-2654.

[32] M. Herman, R. Capote, B.V. Carlson, P. Obložinský, M. Sin, A. Trkov, H. Wienke, V. Zerkin (2007), "EMPIRE: Nuclear Reaction Model Code System for Data Evaluation", *Nuclear Data Sheets* 108, pp.2655–2715.

[33] A.J. Koning, S. Hilaire and M.C. Duijvestijn (2007), "TALYS-1.0", *Proceedings of International Conference on Nuclear Data for Science and Technology*, ND2007), Session-4: Nuclear models, DOI: 10.1051/ndata:07767.

[34] O. Iwamoto (2007), "Development of a Comprehensive Code for Nuclear Data Evaluation, CCONE, and Validation Using Neutron-Induced Cross Sections for Uranium Isotopes", *Journal of Nuclear Science and Technology*, Vol.44, No.5, pp.687-697.

[35] C. De Saint Jean, B. Habert, P. Archier, G. Noguere, D. Bernard, J. Tommasi, P. Blaise (2011),"Uncertainty Evaluation of Nuclear Reaction Model Parameters Using Integral and Microscopic Measurements with the CONRAD Code", *Journal of Korean Physical Society (Proceedings of International Conference on Nuclear Data for Science and Technology*, ND2010), Vol.59, No.2, pp.1276-1279.

[36] M. Herman, M.T. Pigni, P. Obložinský, S.F. Mughabghab, C.M. Mattoon, R. Capote, Young-Sik Cho, A. Trkov (2008), "Development of Covariance Capabilities in EMPIRE Code", Nuclear Data Sheets 109, pp.2752–2761.

[37] M. Herman, E. Bauge, R. Capote, U. Fisher, A.Yu. Konobeyev, P.E. Pereslavtsev, M. Herman, P. Obložinský, M.T. Pigni, T. Kawano, P. Talou, I. Kodeli, A. Trkov, A. Koning, D. Rochman, H. Leeb, D. Neudecker, D.L. Smith (2011), "Covariance Data in the Fast Neutron Region", Nuclear Energy Agency, International Evaluation Co-operation , Volume 24, NEA/NSC/WPEC/DOC(2010)427.

[38] A.J. Koning (2007), "New working methods for nuclear data evaluation: how to make a nuclear data library?" *Proceedings of International Conference on Nuclear Data for Science and Technology,* (ND2007), Session-11: Evaluated files, methods and processing, DOI: 10.1051/ndata:07683.

[39] D. Rochman, A. J. Koning, S. C. van der Marck, A. Hogenbirk, D. van Veen (2011), "Nuclear Data Uncertainty Propagation: Total Monte Carlo vs. Covariances", *Journal of Korean Physical Society (Proceedings of International Conference on Nuclear Data for Science and Technology*, ND2010), Vol.59, No.2, pp.1236-1241.

[40] B.T. Rearden, M.L. Williams, M.A. Jessee, D.E. Mueller, D.A. Wiarda (2011), "Sensitivity and Uncertainty Analysis Capabilities and Data in SCALE", *Nucl. Technol.* 174(2), 236-288.

[41] E. Dupont, A.J. Koning, N. Otuka (2011), "Exploratory Data Analysis of the EXFOR Database", *Journal of Korean Physical Society (Proceedings of International Conference on Nuclear Data for Science and Technology,* ND2010), Vol.59, No.2, pp.1333-1336.

[42] J.B. Dragt *et al.* (1977), "Methods of Adjustment and Error Evaluation of Neutron Capture Cross Sections, Application to Fission Product Nuclides", *Nucl. Sci. Eng.*, 62, 117-129.

[43] T.T. Ivanova *et al.* (2003), "Influence of the Correlations of Experimental Uncertainties on Criticality Prediction", *Nucl. Sci. Eng.*, 145(1), 97-104.

[44] T.T. Ivanova *et al.* (2009), "Towards validation of criticality calculations for systems with MOX powders", Annals of Nuclear Energy, 36, 305–309.

[45] O. Buss, A. Hoefer, J.C. Neuber, M. Schmid (2010), "Hierarchical Monte-Carlo Approach to Bias Estimation for Criticality Safety Calculations", *Proc. of PHYSOR 2010, Advances in Reactor Physics to Power the Nuclear Renaissance*, Pittsburgh, PA, 9-14 May 2010.

[46] B.T. Rearden, K. Dugan (2013), Private communication.

[47] OECD/NEA (2012), "International Handbook of Evaluated Criticality Safety Benchmark Experiments", NEA/NSC/DOC(95)03, September 2012 Edition.

[48] OECD/NEA (2013), "International Handbook of Evaluated Reactor Physics Benchmark Experiments", NEA/NSC/DOC(2006)1, March 2013 Edition.

[49] T. Ikegami (2011), "ZPPR-9 Experiment: A 650 MWe-class Sodium-cooled MOX-fuelled FBR Core Mock-up Critical Experiment with Clean Core of Two Homogeneous Zones", International Handbook of Evaluated Reactor Physics Benchmark Experiments (IRPhE), ZPPR-LMFR-EXP-002, NEA/NSC/DOC(2006)1, OECD/NEA.

[50] V.G. Dean (2003), "The Benchmark Evaluation Process: From Experimental Data to Benchmark Model", *Nuclear Science and Engineering* 145, pp.20-38.

[51] "ZPPR-11 Monthly Report for February 1980", ZPR-TM-361, Argonne National Laboratory.

[52] R.M. Lell, J.A. Morman, R.W. Schaefer, R.D. McKnight (2011), "ZPR-6 Assembly 7 Experiments: A Fast Reactor Core with Mixed (Pu,U)-Oxide Fuel and Sodium with a Thick Depleted Uranium Reflector", International Handbook of Evaluated Reactor Physics Benchmark Experiments (IRPhE), ZPR-LMFR-EXP-001, NEA/NSC/DOC(2006)1, OECD/NEA.

[53] T. Ueki, T. Mori, M. Nakagawa (1997), "Error Estimations and Their Biases in Monte Carlo Eigenvalue Calculations", *Nucl. Sci. Eng.*, 125, 1-11.

[54] H.J. Shim, C.H. Kim (2009), "Real Variance Estimation Using an Intercycle Fission Source Correlation for Monte Carlo Eigenvalue Calculations", *Nucl. Sci. Eng.*, 162, 98-108.

[55] K. Yokoyama, A. Shono (2011), "Japan's Experimental Fast Reactor JOYO Mk-I Core: Sodium-cooled Uranium-Plutonium Mixed Oxide Fuelled Fast Core Surrounded by UO_2 Blanket", International Handbook of Evaluated Reactor Physics Benchmark Experiments (IRPhE), JOYO-LMFR-RESR-001, NEA/NSC/DOC(2006)1, OECD/NEA.

[56] M. Ishikawa, R. D. McKnight (2011), "ZPPR-10A Experiment: A 650 MWe-class Sodium-cooled MOX-fuelled FBR Homogeneous Core Mock-up Critical Experiment with Two Enrichment Zones and Nineteen Control Rod Positions", International Handbook of Evaluated Reactor Physics Benchmark Experiments (IRPhE), ZPPR-LMFR-EXP-001, NEA/NSC/DOC(2006)1, OECD/NEA.

[57] T. Sanda (2011), "ZPPR-10C Experiment: A 800 MWe-class Sodium-cooled MOX-fuelled FBR Homogeneous Core Mock-up Critical Experiment with Two Enrichment Zones and Nineteen Control Rod Positions", International Handbook of Evaluated Reactor Physics Benchmark Experiments (IRPhE), ZPPR-LMFR-EXP-006, NEA/NSC/DOC(2006)1, OECD/NEA.

[58] OECD/NEA (2011), "Assessment of Existing Nuclear Data Adjustment Methodologies", International Evaluation Co-operation, Intermediate Report of WPEC Subgroup 33, NEA/NSC/WPEC/DOC(2010)429.

[59] R.W. Schaefer, K.A. Bunde, P.J. Collins (2011), "The Uranium/Iron Benchmark Assembly: A ^{235}U(93%) Iron Cylinder Reflected by Stainless Steel", International Handbook of Evaluated Criticality Safety Benchmark Experiment (ICSBEP), Volume II, NEA/NSC/DOC(95)03.

[60] R.M. Lell (2011), "ZPR-3 Assembly 53: A Cylindrical Assembly of Plutonium Metal, Depleted Uranium and Graphite with A Thick Depleted Uranium Reflector", International Handbook of Evaluated Criticality Safety Benchmark Experiment (ICSBEP), Volume II, NEA/NSC/DOC(95)03.

[61] R.M. Lell (2011), "ZPR-3 Assembly 54: A Cylindrical Assembly of Plutonium Metal Depleted Uranium and Graphite with A Thick Iron Reflector", International Handbook of Evaluated Criticality Safety Benchmark Experiment (ICSBEP), Volume VI, NEA/NSC/DOC(95)03.

[62] R.M. Lell, M.A. Smith, R.W. Schaefer, R.D. McKnight (2011), "ZPR-6 Assembly 10: A Cylindrical Plutonium/Carbon/StainlessSteel Assembly with Stainless Steel and Iron Reflectors", International Handbook of Evaluated Criticality Safety Benchmark Experiment (ICSBEP), Volume I, NEA/NSC/DOC(95)03.

Appendix A: Models of 1000 MWt Advanced Burner Reactor (ABR) core concepts

2D (r,z) geometry models

Reference 1000 MWt Advanced Burner Reactor (ABR) core concepts were developed at ANL in FY 2007 with ternary metal and mixed oxide fuels. Two core concepts were developed for both metal and oxide cores: start-up and TRU recycled equilibrium cores. Weapons-grade plutonium was used as the TRU feed of the start-up core without recycling the ABR spent fuel. For the recycled core, the TRU recovered from the ABR spent fuel was used as the primary TRU feed and the TRU from LWR spent fuel was used as the make-up feed. Compact core concepts of medium TRU conversion ratio (~0.8 for the start-up core and ~0.7 for the recycled equilibrium core) were developed by trade-off between the burn-up reactivity loss and the TRU conversion ratio.

The planar layouts of the ABR oxide and metal core concepts are shown in Figures A.1 and A.2, respectively. Both cores consist of 180 drivers, 114 reflectors, 66 radial shields, and 15 primary and four secondary control assemblies. Three enrichment zones are used for the oxide core, whereas two enrichment zones are used for the metal core. The primary control system consists of three control assemblies in the fourth row and 12 control assemblies in the seventh row, and the secondary system contains four control assemblies located at the core centre and in the fourth row. The primary control assemblies are axially moved to maintain criticality, while the secondary control assemblies are positioned at the top of the active core all the time.

Figures A.3 and A.4, respectively, show the (r,z) geometry models of the ABR oxide and metal core concepts. All the dimensions represent the values at the operating conditions, accounting for the thermal expansions of fuel and structural materials. In these R-Z models, the primary control assemblies in the fourth row are homogenised together with the secondary control assemblies in the fourth row and positioned at the top of the active core. In the oxide core, the axial position of the primary control assemblies in the seventh row is 68.6 cm from the bottom of the active core for the start-up core and 79.5 cm and for the recycled core. For the metal core, the primary control assembly positions of the start-up and recycled cores are 57.9 cm and 63.3 cm, respectively.

Region-wise, homogenised nuclide densities at the beginning of equilibrium cycle (BOEC) of the start-up oxide core, start-up metal core, and recycled oxide core are provided below. The fuel compositions are prepared separately for five axial burn regions of each of inner, middle (oxide core only), and outer core zones. Fission products are modelled five lumped fission products, depending on fissionable isotopes. Average material temperatures for multi-group cross-section preparation are provided below.

As noted above, fission products are modelled with five lumped fission products. In order to simplify the proposed cross-section adjustment exercise, it is suggested to replace these lumped fission products by a single element (e.g. Mo) or remove the lumped fission products.

Figure A.1: Planar layout of reference 1000 MWt ABR oxide core concept

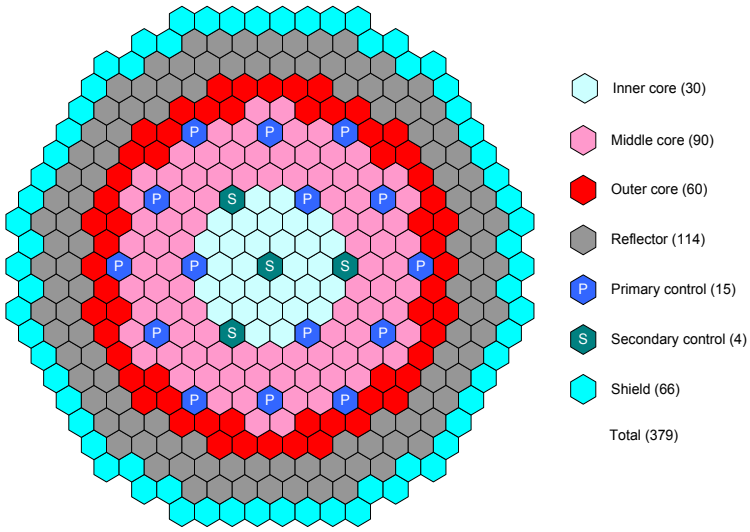

Figure A.2: Planar layout of reference 1000 MWt ABR metal core concept

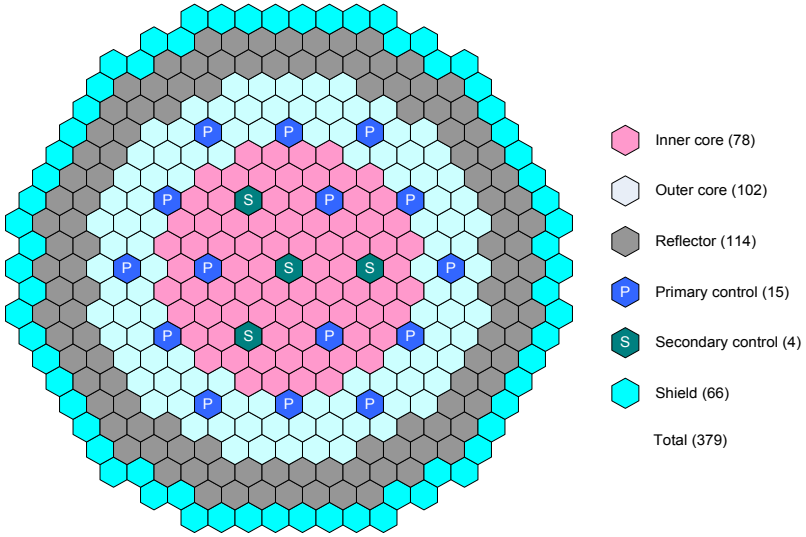

Figure A.3: 2D (r,z) geometry model of 1000 MWt ABR oxide core

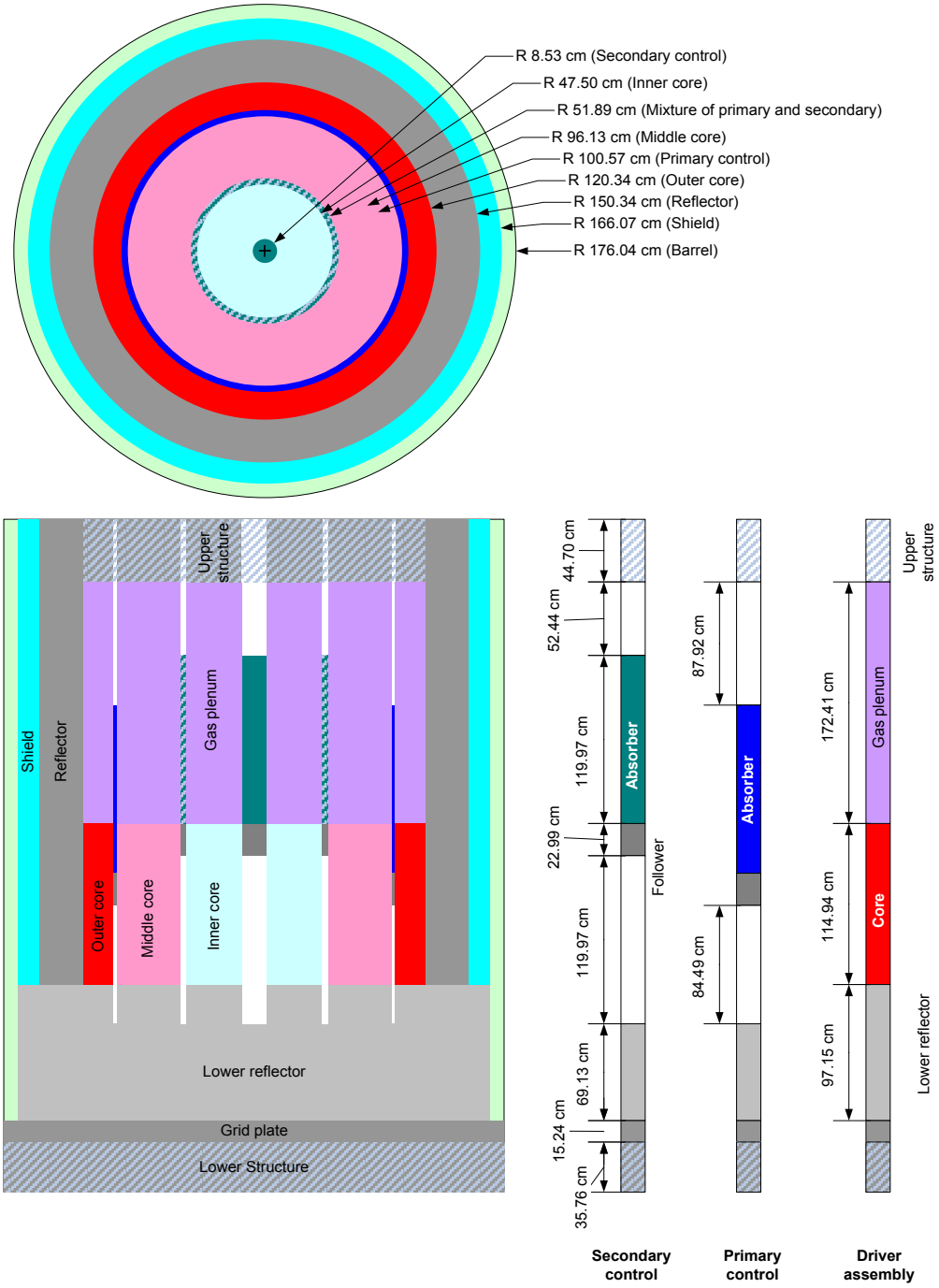

Figure A.4: 2D (r,z) geometry model of 1000 MWt ABR metal core

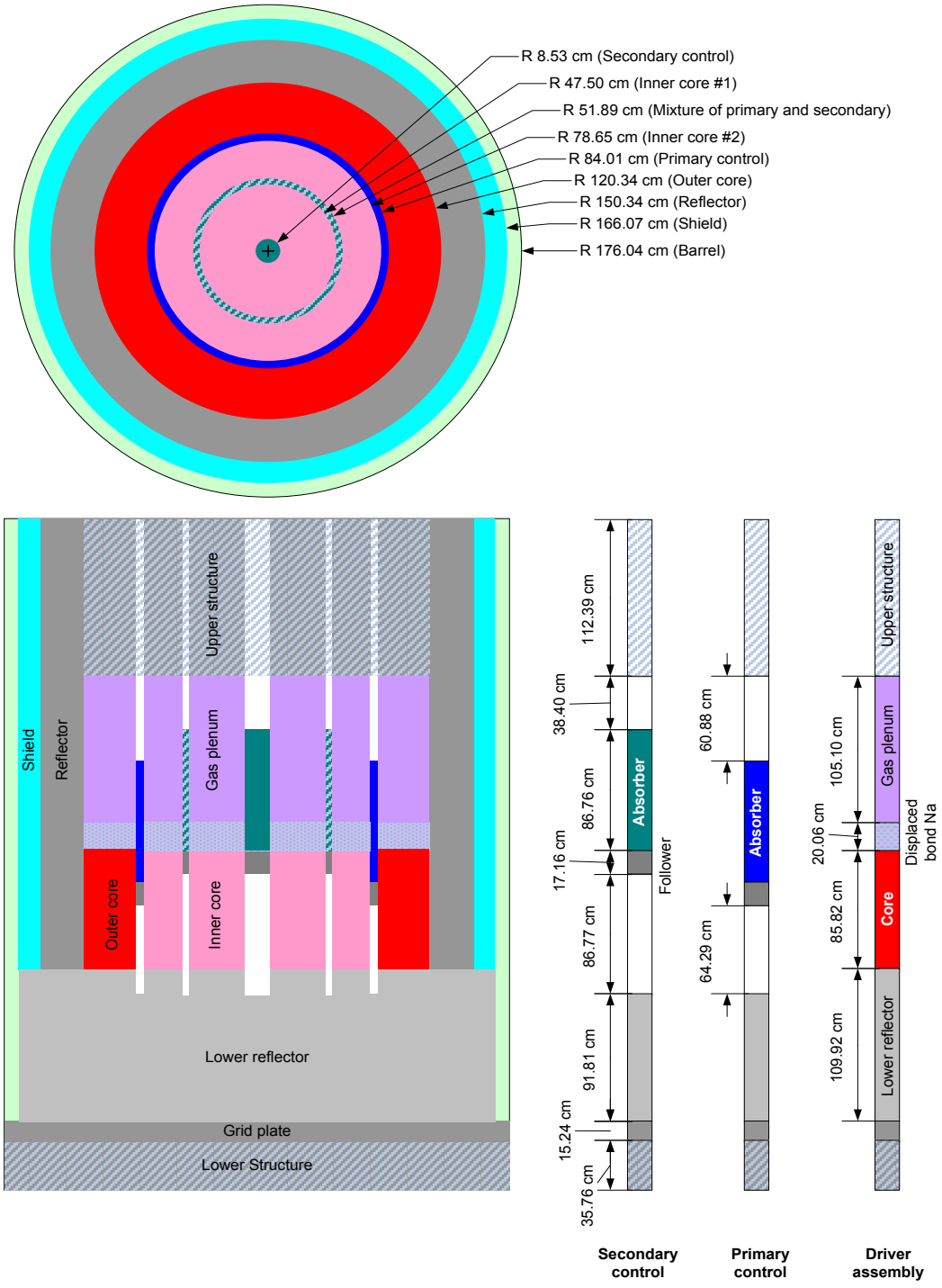

BOEC Nuclide number densities (#/barn-cm) of start-up oxide core

Inner core

Material	Nuclide	Axial node from core bottom				
		1	2	3	4	5
Coolant	Na23	8.1322E-03	8.1322E-03	8.1322E-03	8.1322E-03	8.1322E-03
Structure	Fe	1.8573E-02	1.8573E-02	1.8573E-02	1.8573E-02	1.8573E-02
	Cr	2.7616E-03	2.7616E-03	2.7616E-03	2.7616E-03	2.7616E-03
	Mn55	1.2234E-04	1.2234E-04	1.2234E-04	1.2234E-04	1.2234E-04
	Ni	1.1452E-04	1.1452E-04	1.1452E-04	1.1452E-04	1.1452E-04
	Mo	1.3056E-04	1.3056E-04	1.3056E-04	1.3056E-04	1.3056E-04
Fuel	U234	6.7199E-09	8.7656E-09	9.3294E-09	8.2960E-09	5.5856E-09
	U235	7.8935E-06	7.1198E-06	6.8689E-06	7.3348E-06	8.6984E-06
	U236	1.1065E-06	1.1929E-06	1.2288E-06	1.1584E-06	9.3539E-07
	U238	5.9477E-03	5.8233E-03	5.7834E-03	5.8556E-03	6.0360E-03
	Np237	1.2447E-06	1.6289E-06	1.6950E-06	1.5731E-06	1.1060E-06
	Pu236	5.1177E-12	9.2945E-12	1.0236E-11	8.5477E-12	3.9005E-12
	Pu238	5.3775E-07	7.3123E-07	7.9225E-07	6.8063E-07	4.1150E-07
	Pu239	9.9775E-04	9.6991E-04	9.6103E-04	9.7696E-04	1.0209E-03
	Pu240	1.6777E-04	1.7662E-04	1.8188E-04	1.7159E-04	1.4630E-04
	Pu241	1.5038E-05	1.6764E-05	1.7800E-05	1.5826E-05	1.1514E-05
	Pu242	1.4192E-06	1.8015E-06	2.0053E-06	1.6345E-06	9.5614E-07
	Am241	9.5142E-07	1.0019E-06	1.0408E-06	9.6439E-07	7.8872E-07
	Am242m	3.1938E-08	3.7965E-08	4.1053E-08	3.5258E-08	2.2559E-08
	Am243	8.7649E-08	1.2259E-07	1.4307E-07	1.0660E-07	4.8201E-08
	Cm242	5.3289E-08	6.8596E-08	7.6420E-08	6.2100E-08	3.4313E-08
	Cm243	2.0926E-09	2.7000E-09	3.1449E-09	2.3319E-09	1.0166E-09
	Cm244	1.3752E-08	2.1979E-08	2.7036E-08	1.8235E-08	6.1530E-09
	Cm245	1.0189E-09	1.8547E-09	2.3896E-09	1.4763E-09	3.7794E-10
	Cm246	2.8954E-11	6.5570E-11	9.0122E-11	4.9397E-11	8.6709E-12
	O	1.5205E-02	1.5205E-02	1.5205E-02	1.5205E-02	1.5205E-02
Fission product	LFP35 [a)]	3.7928E-06	4.4393E-06	4.6357E-06	4.2740E-06	3.2024E-06
	LFP38 [b)]	4.7811E-05	6.7659E-05	7.2170E-05	6.4110E-05	4.0575E-05
	LFP39 [c)]	3.9350E-04	5.0622E-04	5.4083E-04	4.7907E-04	3.2044E-04
	LFP40 [d)]	1.0504E-05	1.5766E-05	1.7459E-05	1.4457E-05	7.7439E-06
	LFP41 [e)]	6.6157E-06	9.3915E-06	1.0702E-05	8.3608E-06	4.0945E-06

LFP35: lumped fission product from U234, U235, U236, and Pu236 fissions

LFP38: lumped fission product from U238, Np237, and Pu238 fissions

LFP39: lumped fission product from Pu239 fission

LFP40: lumped fission product from Pu240 fission

LFP41: lumped fission products from Pu241 and higher actinides fissions

Middle core

Material	Nuclide	Axial node from core bottom				
		1	2	3	4	5
Coolant	Na23	8.1322E-03	8.1322E-03	8.1322E-03	8.1322E-03	8.1322E-03
Structure	Fe	1.8573E-02	1.8573E-02	1.8573E-02	1.8573E-02	1.8573E-02
	Cr	2.7616E-03	2.7616E-03	2.7616E-03	2.7616E-03	2.7616E-03
	Mn55	1.2234E-04	1.2234E-04	1.2234E-04	1.2234E-04	1.2234E-04
	Ni	1.1452E-04	1.1452E-04	1.1452E-04	1.1452E-04	1.1452E-04
	Mo	1.3056E-04	1.3056E-04	1.3056E-04	1.3056E-04	1.3056E-04
Fuel	U234	6.2284E-09	8.0473E-09	8.5465E-09	7.6313E-09	5.2326E-09
	U235	8.2850E-06	7.5198E-06	7.2752E-06	7.7300E-06	9.0710E-06
	U236	9.7752E-07	1.0754E-06	1.1140E-06	1.0388E-06	8.0344E-07
	U238	5.8987E-03	5.7887E-03	5.7539E-03	5.8171E-03	5.9784E-03
	Np237	1.1634E-06	1.5429E-06	1.6106E-06	1.4863E-06	1.0229E-06
	Pu236	4.4663E-12	8.2636E-12	9.1383E-12	7.5738E-12	3.3416E-12
	Pu238	4.7301E-07	6.4144E-07	6.9441E-07	5.9743E-07	3.6440E-07
	Pu239	1.0819E-03	1.0467E-03	1.0360E-03	1.0553E-03	1.1104E-03
	Pu240	1.6604E-04	1.7486E-04	1.7987E-04	1.6998E-04	1.4462E-04
	Pu241	1.3782E-05	1.5448E-05	1.6381E-05	1.4593E-05	1.0577E-05
	Pu242	1.1998E-06	1.5219E-06	1.6855E-06	1.3862E-06	8.2383E-07
	Am241	9.2034E-07	9.7417E-07	1.0111E-06	9.3833E-07	7.6743E-07
	Am242m	2.7876E-08	3.3703E-08	3.6504E-08	3.1236E-08	1.9403E-08
	Am243	6.6615E-08	9.3630E-08	1.0881E-07	8.1615E-08	3.6670E-08
	Cm242	4.3862E-08	5.7277E-08	6.3812E-08	5.1798E-08	2.7875E-08
	Cm243	1.4926E-09	1.9814E-09	2.3133E-09	1.7037E-09	6.9840E-10
	Cm244	9.2702E-09	1.5025E-08	1.8422E-08	1.2472E-08	4.0706E-09
	Cm245	6.1835E-10	1.1545E-09	1.4857E-09	9.1710E-10	2.2067E-10
	Cm246	1.5554E-11	3.6406E-11	5.0048E-11	2.7314E-11	4.4006E-12
	O	1.5205E-02	1.5205E-02	1.5205E-02	1.5205E-02	1.5205E-02
Fission product	LFP35	3.3289E-06	3.9624E-06	4.1536E-06	3.8009E-06	2.7506E-06
	LFP38	4.3115E-05	6.1322E-05	6.5452E-05	5.8072E-05	3.6341E-05
	LFP39	3.6847E-04	4.7685E-04	5.0941E-04	4.5115E-04	2.9705E-04
	LFP40	9.4816E-06	1.4286E-05	1.5800E-05	1.3109E-05	6.9493E-06
	LFP41	5.3210E-06	7.6435E-06	8.6948E-06	6.8082E-06	3.2720E-06

Outer core

Material	Nuclide	Axial node from core bottom				
		1	2	3	4	5
Coolant	NA23	8.1322E-03	8.1322E-03	8.1322E-03	8.1322E-03	8.1322E-03
Structure	Fe	1.8573E-02	1.8573E-02	1.8573E-02	1.8573E-02	1.8573E-02
	Cr	2.7616E-03	2.7616E-03	2.7616E-03	2.7616E-03	2.7616E-03
	Mn55	1.2234E-04	1.2234E-04	1.2234E-04	1.2234E-04	1.2234E-04
	Ni	1.1452E-04	1.1452E-04	1.1452E-04	1.1452E-04	1.1452E-04
	Mo	1.3056E-04	1.3056E-04	1.3056E-04	1.3056E-04	1.3056E-04
Fuel	U234	5.4966E-09	6.6707E-09	6.9923E-09	6.4207E-09	4.9543E-09
	U235	8.8784E-06	8.2480E-06	8.0441E-06	8.4113E-06	9.3916E-06
	U236	6.9547E-07	7.9526E-07	8.3352E-07	7.6266E-07	5.7594E-07
	U238	5.6236E-03	5.5524E-03	5.5299E-03	5.5698E-03	5.6686E-03
	Np237	8.7117E-07	1.1780E-06	1.2372E-06	1.1317E-06	7.6202E-07
	Pu236	2.6168E-12	4.9541E-12	5.5197E-12	4.5355E-12	1.9594E-12
	Pu238	3.7229E-07	4.7528E-07	5.0821E-07	4.4977E-07	3.1591E-07
	Pu239	1.4136E-03	1.3602E-03	1.3442E-03	1.3725E-03	1.4497E-03
	Pu240	1.7878E-04	1.8850E-04	1.9341E-04	1.8410E-04	1.6240E-04
	Pu241	1.2844E-05	1.4332E-05	1.5119E-05	1.3668E-05	1.0708E-05
	Pu242	9.4921E-07	1.1586E-06	1.2606E-06	1.0791E-06	7.4824E-07
	Am241	9.6838E-07	1.0249E-06	1.0600E-06	9.9424E-07	8.6038E-07
	Am242m	2.2054E-08	2.7242E-08	2.9584E-08	2.5343E-08	1.6421E-08
	Am243	4.1117E-08	5.5381E-08	6.3328E-08	4.9362E-08	2.6364E-08
	Cm242	3.0421E-08	4.0013E-08	4.4473E-08	3.6517E-08	2.1246E-08
	Cm243	7.5621E-10	1.0475E-09	1.2275E-09	9.0732E-10	4.0606E-10
	Cm244	4.1154E-09	6.4717E-09	7.8335E-09	5.4874E-09	2.1215E-09
	Cm245	2.0007E-10	3.6963E-10	4.7252E-10	2.9879E-10	8.3317E-11
	Cm246	3.3776E-12	7.9080E-12	1.0835E-11	6.0286E-12	1.1087E-12
	O	1.5205E-02	1.5205E-02	1.5205E-02	1.5205E-02	1.5205E-02
Fission product	LFP35	2.2522E-06	2.7642E-06	2.9222E-06	2.6394E-06	1.8722E-06
	LFP38	2.9434E-05	4.1915E-05	4.4744E-05	3.9791E-05	2.5041E-05
	LFP39	3.1740E-04	4.1258E-04	4.4057E-04	3.9149E-04	2.6247E-04
	LFP40	7.2373E-06	1.0892E-05	1.1994E-05	1.0077E-05	5.5871E-06
	LFP41	3.4230E-06	4.8913E-06	5.5242E-06	4.4159E-06	2.3413E-06

Lower structure, grid plate and lower reflector

Nuclide	Lower structure	Grid plate	Lower reflector
Na23	1.5591E-02	1.5591E-02	8.1322E-03
Fe	1.5878E-02	1.5878E-02	4.4260E-02
Cr	3.2355E-03	3.2355E-03	6.5809E-03
Mn55	5.0846E-04	5.0846E-04	2.9155E-04
Ni	3.2604E-03	3.2604E-03	2.7289E-04
Mo	4.3524E-04	4.3524E-04	3.1113E-04

Fission gas plenum and upper structure

Nuclide	Gas plenum	Upper structure
Na23	8.1322E-03	8.1322E-03
Fe	1.8573E-02	4.4260E-02
Cr	2.7616E-03	6.5809E-03
Mn55	1.2234E-04	2.9155E-04
Ni	1.1452E-04	2.7289E-04
Mo	1.3056E-04	3.1113E-04

Radial reflector, shield and barrel

Nuclide	Radial reflector	Shield	Barrel
Na23	3.45173E-03	3.80767E-03	1.23563E-02
Fe	5.89102E-02	2.06903E-02	1.83018E-02
Cr	8.75918E-03	3.07638E-03	3.72938E-03
Mn55	3.88047E-04	1.36289E-04	5.86069E-04
Ni	3.63219E-04	1.27569E-04	3.75801E-03
Mo	4.14113E-04	1.45444E-04	5.01672E-04
C12		1.67189E-03	
B10		7.05028E-03	
B11		2.83782E-02	

Control assemblies

Nuclide	Under follower	Follower	Absorber		Above absorber	Upper structure
			Secondary	Primary		
Na23	2.02091E-02	1.64105E-02	6.42006E-03	6.42006E-03	6.42006E-02	7.87124E-03
Fe	6.45825E-03	1.83482E-02	1.44809E-02	1.44809E-02	1.44809E-03	4.50768E-02
Cr	9.60257E-04	2.72814E-03	2.15312E-03	2.15312E-03	2.15312E-04	6.70233E-03
Mn55	4.25411E-05	1.20862E-04	9.53870E-05	9.53870E-05	9.53870E-03	2.77927E-04
Ni	3.98192E-05	1.13129E-04	8.92839E-05	8.92839E-05	8.92839E-04	2.96925E-04
Mo	4.53987E-05	1.28980E-04	1.01794E-04	1.01794E-04	1.01794E-04	3.16870E-04
C12			1.05367E-02	1.05367E-02		
B10			8.38725E-03	2.70650E-02		
B11			3.37598E-02	1.64104E-02		

BOEC Nuclide number densities (#/barn-cm) of start-up metal core

Inner core

Material	Nuclide	Axial node from core bottom				
		1	2	3	4	5
Coolant	Na23	7.8712E-03	7.8712E-03	7.8712E-03	7.8712E-03	7.8712E-03
Structure	Fe	1.7889E-02	1.7889E-02	1.7889E-02	1.7889E-02	1.7889E-02
	Cr	2.6599E-03	2.6599E-03	2.6599E-03	2.6599E-03	2.6599E-03
	Mn55	1.1784E-04	1.1784E-04	1.1784E-04	1.1784E-04	1.1784E-04
	Ni	1.1030E-04	1.1030E-04	1.1030E-04	1.1030E-04	1.1030E-04
	Mo	1.2575E-04	1.2575E-04	1.2575E-04	1.2575E-04	1.2575E-04
Fuel	U234	4.0295E-09	4.8981E-09	5.0728E-09	4.5923E-09	3.4048E-09
	U235	1.2393E-05	1.1988E-05	1.1839E-05	1.2291E-05	1.3307E-05
	U236	9.8706E-07	9.8735E-07	1.0036E-06	9.3054E-07	7.8523E-07
	U238	8.1520E-03	8.0962E-03	8.0799E-03	8.1281E-03	8.2317E-03
	Np237	1.4157E-06	1.8799E-06	1.9589E-06	1.7810E-06	1.2277E-06
	Pu236	5.4725E-12	9.7820E-12	1.0659E-11	8.6882E-12	4.0093E-12
	Pu238	3.9039E-07	4.7112E-07	4.9178E-07	4.2932E-07	3.0052E-07
	Pu239	1.1108E-03	1.0924E-03	1.0874E-03	1.0969E-03	1.1219E-03
	Pu240	1.2913E-04	1.2427E-04	1.2470E-04	1.2009E-04	1.1365E-04
	Pu241	9.3163E-06	8.8364E-06	8.9178E-06	8.3205E-06	7.4811E-06
	Pu242	7.1302E-07	7.0395E-07	7.2058E-07	6.4547E-07	5.3337E-07
	Am241	4.1883E-07	3.9418E-07	3.9476E-07	3.7992E-07	3.6305E-07
	Am242m	1.0928E-08	1.0767E-08	1.1026E-08	9.8067E-09	7.7424E-09
	Am243	3.1810E-08	3.0351E-08	3.1577E-08	2.6027E-08	1.8201E-08
	Cm242	2.1105E-08	2.1178E-08	2.1910E-08	1.8819E-08	1.3863E-08
	Cm243	4.7419E-10	3.8391E-10	3.9521E-10	3.1263E-10	2.1534E-10
	Cm244	3.4723E-09	3.3275E-09	3.5334E-09	2.6614E-09	1.5403E-09
	Cm245	1.8458E-10	1.8191E-10	1.9751E-10	1.3633E-10	6.4641E-11
	Cm246	3.5803E-12	3.8485E-12	4.3143E-12	2.6645E-12	9.6769E-13
	Zr	2.8392E-03	2.8392E-03	2.8392E-03	2.8392E-03	2.8392E-03
Fission product	LFP35 [a)]	3.6820E-06	4.0818E-06	4.2105E-06	3.8449E-06	2.9973E-06
	LFP38 [b)]	4.8050E-05	6.5436E-05	6.8846E-05	6.1089E-05	4.0355E-05
	LFP39 [c)]	3.0782E-04	3.6706E-04	3.8367E-04	3.4122E-04	2.4548E-04
	LFP40 [d)]	6.8704E-06	8.9595E-06	9.5115E-06	8.0912E-06	5.0941E-06
	LFP41 [e)]	4.8050E-05	6.5436E-05	6.8846E-05	6.1089E-05	4.0355E-05

Outer core

Material	Nuclide	Axial node from core bottom				
		1	2	3	4	5
Coolant	NA23	7.8712E-03	7.8712E-03	7.8712E-03	7.8712E-03	7.8712E-03
Structure	Fe	1.7889E-02	1.7889E-02	1.7889E-02	1.7889E-02	1.7889E-02
	Cr	2.6599E-03	2.6599E-03	2.6599E-03	2.6599E-03	2.6599E-03
	Mn55	1.1784E-04	1.1784E-04	1.1784E-04	1.1784E-04	1.1784E-04
	Ni	1.1030E-04	1.1030E-04	1.1030E-04	1.1030E-04	1.1030E-04
	Mo	1.2575E-04	1.2575E-04	1.2575E-04	1.2575E-04	1.2575E-04
Fuel	U234	3.7347E-09	4.4002E-09	4.5345E-09	4.1995E-09	3.3348E-09
	U235	1.2928E-05	1.2558E-05	1.2432E-05	1.2785E-05	1.3566E-05
	U236	7.0220E-07	7.2116E-07	7.3772E-07	6.7631E-07	5.5745E-07
	U238	7.8153E-03	7.7737E-03	7.7618E-03	7.7944E-03	7.8661E-03
	Np237	1.1259E-06	1.5091E-06	1.5777E-06	1.4302E-06	9.7366E-07
	Pu236	3.6853E-12	6.6851E-12	7.3254E-12	5.9596E-12	2.7010E-12
	Pu238	3.3575E-07	3.9160E-07	4.0583E-07	3.6651E-07	2.8369E-07
	Pu239	1.4658E-03	1.4368E-03	1.4287E-03	1.4466E-03	1.4905E-03
	Pu240	1.5013E-04	1.4713E-04	1.4774E-04	1.4342E-04	1.3723E-04
	Pu241	1.0007E-05	9.7125E-06	9.8037E-06	9.2864E-06	8.5695E-06
	Pu242	6.9407E-07	7.0081E-07	7.1532E-07	6.5908E-07	5.7201E-07
	Am241	4.9508E-07	4.7588E-07	4.7698E-07	4.6354E-07	4.4946E-07
	Am242m	9.7697E-09	9.9724E-09	1.0267E-08	9.1338E-09	7.1585E-09
	Am243	2.5393E-08	2.3845E-08	2.4720E-08	2.0848E-08	1.5695E-08
	Cm242	1.7193E-08	1.7852E-08	1.8538E-08	1.6043E-08	1.1901E-08
	Cm243	2.8688E-10	2.5150E-10	2.6173E-10	2.0701E-10	1.4114E-10
	Cm244	2.0635E-09	1.9589E-09	2.0797E-09	1.5890E-09	9.7082E-10
	Cm245	8.2083E-11	8.1361E-11	8.8703E-11	6.1436E-11	2.9703E-11
	Cm246	1.1356E-12	1.2379E-12	1.3971E-12	8.5922E-13	3.0684E-13
	Zr	2.8392E-03	2.8392E-03	2.8392E-03	2.8392E-03	2.8392E-03
Fission product	LFP35	2.5541E-06	2.9001E-06	3.0075E-06	2.7234E-06	2.0735E-06
	LFP38	3.5709E-05	4.8878E-05	5.1517E-05	4.5820E-05	3.0166E-05
	LFP39	2.8078E-04	3.3873E-04	3.5464E-04	3.1656E-04	2.2767E-04
	LFP40	6.0384E-06	8.0535E-06	8.5656E-06	7.3565E-06	4.6505E-06
	LFP41	3.5709E-05	4.8878E-05	5.1517E-05	4.5820E-05	3.0166E-05

Lower structure, grid plate and lower reflector

Nuclide	Lower structure	Grid plate	Lower reflector
Na23	1.5591E-02	1.5591E-02	7.8712E-03
Fe	1.5878E-02	1.5878E-02	4.5077E-02
Cr	3.2355E-03	3.2355E-03	6.7023E-03
Mn55	5.0846E-04	5.0846E-04	2.9693E-04
Ni	3.2604E-03	3.2604E-03	2.7793E-04
Mo	4.3524E-04	4.3524E-04	3.1687E-04

Fission gas plenum and upper structure

Nuclide	Gas Plenum with displaced bond Na	Gas plenum	Upper structure
Na23	1.6557E-02	7.8712E-03	7.8712E-03
Fe	1.7889E-02	1.7889E-02	4.5077E-02
Cr	2.6599E-03	2.6599E-03	6.7023E-03
Mn55	1.1784E-04	1.1784E-04	2.9693E-04
Ni	1.1030E-04	1.1030E-04	2.7793E-04
Mo	1.2575E-04	1.2575E-04	3.1687E-04

Radial reflector, shield and barrel

Nuclide	Radial reflector	Shield	Barrel
Na23	3.4517E-03	3.8077E-03	1.2356E-02
Fe	5.8910E-02	2.0690E-02	1.8302E-02
Cr	8.7592E-03	3.0764E-03	3.7294E-03
Mn55	3.8805E-04	1.3629E-04	5.8607E-04
Ni	3.6322E-04	1.2757E-04	3.7580E-03
Mo	4.1411E-04	1.4544E-04	
C12		1.0858E-02	
B10		2.2744E-02	
B11		2.0686E-02	

Control assemblies

Nuclide	Under follower	Follower	Absorber		Above absorber	Upper structure
			Secondary	Primary		
Na23	2.0209E-02	1.6411E-02	6.4201E-03	6.4201E-03	6.4201E-03	7.8712E-03
Fe	6.45823-03	1.8348E-02	1.4481E-02	1.4481E-02	1.4481E-02	4.5077E-02
Cr	9.6026E-04	2.7281E-03	2.1531E-03	2.1531E-03	2.1531E-03	6.7023E-03
Mn55	4.2541E-05	1.2086E-04	9.5387E-05	9.5387E-05	9.5387E-05	2.9693E-04
Ni	3.9819E-05	1.1313E-04	8.9284E-05	8.9284E-05	8.9284E-05	2.7793E-04
Mo	4.5399E-05	1.2898E-04	1.0179E-04	1.0179E-04	1.0179E-04	3.1687E-04
C12			1.0537E-02	1.0869E-02		
B10			8.3873E-03	2.7065E-02		
B11			3.3760E-02	1.6410E-02		

BOEC Nuclide number densities (#/barn-cm) of recycled oxide core

Inner core

Material	Nuclide	Axial node from core bottom				
		1	2	3	4	5
Coolant	Na23	8.1322E-03	8.1322E-03	8.1322E-03	8.1322E-03	8.1322E-03
Structure	Fe	1.8573E-02	1.8573E-02	1.8573E-02	1.8573E-02	1.8573E-02
	Cr	2.7616E-03	2.7616E-03	2.7616E-03	2.7616E-03	2.7616E-03
	Mn55	1.2234E-04	1.2234E-04	1.2234E-04	1.2234E-04	1.2234E-04
	Ni	1.1452E-04	1.1452E-04	1.1452E-04	1.1452E-04	1.1452E-04
	Mo	1.3056E-04	1.3056E-04	1.3056E-04	1.3056E-04	1.3056E-04
Fuel	U234	6.4319E-07	6.0429E-07	5.9246E-07	6.1463E-07	6.6954E-07
	U235	8.2377E-06	7.5720E-06	7.3559E-06	7.7711E-06	8.8939E-06
	U236	9.0366E-07	9.9269E-07	1.0280E-06	9.5752E-07	7.5727E-07
	U238	5.5788E-03	5.4894E-03	5.4608E-03	5.5146E-03	5.6426E-03
	Np237	1.3251E-05	1.2756E-05	1.2532E-05	1.2966E-05	1.4022E-05
	Pu236	1.1814E-10	1.3241E-10	1.3410E-10	1.3073E-10	1.1558E-10
	Pu238	5.0045E-05	4.8018E-05	4.7474E-05	4.8468E-05	5.0863E-05
	Pu239	7.0883E-04	7.0714E-04	7.0646E-04	7.0745E-04	7.0825E-04
	Pu240	5.3934E-04	5.2951E-04	5.2752E-04	5.3103E-04	5.4112E-04
	Pu241	8.9976E-05	8.8296E-05	8.8408E-05	8.8026E-05	8.7409E-05
	Pu242	1.3138E-04	1.2931E-04	1.2871E-04	1.2982E-04	1.3262E-04
	Am241	4.7040E-05	4.3767E-05	4.2701E-05	4.4746E-05	5.0108E-05
	Am242m	4.0083E-06	3.8425E-06	3.7845E-06	3.8921E-06	4.1120E-06
	Am243	4.4696E-05	4.3813E-05	4.3637E-05	4.3958E-05	4.4794E-05
	Cm242	2.4461E-06	2.7751E-06	2.8955E-06	2.6591E-06	2.0095E-06
	Cm243	3.0981E-07	3.1436E-07	3.2302E-07	3.0570E-07	2.7710E-07
	Cm244	3.4300E-05	3.4309E-05	3.4478E-05	3.4126E-05	3.3355E-05
	Cm245	1.0142E-05	9.9622E-06	9.9750E-06	9.9395E-06	9.9578E-06
	Cm246	6.1911E-06	6.1773E-06	6.1804E-06	6.1746E-06	6.1733E-06
	O	1.5205E-02	1.5205E-02	1.5205E-02	1.5205E-02	1.5205E-02
Fission product	LFP35	2.7919E-06	3.3563E-06	3.5303E-06	3.1979E-06	2.2933E-06
	LFP38	4.1564E-05	5.9267E-05	6.3578E-05	5.5523E-05	3.4233E-05
	LFP39	1.9748E-04	2.6283E-04	2.8346E-04	2.4526E-04	1.5538E-04
	LFP40	2.8395E-05	4.0454E-05	4.3542E-05	3.7849E-05	2.3346E-05
	LFP41	5.4126E-05	7.0362E-05	7.5814E-05	6.5582E-05	4.1719E-05

Middle core

Material	Nuclide	Axial node from core bottom				
		1	2	3	4	5
Coolant	Na23	8.1322E-03	8.1322E-03	8.1322E-03	8.1322E-03	8.1322E-03
Structure	Fe	1.8573E-02	1.8573E-02	1.8573E-02	1.8573E-02	1.8573E-02
	Cr	2.7616E-03	2.7616E-03	2.7616E-03	2.7616E-03	2.7616E-03
	Mn55	1.2234E-04	1.2234E-04	1.2234E-04	1.2234E-04	1.2234E-04
	Ni	1.1452E-04	1.1452E-04	1.1452E-04	1.1452E-04	1.1452E-04
	Mo	1.3056E-04	1.3056E-04	1.3056E-04	1.3056E-04	1.3056E-04
Fuel	U234	7.2436E-07	6.8348E-07	6.7144E-07	6.9355E-07	7.4990E-07
	U235	8.4243E-06	7.7788E-06	7.5734E-06	7.9608E-06	9.0285E-06
	U236	7.9339E-07	8.8688E-07	9.2208E-07	8.5334E-07	6.5603E-07
	U238	5.4589E-03	5.3797E-03	5.3547E-03	5.4010E-03	5.5148E-03
	Np237	1.5088E-05	1.4514E-05	1.4274E-05	1.4733E-05	1.5892E-05
	Pu236	1.3171E-10	1.4811E-10	1.5031E-10	1.4608E-10	1.2822E-10
	Pu238	5.5515E-05	5.3452E-05	5.2914E-05	5.3877E-05	5.6260E-05
	Pu239	7.5244E-04	7.4540E-04	7.4334E-04	7.4687E-04	7.5519E-04
	Pu240	5.9181E-04	5.8062E-04	5.7817E-04	5.8246E-04	5.9441E-04
	Pu241	9.6761E-05	9.5219E-05	9.5311E-05	9.4966E-05	9.4289E-05
	Pu242	1.4508E-04	1.4290E-04	1.4227E-04	1.4341E-04	1.4635E-04
	Am241	5.3951E-05	5.0420E-05	4.9293E-05	5.1418E-05	5.7114E-05
	Am242m	4.4755E-06	4.3196E-06	4.2663E-06	4.3629E-06	4.5560E-06
	Am243	4.9278E-05	4.8383E-05	4.8202E-05	4.8525E-05	4.9392E-05
	Cm242	2.3574E-06	2.7301E-06	2.8625E-06	2.6077E-06	1.8962E-06
	Cm243	3.1564E-07	3.1937E-07	3.2647E-07	3.1252E-07	2.9142E-07
	Cm244	3.6933E-05	3.6974E-05	3.7139E-05	3.6798E-05	3.6021E-05
	Cm245	1.0983E-05	1.0786E-05	1.0788E-05	1.0773E-05	1.0833E-05
	Cm246	6.7801E-06	6.7589E-06	6.7595E-06	6.7581E-06	6.7658E-06
	O	1.5205E-02	1.5205E-02	1.5205E-02	1.5205E-02	1.5205E-02
Fission product	LFP35	2.4015E-06	2.9471E-06	3.1133E-06	2.8019E-06	1.9394E-06
	LFP38	3.8540E-05	5.5371E-05	5.9480E-05	5.1951E-05	3.1654E-05
	LFP39	1.8253E-04	2.4497E-04	2.6422E-04	2.2909E-04	1.4304E-04
	LFP40	2.8576E-05	4.1006E-05	4.4171E-05	3.8441E-05	2.3447E-05
	LFP41	5.0892E-05	6.7355E-05	7.2694E-05	6.2840E-05	3.9027E-05

Outer core

Material	Nuclide	Axial node from core bottom				
		1	2	3	4	5
Coolant	NA23	8.1322E-03	8.1322E-03	8.1322E-03	8.1322E-03	8.1322E-03
Structure	Fe	1.8573E-02	1.8573E-02	1.8573E-02	1.8573E-02	1.8573E-02
	Cr	2.7616E-03	2.7616E-03	2.7616E-03	2.7616E-03	2.7616E-03
	Mn55	1.2234E-04	1.2234E-04	1.2234E-04	1.2234E-04	1.2234E-04
	Ni	1.1452E-04	1.1452E-04	1.1452E-04	1.1452E-04	1.1452E-04
	Mo	1.3056E-04	1.3056E-04	1.3056E-04	1.3056E-04	1.3056E-04
Fuel	U234	1.1303E-06	1.0941E-06	1.0847E-06	1.1009E-06	1.1421E-06
	U235	7.6389E-06	7.1780E-06	7.0335E-06	7.2933E-06	7.9544E-06
	U236	5.6786E-07	6.4334E-07	6.7063E-07	6.2053E-07	4.9571E-07
	U238	4.5422E-03	4.4948E-03	4.4800E-03	4.5063E-03	4.5693E-03
	Np237	4.8957E-05	4.6780E-05	4.6027E-05	4.7391E-05	5.0686E-05
	Pu236	2.5009E-10	3.0342E-10	3.1247E-10	2.9597E-10	2.3346E-10
	Pu238	8.5618E-05	8.4378E-05	8.4173E-05	8.4481E-05	8.5296E-05
	Pu239	1.1142E-03	1.0788E-03	1.0686E-03	1.0867E-03	1.1339E-03
	Pu240	8.4812E-04	8.3515E-04	8.3211E-04	8.3729E-04	8.5140E-04
	Pu241	1.6073E-04	1.5773E-04	1.5740E-04	1.5787E-04	1.6002E-04
	Pu242	2.1785E-04	2.1556E-04	2.1492E-04	2.1604E-04	2.1888E-04
	Am241	1.0593E-04	1.0042E-04	9.8670E-05	1.0181E-04	1.0968E-04
	Am242m	6.1910E-06	6.2158E-06	6.2220E-06	6.2046E-06	6.0838E-06
	Am243	6.8657E-05	6.7880E-05	6.7768E-05	6.7954E-05	6.8611E-05
	Cm242	3.0806E-06	3.6982E-06	3.9138E-06	3.5211E-06	2.5457E-06
	Cm243	3.8842E-07	3.9839E-07	4.0717E-07	3.9129E-07	3.7072E-07
	Cm244	4.4791E-05	4.5091E-05	4.5338E-05	4.4876E-05	4.4011E-05
	Cm245	1.2811E-05	1.2667E-05	1.2679E-05	1.2651E-05	1.2709E-05
	Cm246	7.6435E-06	7.6202E-06	7.6200E-06	7.6203E-06	7.6370E-06
	O	1.5205E-02	1.5205E-02	1.5205E-02	1.5205E-02	1.5205E-02
Fission product	LFP35	1.4560E-06	1.8497E-06	1.9689E-06	1.7556E-06	1.2064E-06
	LFP38	3.0330E-05	4.3537E-05	4.6793E-05	4.1048E-05	2.5399E-05
	LFP39	1.9033E-04	2.5417E-04	2.7287E-04	2.3990E-04	1.5705E-04
	LFP40	3.0958E-05	4.4616E-05	4.8030E-05	4.2051E-05	2.5981E-05
	LFP41	5.6459E-05	7.5735E-05	8.1708E-05	7.1125E-05	4.5652E-05

Lower structure, grid plate and lower reflector

Nuclide	Lower structure	Grid plate	Lower reflector
Na23	1.5591E-02	1.5591E-02	8.1322E-03
Fe	1.5878E-02	1.5878E-02	4.4260E-02
Cr	3.2355E-03	3.2355E-03	6.5809E-03
Mn55	5.0846E-04	5.0846E-04	2.9155E-04
Ni	3.2604E-03	3.2604E-03	2.7289E-04
Mo	4.3524E-04	4.3524E-04	3.1113E-04

Fission gas plenum and upper structure

Nuclide	Gas plenum	Upper structure
Na23	8.1322E-03	8.1322E-03
Fe	1.8573E-02	4.4260E-02
Cr	2.7616E-03	6.5809E-03
Mn55	1.2234E-04	2.9155E-04
Ni	1.1452E-04	2.7289E-04
Mo	1.3056E-04	3.1113E-04

Radial reflector, shield and barrel

Nuclide	Radial reflector	Shield	Barrel
Na23	3.45173E-03	3.80767E-03	1.23563E-02
Fe	5.89102E-02	2.06903E-02	1.83018E-02
Cr	8.75918E-03	3.07638E-03	3.72938E-03
Mn55	3.88047E-04	1.36289E-04	5.86069E-04
Ni	3.63219E-04	1.27569E-04	3.75801E-03
Mo	4.14113E-04	1.45444E-04	5.01672E-04
C12		1.67189E-03	
B10		7.05028E-03	
B11		2.83782E-02	

Control assemblies

Nuclide	Under follower	Follower	Absorber		Above absorber	Upper structure
			Secondary	Primary		
Na23	2.02091E-02	1.64105E-02	6.42006E-03	6.42006E-03	6.42006E-02	7.87124E-03
Fe	6.45825E-03	1.83482E-02	1.44809E-02	1.44809E-02	1.44809E-03	4.50768E-02
Cr	9.60257E-04	2.72814E-03	2.15312E-03	2.15312E-03	2.15312E-04	6.70233E-03
Mn55	4.25411E-05	1.20862E-04	9.53870E-05	9.53870E-05	9.53870E-03	2.77927E-04
Ni	3.98192E-05	1.13129E-04	8.92839E-05	8.92839E-05	8.92839E-04	2.96925E-04
Mo	4.53987E-05	1.28980E-04	1.01794E-04	1.01794E-04	1.01794E-04	3.16870E-04
C12			1.05367E-02	1.05367E-02		
B10			8.38725E-03	2.70650E-02		
B11			3.37598E-02	1.64104E-02		

Average temperatures (°C)

	Metal core	Oxide core
Lower structure	355	355
Grid place	355	355
Lower reflector	355	355
Active core - Fuel - Structure - Coolant	581 450 433	1056 445 433
Upper gas plenum	510	510
Upper structure	510	510
Radial reflector	355	355
Radial shield	355	355
Barrel	355	355

Appendix B: Models of the 600 MWe Fast Breeder Reactor (FBR) core

A 600 MWe Fast Breeder Reactor (FBR) core concept with mixed oxide fuels was developed at PNC (the former of JAEA) in 1992 [B.1]. The purpose of the design study is to present a plant concept which could stand both the reality at the demonstration stage of FBR development, and the innovativeness through commercialisation, as well as to establish the technological basis of the design study. The major design targets of the plant performance are as follows:

- thermal power of the core: 1 600 MWt, i.e. thermal efficiency of the plant: 38%;
- power operating length per cycle: 375 days (3 batches for core fuels and 4 for blankets);
- breeding ratio: approximately 1.2;
- other characteristics: see Table B.1.

The planar layouts of the 600 MWe FBR core are shown in Figure B.1. The core consists of 246 fuel subassemblies with two Pu-enrichment zones, 126 radial blankets, 72 stainless steel shields, 78 B_4C shields, 13 primary control rods and 9 back-up ones. The primary control rods are axially moved to maintain criticality, while the back-up ones are positioned at the top of the active core during the power operation. The equivalent diameter and height of the active core are 2.75 and 1.00 meter, respectively. Figure B.2 shows the (r,z) model of the 600 MWe FBR core. All the dimensions present the values at a room temperature. All primary control rods are moved to the fully-withdrawal positions, which are followed by coolant, that is, sodium. Region-wise, homogenised nuclide number densities at the beginning of equilibrium cycle (BOEC) are provided in Tables B.2 and B.3 with the temperature. It should be emphasised that the minor actinides and the lumped fission-product (FP) isotopes are intentionally removed from the table to make the preparation work of the input data simple. The k_{eff} value of this (r,z) model by JENDL-4.0 is 1.0522 with a diffusion-theory, homogeneous-cell, 70 energy-group calculation.

Table B.1: Characteristics of 600 MWe fast breeder reactor core

Specification		Value
Thermal power (MWt)		1,600
Primary coolant	Inlet Temperature (C)	380
	Outlet temperature (C)	530
	Flow rate (kg/s)	8.41E3
Operating cycle length (days)		375
Fuel type, Batch number		MOX, 3
Pu enrichment (Inner/Outer core) (weight %)		17.1/ 20.9
Pu isotopic ratio (Pu-238:239: 240:241:242) (weight %)		3:53: 55:12:7

Performance		Value
Maximum linear power at BOC (w/cm)	BOEC (Inner/Outer core)	470/460
	EOEC (Inner/Outer core)	442/434
Breeding Ratio (BOEC/EOEC)		1.24/1.23
Burnup reactivity loss per cycle (%dk/kk')		2.70
Average burnup rate of discharged fuel		85,700
Control rod worth (Primary/Backup) (%dk/kk')		7.9/2.7
Sodium void reactivity (BOEC) ($)		4.3
Doppler reactivity (BOEC) (Tdk/dT)		-1.0E-2

Figure B.1: Planar layout of 600 MWe fast breeder reactor core

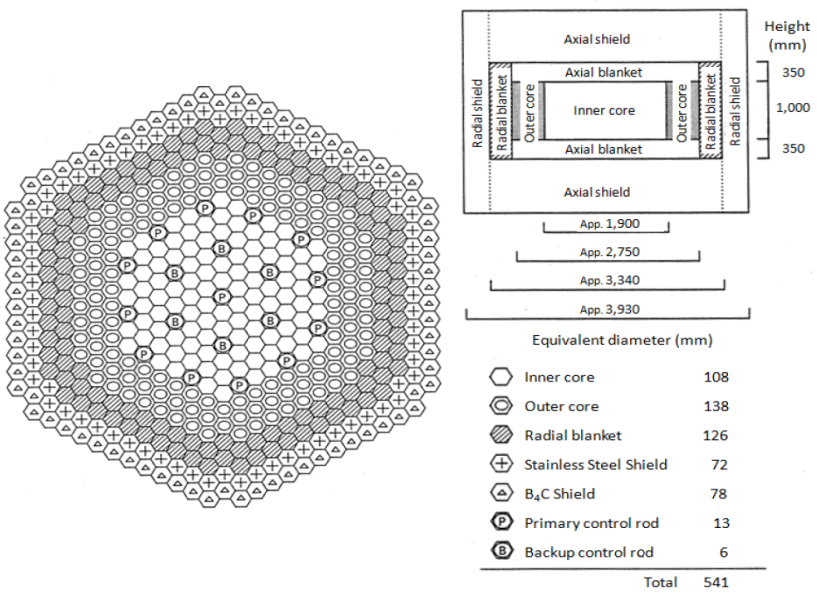

Figure B.2: 2D (r,z) geometry model of 600 MWe fast breeder reactor core

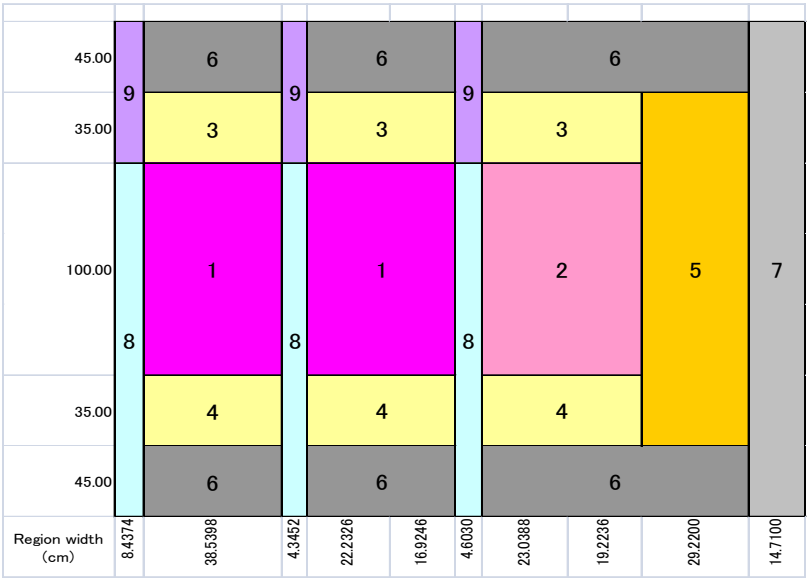

Note: Region 1: inner core, 2: outer core, 3: upper axial blanket, 4: lower axial blanket, 5: radial blanket, 6: axial shield, 7: stainless steel shield, 8: sodium follower,9: control rod absorber.

Table B.2: BOEC Nuclide number densities (#/barn-cm) of 600 MWe fast breeder reactor core (1/2)

	Inner core	Outer core	Upper axial blanket	Lower axial blanket	Radial blanket
	Region 1	Region 2	Region 3	Region 4	Region 5
Temperature (K)	1373.15	1373.15	1073.15	1073.15	1073.15
U-235	1.7008E-05	1.8308E-05	2.6295E-05	2.6858E-05	3.3177E-05
U-238	7.0638E-03	7.0045E-03	9.1420E-03	9.4891E-03	1.1618E-02
Pu-239	8.6457E-04	9.6727E-04	2.1070E-04	8.4859E-05	9.1092E-05
Pu-240	4.1172E-04	4.6652E-04	7.2647E-05	2.0851E-06	1.8599E-06
Pu-241	1.5432E-04	1.8687E-04	3.1348E-05	4.2087E-08	3.2620E-08
Pu-242	1.1100E-04	1.2793E-04	1.9798E-05	5.2394E-10	3.6458E-10
O-16	1.7823E-02	1.7854E-02	1.9230E-02	1.9230E-02	2.3515E-02
Cr-50	1.3541E-04	1.3541E-04	1.3541E-04	1.3541E-04	1.1459E-04
Cr-52	2.6112E-03	2.6112E-03	2.6112E-03	2.6112E-03	2.2097E-03
Cr-53	2.9609E-04	2.9609E-04	2.9609E-04	2.9609E-04	2.5056E-04
Cr-54	7.3702E-05	7.3702E-05	7.3702E-05	7.3702E-05	6.2369E-05
Mn-55	3.8608E-04	3.8608E-04	3.8608E-04	3.8608E-04	3.2671E-04
Fe-54	6.8707E-04	6.8707E-04	6.8707E-04	6.8707E-04	5.8142E-04
Fe-56	1.0785E-02	1.0785E-02	1.0785E-02	1.0785E-02	9.1270E-03
Fe-57	2.4908E-04	2.4908E-04	2.4908E-04	2.4908E-04	2.1078E-04
Fe-58	3.3149E-05	3.3149E-05	3.3149E-05	3.3149E-05	2.8051E-05
Ni-58	2.4354E-03	2.4354E-03	2.4354E-03	2.4354E-03	2.0609E-03
Ni-60	9.3812E-04	9.3812E-04	9.3812E-04	9.3812E-04	7.9387E-04
Ni-61	4.0780E-05	4.0780E-05	4.0780E-05	4.0780E-05	3.4509E-05
Ni-62	1.3002E-04	1.3002E-04	1.3002E-04	1.3002E-04	1.1003E-04
Ni-64	3.3113E-05	3.3113E-05	3.3113E-05	3.3113E-05	2.8021E-05
Mo-92	4.1801E-05	4.1801E-05	4.1801E-05	4.1801E-05	3.5373E-05
Mo-94	2.6055E-05	2.6055E-05	2.6055E-05	2.6055E-05	2.2049E-05
Mo-95	4.4843E-05	4.4843E-05	4.4843E-05	4.4843E-05	3.7948E-05
Mo-96	4.6984E-05	4.6984E-05	4.6984E-05	4.6984E-05	3.9759E-05
Mo-97	2.6900E-05	2.6900E-05	2.6900E-05	2.6900E-05	2.2764E-05
Mo-98	6.7969E-05	6.7969E-05	6.7969E-05	6.7969E-05	5.7517E-05
Mo-100	2.7126E-05	2.7126E-05	2.7126E-05	2.7126E-05	2.2955E-05
Na-23	7.5616E-03	7.5616E-03	7.5616E-03	7.5616E-03	6.4029E-03
B-10					
B-11					
C-12					

a) The number densities are the region-averaged values.

b) Minor actinides and lumped FP isotopes are removed from the table for simplicity.

c) The k_{eff} value of this (r,z) model by JENDL-4.0 is 1.0522 with a diffusion-theory, homogeneous-cell, 70 energy-group calculation.

Table B.3: BOEC Nuclide number densities (#/barn-cm) of 600 MWe fast breeder reactor core (2/2)

	Axial shield	Stailess steel shield	Soidum follower	Control rod absorber
	Region 6	Region7	Region 8	Region 9
Temperature (K)	703.15	703.15	703.15	703.15
U-235				
U-238				
Pu-239				
Pu-240				
Pu-241				
Pu-242				
O-16				
Cr-50	1.3541E-04	3.9447E-04	5.6441E-05	1.0745E-04
Cr-52	2.6112E-03	7.6069E-03	1.0884E-03	2.0721E-03
Cr-53	2.9609E-04	8.6256E-04	1.2342E-04	2.3496E-04
Cr-54	7.3702E-05	2.1471E-04	3.0721E-05	5.8486E-05
Mn-55	3.8608E-04		1.0848E-04	3.0638E-04
Fe-54	6.8704E-04	2.9802E-03	2.7861E-04	5.4520E-04
Fe-56	1.0785E-02	4.6783E-02	4.3736E-03	8.5584E-03
Fe-57	2.4907E-04	1.0804E-03	1.0100E-04	1.9765E-04
Fe-58	3.3147E-05	1.4378E-04	1.3442E-05	2.6304E-05
Ni-58	2.4353E-03	2.4366E-04	5.5267E-04	1.9326E-03
Ni-60	9.3807E-04	9.3858E-05	2.1289E-04	7.4442E-04
Ni-61	4.0777E-05	4.0799E-06	9.2541E-06	3.2359E-05
Ni-62	1.3002E-04	1.3009E-05	2.9506E-05	1.0318E-04
Ni-64	3.3111E-05	3.3129E-06	7.5144E-06	2.6276E-05
Mo-92	4.1801E-05	1.7477E-05	1.5372E-05	3.3173E-05
Mo-94	2.6055E-05	1.0894E-05	9.5813E-06	2.0677E-05
Mo-95	4.4843E-05	1.8749E-05	1.6490E-05	3.5588E-05
Mo-96	4.6984E-05	1.9644E-05	1.7277E-05	3.7286E-05
Mo-97	2.6900E-05	1.1247E-05	9.8921E-06	2.1348E-05
Mo-98	6.7969E-05	2.8418E-05	2.4994E-05	5.3940E-05
Mo-100	2.7126E-05	1.1341E-05	9.9749E-06	2.1527E-05
Na-23	7.5616E-03	5.9621E-03	2.0932E-02	1.1277E-02
B-10				2.9763E-02
B-11				3.0080E-03
C-12				8.1927E-03

Reference

[B.1] H. Hayashi, K. Nagata, M. Moriyama, M. Ishikawa, M. Nakaoji, S. Kuroki, M. Yamaoka, T. Onihashi, T. Wakabayashi, K. Maeda, M. Ichimiya Y. Yamashita (1992), "Progress Report of the Design Study on a Large Scale Reactor", Power reactor and Nuclear fuel development Corporation, PNC TN9410 92-137.

Appendix C: Corrective factors and S_n Quadratures

The following S_4 angular data have been used for one-dimensional calculations:

Direc.	Weight	μ
1	0.0000000E+00	-0.9367418E+00
2	0.1666667E+00	-0.8688903E+00
3	0.3333333E+00	-0.3500212E+00
4	0.3333333E+00	0.3500212E+00
5	0.1666667E+00	0.8688903E+00

For two dimensional calculations the following data have been used:

Direc.	Weight	η	μ
1	0.0000000E+00	-0.8819200E+00	-0.4714000E+00
2	0.8333331E-01	-0.8819200E+00	-0.3333333E+00
3	0.8333331E-01	-0.8819200E+00	0.3333333E+00
4	0.0000000E+00	-0.3333333E+00	-0.9428100E+00
5	0.8333331E-01	-0.3333333E+00	-0.8819200E+00
6	0.8333331E-01	-0.3333333E+00	-0.3333333E+00
7	0.8333331E-01	-0.3333333E+00	0.3333333E+00
8	0.8333331E-01	-0.3333333E+00	0.8819200E+00
9	0.0000000E+00	0.8819200E+00	-0.4714000E+00
10	0.8333331E-01	0.8819200E+00	-0.3333333E+00
11	0.8333331E-01	0.8819200E+00	0.3333333E+00
12	0.0000000E+00	0.3333333E+00	-0.9428100E+00
13	0.8333331E-01	0.3333333E+00	-0.8819200E+00
14	0.8333331E-01	0.3333333E+00	-0.3333333E+00
15	0.8333331E-01	0.3333333E+00	0.3333333E+00
16	0.8333331E-01	0.3333333E+00	0.8819200E+00

Directions with zero weight are used only for improving convergence on the curvilinear derivative term and should not affect the final result if not used, as is the case with some S_n codes (e. g. ONETRAN, ONEDANT, TWOTRAN, TWODANT, etc.).

C.1 JEZEBEL ^{239}Pu Corrective factors

The specifications of this experiment are provided in the "International Handbook of Evaluated Criticality Safety Benchmark Experiments" under the name "PU-MET-FAST-001" in the Plutonium Systems Chapter. JEZEBEL ^{239}Pu is a 17,020 gram sphere of plutonium alloy with a density of 15.61 g/cm^3 and has a radius of 6.3849 cm.

The homogeneous compositions are given in Table C.1 (taken from the benchmark DVD).

For the deterministic spherical model, the following meshing has been used with equidistant points in the same region:

Axis			
R	Point	1	33
	Dimension (cm)	0.0	6.3849

Corrective factors have been calculated with the ENDF/B-VII cross-section data. In Table C.2 the corrective factors are provided for the homogenous R model for the deterministic S_4P_1 33-group calculations. Corrective factors are calculated as the ratio between the values obtained by the detailed Monte Carlo calculation and those obtained by the corresponding approximated calculation.

Table C.1: Homogeneous compositions for JEZEBEL ^{239}Pu

Nuclide	Atom Density, atoms/barn-cm
Ga	1.3752×10^{-3}
^{239}Pu	3.7047×10^{-2}
^{240}Pu	1.7512×10^{-3}
^{241}Pu	1.1674×10^{-4}

Table C.2: Corrective factors for R homogeneous deterministic calculations for JEZEBEL ^{239}Pu

Parameters	MC Detailed	S_4 R.	Corr. Fact.	Experiment
k_{eff}	0.99986 ±9pcm	1.00538	0.99451	1.00000
F28/F25	0.2084 ±0.0009	0.2032	1.0256	0.214
F37/F25	0.9707 ±0.0013	0.9620	1.0090	0.962
F49/F25	1.4248 ±0.0018	1.4220	1.0020	1.448

C.2 JEZEBEL ^{240}Pu Corrective factors

The specifications of this experiment are provided in the "International Handbook of Evaluated Criticality Safety Benchmark Experiments" under the name "PU-MET-FAST-002" in the Plutonium Systems Chapter.

JEZEBEL ^{240}Pu is a 19,460 g sphere of plutonium alloy with a density of 15.73 g/cm^3 has a radius of 6.6595 cm. The homogeneous compositions are given in Table C.3 (taken from the benchmark DVD).

For the deterministic spherical model, the following meshing has been used with equidistant points in the same region:

Axis			
R	Point	1	33
	Dimension (cm)	0.0	6.6595

Corrective factors have been calculated with the ENDF/B-VII cross-section data. In Table C.4 the corrective factors are provided for the homogenous R model for the deterministic S_4P_1 33-group calculations. Corrective factors are calculated as the ratio between the values obtained by the detailed Monte Carlo calculation and those obtained by the corresponding approximated calculation.

Table C.3: Homogeneous compositions for JEZEBEL ^{240}Pu

Nuclide	Atom Density, atoms/barn-cm
Ga	1.3722×10^{-3}
^{239}Pu	2.9934×10^{-2}
^{240}Pu	7.8754×10^{-3}
^{241}Pu	1.2146×10^{-3}
^{242}Pu	1.5672×10^{-4}

Table C.4: Corrective factors for R homogeneous deterministic calculations for JEZEBEL ^{240}Pu

Parameters	MC Detailed	S_4 R.	**Corr. Fact.**	Experiment
k_{eff}	0.99981 ±9pcm	1.00459	**0.99527**	1.00000

C.3 FLATTOP ^{239}Pu Corrective factors

The specifications of this experiment are provided in the "International Handbook of Evaluated Criticality Safety Benchmark Experiments" under the name "PU-MET-FAST-006" in the Plutonium Systems Chapter.

The radius of the core, a 6060-gram Pu sphere at a density of 15.53 g/cm3, was 4.5332 cm. The sphere was reflected by 19.6088 cm of normal uranium (outer radius of 24.1420 cm). The homogeneous compositions are given in Table C.5 (taken from the benchmark DVD).

For the deterministic spherical model, the following meshing has been used with equidistant points in the same region:

Axis				
R	Point	1	25	100
	Dimension (cm)	0.0	4.5332	24.142

Corrective factors have been calculated with the ENDF/B-VII cross section data. In Table C.6 the corrective factors are provided for the homogenous R model for the deterministic S_4P_1 33-group calculations. Corrective factors are calculated as the ratio between the values obtained by the detailed Monte Carlo calculation and those obtained by the corresponding approximated calculation.

Table C.5: Homogeneous compositions for FLATTOP ^{239}Pu

Isotope	Atom Densities (atoms/barn-cm)
Core	
^{239}Pu	3.6697×10^{-2}
^{240}Pu	1.8700×10^{-3}
^{241}Pu	1.1639×10^{-4}
Ga	1.4755×10^{-3}
Reflector[(a)]	
^{234}U	2.6438×10^{-6}
^{235}U	3.4610×10^{-4}
^{238}U	4.7721×10^{-2}

Table C.6: Corrective factors for R homogeneous deterministic calculations for FLATTOP ^{239}Pu

Parameters	MC Detailed	S_4 R.	**Corr. Fact.**	Experiment
k_{eff}	1.00097 ±18pcm	0.99815	**1.00283**	1.00000
F28/F25	0.1767 ±0.0013	0.1715	**1.0303**	0.1799
F37/F25	0.8523 ±0.0013	0.8452	**1.0084**	0.8561

C.4 ZPR-6 Assembly 7 Corrective factors

The specifications of this experiment are provided in the "International Handbook of Evaluated Reactor Physics Benchmark Experiments" under the name "ZPR-LMFR-EXP-001" in the Liquid Metal Fast Reactor Chapter.

The homogeneous R-Z model and associated dimension are shown in Figure C.1 and homogeneous compositions are given in Table C.7 (both taken from the benchmark DVD).

For the deterministic model (one quarter only of the geometry was described), the following meshing has been used with equidistant points in the same region:

Axis							
R	Point	1	24	54	74	85	
	Dimension (cm)	0.0	24.3435	80.7984	112.2504	140.2589	
Z	Point	1	51	64	69	74	80
	Dimension (cm)	0.0	76.2813	101.7257	106.6800	110.5357	121.9200

Corrective factors have been calculated with the ENDF/B-VII cross section data. In Tables C.8 and C.9 the corrective factors are provided for the homogenous R-Z model for Monte Carlo (MC) and deterministic S_4P_1 33-group calculations. Spectral indices have been calculated at the central location. Corrective factors are calculated as the ratio between the values obtained by the detailed Monte Carlo calculation and those obtained by the corresponding approximated calculation.

Figure C.1: R-Z homogeneous model for ZPR-6 Assembly 7

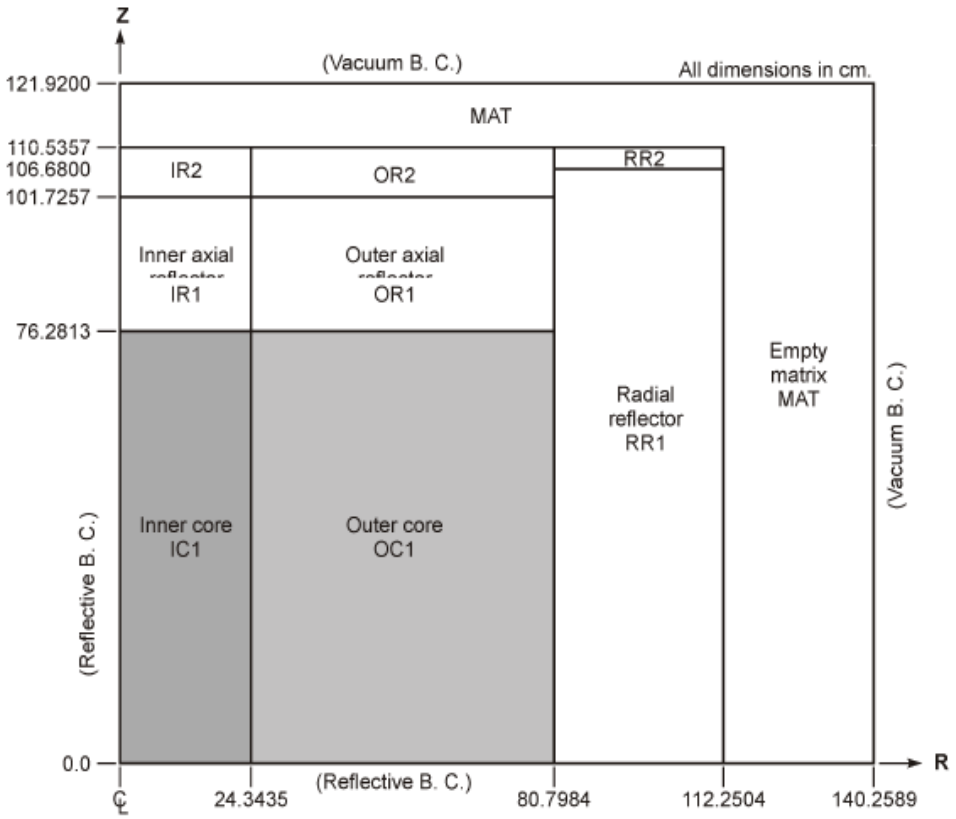

Table C.7: Homogeneous R-Z compositions for ZPR-6 Assembly 7

Nuclide	Inner Core IC1	Outer Core OC1	Inner Axial Reflector 1 (IR1)	Inner Axial Reflector 2 (IR2)
^{240}Pu	1.17621E-04	1.17551E-04	0.00000E+00	0.00000E+00
^{241}Pu	1.32171E-05	1.50239E-05	0.00000E+00	0.00000E+00
^{235}U	1.26065E-05	1.26448E-05	8.29422E-05	8.65264E-05
^{238}U	5.79290E-03	5.81017E-03	3.71167E-02	3.87479E-02
^{239}Pu	8.86521E-04	8.86314E-04	0.00000E+00	0.00000E+00
^{238}Pu	3.33012E-07	4.68474E-07	0.00000E+00	0.00000E+00
^{242}Pu	1.40289E-06	1.76343E-06	0.00000E+00	0.00000E+00
^{241}Am	3.12449E-06	2.58715E-06	0.00000E+00	0.00000E+00
Cr	2.69312E-03	2.68787E-03	1.64641E-03	1.44970E-03
Ni	1.19777E-03	1.18818E-03	6.89374E-04	6.07516E-04
Fe	1.28729E-02	1.32415E-02	6.06025E-03	5.25530E-03
^{27}Al	4.02097E-06	1.63640E-05	0.00000E+00	0.00000E+00
^{23}Na	9.27911E-03	9.11269E-03	0.00000E+00	0.00000E+00
^{16}O	1.37692E-02	1.42601E-02	0.00000E+00	0.00000E+00
C	3.66420E-05	3.40451E-05	3.67281E-05	2.71677E-05
Mo	2.36058E-04	2.38695E-04	1.06205E-05	1.00416E-05
Mn	2.25629E-04	2.23933E-04	1.43193E-04	1.27167E-04
Cu	2.46769E-05	2.48245E-05	1.97417E-05	1.90679E-05
Si	1.62355E-04	1.54889E-04	1.06228E-04	9.52030E-05
Ca	2.13014E-06	2.09220E-06	0.00000E+00	0.00000E+00
Cl	2.98536E-07	2.96680E-07	0.00000E+00	0.00000E+00
^{59}Co	8.32422E-07	1.69933E-07	0.00000E+00	0.00000E+00
Nuclide	Outer Axial Reflector 1 (OR1)	Outer Axial Reflector 2 (OR2)	Radial Reflector (RR1)	Matrix (MAT and RR2)
^{240}Pu	0.00000E+00	0.00000E+00	0.00000E+00	0.00000E+00
^{241}Pu	0.00000E+00	0.00000E+00	0.00000E+00	0.00000E+00
^{235}U	8.26986E-05	8.54980E-05	8.66555E-05	0.00000E+00
^{238}U	3.70115E-02	3.82849E-02	3.88076E-02	0.00000E+00
^{239}Pu	0.00000E+00	0.00000E+00	0.00000E+00	0.00000E+00
^{238}Pu	0.00000E+00	0.00000E+00	0.00000E+00	0.00000E+00
^{242}Pu	0.00000E+00	0.00000E+00	0.00000E+00	0.00000E+00
^{241}Am	0.00000E+00	0.00000E+00	0.00000E+00	0.00000E+00
Cr	1.65503E-03	1.46815E-03	1.17821E-03	1.19186E-03
Ni	6.92826E-04	6.15041E-04	4.75780E-04	4.82129E-04
Fe	6.08806E-03	5.31944E-03	4.23998E-03	4.31040E-03
^{27}Al	0.00000E+00	0.00000E+00	0.00000E+00	0.00000E+00
^{23}Na	0.00000E+00	0.00000E+00	0.00000E+00	0.00000E+00
^{16}O	0.00000E+00	0.00000E+00	0.00000E+00	0.00000E+00
C	3.66408E-05	2.73038E-05	1.85721E-05	1.98538E-05
Mo	1.06734E-05	1.02040E-05	8.18136E-06	8.27768E-06
Mn	1.43786E-04	1.28519E-04	1.04936E-04	1.06060E-04
Cu	1.98177E-05	1.92138E-05	1.70748E-05	1.71923E-05
Si	1.06088E-04	9.54624E-05	6.76848E-05	6.88726E-05
Ca	0.00000E+00	0.00000E+00	0.00000E+00	0.00000E+00
Cl	0.00000E+00	0.00000E+00	0.00000E+00	0.00000E+00
^{59}Co	0.00000E+00	0.00000E+00	0.00000E+00	0.00000E+00

Table C.8: Corrective factors for R-Z homogeneous Monte Carlo calculations

Parameters	MC Detailed	MC R-Z Hom.	**Corr. Fact.**	Experiment
k_{eff}	1.00094 ±7 pcm	0.98680	**1.01433**	1.00051
F49/F25	0.9093 ±0.0065	0.9213	**0.9870**	0.9414
F28/F25	0.0224 ±0.0002	0.0214	**1.04673**	0.0233
C28/F25	0.1336 ±0.0008	0.1388	**0.9625**	0.1323

Table C.9: Corrective factors for R-Z homogeneous deterministic calculations

Parameters	MC Detailed	S_4 R-Z Hom.	**Corr. Fact.**	Experiment
k_{eff}	1.00094 ±7 pcm	0.98915	**1.01192**	1.00051
F49/F25	0.9093 ±0.0065	0.9232	**0.9849**	0.9435
F28/F25	0.0224 ±0.0002	0.0218	**1.0275**	0.0233
C28/F25	0.1336 ±0.0008	0.1387	**0.9632**	0.1323

C.5 ZPR-6 Assembly 7 High ^{240}Pu corrective factors

The specifications of this experiment are provided in the "International Handbook of Evaluated Reactor Physics Benchmark Experiments" under the name "ZPR-LMFR-EXP-002" in the Liquid Metal Fast Reactor Chapter.

The homogeneous R-Z model and associated dimension are shown in Figure C.2 and homogeneous compositions are given in Table C.10 (both taken from the benchmark DVD).

For the deterministic model (one quarter only of the geometry was described), the following meshing has been used with equidistant points in the same region:

Axis							
R	Point	1	24	51	53	74	85
	Dimension (cm)	0.0	24.3435	75.0028	78.0496	111.5583	140.2589
Z	Point	1	51	64	69	74	80
	Dimension (cm)	0.0	76.2813	101.7257	106.6800	110.5357	121.9200

Corrective factors have been calculated with the ENDF/B-VII cross-section data. In Tables C.11 and C.12 the corrective factors are provided for the homogenous R-Z model for Monte Carlo (MC) and deterministic S_4P_1 33-group calculations. Corrective factors are calculated as the ratio between the values obtained by the detailed Monte Carlo calculation and those obtained by the corresponding approximated calculation.

Figure C.2: R-Z homogeneous model for ZPR-6 Assembly 7 High ^{240}Pu

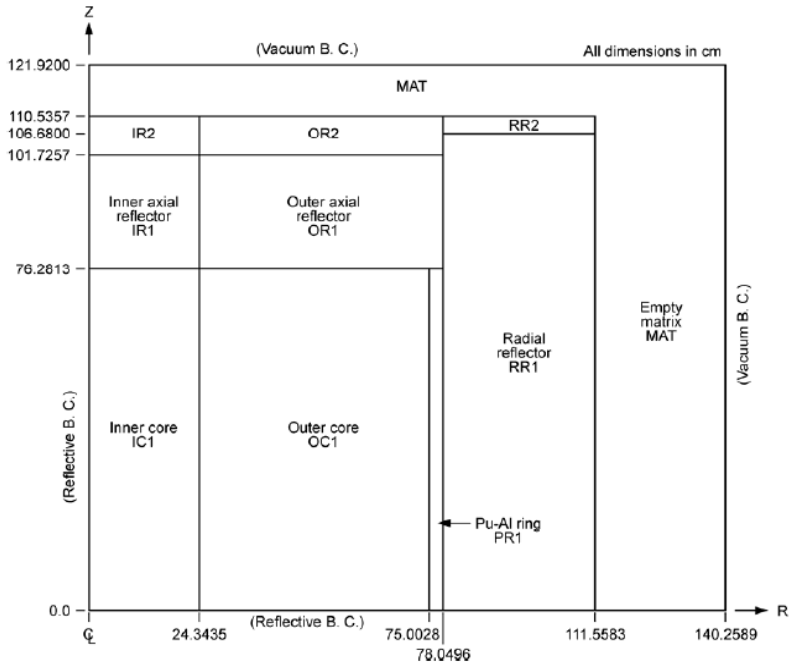

Table C.10: Homogeneous R-Z compositions for ZPR-6 Assembly 7 High ^{240}Pu

Nuclide	Inner Core	Outer Core	Pu-Al Ring
^{240}Pu	3.2178E-04	1.1749E-04	5.0694E-05
^{241}Pu [a]	5.3569E-05	1.4641E-05	2.8433E-06
^{235}U	1.1872E-05	1.2575E-05	1.2151E-05
^{238}U	5.5620E-03	5.7820E-03	5.7042E-03
^{239}Pu	8.3844E-04	8.8583E-04	1.0697E-03
^{238}Pu	1.1083E-06	4.6444E-07	1.6248E-09
^{242}Pu	1.7447E-05	1.7620E-06	1.1005E-07
^{241}Am [a(	1.4681E-05	2.9643E-06	1.9758E-06
Cr	2.6792E-03	2.6909E-03	2.6230E-03
Ni	1.1908E-03	1.1885E-03	1.1648E-03
Fe	1.2805E-02	1.3230E-02	1.3160E-02
Al	4.1057E-06	1.8593E-05	1.1477E-04
Na	9.1676E-03	9.0718E-03	9.3420E-03
O	1.3684E-02	1.4192E-02	1.4386E-02
C	3.6621E-05	3.3605E-05	4.0021E-05
Mo	2.3662E-04	2.3875E-04	1.3306E-05
Mn	2.2447E-04	2.2395E-04	2.2020E-04
Cu	2.4580E-05	2.4882E-05	2.5731E-05
Si	1.6182E-04	1.5377E-04	1.5879E-04
Ca	2.1044E-06	2.0828E-06	2.1452E-06
Cl	2.9484E-07	2.9546E-07	3.0352E-07
Co	8.2889E-07	5.4095E-08	8.2412E-07

Nuclide	Inner Reflector 1	Inner Reflector 2	Outer Reflector 1	Outer Reflector 2
^{235}U	8.1353E-05	8.5866E-05	8.1048E-05	8.4740E-05
^{238}U	3.7936E-02	4.0055E-02	3.7795E-02	3.9527E-02
Cr	1.6464E-03	1.4497E-03	1.6557E-03	1.4696E-03
Ni	6.8937E-04	6.0752E-04	6.9310E-04	6.1564E-04
Fe	6.0603E-03	5.2553E-03	6.0903E-03	5.3245E-03
C	3.6728E-05	2.7168E-05	3.6634E-05	2.7315E-05
Mo	1.0620E-05	1.0042E-05	1.0678E-05	1.0217E-05
Mn	1.4319E-04	1.2717E-04	1.4383E-04	1.2863E-04
Cu	1.9742E-05	1.9068E-05	1.9824E-05	1.9225E-05
Si	1.0623E-04	9.5203E-05	1.0608E-04	9.5483E-05

Nuclide	Radial Reflector 1	Radial Reflector 2	Matrix
^{235}U	8.5846E-05	0.0000E+00	0.0000E+00
^{238}U	4.0046E-02	0.0000E+00	0.0000E+00
Cr	1.1782E-03	1.1910E-03	1.1910E-03
Ni	4.7578E-04	4.8172E-04	4.8172E-04
Fe	4.2400E-03	4.3056E-03	4.3056E-03
C	1.8572E-05	1.9752E-05	1.9752E-05
Mo	8.1814E-06	8.2719E-06	8.2719E-06
Mn	1.0494E-04	1.0599E-04	1.0599E-04
Cu	1.7075E-05	1.7186E-05	1.7186E-05
Si	6.7685E-05	6.8789E-05	6.8789E-05

Table C.11: Corrective factors for R-Z homogeneous Monte Carlo calculations

Parameters	MC Detailed	MC R-Z Hom.	**Corr. Fact.**	Experiment
k_{eff}	1.00017 ±11pcm	0.98589	**1.01448**	1.00080

Table C.12: Corrective factors for R-Z homogeneous deterministic calculations

Parameters	MC Detailed	S_4 R-Z Hom.	**Corr. Fact.**	Experiment
k_{eff}	1.00017 ±11pcm	0.98781	**1.01251**	1.00080

C.6 ZPPR-9 Corrective factors (ANL-INL-JAEA)

The specifications of this experiment are provided in the "International Handbook of Evaluated Reactor Physics Benchmark Experiments" under the name "ZPPR-LMFR-EXP-002" in the Liquid Metal Fast Reactor Chapter [C.1].

The homogeneous R-Z model and associated dimension are shown in Figure C.3 and homogeneous compositions are given in Table C.13.

For the deterministic model (one quarter only of the geometry was described), the following meshing has been used with equidistant points in the same region:

Corrective factors have been calculated using as-built detailed model in Monte Carlo calculations. Two sets of reference calculations have been used. The first uses 300K temperature, JENDL-4 cross-sections and the MVP code [C.2]. The second one uses 293K temperature, ENDF/B-VII.0 cross-sections and MCNP5 code. In Tables C.14 (JENDL-4-based) and C.15 (ENDF/B-VII.0 based) the corrective factors are provided with respect to the corresponding homogenous R-Z model for Monte Carlo (MC) calculations. Table C.16 reports the corrective factors (only ENDF/B-VII.0 based) for deterministic S_4P_1 33-group calculations. Corrective factors are calculated as the ratio between the values obtained by the detailed Monte Carlo calculation and those obtained by the corresponding approximated calculation. The experimental values (and associated uncertainties) are those relative to the as-built detailed model. Experimental reactivity worth for the sodium void configurations is calculated using a $ value of 355 pcm. The $ value has been calculated using Tuttle (1979)'s delayed neutron yield data and Saphier (1977)'s delayed neutron spectrum data.

ZPPR-9

R-axis	Point	1	2	3	5	7	19	25	30	33
	Dimension	0.000	3.117	9.351	18.959	30.698	88.872	119.949	142.594	159.448
	Coarse mesh width	-	3.117	6.234	9.608	11.739	58.174	31.077	22.645	16.854
	Fine mesh width	-	3.117	6.234	4.804	5.870	4.848	5.180	4.529	5.618
Z-axis	Point	1	5	11	16	17	19	21		
	Dimension	0.000	20.396	50.876	76.276	81.359	91.516	104.810		
	Coarse mesh width	-	20.396	30.480	25.400	5.083	10.157	13.294		
	Fine mesh width	-	5.099	5.080	5.080	5.083	5.079	6.647		

Unit: cm

Figure C.3: R-Z Homogeneous model for ZPPR-9

[1] Inner Core
[2] Outer Core
[3] Radial Blanket (Lower)
[4] Radial Blanket (Upper)
[5] Axial Blanket (Lower)
[6] Axial Blanket (Upper)
[7] Radial Reflector
[8] Axial Reflector
[9] Matrix
[10] Na voided Inner Core

(1) For criticality

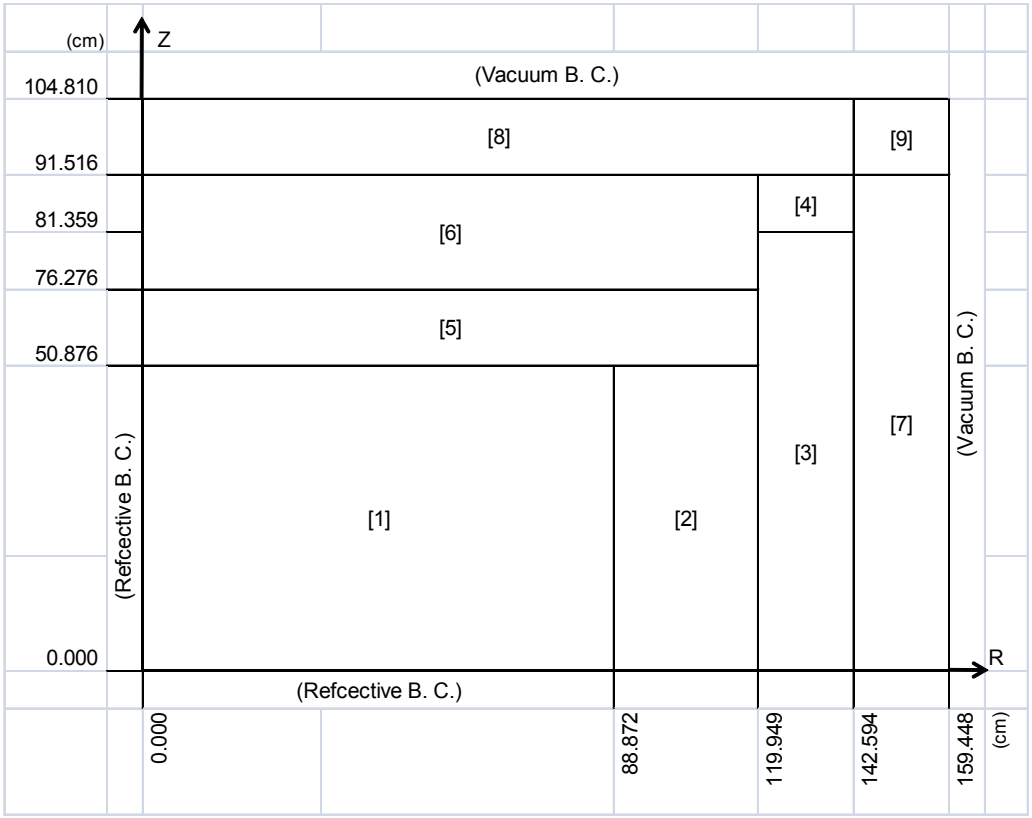

(2) For spectral indices (F28/F25, F49/F25, C28/F25)

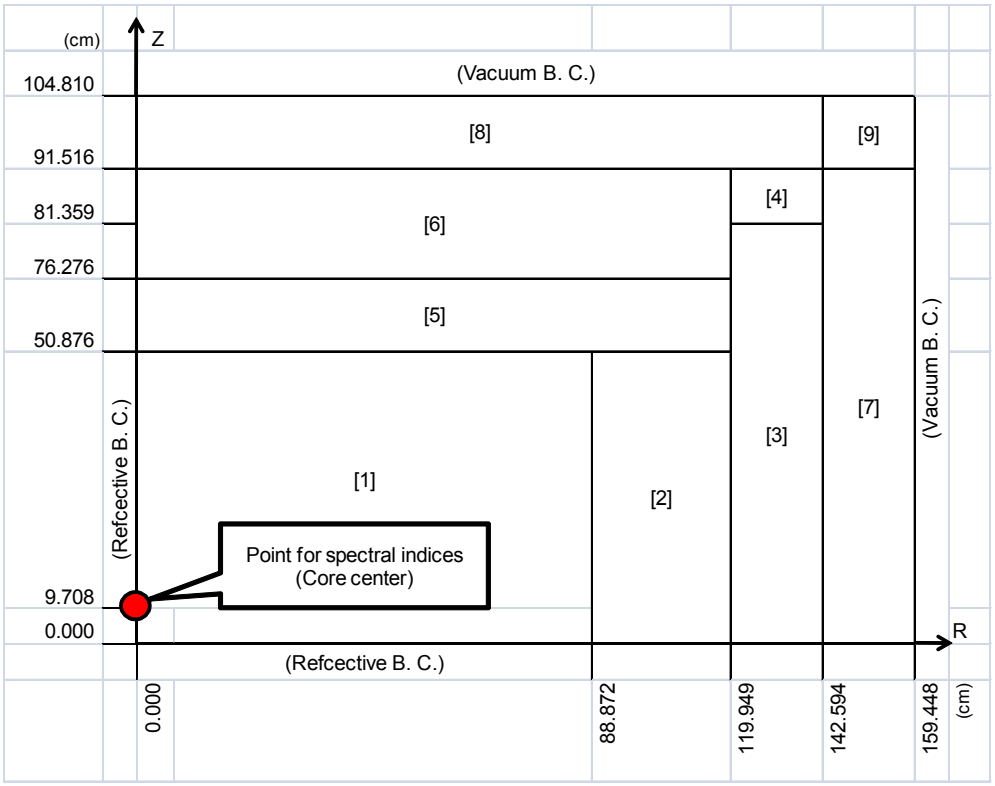

(3) For sodium void reactivity (Step 3, Step 5)

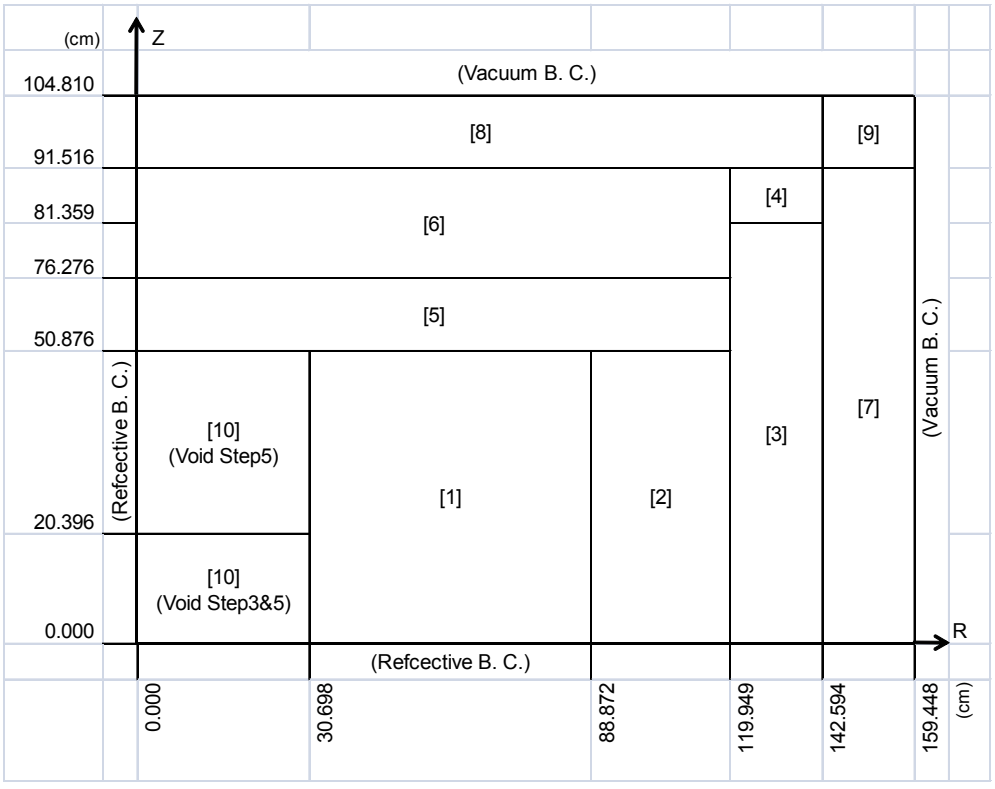

Table C.13: Homogeneous R-Z compositions for ZPPR-9

Table Region-wise homogeneous model composition data

(UNIT:1.0E+24/cc)

Nuclide	[1] Inner Core	[2] Outer Core	[3] Radial Blanket (Lower)	[4] Radial Blanket (Upper)	[5] Axial Blanket (Lower)	[6] Axial Blanket (Upper)	[7] Radial Reflector	[8] Axial Reflector	[9] Matrix	[10] Na Voided Inner Core
U-235	1.81195E-05	1.66427E-05	2.88484E-05	8.92170E-05	2.06540E-05	2.06540E-05	-	-	-	1.81374E-05
U-238	8.24292E-03	7.55916E-03	1.32520E-02	3.99934E-02	9.38616E-03	9.38616E-03	-	-	-	8.24836E-03
Pu-238	5.25465E-07	7.16465E-07	-	-	-	-	-	-	-	5.48400E-07
Pu-239	8.86669E-04	1.26613E-03	-	-	-	-	-	-	-	8.87323E-04
Pu-240	1.17426E-04	1.67660E-04	-	-	-	-	-	-	-	1.17514E-04
Pu-241	1.11237E-05	1.55657E-05	-	-	-	-	-	-	-	1.12966E-05
Pu-242	1.89890E-06	2.63347E-06	-	-	-	-	-	-	-	1.93167E-06
Am-241	6.95678E-06	9.90637E-06	-	-	-	-	-	-	-	6.88803E-06
H-1	9.36509E-06	9.47193E-06	-	-	9.55310E-06	-	-	-	-	9.61957E-06
C	1.05369E-03	1.06073E-03	3.18302E-05	2.91048E-05	1.06754E-03	4.18385E-05	2.13937E-04	5.71292E-04	1.85099E-05	1.07013E-03
O-16	1.44792E-02	1.36044E-02	2.24174E-02	3.57691E-06	1.43528E-02	1.12709E-02	-	-	-	1.46460E-02
Na-23	8.77014E-03	8.80109E-03	4.65010E-03	-	8.73658E-03	9.04687E-03	-	-	-	2.07535E-03
Al-27	4.70703E-06	5.24462E-06	1.40335E-06	-	3.42778E-06	3.17620E-06	-	-	-	4.81478E-06
Si-28	1.53281E-04	1.58949E-04	1.18333E-04	1.02547E-04	1.58537E-04	1.53084E-04	7.94601E-04	6.75406E-05	6.21724E-05	1.53861E-04
Si-29	7.78324E-06	8.07103E-06	6.00864E-06	5.20711E-06	8.05014E-06	7.77322E-06	4.03479E-05	3.42955E-06	3.15696E-06	7.81270E-06
Si-30	5.13077E-06	5.32048E-06	3.96094E-06	3.43257E-06	5.30671E-06	5.12417E-06	2.65976E-05	2.26078E-06	2.08109E-06	5.15019E-06
P-31	5.22693E-06	5.22711E-06	4.37334E-06	4.01289E-06	2.22912E-05	2.23999E-05	5.32680E-05	2.13939E-05	2.72366E-06	5.22798E-06
S-32	1.10601E-06	1.10517E-06	1.14990E-06	1.14990E-06	1.45948E-06	1.28955E-06	2.38539E-05	2.89565E-05	6.81643E-07	1.10363E-06
S-33	8.85461E-09	8.84784E-09	9.20596E-09	9.20596E-09	1.16845E-08	1.03240E-08	1.90972E-07	2.31823E-07	5.45716E-09	8.83553E-09
S-34	4.99819E-08	4.99438E-08	5.19652E-08	5.19652E-08	6.59557E-08	5.82762E-08	1.07799E-06	1.30858E-06	3.08043E-08	4.98743E-08
S-36	2.33016E-10	2.32838E-10	2.42262E-10	2.42262E-10	3.07486E-10	2.71684E-10	5.02558E-09	6.10060E-09	1.43610E-10	2.32514E-10
Cl-35	2.21309E-06	2.22759E-06	1.14470E-07	-	2.22036E-06	2.20971E-07	-	-	-	2.08080E-06
Cl-37	7.07323E-07	7.11959E-07	3.65858E-08	-	7.09648E-07	7.06243E-08	-	-	-	6.65042E-07
Ca-40	1.49676E-06	1.50057E-06	1.03441E-06	-	1.48720E-06	2.01366E-06	-	-	-	-
Ca-42	9.98962E-09	1.00150E-08	6.90381E-09	-	9.92582E-09	1.34395E-08	-	-	-	-
Ca-43	2.08439E-09	2.08969E-09	1.44052E-09	-	2.07108E-09	2.80422E-09	-	-	-	-
Ca-44	3.22076E-08	3.22896E-08	2.22587E-08	-	3.20020E-08	4.33304E-08	-	-	-	-
Ca-46	6.17596E-11	6.19168E-11	4.26820E-11	-	6.13652E-11	8.30880E-11	-	-	-	-
Ca-48	2.88726E-09	2.89461E-09	1.99538E-09	-	2.86882E-09	3.88436E-09	-	-	-	-
Cr-50	1.24509E-04	1.29991E-04	9.11685E-05	7.93401E-05	1.29411E-04	1.23108E-04	6.52619E-04	5.56751E-05	5.09812E-05	1.24914E-04
Cr-52	2.40104E-03	2.50674E-03	1.75809E-03	1.53000E-03	2.49555E-03	2.37401E-03	1.25851E-02	1.07364E-03	9.83121E-04	2.40884E-03
Cr-53	2.72259E-04	2.84244E-04	1.99354E-04	1.73489E-04	2.82976E-04	2.69194E-04	1.42705E-03	1.21742E-04	1.11478E-04	2.73143E-04
Cr-54	6.77710E-05	7.07544E-05	4.96234E-05	4.31851E-05	7.04387E-05	6.70080E-05	3.55223E-04	3.03042E-05	2.77493E-05	6.79911E-05
Mn-55	2.42702E-04	2.53496E-04	1.82106E-04	1.61906E-04	2.50724E-04	2.40480E-04	1.52182E-03	6.04716E-04	1.04506E-04	2.43382E-04
Fe-54	6.99413E-04	7.64216E-04	4.38231E-04	3.83016E-04	7.26703E-04	6.97911E-04	3.09928E-03	4.23201E-03	2.46809E-04	7.06544E-04
Fe-56	1.09793E-02	1.19966E-02	6.87929E-03	6.01253E-03	1.14077E-02	1.09557E-02	4.86520E-02	6.64335E-02	3.87438E-03	1.10912E-02
Fe-57	2.53560E-04	2.77053E-04	1.58873E-04	1.38856E-04	2.63453E-04	2.53015E-04	1.12359E-03	1.53424E-03	8.94763E-05	2.56145E-04
Fe-58	3.37441E-05	3.68707E-05	2.11431E-05	1.84791E-05	3.50608E-05	3.36716E-05	1.49529E-04	2.04179E-04	1.19076E-05	3.40882E-05
Co-59	7.94274E-07	7.89194E-07	4.15621E-06	3.69088E-06	7.91705E-07	9.34345E-07	-	2.05260E-07	-	7.82939E-07
Ni-58	8.61962E-04	9.04973E-04	6.13393E-04	5.17734E-04	8.87056E-04	8.38714E-04	4.52970E-03	3.47385E-04	3.22648E-04	8.65074E-04
Ni-60	3.32026E-04	3.48594E-04	2.36278E-04	1.99430E-04	3.41692E-04	3.23071E-04	1.74483E-03	1.33812E-04	1.24284E-04	3.33225E-04
Ni-61	1.44330E-05	1.51531E-05	1.02708E-05	8.66909E-06	1.48531E-05	1.40437E-05	7.58467E-05	5.81672E-06	5.40252E-06	1.44851E-05
Ni-62	4.60186E-05	4.83149E-05	3.27479E-05	2.76408E-05	4.73583E-05	4.47774E-05	2.41832E-04	1.85462E-05	1.72256E-05	4.61847E-05
Ni-64	1.17196E-05	1.23044E-05	8.33993E-06	7.03931E-06	1.20608E-05	1.14035E-05	6.15876E-05	4.72318E-06	4.38685E-06	1.17619E-05
Cu-63	2.16911E-05	2.21902E-05	2.13937E-05	2.00397E-05	2.32359E-05	2.28168E-05	1.17953E-05	1.25580E-05	1.17643E-05	2.17044E-05
Cu-65	9.66801E-06	9.89048E-06	9.53547E-06	8.93194E-06	1.03565E-05	1.01698E-05	5.25732E-06	5.59725E-06	5.24350E-06	9.67396E-06
Mo-92	3.56028E-05	4.99963E-05	2.18282E-06	2.16292E-06	2.34410E-06	2.26522E-06	1.21264E-06	1.30443E-06	1.20945E-06	3.56123E-05
Mo-94	2.21918E-05	3.11634E-05	1.36058E-06	1.34818E-06	1.46111E-06	1.41195E-06	7.55858E-07	8.13069E-07	7.53869E-07	2.21977E-05
Mo-95	3.81938E-05	5.36348E-05	2.34167E-06	2.32032E-06	2.51469E-06	2.43008E-06	1.30089E-06	1.39936E-06	1.29747E-06	3.82040E-05
Mo-96	4.00172E-05	5.61953E-05	2.45346E-06	2.43109E-06	2.63474E-06	2.54609E-06	1.36300E-06	1.46616E-06	1.35941E-06	4.00278E-05
Mo-97	2.29115E-05	3.21741E-05	1.40471E-06	1.39190E-06	1.50850E-06	1.45774E-06	7.80373E-07	8.39439E-07	7.78319E-07	2.29176E-05
Mo-98	5.78905E-05	8.12945E-05	3.54928E-06	3.51692E-06	3.81153E-06	3.68328E-06	1.97177E-06	2.12101E-06	1.96658E-06	5.79060E-05
Mo-100	2.31034E-05	3.24437E-05	1.41648E-06	1.40356E-06	1.52114E-06	1.46995E-06	7.86910E-07	8.46471E-07	7.84839E-07	2.31096E-05

Table C.14: Corrective factors for R-Z homogeneous Monte Carlo calculations (JENDL-4)

(The corrective factor and experimental value of k_{eff} is corresponding to the 300K data of the ZPPR-9 experiment.)

Parameters	Most detailed	Base*1	(Uncertainty)	Corrections	(Uncertainty)	Experiment	(Uncertainty)
Keff	1.00237	0.99121	±0.00004	1.01126	0.00005	1.00077	±117pcm
S-Index (F28/F25)	0.02116	0.02004	±0.00018	1.056	0.009	0.0207	±2.7%
S-Index (F49/F25)	0.9172	0.9261	±0.0044	0.990	0.005	0.9225	±2.0%
S-Index (C28/F25)	0.1411	0.1395	±0.0009	1.012	0.006	0.1296	±1.9%
Na void (Step 3)	32.84 ¢	34.76 ¢	±1.85 ¢	0.945	0.050	29.39 ¢	±1.9%
Na void (Step 5)	33.20 ¢	43.71 ¢	±1.83 ¢	0.760	0.032	31.68 ¢	±1.9%

Effective delayed neutron fraction (with Tuttle and Saphier): 3.550E-03

*1: Continuous-energy Monte-Carlo R-Z Homogeneous model

Table C.15: Corrective factors for R-Z homogeneous Monte Carlo calculations (ENDF/B-VII.0)

Parameters	MC Detailed	MC R-Z Hom.	**Corr. Fact.**	Experiment
K_{eff}	1.00028 ±3pcm	0.98658	**1.01389** ±100pcm	1.00106 ±117pcm
Na void Step 3 Δk/kk' (pcm)	106 ±4pcm	103	**1.029** ±4pcm	104 pcm ±1.9%
Na void Step 5 Δk/kk' (pcm)	109 ±4pcm	137	**0.796** ±4pcm	112 pcm ±1.9%
F28/F25	0.0201 ±0.55%	0.0198	**1.0152** ±1.0%	0.0207 ±2.7%
F49/F25	0.9048 ±0.37%	0.9091	**0.9953** ±1.0%	0.9225 ±2.0%
C28/F25	0.1308 ±0.33%	0.1382	**0.9465** ±1.0%	0.1296 ±1.9%

Table C.16: Corrective factors for R-Z homogeneous deterministic calculations

Parameters	MC Detailed	S_4 R-Z Hom.	**Corr. Fact.**	Experiment
K_{eff}	1.00028 ±3pcm	0.98809	**1.01234** ±100pcm	1.00106 ±117pcm
Na void Step 3 Δk/kk' (pcm)	106 ±4pcm	106	**1.0** ±4pcm	104 pcm ±1.9%
Na void Step 5 Δk/kk' (pcm)	109 ±4pcm	141	**0.773** ±4pcm	112 pcm ±1.9%
F28/F25	0.0201 ±0.55%	0.0198	**1.0152** ±1.0%	0.0207 ±2.7%
F49/F25	0.9048 ±0.37%	0.9141	**0.9898** ±1.0%	0.9225 ±2.0%
C28/F25	0.1308 ±0.33%	0.1371	**0.9540** ±1.0%	0.1296 ±1.9%

C.7 JOYO Corrective factors (INL-JAEA)

The specifications of this experiment are provided in the "International Handbook of Evaluated Reactor Physics Benchmark Experiments" under the name "JOYO-LMFR-RESR-001" in the Liquid Metal Fast Reactor Chapter [C.1].

The homogeneous R-Z model and associated dimension are shown in Figure C.4 and homogeneous compositions are given in Tables C.17 and C.18.

For the deterministic model, the following meshing has been used with equidistant points in the same region:

Corrective factors have been calculated using as-built detailed model in Monte Carlo calculations. Two sets of reference calculations have been used. The first uses JENDL-4 cross-sections and the MVP code [C.2]. The second one uses ENDF/B-VII.0 cross-sections and MCNP5 code. In Tables C.19 (JENDL-4-based) and C.20 (ENDF/B-VII.0 based) the corrective factors are provided with respect to the corresponding homogenous R-Z model for Monte Carlo (MC) calculations. Table C.21 reports the corrective factors (only ENDF/B-VII.0-based) for deterministic S_4P_1 33-group calculations. Corrective factors are calculated as the ratio between the values obtained by the detailed Monte Carlo calculation and those obtained by the corresponding approximated calculation.

Joyo MK-I										
R-axis	Point	1	5	6	9	16	17	22		
	Dimension	0.000	20.368	22.925	35.940	69.929	75.999	100.468		
	Coarse mesh width	-	20.368	2.557	13.015	33.989	6.070	24.469		
	Fine mesh width	-	5.092	2.557	4.338	4.856	6.070	4.894		
Z-axis	Point	1	5	13	19	23	25	30	33	37
	Dimension	0.000	20.078	60.163	91.000	111.078	120.291	146.214	160.376	180.454
	Coarse mesh width	-	20.078	40.085	30.837	20.078	9.213	25.923	14.162	20.078
	Fine mesh width	-	5.019	5.011	5.139	5.019	4.607	5.185	4.721	5.019
Unit: cm										

Figure C.4: R-Z homogeneous model for JOYO

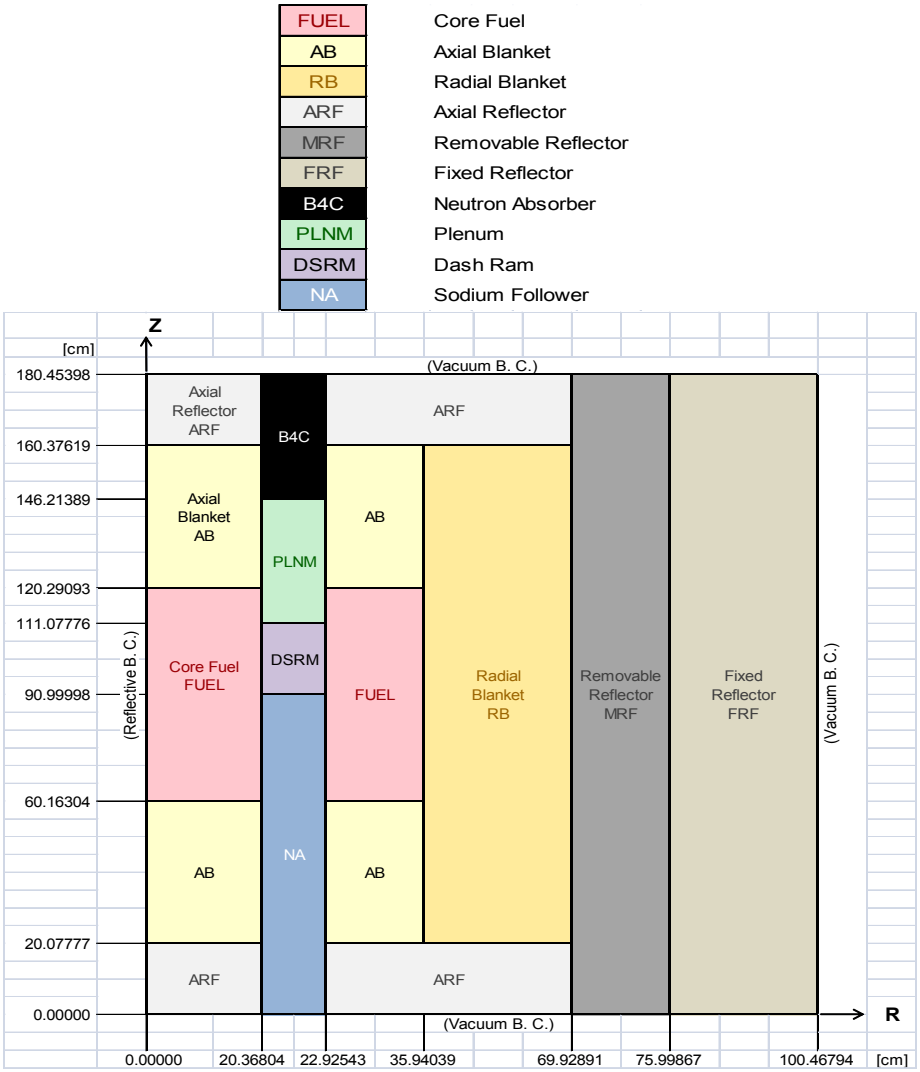

Table C.17: Homogeneous R-Z compositions (1/2) for JOYO

Nuclide	Core Fuel FUEL	Axial Blanket AB	Radial Blanket RB	Axial Reflector ARF	Removable Reflector MRF
U-235	1.58011E-03	1.66524E-05	2.21488E-05	-	-
U-238	5.22603E-03	8.20473E-03	1.09125E-02	-	-
Pu-238	1.45673E-06	-	-	-	-
Pu-239	1.11451E-03	-	-	-	-
Pu-240	2.77791E-04	-	-	-	-
Pu-241	3.82746E-05	-	-	-	-
Pu-242	7.87932E-06	-	-	-	-
Am-241	9.19779E-06	-	-	-	-
B-10	-	-	-	-	-
B-11	-	-	-	-	-
C	-	-	-	-	-
O-16	1.65356E-02	1.64128E-02	2.19755E-02	-	-
Na-23	9.34840E-03	9.34840E-03	7.54820E-03	9.34840E-03	4.56060E-03
Cr-50	1.41909E-04	1.41909E-04	1.23447E-04	1.41909E-04	5.83264E-04
Cr-52	2.73658E-03	2.73658E-03	2.38055E-03	2.73658E-03	1.12477E-02
Cr-53	3.10306E-04	3.10306E-04	2.69935E-04	3.10306E-04	1.27540E-03
Cr-54	7.72418E-05	7.72418E-05	6.71925E-05	7.72418E-05	3.17473E-04
Fe-54	6.95070E-04	6.95070E-04	6.04654E-04	6.95070E-04	2.79900E-03
Fe-56	1.09111E-02	1.09111E-02	9.49177E-03	1.09111E-02	4.39383E-02
Fe-57	2.51985E-04	2.51985E-04	2.19206E-04	2.51985E-04	1.01473E-03
Fe-58	3.35346E-05	3.35346E-05	2.91723E-05	3.35346E-05	1.35042E-04
Ni-58	1.42471E-03	1.42471E-03	1.23939E-03	1.42471E-03	4.21201E-03
Ni-60	5.48794E-04	5.48794E-04	4.77410E-04	5.48794E-04	1.62246E-03
Ni-61	2.38557E-05	2.38557E-05	2.07527E-05	2.38557E-05	7.05271E-05
Ni-62	7.60625E-05	7.60625E-05	6.61686E-05	7.60625E-05	2.24871E-04
Ni-64	1.93709E-05	1.93709E-05	1.68512E-05	1.93709E-05	5.72681E-05
Mo-92	3.49206E-05	3.49206E-05	3.03778E-05	3.49206E-05	-
Mo-94	2.17665E-05	2.17665E-05	1.89349E-05	2.17665E-05	-
Mo-95	3.74620E-05	3.74620E-05	3.25886E-05	3.74620E-05	-
Mo-96	3.92504E-05	3.92504E-05	3.41443E-05	3.92504E-05	-
Mo-97	2.24725E-05	2.24725E-05	1.95490E-05	2.24725E-05	-
Mo-98	5.67813E-05	5.67813E-05	4.93946E-05	5.67813E-05	-
Mo-100	2.26607E-05	2.26607E-05	1.97128E-05	2.26607E-05	-

Unit: 1E+24/cc

Remark: Temperatures of all regions are 250°C.

Table C.18: Homogeneous R-Z compositions (2/2) for JOYO

Nuclide	Fixed Reflector FRF	Neutron Absorber B4C	Plenum PLNM	Dash Ram DSRM	Na Follower NA
U-235	-	-	-	-	-
U-238	-	-	-	-	-
Pu-238	-	-	-	-	-
Pu-239	-	-	-	-	-
Pu-240	-	-	-	-	-
Pu-241	-	-	-	-	-
Pu-242	-	-	-	-	-
Am-241	-	-	-	-	-
B-10	-	2.16249E-02	-	-	-
B-11	-	1.78019E-03	-	-	-
C	-	5.61935E-03	-	-	-
O-16	-	-	-	-	-
Na-23	1.53460E-02	1.30400E-02	1.30400E-02	1.94040E-02	2.15070E-02
Cr-50	2.64090E-04	1.49245E-04	1.49245E-04	1.14505E-04	5.37954E-05
Cr-52	5.09270E-03	2.87804E-03	2.87804E-03	2.20812E-03	1.03739E-03
Cr-53	5.77472E-04	3.26347E-04	3.26347E-04	2.50383E-04	1.17632E-04
Cr-54	1.43745E-04	8.12347E-05	8.12347E-05	6.23256E-05	2.92811E-05
Fe-54	1.26737E-03	7.31005E-04	7.31005E-04	5.60857E-04	2.63498E-04
Fe-56	1.98950E-02	1.14752E-02	1.14752E-02	8.80426E-03	4.13636E-03
Fe-57	4.59463E-04	2.65013E-04	2.65013E-04	2.03329E-04	9.55266E-05
Fe-58	6.11461E-05	3.52683E-05	3.52683E-05	2.70593E-05	1.27128E-05
Ni-58	1.90717E-03	1.49839E-03	1.49839E-03	1.14963E-03	5.40086E-04
Ni-60	7.34638E-04	5.77176E-04	5.77176E-04	4.42835E-04	2.08040E-04
Ni-61	3.19342E-05	2.50894E-05	2.50894E-05	1.92497E-05	9.04336E-06
Ni-62	1.01820E-04	7.99961E-05	7.99961E-05	6.13765E-05	2.88342E-05
Ni-64	2.59306E-05	2.03726E-05	2.03726E-05	1.56308E-05	7.34322E-06
Mo-92	-	3.67262E-05	3.67262E-05	2.81776E-05	1.32377E-05
Mo-94	-	2.28920E-05	2.28920E-05	1.75635E-05	8.25129E-06
Mo-95	-	3.93990E-05	3.93990E-05	3.02283E-05	1.42011E-05
Mo-96	-	4.12798E-05	4.12798E-05	3.16713E-05	1.48791E-05
Mo-97	-	2.36344E-05	2.36344E-05	1.81332E-05	8.51890E-06
Mo-98	-	5.97172E-05	5.97172E-05	4.58171E-05	2.15247E-05
Mo-100	-	2.38324E-05	2.38324E-05	1.82851E-05	8.59026E-06

Unit: 1E+24/cc

Remark: Temperatures of all regions are 250℃.

Table C.19: Corrective factors for R-Z homogeneous Monte Carlo calculations (JENDL-4)

Parameters	Most detailed	Base*1	(Uncertainty)	Corrections	(Uncertainty)	Experiment	(Uncertainty)
Keff	0.99923	1.00410	0.00014	0.99515	0.00014	1.00105	±0.00180

*1: Continuous-energy Monte-Carlo R-Z Homogeneous model

Table C.20: Corrective factors for R-Z homogeneous Monte Carlo calculations (ENDF/B-VII.0)

Parameters	MC Detailed	MC R-Z Hom.	**Corr. Fact.**	Experiment
k_{eff}	0.99851 ±9pcm	1.00186	**0.99666** ±100pcm	1.00105 ±180pcm

Table C.21: Corrective factors for R-Z homogeneous deterministic calculations

Parameters	MC Detailed	S_4 R-Z Hom.	**Corr. Fact.**	Experiment
k_{eff}	0.99851 ±9pcm	1.00107	**0.99744** ±100pcm	1.00105 ±180pcm

References

[C.1] T. Ikegami (2011), "ZPPR-9 Experiment: A 650 MWe-class Sodium-cooled MOX-fuelled FBR Core Mock-up Critical Experiment with Clean Core of Two Homogeneous Zones", ZPPR-LMFR-EXP-002, NEA/NSC/DOC (2006)01, International Handbook of Evaluated Reactor Physics Benchmark Experiments.

[C.2] Y. Nagaya, K. Okumura, T. Mori, M. Nakagawa (2005), "MVP/GMVP II: General Purpose Monte Carlo Codes for Neutron and Photon Transport Calculations based on Continuous Energy and Multi-group Methods", JAERI 1348, Japan Atomic Energy Research Institute.

Appendix D: In-depth comparison of JAEA and PSI sensitivity coefficients

The JAEA solution was provided on the basis of the Generalised Perturbation Theory code SAGEP [D.1] using diffusion theory in (r,z) geometry and JENDL-4 nuclear data. PSI used finite-difference discrete-ordinates transport theory with P_1S_4 approximations in either spherical or (r,z) geometry depending on the benchmark set, and JEFF-3.1 nuclear data. In order to understand the main differences of the two solutions, the two parties made consistent complementary analyses for the spherical systems FLATTOP and JEZEBEL (Pu configurations) using (a) 1D transport theory, (b) 2D transport theory for a cylinder of height equal to diameter in each of the two zones in the case of FLATTOP, maintaining the original spherical volumes but not their outer surface areas, which correspond to the SAGEP model, (c) 1D diffusion theory, and (d) 2D diffusion theory for the same geometrical model as in (b).

Figure D.1 illustrates and clearly indicates that for the effective multiplication factor k the main differences between the JAEA and PSI reference solutions obtained with the Standard Perturbation Theory (SPT) can be attributed to the different flux and adjoint flux calculation options, i.e. diffusion or transport theory. These differences appear more clearly in the case of FLATTOP having a natural U reflector than in that of the bare sphere JEZEBEL, i.e. with no reflector.

Similar conclusions could also be drawn for the central reaction rate ratios obtained by using the Generalised Perturbation Theory (GPT).

For the void effect in ZPPR9, however, no significant effect was found to result from the use of diffusion or transport theory in the calculations based on Equivalent Generalised Perturbation Theory (EGPT) and the differences between JAEA and PSI might be attributed to nuclear data differences, in this case.

Figure D.1: Sensitivity coefficients of *k* to the ^{239}Pu inelastic scattering cross-section for (a) FLATTOP and (b) JEZEBEL (Pu configurations), computed using different models

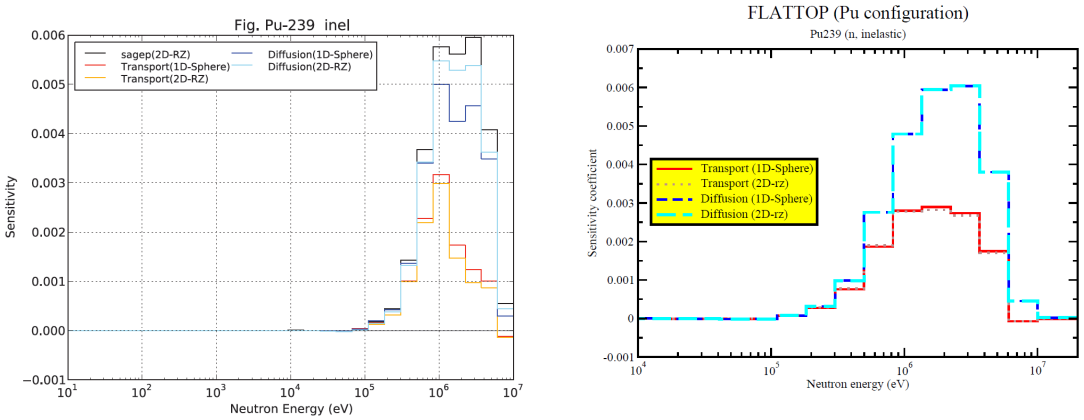

(a)

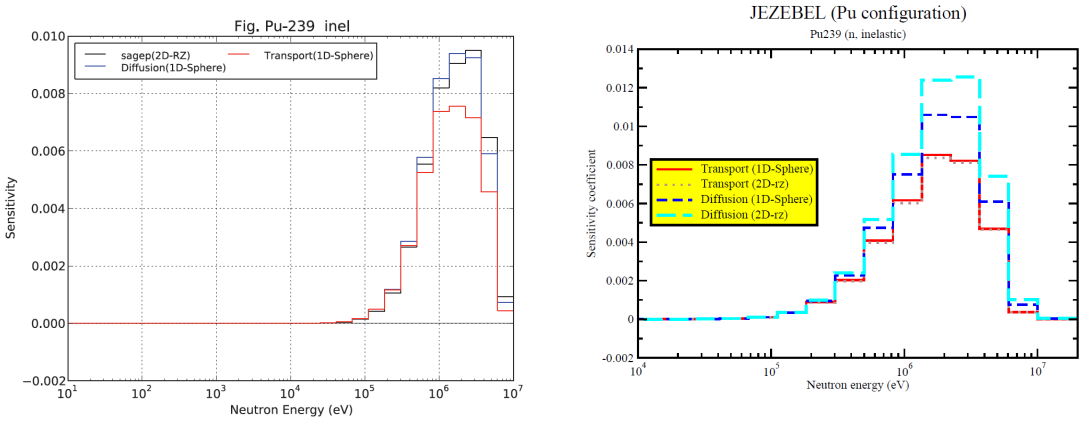

(b)

On the left: JAEA results; on the right: PSI results.

Reference

[D.1] A. Hara, T. Takeda, Y. Kikuchi (1984), "SAGEP: Two-Dimensional Sensitivity Analysis Code Based on Generalised Perturbation Theory", JAERI-M 84-027, Japan Atomic Energy Research Institute.

Appendix E: Teaching example of adjustment method characteristics

Introduction

In the cross-section adjustment procedure, various kinds of differential and integral parameters affect the adjusted results in very complicated manners. Based on an analysis of a simple problem, this appendix aims to illustrate the physical meaning of each parameter used in the adjustment.

Theory of cross-section adjustment

The cross-section adjustment methodology is based on the Bayesian theory and the generalised least-square technique (for example, [E.1]), where all related information including cross-section covariance data, sensitivity coefficients, integral C/E (calculation/experiment) values, experimental and analytical modelling uncertainty, is synthesised with physical consistency. Based on the Bayes theorem, i.e. the conditional probability estimation method, the posterior probability that a cross-section set, ***T***, is true, is maximised under the condition that the information of integral experiments, ***R***, is obtained:

$$J(T) = (T\text{-}To)^t M^{-1}(T\text{-}To) + [Re\text{-}Rc(T)]^t[Ve+Vm]^{-1}[Re\text{-}Rc(T)] \quad (E.1)$$

where:

J(T): an error[18] function targeted for the combined set of differential and integral data;

To : *a prior* cross-section set before adjustment;

M : covariance of the prior cross-section set ***To*** before adjustment;

Re : measured values of the integral experiment set;

Rc(T) : analytical values of the integral experiment set obtained with the cross-section set ***T***;

Ve : experimental error matrix of an integral experiment set ***Re***;

Vm : analytical modelling error matrix of the analysed integral experiment set ***Rc***.

In order to minimise the error function ***J(T)***, its differentiation with respect to ***T*** is required to be zero:

$$dJ(T)/dT = 0. \quad (E.2)$$

After analytical derivations with the linearity assumption between ***Rc(T)*** and ***T***, the posterior cross-section set, ***T'***, and its covariance, ***M'***, after adjustment, are obtained as follows:

$$T' = To + MG^t[GMG^t+Ve+Vm]^{-1}[Re\text{-}Rc(To)] \quad (E.3)$$

$$M' = M - MG^t[GMG^t+Ve+Vm]^{-1}GM \quad (E.4)$$

[18] The word "error" does not mean the "mistake" here, but as same with the "uncertainty" in the statistical usage.

where:

G*:** sensitivity coefficients of the integral parameter set, **R**, with respect to ***T, that is,

$$\boldsymbol{G} = (d\boldsymbol{R}/\boldsymbol{R})/(d\ \boldsymbol{T}/\boldsymbol{T}). \quad \text{(E.5)}$$

The minimised ***J(T')*** function is generally called the minimised chi-square, χ^2_{min} [E.2]. Note that the second term of the right-hand side in Equation (E.6) applies the optimised posterior analytical values of integral parameters, ***Rc(T')***, in contrast, the prior values, ***Rc(To)***, are used in the right-hand side of Equation (E.7):

$$\chi^2_{min} = (T'-To)^t M^{-1}(T'-To) + [Re-Rc(T')]^t[Ve+Vm]^{-1}[Re-Rc(T')] \quad \text{(E.6)}$$

$$= [Re-Rc(To)]^t[GMG^t + Ve+Vm]^{-1}[Re-Rc(To)] \quad \text{(E.7)}$$

where,

$$Rc(T') = Rc(To)+G(T'-To). \quad \text{(E.8)}$$

The prior and posterior uncertainties of integral parameters induced by the cross-section error are calculated with $\boldsymbol{GMG^t}$ and $\boldsymbol{GM'G^t}$, respectively. Here, some characteristics of the posterior cross-section-induced uncertainty can be found, $\boldsymbol{GM'G^t}$, and we can also observe a product of Equation (E.4) multiplied by the sensitivity ***G*** from the left- and right-sides with some approximations:

$$\text{If } GMG^t << Ve+Vm, \text{ then } T' \fallingdotseq To \text{ and } GM'G^t \fallingdotseq GMG^t \quad \text{(E.9)}$$

$$\text{If } GMG^t >> Ve+Vm, \text{ then } GM'G^t \fallingdotseq Ve+Vm \quad \text{(E.10)}$$

$$\text{If } GMG^t \fallingdotseq Ve+Vm, \text{ then } GM'G^t \fallingdotseq 1/2 \times GMG^t \quad \text{(E.11)}$$

Simulation of the adjustment procedure

Here, we treat a very simple data set to simulate the adjustment procedure. This system is comprised of three cross-sections (**s1**, **s2** and **s3**) and two integral parameters (**R1** and **R2**).

Standard case

Figure E.1 summarises the input set of the standard case and the results of adjustment, i.e. output in the form of both tables and graphs. The cross-section covariance is composed of a 3-by-3 square matrix. The prior values of the matrix components are given as 1.0 for the diagonal terms, that is, the variance (=cov(x_i, x_i)) or the square of the standard deviation (=[std(x_i)]^2). For the non-diagonal terms of the matrix [=cov(x_i, x_j), $i \neq j$], the values of 0.0 are given, that is, there are no-correlations among three cross-sections. The sensitivity is also a matrix with 2-by-3 elements. The sensitivity coefficients of integral parameter **R1** with respect to cross-sections are set as 1.0 for all three cross-sections, and those of **R2** to cross-sections **s1**, **s2** and **s3** are 1.01, 1.0 and 0.99, respectively. Namely, the sensitivity coefficient vectors of **R1** and **R2** are set to be very similar, but not completely identical to avoid mathematical irregularity. The uncertainty of integral parameters, that is, the summation of experimental error ***Ve*** and analytical modelling error ***Vm***, is a 2-by-2 matrix. The matrix elements are given as 0.1 for the diagonal terms, and zero for non-diagonal terms. These values mean there is no correlation between the error of **R1** and **R2**, and the integral error matrix, ***Ve+Vm***, are extremely small compared with the cross-section-induced uncertainty, $\boldsymbol{GMG^t}$, which corresponds to the case of Equation (E.10). The prior **E-C** value vector is set as 1.0 for both **R1** and **R2**.

The χ^2_{min} value of this standard case is calculated as 0.33 using Equation (E.7). From the statistical viewpoint, the χ^2_{min} value is expected to be close to the degree of freedom

in the dataset, that is, the number of the integral parameters. Though the value of 0.33 is quite smaller than 2, it has no impact on these simulations[19].

As the consequence of the adjustment operation, first, all cross-sections are changed by +0.33. When the cross-section alterations are multiplied by the sensitivity coefficients as Equation (E.8), the posterior **E-C** values become approximately zero for both integral parameters **R1** and **R2**, as shown in Equation (E.10). It is also reasonable that the values of cross-section alterations are same among **s1**, **s2** and **s3**. The variances and the sensitivity coefficients are practically identical among three cross-sections, therefore, the contribution from each cross-section must be equal, as shown in Equation (E.3), if there is no correlation among cross-sections. Second, every diagonal-term of the posterior cross-section covariance decreases to a value of 0.67, which is just two-third of the prior variance. The important thing to be noticed here is that all non-diagonal terms of the posterior covariance shift to the negative values by -0.33 (= -0.49 as the correlation factor (=ρ_{ij}))[20] in this case. As shown in Equation (E.4), the non-diagonal terms of the cross-section covariance would move to the negative direction, as well as the diagonal terms. The posterior cross-section-induced uncertainty, $\boldsymbol{GM'G^t}$, is found to be very close to the integral parameter error matrix, ***Ve+Vm***, which is consistent with Equation (E.10). It should be noted that the contributions to the reduction of the cross-section-induced uncertainty consist of one-third from the diagonal terms, and two-third from the non-diagonal terms.

Figure E.1: Simulation of cross-section adjustment (standard case)

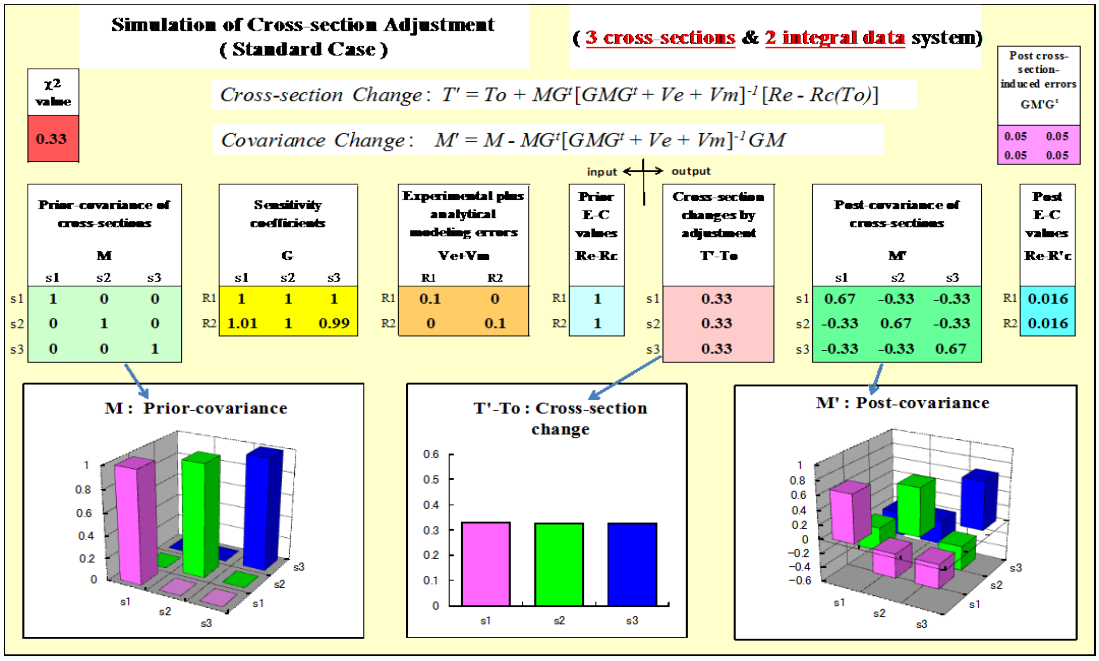

Hereafter, we change an input value of the standard case, one by one, to understand the effect of each parameter in the adjustment procedure.

[19] If one would like to force the χ^2_{min} value to be approximately the degree of freedom, it can be easily attained. Setting the prior **E/C** values as 2.5 for both **R1** and **R2** will make χ^2_{min} to be the value of 2.05. However, we avoid it here since the adjusted results will become difficult to understand intuitively.

[20] Correlation factor between elements x_i and x_j: $\rho_{ij} = \dfrac{\mathrm{cov}(x_i, x_j)}{std(x_i) \times std(x_j)}$, where, $-1 \le \rho_{ij} \le +1$

Case 1: Effect of cross-section standard deviation (or variance)

In Figure E.2, the variance of the prior cross-section **s1** is changed to 2.0, which is twice of the standard case. The grey-coloured figures in the input mean that they are unchanged from the standard case.

The posterior **E-C** values are almost zeros like the standard case, but the contributions of cross-sections are quite different. The cross-sections **s1** is altered by +0.49, which is roughly double with the value of other **s2** and **s3**, +0.25. As shown in Equation (E.3), the cross-section alteration rate, **T'-To**, appears to be rather proportional with the value of covariance, **M**, though the degree is somewhat mitigated by the denominator which includes **M**. In fact, a cross-section with large uncertainty would tend to be altered significantly by the adjustment, if its sensitivity is comparable with other cross-sections.

The posterior variance of the cross-section **s1** reduces to 1.0, which is a half of the prior value, 2.0, but the values of other **s2** and **s3** are around 0.75, which is three fourths of the prior. The non-diagonal terms of the posterior covariance also move to more negative for the elements related to **s1** than the other correlation between **s2** and **s3**. Converting the values of covariance elements to the correlation factors, the posterior ones are -0.57 between **s1** and **s2**, and -0.32 between **s2** and **s3**. In summary, the reduction of cross-section covariance is also significant for the cross-section with large uncertainty, as well as the cross-section alteration, when other conditions are the same among these cross-sections.

The χ^2_{min} value becomes 0.25, which is smaller than that of the standard case 0.33, since the denominator of Equation (E.7) becomes larger due to the prior covariance.

Figure E.2: Simulation of cross-section adjustment (Case 1)

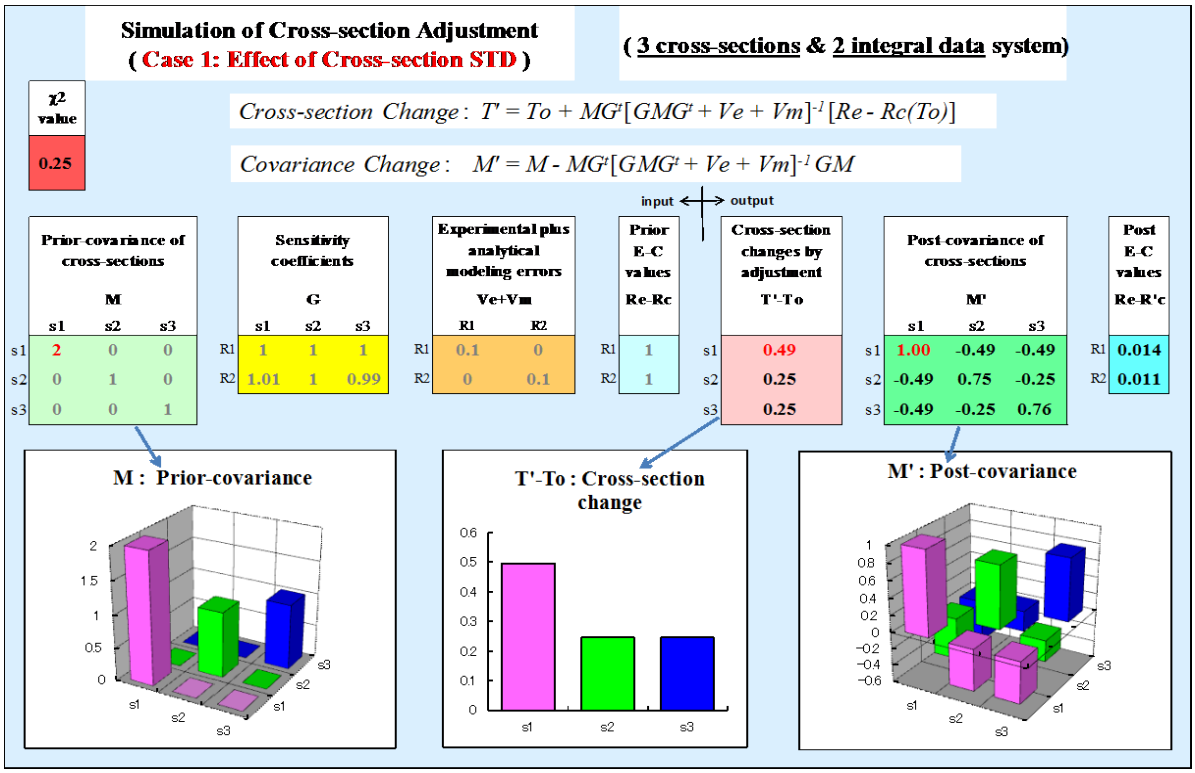

Case 2: Effect of cross-section correlation

In Figure E.3, a strong positive correlation between the cross-sections **s1** and **s2** is given as +0.9, which is zero in the standard case. The other inputs are not changed.

The posterior **E-C** values are almost zeros like the standard case, but the contributions of cross-sections are quite different like Case 1. The cross-section **s1** and **s2** are altered by +0.39 both, which is double with that of **s3**, +0.20. If we gave a value of 2 to the variance of **s2** as well as **s1** as a modification of Case 1, practically comparable cross-section alterations with this Case 2 would be obtained. As a result, it is to be noted that giving the correlation among cross-sections would play a similar role to change their variances in some situations. In other words, the correlation in covariance would be also a kind of error values in the adjustment.

The posterior variances of the cross-sections **s1** and **s2** reduce to 0.25 for both, which is one-fourth of the prior value, while the posterior of uncorrelated **s3** is 0.80, the reduction of which is much smaller than those of correlated **s1** and **s2**. The non-diagonal term of the posterior covariance between **s1** and **s2** still has a positive value of +0.15, but the reduction from the prior value is quite large. As the correlation factor values, the posterior one between **s1** and **s2** is +0.6, which reduces from the prior value, +0.9. The non-diagonal correlation factors related to the uncorrelated **s3** are -0.87, which is larger in absolute than the value of the standard case -0.49. However, the quantitative trends of the posterior covariance do not seem easy to understand in this Case 2.

The χ^2_{min} value of Case 2 is 0.21, which is smaller than that of the standard case 0.33, due to the larger prior covariance as well as Case 1.

Figure E.3: Simulation of cross-section adjustment (Case 2)

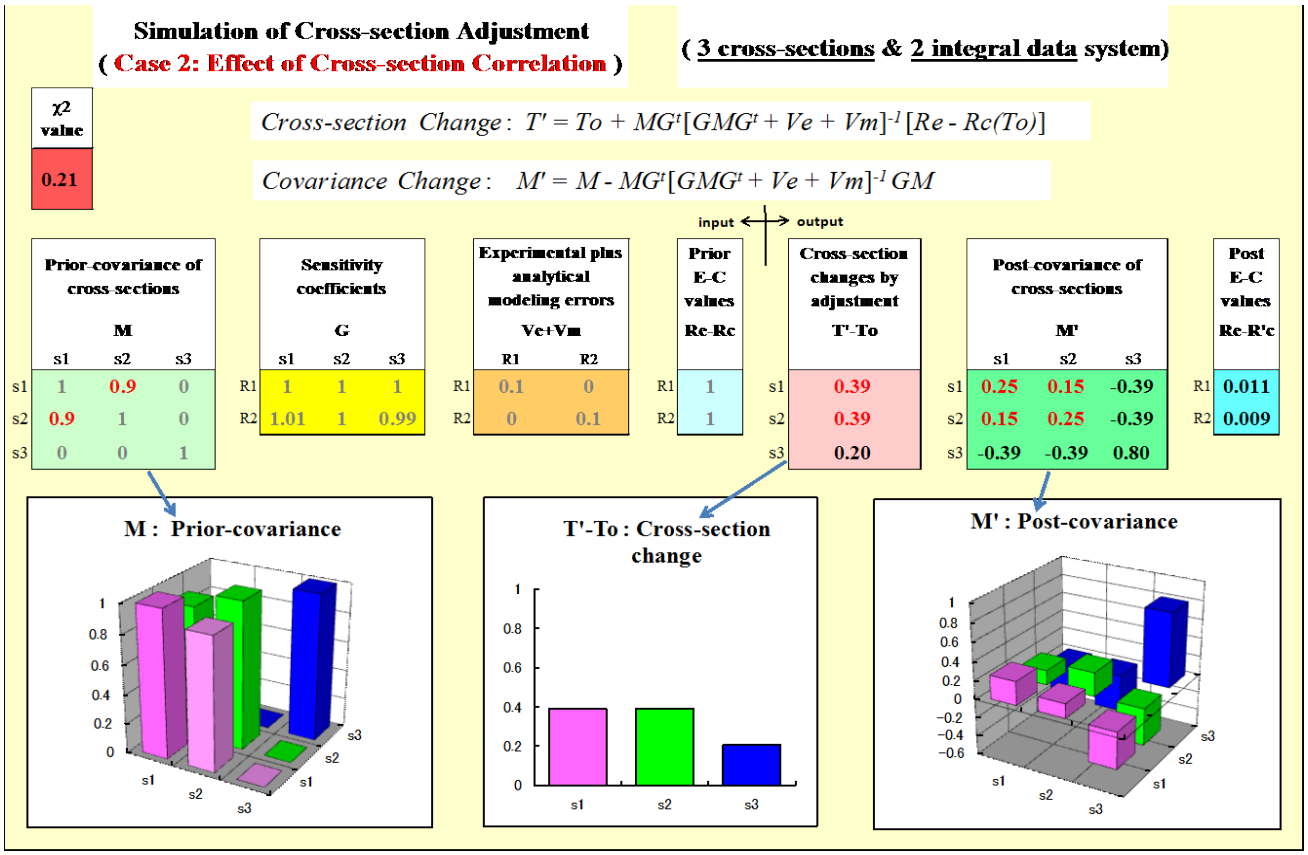

Case 3: Effect of sensitivity coefficient

In Figure E.4, the sensitivity coefficients of the integral parameters **R1** and **R2** with respect to the cross-section **s1** are made twice with those of the standard case. The other inputs are not changed.

The posterior **E-C** values are almost zeros like the standard case, but the contributions of three cross-sections are also different. The altered value of the cross-section **s1** is +0.33, which is roughly double with the value of the other **s2** and **s3**, around +0.16. As can be seen in Equation (E.3), the cross-section alteration rate, ***T'-To***, is suggested to be rather proportional with the value of sensitivity coefficients, **G**, as well as the cross-section covariance, **M**. In this Case 3, the contribution of **s1** to the **E-C** changes is 4-times larger than those of the other **s2** and **s3**. Coupling with the conclusion of Case 1, a cross-section with large uncertainty and/or large sensitivity would tend to be altered significantly by the adjustment.

The posterior variance of the cross-section **s1** reduces to 0.34, which is one third of the prior value, but the values of other **s2** and **s3** are around 0.83, which is rather close to the prior values. The non-diagonal terms of the posterior covariance also move to more negative for the elements related to **s1** than the other correlation between **s2** and **s3**. As the correlation factors, the posterior ones are -0.62 between **s1** and **s2**, and -0.20 between **s2** and **s3**. In summary, the reduction of cross-section uncertainty is significant for the cross-section with large sensitivity, as well as the cross-section alteration.

The χ^2_{min} value is 0.17, which is smaller than that of the standard case 0.33, since the denominator of Equation (E.7) becomes larger due to the sensitivity coefficients. Note that the sensitivity coefficients, **G**, contributes to the accuracy of integral data as the square of the values with the term, $\boldsymbol{GMG^t}$.

Figure E.4: Simulation of cross-section adjustment (Case 3)

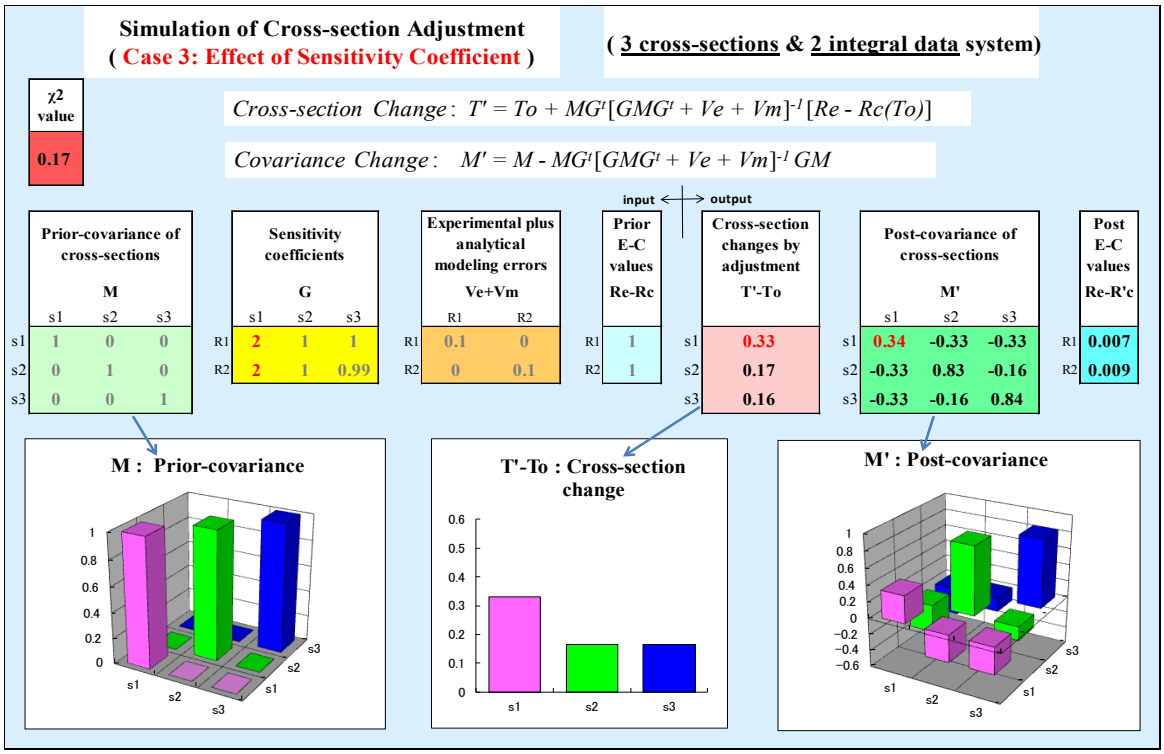

Case 4: Effect of integral parameter uncertainty

In Figure E.5, the diagonal terms of the integral parameters error matrix, ***Ve+Vm***, are made extremely large for both **R1** and **R2** to be a value of 100, compared with those of the standard case, 0.1. The other inputs are not changed.

The posterior **E-C** values are 0.94 for both **R1** and **R2**, which are hardly altered from the prior values, 1.0. The cross-sections and their covariance are hardly changed by the adjustment either. These results are consistent with Equation (E.9). When the integral parameters possess very large errors, ***Ve+Vm***, compared with the cross-section-induced uncertainty, ***GMG***^{t}, these integral data have no influence on the adjusted results. In this Case 4, the posterior dataset is almost the same as the prior one. It should be emphasised that the integral data with large uncertainty have no impact on the adjusted results, since they are simply ignored in the adjustment procedure. In contrast, the integral data with too small errors which is improbable physically, must not to be adopted in the adjustment, since it will alter the posterior covariance (and related cross-sections) too much largely, as shown in Equation (E.10).

The χ^2_{min} value is 0.02, which is much smaller than that of the standard case 0.33, since the denominator of Equation (E.7) is extremely large.

Figure E.5: Simulation of cross-section adjustment (Case 4)

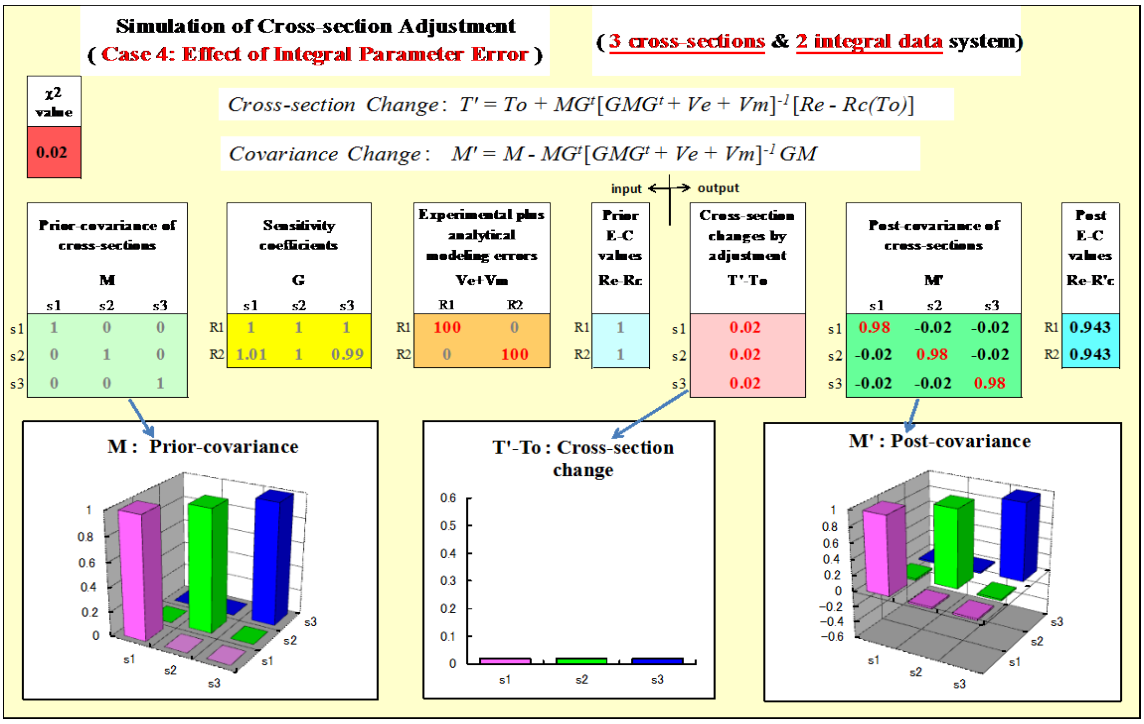

Case 5: Effect of abnormal E-C value

In Figure E.6, the **E-C** value of the integral parameter **R1** is changed to -1.0 from that of the standard case, +1.0. The other inputs including the **C-E** value of **R2** are not changed. Since the integral error matrix, ***Ve+Vm***, is sufficiently small compared with the prior cross-section-induced uncertainty, ***GMG***^{t}, the prior **E-C** values are practically determined only by the cross-section errors. In addition, the sensitivity coefficients of both **R1** and **R2** are nearly identical here. Hence, it should be emphasised that the prior **E-C** values of **R1** and **R2**, -1.0 and +1.0 are obviously inconsistent with each other. In other words, we should consider that there would be some serious mistakes to evaluate the value of **E** or **C**

or ***Ve+Vm***, or everything in this Case 5. The posterior **E-C** values are -1.0 for **R1**, and +0.999 for **R2**, which are hardly altered from the prior values. The posterior cross-section covariance **M'** is identical with the standard case, that is, +0.67 for the diagonal terms, and -0.33 for the non-diagonal.

The posterior cross-section-induced uncertainty $\boldsymbol{GM'G^t}$ is also identical with that of the standard case, where large accuracy improvement is obtained by the adjustment. These results may seem puzzling, since the accuracy of cross-sections is improved, while there are no alterations in the posterior **E-C** values. The answer can be found in Equation (E.4), that is, the posterior covariance is not concerned with the **E-C** values at all in the adjustment procedure. On the other hand, the alterations of cross-sections ***T'-To*** are rather significant, +0.10 for **s1** and -0.10 for **s3**. The contributions of **s1** and **s3** to the posterior **E-C** values are totally cancelled, therefore the **E-C** values are not altered. Note that this large difference of cross-section alterations between **s1** and **s3** stems from very tiny differences of the sensitivity coefficients, +1.01 for **s1** and +0.99 for **s3**. This situation would be very dangerous for the use of the adjustment, since physically meaningless difference of the sensitivity coefficients would result in the large movement of the cross-sections. Fortunately, we can find the anomaly of this Case 5 input from the statistical analysis. The χ^2_{min} value is 19.98, which exceeds extremely the degree of freedom, 2. We could judge that the input should not be adopted in this Case 5 from the χ^2_{min} value, however, it would be difficult to find this kind of abnormal data if we were dealing with in the adjustment. In this case, we might need to apply other screening system such as the comparison of individual **E-C** value with the corresponding total uncertainty of the integral parameter, that is, $\boldsymbol{GMG^t + Ve + Vm}$, in Equation (E.7).

Figure E.6: Simulation of cross-section adjustment (Case 5: Effect of abnormal E-C value)

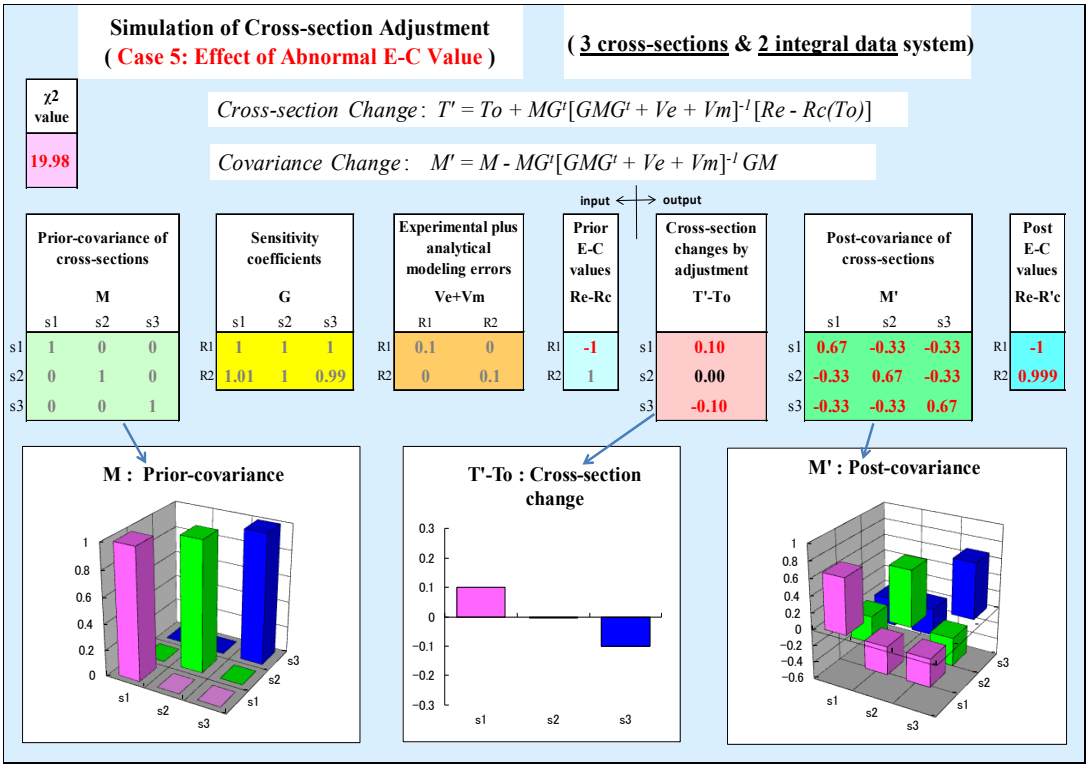

Concluding remarks

The lessons learnt from this adjustment exercise with a very simple problem are summarised as follows:

- The accuracy improvement of the integral parameters is caused by the shrinkage of the cross-section covariance data, especially by the addition of negative correlation among cross-sections.
- If the standard deviation value of a cross-section is large, the alteration rate of the cross-section by the adjustment is also large.
- Positive correlation between cross-sections behaves like large standard deviation values of the cross-sections, if the sensitivity coefficients and other integral parameters are consistent.
- Large sensitivity coefficients work like large standard deviation values of the cross-sections, if the prior **E-C** values are consistent with other parameters.
- Large uncertainty values of integral parameters mean that the data have less weight or little influence on the adjusted results.
- If the sensitivity coefficients and the prior **E-C** values are inconsistent with small uncertainty values of integral parameters, the adjusted results tend to be dangerously fictitious. Some statistical analysis would help eliminate such erroneous data.

References

[E.1] J.B. Dragt *et al.* (1977), "Methods of Adjustment and Error Evaluation of Neutron Capture Cross Sections; Application to Fission Product Nuclides", *Nuclear Science and Engineering* 62, pp.117-129.

[E.2] D.L. Smith (1991), "Probability, Statistics, and Data Uncertainties in Nuclear Science and Technology", An OECD Nuclear Energy Agency Nuclear Data Committee Series, Volume 4, *American Nuclear Society*.

Appendix F: IRSN adjustment methodology and assessment questionnaire

Introduction

In order to be able to assess the safety of future sodium fast reactor project, IRSN develops a methodology for validation of neutronics calculations to address safety needs. The BERING code package is a key element of this methodology. It applies the Generalised Linear-Least-Square Method (GLLSM), which is the linearisation of the maximum likelihood approach [F.1]. The code was written in 2012 and it has not been published to date.

The method modifies or "adjust" nuclear data to improve agreement between computed and measured values in a set of integral experiments, taking into account uncertainties and correlations in nuclear data and in the measured data [F.1] [F.2]. However, the major function of BERING is not to obtain an adjusted library of nuclear data and cross-section covariances, but rather to establish the high-confidence bias and the bias uncertainty for validation of neutronics computations. Nevertheless, the post-adjusted data, e.g. cross-sections and cross-section covariance data, are given in the output of the tool and can be analysed to avoid non-physical data changes [F.3].

Theoretical background

Let us assume that there are available *I* benchmark experiment values (with associated benchmark uncertainties and calculation results) modelled correctly using a finite number of neutron cross-sections presented in *NG* groups, for *NI* nuclides and *NR* reactions. If covariance matrices of the nuclear data and sensitivity coefficients of measured parameters to the neutron cross-sections are also available, it is possible, following Bayes' theorem, to adjust these parameters within their uncertainty bounds in such a way as to provide the best fit with *I* experimentally measured values. The corrections to the neutron cross sections are such that the new cross-sections satisfy the following relation:

$$\sigma_x = \sigma_{x,0} \cdot \left(1 + \Delta\sigma_{\sigma,x}\right), \qquad \text{(F.1)}$$

where σ_x is the nuclear data corrected to be close to true, $\sigma_{x,0}$ is initial nuclear data and $\Delta\sigma_{\sigma,x}$ is the element of vector $\vec{\Delta}_\sigma$ of corrections to nuclear data for *x*-th reaction, where *x* corresponds to nuclide *in*, reaction *ir* and group *ig* as:

$$x = NR \cdot NG \cdot (in - 1) + NG \cdot (ir - 1) + ig\,. \qquad \text{(F.2)}$$

The correction vector $\vec{\Delta}_\sigma$ is determined under the condition of minimising the following quadratic form [F.2]:

$$\chi^2 = \vec{\Delta}_\sigma^T \cdot \hat{S}_k^T \cdot \hat{W} \cdot \hat{S}_k \cdot \vec{\Delta}_\sigma + \vec{\Delta}k_{C-E}^T \cdot \hat{V} \cdot \vec{\Delta}k_{C-E}\,, \qquad \text{(F.3)}$$

where χ^2 is the quadratic form of off-sets; $\hat{W}$ is the covariance matrix of nuclear data; $\hat{S}_k$ is the rectangular matrix of sensitivity coefficients to the nuclear data, $\hat{V}$ is the covariance matrix of integral experiments [F.4]; $\vec{\Delta}_\sigma$ is the vector of corrections to the nuclear data (relative values); and $\vec{\Delta}k_{C-E}$ is the vector of relative calculation-to-experiment discrepancies. The correction to nuclear data can be expressed as:

$$\Delta_\sigma = \frac{\sigma_{0,x} - \sigma_x}{\sigma_{0,x}}, \forall x \in [1, NI \cdot NR \cdot NG], \tag{F.4}$$

where σ is an element of nuclear data vector that are close to the true values; $\sigma_{o,x}$ is an element the original vector of nuclear parameters. The relative calculation-to-experiment discrepancies are calculated as follows:

$$\Delta k_{C-E,l} = \frac{E_l - C_l}{E_l}, \forall l \in [1, I], \tag{F.5}$$

where C_l and E_l is calculated and measured *l-th* benchmark parameter, respectively.

The rectangular $[I \times (NI \cdot NR \cdot NG)]$ ranking matrix of the sensitivity coefficients can be expressed as:

$$\hat{S}_k = \begin{bmatrix} S_{1,1} & \ldots & S_{k,1} & S_{I,1} \\ S_{1,2} & \ldots & S_{k,2} & S_{I,2} \\ \ldots & \ldots & \ldots & \ldots \\ S_{1,X} & \ldots & S_{k,X} & S_{I,X} \end{bmatrix} = [\vec{S}_k], \tag{F.6}$$

$$\vec{S}_k = \begin{bmatrix} S_{k,1} \\ S_{k,2} \\ \ldots \\ S_{k,X} \end{bmatrix} \forall k \in [1, I]$$

where $S_{k,x}$ is the sensitivity to *x-th* cross-section calculated as follows:

$$S_{k,x} = \frac{\sigma_x}{k_{eff}} \cdot \frac{\partial k_{eff}}{\partial \sigma_x}. \tag{F.7}$$

Differentiating $S_{k,x}$ with respect to the elements of Δ_σ and setting all the partial derivatives to zero, the system of linear equations:

$$(\hat{W}^{-1} + \hat{S}_k^T \cdot \hat{V}^{-1} \cdot \hat{S}_k) \cdot \vec{\Delta}_\sigma = -\hat{S}_k^T \cdot \hat{V}^{-1} \cdot \vec{\Delta}k_{C-E} \tag{F.8}$$

produces the following correction vector:

$$\vec{\Delta}_\sigma = (\hat{W}^{-1} + \hat{S}_k^T \cdot \hat{V}^{-1} \cdot \hat{S}_k)^{-1} \cdot (-\hat{S}_k^T \cdot \hat{V}^{-1} \cdot \vec{\Delta}k_{C-E}) . \quad \text{(F.9)}$$

In order to solve Equation (F.9), it is transformed into:

$$\vec{\Delta}_\sigma = \hat{W} \cdot \hat{S}_k \cdot \left[\hat{V} + \hat{S}_k^T \cdot \hat{W} \cdot \hat{S}_k\right]^{-1} \cdot \vec{\Delta}k_{C-E} . \quad \text{(F.10)}$$

As can be seen, the kernel of adjustment is the matrix $\hat{B}$ to be inversed is:

$$\hat{B} = \left[\hat{V} + \hat{S}_k^T \cdot \hat{W} \cdot \hat{S}_k\right]. \quad \text{(F.11)}$$

It has the rank of the integral experiments used in the adjustment.

The previously determined correction vector $\vec{\Delta}_\sigma$ gives rise to the new vector of calculation-to-experiment deviation:

$$\vec{k} = \vec{k}_0 + \hat{S}_k^T \cdot \vec{\Delta}_\sigma , \quad \text{(F.12)}$$

where $\vec{k}$ and $\vec{k}_0$ are the vectors of adjusted and of initial reactor parameters, accordingly.

It is demonstrated in [F.2] that the new cross-section-covariance matrix $\hat{W}'$ can be presented as:

$$\hat{W}' = \hat{W} - \hat{W} \cdot \hat{S}_k \cdot \left[\hat{V} + \hat{S}_k^T \cdot \hat{W} \cdot \hat{S}_k\right]^{-1} \cdot \hat{S}_k \cdot \hat{W} . \quad \text{(F.13)}$$

Using this matrix in the "sandwich equation", the calculation uncertainties due to the adjusted nuclear data can be calculated as:

$$\delta\vec{k} = \sqrt{\hat{S}_k^T \cdot \hat{W}' \cdot \hat{S}_k} . \quad \text{(F.14)}$$

An application object can be defined as calculated values to be predicted through the adjustment [F.5]. This object plays a passive role in the GLLS procedure. Since the application has no experimental results, it does not impact the values included in the consolidation procedure; but the GLLS procedure may modify the calculated value of the application object if it is similar to the experimental configurations. The bias for the application object (AO) and its uncertainty are, respectively, calculated as:

$$\vec{k}_{AO} = \vec{k}_{AO}^C + \vec{S}_{AO}^T \cdot \vec{\Delta}_\sigma \quad \text{(F.15)}$$

and

$$\delta\vec{k}_{AO} = \sqrt{\vec{S}_{AO}^T \cdot \hat{W}' \cdot \vec{S}_{AO}} . \quad \text{(F.16)}$$

Data consistency test

A χ^2 test is used to check the consistency of nuclear data and integral information. The minimised value $\chi^2_{\min}$ of quadratic form (F.3) with respect to the vector Δ_σ can be presented as:

$$\chi^2_{\min} = \vec{\Delta}k_{C-E}^T \cdot \hat{B}^{-1} \cdot \vec{\Delta}k_{C-E} . \quad \text{(F.17)}$$

Generally speaking, $\chi^2_{\min}$ is a random quantity originated from random character of vector Δk elements. Using Equation (F.17), it is possible to determine the value of chi-square likelihood criterion of consistency:

$$\chi^2 = \chi^2_{\min} / I' , \qquad \text{(F.18)}$$

where I' is the number of freedom degrees that are equal to the number of experiments if they are independent, otherwise it should be calculated upon the experimental covariance matrix [F.5]. This criterion is used as a measure between the dispersion of calculation-to-experiment discrepancies that is expected based on the estimated uncertainties of benchmark values and the actually observed dispersion of calculation-to-experiment discrepancies. If the experimental results used for adjustment are consistent within their experimental uncertainties and correlations, the χ^2 value is distributed according to the χ^2 statistical law with I' degrees of freedom. This being close to a normal distribution with central tendency equal to uniform and variance equal to $2/I'$, it confirms that the set of benchmarks is representative.

The considerable difference of χ^2 from unity indicates the presence of contradictions within the selected benchmarks. In this case, the accuracy of the calculated values $\vec{k}$ should be characterised not by the expected uncertainties (F.14) but by the more conservative value:

$$\delta\vec{k}' = \sqrt{\chi^2 \cdot \left[\hat{S}_k^T \cdot \hat{W}' \cdot \hat{S}_k\right]} . \qquad \text{(F.19)}$$

When the difference between the χ^2 value and 1 is very large, it is necessary to perform a comprehensive examination of the integral data used in the adjustment in order to detect questionable practices and to re-estimate or exclude them from the adjustment procedure [F.5].

BERING Code package

The algorithm described above has been implemented into the BERING code package.

The sensitivity coefficients, input to BERING, can be calculated in any energy group structure. BERING converts them into the group structure of available covariance matrices. For example, for this exercise the 238-group sensitivities produced by SCALE6.1/TSUNAMI-3D [F.6] are collapsed into 33 groups as follows:

$$\vec{S}_{k,33gr} = \hat{T}_{238\Rightarrow 33} \cdot \begin{bmatrix} S_{k,\Sigma(1)} \\ S_{k,\Sigma(2)} \\ \cdots \\ S_{k,\Sigma(238\ gr)} \end{bmatrix} , \qquad \text{(F.20)}$$

where $\vec{S}_{k,33gr}$ is matrix of sensitivity coefficients in a targeted energy structure and $\hat{T}_{238\Rightarrow 33}$ is the transformation operator.

The conventional adjustment approach demonstrated above performs the one through adjustment for all nuclear data. The adjustment results of the new cross-correlations might be non-physical. Therefore, an option is added to BERING that allows

suppressing undesirable cross-correlations. In this case, the cross-section-covariance matrix can be presented as a junction of sub-matrices:

$$\hat{W} = \hat{W}_0 \cup \hat{W}_1, \tag{F.21}$$

where $\hat{W}_1$ is an extracted fragment and $\hat{W}_0$ is the residual part of the matrix. The sensitivity coefficients in this case can be presented similarly:

$$\hat{S}_k = \hat{S}_0 \cup \hat{S}_1, \tag{F.22}$$

where $\hat{S}_1$ is an extracted fragment and $\hat{S}_0$ is the residual vector.

The adjustment is conducted as a chain of subsequent steps. On each step, the calculation uncertainty due to extracted part of nuclear data is added to benchmark uncertainty as follows:

$$\hat{V}_1 = \hat{V} + \hat{S}_1^T \cdot \hat{W}_1 \cdot \hat{S}_1, \tag{F.23}$$

where $\hat{V}_1$ is the new benchmark uncertainty covariance matrix. Then the correction factor is calculated with the residual matrix and sensitivity coefficients as:

$$\vec{\Delta}_0 = \hat{W}_0 \cdot \hat{S}_0 \cdot \left[\hat{V}_1 + \hat{S}_0^T \cdot \hat{W}_0 \cdot \hat{S}_0\right]^{-1} \cdot \Delta\vec{k}_{C-E}, \tag{F.24}$$

where $\vec{\Delta}_0$ is the reduced vector of corrections. The correction ($\Delta\vec{k}_0$) obtained on this step can be presented as follows:

$$\vec{\Delta}k_0 = \vec{S}_0^T \cdot \vec{\Delta}_0. \tag{F.25}$$

The new reduced covariance matrix is calculated similar to Equation (F.13):

$$\hat{W}'_0 = \hat{W}_0 - \hat{W}_0 \cdot \hat{S}_0 \cdot \left[\hat{V}_1 + \hat{S}_0^T \cdot \hat{W}_0 \cdot \hat{S}_0\right]^{-1} \cdot \hat{S}_0 \cdot \hat{W}_0, \tag{F.26}$$

where $\hat{W}'_0$ is the reduced covariance matrix. The uncertainty of calculated parameters on this step is:

$$\delta\vec{k}_0 = \sqrt{\hat{S}_0^T \cdot \hat{W}_0' \cdot \hat{S}_0}, \tag{F.27}$$

where $\delta\vec{k}_0$ is a partial bias uncertainty.

Calculated parameters for the next step include the corrections generated on each preceded step using a new vector: $\vec{\Delta}k_{E-C}^0 = \dfrac{\vec{E} - \vec{k}_0}{\vec{E}}$.

The integral experiments covariance matrix will be a composition of the initial matrix and contribution due to partially adjusted nuclear data:

$$\hat{V}_0 = \hat{V} + \hat{S}_0^T \cdot \hat{W}'_0 \cdot \hat{S}_0, \tag{F.28}$$

where $\hat{V}_0$ is the covariance matrix of the benchmarks for the second step.

The corrections to the nuclear data are presented as:

$$\vec{\Delta}_{\sigma 1} = \hat{W}_1 \cdot \hat{S}_1 \cdot \left[\hat{V}_0 + \hat{S}_1^T \cdot \hat{W}_1 \cdot \hat{S}_1\right]^{-1} \cdot \vec{\Delta} k_0 , \quad \text{(F.29)}$$

where $\vec{\Delta}_{\sigma 1}$ is a partial correction for this step.

The new corrected partial covariance matrix of nuclear data is similar to Equation (F.13) and (F.26):

$$\hat{W}'_1 = \hat{W}_1 - \hat{W}_1 \cdot \hat{S}_1 \cdot \left[\hat{V}_0 + \hat{S}_1^T \cdot \hat{W}_1 \cdot \hat{S}_1\right]^{-1} \cdot \hat{S}_1 \cdot \hat{W}_1 , \quad \text{(F.30)}$$

where $\hat{W}'_1$ is the corrected partial covariance matrix.

The chain of partial adjustments results in correction factors for all nuclear data:

$$\hat{W}' = \hat{W}_0' \cup \hat{W}_1' , \quad \text{(F.31)}$$

and

$$\vec{\Delta} = \vec{\Delta}_0 \cup \vec{\Delta}_1 . \quad \text{(F.32)}$$

Generated as presented above, the cross-section covariances contain only desirable correlations.

References

[F.1] L. N. Usachev, Yu. G. Bobkov (1980), "Perturbation Theory and Planning of Experiment at the Problem of Nuclear Data for Reactors", Atomizdat, Moscow, (in Russian).

[F.2] M. Kendall, A. Stewart (1967), "The Advanced Theory of Statistics, Vol. II, Inferences and Relationships", 2nd ed., Charles Griffin and Company, London.

[F.3] T. Ivanova, E. Létang, I. Duhamel (2011), "Impact of Cross-Section-Covariance Data on Results of High-Confidence Criticality Validation", *Journal of Korean Physical Society*, V. 59, N. 23, Page: 1170 – 1173.

[F.4] T. T. Ivanova, M. N. Nikolaev, K. F. Raskach, E. V. Rozhikhin, A. M. Tsiboulia, "Influence of the Correlations of Experimental Uncertainties on Criticality Prediction", NSE, V. 145 (1), September 2003, pp. 97-104.

[F.5] T. T. Ivanova, M. N. Nikolaev, K. F. Raskach, E. V. Rozhikhin, A. M. Tsiboulia, "Use of International Criticality Safety Benchmark Evaluation Project Data for Validation of the ABBN Cross-Section Library with the MMK-KENO Code", NSE, V. 145 (2), October 2003, pp. 247-255.

[F.6] SCALE: A Comprehensive Modelling and Simulation Suite for Nuclear Safety Analysis and Design, ORNL/TM-2005/39, Version 6.1, Oak Ridge National Laboratory, Oak Ridge, Tennessee, June 2011.

IRSN Assessment Questionnaire

This section summarises the IRSN methodology used in the benchmark exercise by answering the questionnaire proposed in the NEA Report, "Assessment of Existing Nuclear Data Adjustment Methodologies", International Evaluation Co-operation, Intermediate Report of WPEC Subgroup 33, NEA/NSC/WPEC/DOC(2010)429, OECD/NEA, Paris, 2011.

Quantitative criteria

Computational efforts

What is the rank of the matrix (or matrices) to be inverted?

The matrix to be inversed has rank equal to number of benchmarks' values used in the data assimilation.

Does your adjustment use an iterative method?

The iterative (in other words step-wise) solution is optional. It can be applied to suppress generation of undesirable cross-correlations in cross-section covariances.

Is there any computational limitation (number of variables, experiments, etc.)?

There is no computational limitation with respect to number of benchmarks, reaction, groups and other variables.

What is a typical running time for a defined number of variables/experiments?

The running time is around 3÷5 minutes for 4000 parameters adjustment on 20 measured values on a 1.6 GHz, 1GB RAM, 32-bit architecture personal computer.

Input/output burden

Are all cross-sections taken into account? (If not, please, specify cross-section selection strategy.)

The method allows calculating relative corrections to all cross-sections.

Qualitative criteria

Are all reactions taken into account?

All reactions can be treated if specified by the user and if associated sensitivity coefficients and covariances are provided.

Can self-shielding effects be explicitly treated?

The self-shielding can be treated explicitly if the corresponded covariance matrices and sensitivities are available.

Can high order effects be taken into account?

No, they are not recommended to be taken into account.

Can method uncertainties/bias be accounted for?

Methodical component of uncertainty are combined with uncertainty of measurements. However, it could be considered separately using surrogate covariance matrix and associated sensitivity.

How are inelastic matrices and secondary energy distributions treated?

The total inelastic cross-section is adjusted. Secondary energy distribution is adjusted depending on the capability of calculating associated sensitivity coefficients. But its applicability remains to be an open question.

Fission prompt and delayed neutron spectra/data?

Yes, they can be treated in the same manner as other nuclear parameters.

Is consistency test present?

Yes, chi-square test is present.

Are cross-correlations among nuclear data taken into account?

Yes, cross-correlations are taken into account.

Are correlations among experiments taken into account?

Yes, if they are provided by user.

Are correlations among nuclear data and experiments taken into account?

No.

Is a new covariance data set produced?

Yes, a new covariance data set is produced. However, it is valid only for an application area of the adjustment.

Is the solution unique (local minima)?

Yes, the solution is unique.

Appendix G: Detailed benchmark results

Detailed benchmark results provided by the participants are available on the NEA website (www.oecd-nea.org/science/wpec/sg33/benchmark/results/).

This website gives access to raw results (text files) and plot comparisons for integral parameters and nuclear data.